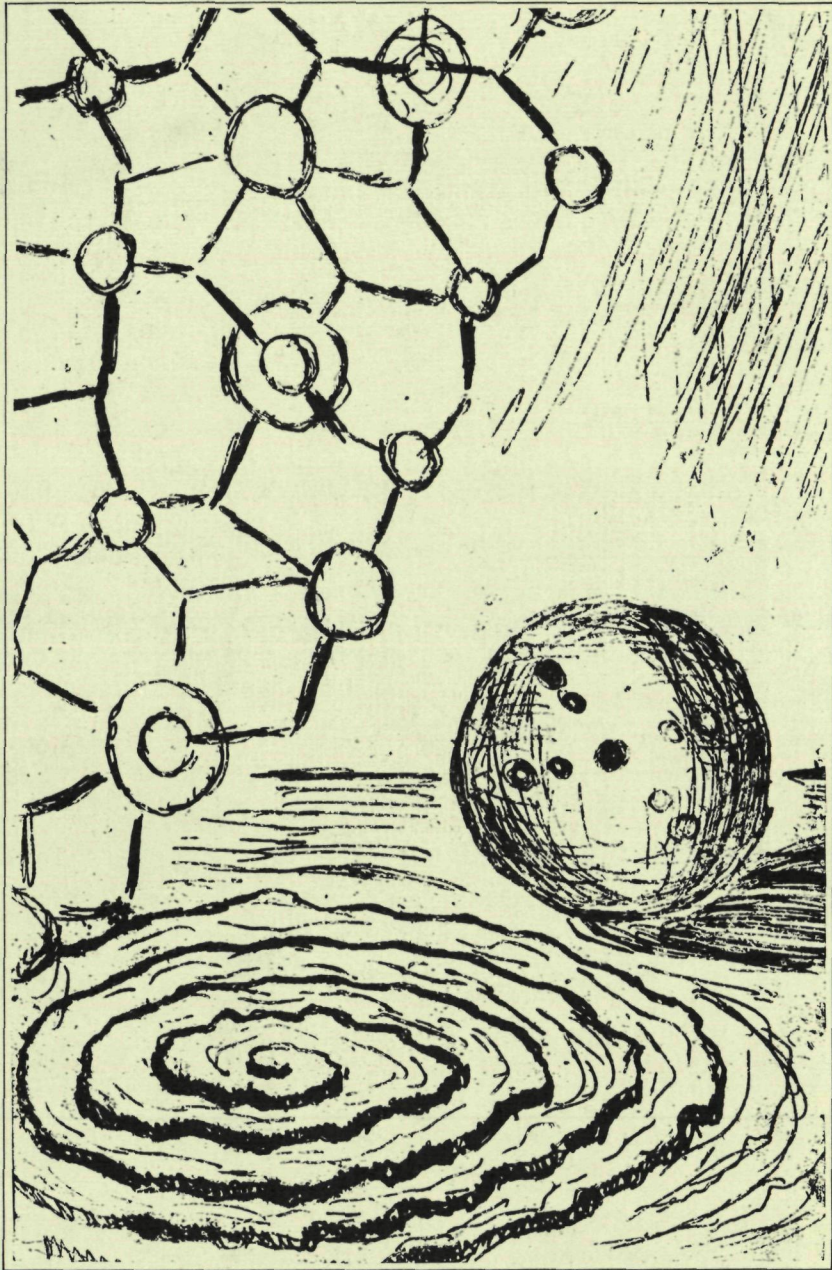


2354



**CONTRIBUTIONS TO THE THEORY
OF CRYSTAL GROWTH**

J. P. VAN DER EERDEN

CONTRIBUTIONS TO THE THEORY OF CRYSTAL GROWTH

PROMOTOR: DR. P. BENNEMA

CONTRIBUTIONS TO THE THEORY OF CRYSTAL GROWTH

PROEFSCHRIFT

ter verkrijging van de graad van doctor in de
wiskunde en natuurwetenschappen aan de
Katholieke Universiteit te Nijmegen, op gezag
van de rector magnificus Prof. dr. P. G. A. B. Wijdeveld,
volgens besluit van het College van Decanen,
in het openbaar te verdedigen op vrijdag 15 juni 1979
des namiddags te 2.00 uur precies

door

Johannes Petrus Josef Maria van der Eerden

geboren te Amsterdam

1979

Druk: Krips Repro Meppel

Dankwoord

Ik bedank iedereen die, op welke manier dan ook, heeft bijgedragen aan het tot stand komen van dit proefschrift.

Enigen wil ik in het bijzonder noemen. Mijn vrouw, die mij door haar belangstelling en kritische vragen stimuleert om een helder zicht te krijgen en te geven op de zin en de problemen van mijn onderzoek.

Cor van Leeuwen, die tijd noch moeite heeft gespaard om mij snel in te werken in de theorie van de kristalgroei, in het bijzonder de Monte Carlo simulaties.

De medewerkers van de laboratoria in Delft en in Nijmegen, waar het onderzoek werd uitgevoerd, Willem van Enckevort, Bas van der Hoek, Hans Human, Renée Janssen, Ronald Kalf, Henk Keller, John van Krieken, Wim van der Linden, Erik Mischgofsky, Joo Odekerken en Katsuo Tsukamoto, die bijdragen tot wetenschappelijk en sociaal optimale werkomstandigheden.

De overige medeschrijvers van de artikelen in dit proefschrift, Prof. E. Budevski, Dr. T. Cherepanova, Dr. Kashchiev, Dr. H. Knops, Dr. G. Staikov en Prof. B.P.Th. Veltman, aan wie ik een aanzienlijke verzuiming van mijn wetenschappelijk blikveld dank.

Tenslotte degenen die slordige manuscripten hebben omgezet in net typewerk, in het bijzonder Wilma Philipse, die dat in de tijdnoodfase heeft gedaan met de paragrafen 4.5 en 4.6.

In feite is de opvatting dat wij kunnen gaan waarnemen zonder over iets als een theorie te beschikken, absurd.

K. Popper

CONTENTS

Omslag	2
Voorwoord	3
Preface	4
1. Introduction	
1.1 The object of the theory of crystal growth	5
1.2 The network model for crystal-fluid systems	7
1.3 The values of the model parameters	12
1.4 Faceting	17
1.5 Summary of the reprinted papers	21
References to chapter 1	23
2. Survey papers	
2.1 Crystal growth from solution: development in computer simulation	24
2.2 Survey of Monte Carlo simulations of crystal surfaces and crystal growth	37
3. Equilibrium surface roughening	
3.1 Roughening transition in mean-field and pair approximation of Ising models	70
3.2 Correlations in the XY model and screw dislocations in the solid on solid model	77
4. Growth and evaporation	
4.1 Crystal growth: a comparison of Monte Carlo simulation, nucleation and normal growth theories	80
4.2 Nucleation growth processes: a Monte Carlo simulation	87
4.3 Evaporation at high underpressure: confrontation of theory and experiment	101
4.4 Fast growth of ordered AB crystals, a Monte Carlo simulation for ionic crystal growth	105
4.5 On the influence of surface diffusion and step integration kinetics on spiral growth	113
4.6 On the diffusion problem for a free spiral-shaped boundary	129
5. Thin films and adsorption layers	
5.1 Transition from island to layer growth of thin films: a Monte Carlo simulation	149
5.2 Surface migration of small crystallites: a Monte Carlo simulation with continuous time	161
5.3 Mean field theory and Monte Carlo simulation of multisite adsorption	165
Curriculum vitae	185

Op de omslag zijn de uitgangspunten van dit proefschrift gesymboliseerd. De bol staat voor de zogenaamde bolproef. In dit experiment wordt een kristal eerst bolvormig geslepen en vervolgens in een licht oververzadigde omgeving gebracht (bijvoorbeeld een oplossing, een smelt, een damp enz.). In die omgeving groeit de bol in alle richtingen uit, echter niet in alle richtingen even snel. In richtingen die langzamer groeien ontstaan daardoor "deuken" op die bol. Wanneer de groeisnelheid slechts geleidelijk zou veranderen bij een kleine richtingsverandering, dan zou de bol alleen wat afgeplat zijn maar nog wel glad. In werkelijkheid echter ontstaan er een aantal cirkelvormige gladde gebiedjes, de zogenaamde facetten. Dit betekent dat er abrupte groeisnelheids veranderingen optreden bij sommige richtingsveranderingen. Wanneer men de bol lang genoeg zou laten doorgroeien dan zouden op den duur alleen enige facetten overblijven en zou de vorm ontstaan die meestal met kristal wordt geassocieerd (zout, suiker, mineralen, etc).

Dit proefschrift probeert een antwoord te geven op de vraag waarom zulke facetten voorkomen, hoe je ze zou kunnen karakteriseren, onder welke voorwaarden ze ontstaan en wat voor gevolg ze hebben voor de groei van kristallen in het algemeen.

Om de eerste vragen te kunnen beantwoorden gaan we terug naar de atomaire modellen. Daarbij nemen we aan dat het kristal gezien kan worden als een verzameling atomen (ionen, moleculen etc) die door sterke bindingen tussen burens bijeen wordt gehouden. In zo'n netwerk van deeltjes en bindingen is een grote regelmaat te vinden. Het zal mogelijk zijn het hele netwerk opgebouwd te denken uit steeds gelijke lagen die op een bepaalde manier gestapeld zijn. In een aantal richtingen is zo'n laag een stevig "matje" van deeltjes en bindingen. Een voorbeeld van zo'n matje in een granaatkristal is afgebeeld op de omslag.

Als men nu probeert een echt kristal te splijten dan zal dat alleen lukken als de stevigste matjes zoveel mogelijk intact blijven. Om die reden kunnen we spreken van splijtvlakken en splijtrichtingen. Een belangrijke konklusie die in dit proefschrift wordt getrokken is dat de bovengenoemde facetten op de bol optreden in die richtingen waarin het dunst mogelijke matje (dwz de deeltjes tussen twee opeenvolgende splijtvlakken) nog bijeen wordt gehouden door sterke bindingen.

De kristalgroei op zo'n vlak zal langzaam gaan. Immers als er atomen arriveren die een nieuw matje zouden gaan vormen dan hebben ze nog geen mogelijkheid om al de bindingen aan te gaan die ze in dat matje zullen krijgen, ze zullen dus gemakkelijk weer van dat vlak verdwijnen. In de praktijk wordt dit probleem vaak overwonnen doordat een bepaalde kristalfout (de schroefdislokatie) er voor zorgt dat er treden op zo'n oppervlak voorkomen waaraan de nieuwe atomen kunnen aanleggen. Zo'n trede rolt zich dan op tot een spiraal, zoals ook op de omslag is te zien. De groeisnelheid van de zo opgebouwde groeiheuvel wordt besproken.

VOORWOORD

Dit proefschrift is een weerslag van het werk dat ik in de periode september 1974 tot februari 1979 heb gedaan. Het onderzoek werd uitgevoerd in het kader van een promotie onderzoek. Het heeft zich bewogen in verschillende gebieden van de theorie van de kristal groei. Het heeft geleid tot een aantal publikaties en het proefschrift bestaat grotendeels uit herdrukken van die publikaties. Er kunnen drie aspecten onderscheiden worden.

Ten eerste zijn er stukken onderzoek die vrij direkt werden geïnspireerd door bepaalde experimentele situaties. Voorbeelden zijn de waargenomen groeikinetic bij groei uit een oplossing (zie bijvoorbeeld 2.1), molecular beam experimenten (4.3) en metaalionen adsorptie uit een elektrolytische oplossing (5.3).

Ten tweede kent de theorie van de kristal groei een aantal eenvoudige modellen die als een eerste benadering voor in de praktijk zeer uiteenlopende situaties gebruikt worden (1.2). Ondanks de eenvoud van die modellen is het vaak moeilijk om de interessante grootheden (groeisnelheid, oppervlaktestructuur) met enige nauwkeurigheid te berekenen. In zo'n gevallen neemt men zijn toevlucht tot numerieke methodes, waarbij vooral de Monte Carlo simulaties een machtig hulpmiddel blijken te zijn (2.2, 4.1, 4.2, 4.4, 5.1 en 5.2).

En ten derde komt het voor dat, hoewel numerieke methodes kwantitatieve antwoorden opleveren, er toch gezocht moet worden naar analytische methodes om werkelijk begrip en inzicht te verkrijgen. Voorbeelden zijn de verruwingstemperatuur (3.1 en 3.2) en het oppervlakte diffusie probleem rond een groeispiraal (4.5 en 4.6)

Zoals aangegeven zijn deze drie aspecten vertegenwoordigd in dit proefschrift. Iedere paragraaf in de hoofdstukken twee tot en met vijf is een herdruk van een artikel. Daardoor komen zo nu en dan doublures voor en is er geen volledig consequente symbolen conventie. Tegenover dit nadeel staat dat iedere paragraaf nu als een afgerond geheel gelezen kan worden.

Bij het inleidend hoofdstuk 1 is getracht de interessante aspecten van de kristal groei te verduidelijken op basis van minimale voorkennis. Uitgaande van deze inleiding zullen de volgende hoofdstukken, die zijn geschreven op het niveau van de kristal groei wetenschap, begrijpelijk zijn voor de fysisch geschoolde lezer. De inhoud van dit gedeelte is kort aangegeven in 1.5

PREFACE

This thesis is a reflection of the work which I have carried out in the period of september 1974 to february 1979. The research has covered several fields within the theory of crystal growth. It has led to a number of papers and the present thesis consists mainly out of reprints of these articles. Three aspects can be distinguished.

Firstly, some cases were almost directly inspired by certain experimental situations. Examples are the observed growth kinetics for growth from solution (2.1), molecular beam experiments (4.3), and metal ion adsorption from electrolytic solutions (5.3).

Secondly, in the theory of crystal growth some simple models are used to describe approximately a number of different situations (1.2). Although they are simple, it is often difficult to compute the interesting quantities (growth rate, interface structure etc.) with some precision. In such cases numerical methods have to be used (2.2, 4.1, 4.2, 4.4, 5.1, 5.2). Among them Monte Carlo simulations turn out to be a powerful tool.

And third, it may happen that, although numerical methods lead to quantitative results, it is necessary to use analytical methods in order to obtain a more fundamental understanding. Examples are the roughening temperature (3.1 and 3.2) and the surface diffusion problem in the presence of a growth spiral (4.5 and 4.6)

As indicated these three aspects are present in this thesis. Every section of the chapters two to five is a reprint of an article. Consequently in some cases doublures are present and there is no fully consistent use of symbols. This disadvantage is compensated by the fact that each section is self contained and can be read separately.

In the introductory chapter 1 an attempt is made to indicate the interesting aspects of crystal growth on the basis of minimal a priori knowledge. Using this introduction, the next chapters, which are written on the present level of the science of crystal growth, will be accesible for readers with physical background. This second part is summarized in 1.5.

1.1 THE OBJECT OF THE THEORY OF CRYSTAL GROWTH

Crystal growth is the formation of a crystal out of a mother phase, which may be a vapour, a solution, a melt, a flux etc. The basic process is the change of the mother phase which contains the building units for the crystal, in a low degree of ordering, to the highly ordered crystal phase.

This process is a first order phase transition. This means that at conditions (temperature, pressure etc.) at which the mother phase is in equilibrium with the crystal both phases are distinct, a situation which persists even (not too far) away from equilibrium. Due to this basic property of a first order transition the possibility exists of a mother phase which is in metastable equilibrium with the crystal. This could also be expressed by the statement that the free energy of the system possesses not only the absolute minimum corresponding to the real equilibrium state of the system, but also a relative minimum corresponding to the supersaturated or the undersaturated state. It will take a finite time for the system to change from the metastable state to real equilibrium.

A consequence of this coexistence of two phases is the existence of an interface which separates the crystal and the mother phase. Generally speaking we mean with interface that part of the system which deviates both from the average mother phase and from the crystal. A more precise definition will be given in sect. 1.3. The atoms in the interface are neither in the equilibrium state, nor in the metastable state. Therefore their contribution to the total free energy of the crystal-mother phase system always is larger than when they would belong to either of the two bulk phases. This is equivalent to saying that the interface free energy necessarily is positive.

This positive interface free energy causes the nucleation phenomenon. Here and further on we mean with energies which are ascribed to planes energies per unit area, unless explicitly stated otherwise. To form a small aggregate of the equilibrium state out of the metastable state an interface has to be formed which is, for small particles, large compared to the equilibrated material in the volume of the aggregate. Indeed, there exists a critical size, such that only the formation of larger aggregates lowers the free energy of the system (i.e. is favourable for the system). The critical aggregate is formed by spontaneous local fluctuations of the system.

Thus we conclude that due to the fact that crystallization is a first order transition, the formation of interface acts as a kinetic barrier which height depends in general on supersaturation and on the interface free energy. It is precisely the object of the theory of crystal growth to explain how a supersaturated system overcomes this barrier.

Having thus formulated the problem in general terms we go into more detail now. The crystal growth process involves on one hand atomic processes in the interface itself, on the other hand transport processes from the bulk of the crystal and of the mother phase to the interface and vice versa. Examples for the latter ones are the transport of growth units from the mother phase to the interface and of heat away from the interface.

1.1 The object of the theory of crystal growth

If the transport processes are slow in comparison with the interface processes, the tendency of the crystal to keep its interface as small as possible may be dominated by a tendency of the equilibrium phase to protrude into the metastable phase, thus making contact with a region of higher supersaturation. This morphological instability was first studied by Sekerka [1] for smooth and by Chernov [2] for faceted interfaces. Experimentally it exhibits itself by the loss of well-defined surfaces or by dendrites. Recently Langer and Mueller-Krumbhaar [3] gave a quantitative criterion for the occurrence of this instability. They showed that dendrites grow if the diffusion constant is larger than the product of the growth velocity and the critical particle size mentioned above.

In the opposite case where the interface processes are dominant for the determination of the crystal growth rate, the pioneering work has been done by Burton, Cabrera and Frank [4], and was considerably stimulated by the Monte Carlo simulations, introduced in the field by Gilmer and Bennema [5]. The fundamental assumption which underlies this field of the theory is that every position of the interface has the same temperature, pressure, supersaturation etc. This implies that possible gradients in these quantities are perpendicular to the interface, and, moreover, that they are so small that they are not felt on the scale of the atomic roughness of the interface.

This thesis restricts itself to the description of interface properties and processes. Referring to the survey scheme of fig.1 in sect. 2.2, this means that the thesis deals with all theoretical aspects given there, except the kinematic wave theory and volume diffusion kinetics. Moreover special attention is given to the relation between experimental situations and simple theoretical models, a non-trivial problem which is not indicated in that scheme.

The next three sections of this introductory chapter are intended to describe how a theory of crystal growth could be founded and what features are at present of most interest. This serves as a context in which my contributions can be seen.

In sect. 1.2 of this introductory chapter the Hartman-Perdok [6] theory is discussed. This theory usually serves to predict crystal facets on the basis of a distinction between F, S and K faces, and the linear growth rate of F faces. It will be shown here how the notion of the roughening transition modifies this prediction and solves the fundamental problem that any face would be predicted to be an F-face if enough of the actual interactions are taken into account.

In sect. 1.3 a general route is presented, along which the transfer from a complicated experimental situation to a suitable interface can be achieved. Examples for certain cases are given.

In sect. 1.4 the relation between surface and edge free energy on one hand and the faceting of equilibrium and growth forms of crystals on the other is discussed, using the concepts of the Wulff and growth plot, and the Wulff theorem.

In sect. 1.5 personal contributions are shortly summar-

1.1 The object of the theory of crystal growth

ized and organized in some groups according to the subjects they deal with. Each subject coincides with a chapter in the rest of this thesis, which consists out of a set of reprints. This section can, therefore be used as an index for the rest of the chapters.

1.2 THE NETWORK MODEL FOR CRYSTAL FLUID SYSTEMS

A crystal can be defined as a set of particles (atoms, molecules, ions etc) whose average positions in space form a lattice with translational symmetry in at least three independent space directions. Such a definition applies strictly spoken only to infinite crystals. It is natural, therefore, to extend the lattice mentally outside the actual crystal (or part of the crystal) under consideration. The translational symmetry should be understood to refer to this extended lattice. The actual crystal corresponds to a partial occupation of this lattice by crystal particles.

For a complete description of the crystal all interactions between the occupied lattice points should be taken into account. Since, however we are primarily interested in a suitable description of the crystal-mother phase interface, we shall attempt to refrain from the details of such interactions as long as they are not necessary for a suitable interface model. The first obvious simplification is to treat assemblies of crystal particles, which are present in the same form both in the crystal and in the mother phase, as the basic building units. In this way only those bonds which are actually formed during the crystallization process do enter the interface model.

Let us restrict ourselves to crystals in which short range interactions are dominant, thus excluding e.g. ionic crystals from the discussion. Let us approximate the crystal by a considerably simpler network. The method is expected to be applicable far below the melting point. The vibrations of the particles around their average positions can be neglected in that case. A method, due to Hartman [6], analyses the network of the particle positions connected by "strongest bonds". Of course the definition of strongest bonds is somewhat ambiguous but in most practical cases they coincide with nearest neighbour bonds (see also the end of this section). The bonds must be sufficient in number to connect all lattice points.

The analysis uses as a basic concept the periodic bond chains (PBC). These are one dimensional chains of particles satisfying the following conditions:

- 1) All particles in a PBC are connected by "strongest bonds",
- 2) Each PBC has translational symmetry in one direction,
- 3) Each PBC has the stoichiometry of the crystal,
- 4) The PBC's parallel to a certain direction contain together all particles,
- 5) No PBC contains a complete period of another PBC.

The second basic concept are the slices. These are two dimensional textures of particles and bonds which can be confined between planes whose average distance equals the interplanar dis-

1.2 The network model for crystal-fluid systems

tance $d(hkl)$ (we use Miller indices (hkl) and $[uvw]$ to define planes and vectors). The slices have the stoichiometry of the crystal.

The Hartman Perdok theory classifies (hkl) faces as follows:

F faces (flat faces), at least two non-parallel PBC's in an (hkl) slice,

S faces (stepped faces), an (hkl) slice contains only parallel PBC's, and

K faces (kinked faces), an (hkl) slice contains no PBC.

The prediction of this method is that crystal facets are F faces, and that the facets which really appear on the equilibrium form of a crystal can be found with the Wulff theorem (see sect. 1.4), using the attachment energy, i.e. the energy of the bonds between (hkl) slices, for the determination of the surface energy. Growth on such faces takes place by a layer growth mechanism, like spiral growth or two dimensional nucleation.

In the rest of this section we study these predictions in the light of present insights of the crystal surface theory, in which the concept of surface roughening plays a central role. We first neglect entropy effects, i.e. we discuss the zero temperature interface first, and then continue with the temperature influence on the configurational entropy of the interface, still neglecting phonon excitations. Moreover we assume that no lattice distortion, specific adsorption or surface enrichment takes place. The effect of the latter processes is shortly discussed in sect. 1.3.

Under these assumptions the zero temperature interface can be obtained from an infinite lattice by cleaving the crystal along a (hkl) plane, and replacing one semi infinite crystal by the mother phase. The energy which should be ascribed to this interface is the adhesion energy of the mother phase to the crystal, decreased with half the cleavage energy along a (hkl) plane and half the separation energy of the mother phase. All energies are to be taken per unit area. Note that in this definition all energies are potential energies, the latter three are negative and the interface energy is positive.

A crystal in equilibrium with a surrounding mother phase will keep its total interface energy as small as possible. Neglecting possible differences in the adhesion energy of the mother phase to different crystal faces, this means that a crystal will be bounded by faces with minimal cleavage energy. It is seen immediately that planes parallel to as many PBC's as possible are the first candidates for such faces, since at least these PBC's need not to be interrupted in the cleaving process. Hartman defines the attachment energy as that part of the crystallization energy per unit cell which is not confined in PBC's parallel to the (hkl) plane. The cleavage energy is the attachment energy, divided by the mesh area. The mesh area $M(hkl)$ is the unit cell volume divided by $d(hkl)$. For more complicated structures it may be less in absolute value than the total energy in all non-parallel PBC's because only the weakest (not all) bonds have to be interrupted.

1.2 The network model for crystal-fluid systems

The first result of the PBC method is thus that those planes come into consideration to form crystal facets which are parallel to at least two PBC directions, and that their interface energy $\sigma(hkl)$ equals, at $T=0$, the sum of the interruption energies of the non-parallel PBC's. Indeed this hypothesis is supported by modern interface theories. The essentially new notion is however that such faces possess a roughening transition, i.e. even when they appear as facets at zero temperature they lose this property at a finite temperature T_R . We summarize the idea of surface roughening below, which will explain also what is the reason (and the precise formulation) of Hartmans second demand for F faces (the local confinement of the PBC's parallel to (hkl) within a slice of thickness $d(hkl)$).

Burton, Cabrera and Frank [4] pointed out the similarity of a crystal surface and a two dimensional lattice gas. Since a second order phase transition is known to exist in the latter one, they conjectured that the character of a crystal surface would change from essentially flat to rough above a finite temperature, and that this change over would have the characteristics of a second order phase transition. This transition has been termed roughening transition and remained a central theme of interest in the theory of crystal growth until now.

Proceeding along this line Weeks, Gilmer and Leamy [7] gave low temperature expansions of several surface quantities which characterize surface roughness. Pade analysis of the coefficients suggested singularities of these quantities at a temperature close to the critical temperature of the two dimensional lattice gas. This result thus tends to support the conjecture of Burton, Cabrera and Frank.

A second point of view to approach faceting was given by Temkin [8]. He argued that for a surface to remain flat it must be localized, i.e. the average distance of the interface and a fixed (hkl) plane must at any time equal an integer number of times the interplanar distance $d(hkl)$. He studied therefore (in a mean field approximation) the occurrence of minima in the free energy of the system for such average interface positions. Indeed these minima virtually disappeared above a finite temperature. Monte Carlo simulations of the localization of the interface are described in the thesis of van Leeuwen [9] and support this conclusion. Based on this presupposition of interface localization below T_R I developed a computational procedure to estimate T_R for a number of different interface models [sect. 3.1].

A third approach uses the occurrence of steps on a surface (a monolayer step separates two regions of the interface whose distance to a reference (hkl) layer differ by $d(hkl)$, the interplanar distance). In sect. 1.4 it will be shown in general that an (hkl) plane will appear as a facet on an initially spherical crystal if steps along all directions in the (hkl) plane have a non zero edge free energy (edge free energy is the one dimensional analog of the interface free energy defined in sect. 1.1). Starting from this point of view Leamy, Gilmer and Weeks [10] carried out Monte Carlo simulations on stepped surfaces. The results suggest strongly the vanishing of the edge free energy at

1.2 The network model for crystal-fluid systems

a finite temperature. They mentioned an analogy with the behaviour which has to be expected for a second order phase transition. More accurate simulations by Swendsen and Mueller-Krumbhaar [11], however, showed that this analogy was removed by larger computational precision.

The question about the character of the roughening transition has been solved recently. After the exact results obtained by van Beyeren [12] for a special interface model, and the shown equivalence of the most common interface models and planar XY models (by Knops [13] and simultaneously by Jose, Kirkpatrick and Nelson [14]) it became clear that the roughening transition is a textural transition. Upon varying the temperature in equilibrium systems the transition appears not as a second order but as an infinite order transition (i.e. the singularities are of the weakest possible type). Changing, however, from supersaturated to undersaturated mother phases a first order transition appears below T_R . It is shown in sect. 3.2, and independently by Swendsen [15] that the edge free energy behaves as the spin-spin correlation length in the planar XY model. Thus it could be concluded that the edge free energy vanishes above T_R in a smooth way, which is precisely what is indicated by the precise Monte Carlo simulations [11].

Summarizing, (hkl) faces will become facets on initially spherical crystals if edge energies of steps along all directions in this face are non zero. Moreover, if this condition is met such faces possess a roughening temperature above which the edge free energy vanishes and the facet disappears.

The resemblance of the present textural phase transition and the Ising transition of the two dimensional lattice gas is the fact that in the temperature-supersaturation plane the interval of the temperature axis between 0 and T_R is a line of first order phase transitions. The difference is that, moving along the temperature axis, a second order transition is obtained in the two dimensional lattice gas and an infinite order transition for the textural transition.

Let us now investigate how the roughening transition is related to the F face definition of Hartman. It is sufficient to investigate which faces steps have a non zero edge energy at $T=0$. Such faces will, below their roughening temperature, lead to facets. At $T=0$ any F face would be perfectly flat, i.e. all non parallel PBC's are interrupted just above the (hkl) plane. A step could be created on such a face by the addition of a semi infinite layer on top of this flat face. A non zero step energy is obtained when the total number of interrupted PBC's increases during this process (this follows from the definition of edge energy as the interfacial energy difference of an interface with and without step). Some reflection shows that this is equivalent with the statement that an infinite (hkl) layer is "strongly connected", i.e. can not be divided in two parts without interrupting strong bonds. This in turn leads to the F face definition of Hartman, which could be reformulated as follows:

An (hkl) face is an F face if the particles between successive (hkl) cleaving planes are organized in a strongly con-

1.2 The network model for crystal-fluid systems

nected lattice.

Note that here the second fundamental concept of the PBC method is redefined: the slice between successive cleaving faces, which may have dips on the scale of the crystal particles. From a given cleaving face the next one is in general not obtained by an elementary translation over $d(hkl)$, but by the combination of this operation with an element of the point group of the crystal. Therefore, although the average thickness of the slice is $d(hkl)$, the thickness may vary locally.

In passing we note that in some cases successive cleaving faces have an average distance less than $d(hkl)$. This happens when different stoichiometric slices (which automatically have an average thickness $d(hkl)$) can be defined with the same orientation (hkl) , and when, moreover, these have the same attachment energy. In such a case the slice between successive cleaving faces is only part of the stoichiometric slice. The case that the attachment energies of different stoichiometric (hkl) slices have slightly different attachment energies has to be investigated further.

The analysis of the so defined two dimensional network can be used not only to determine the F character of an (hkl) face. Indeed, although the presence of many parallel (hkl) planes is shown to change the type of critical behaviour close to T_R , the present evidence points towards the conclusion that the position of the critical temperature is hardly influenced. This implies that the critical temperature of the lattice gas on the two dimensional network between successive cleaving faces gives a reasonable estimation of the real roughening temperature.

Here I want to make a remark on a certain incompleteness of the classical PBC method. The fact that only a few orientations lead to F faces is caused by the neglect of all but the "strongest bonds". This can be seen as follows. Take the crystal particles between successive, arbitrary, (hkl) cleaving planes. In general these will not form a connected lattice in the PBC sense. In reality, however, they are connected by (weaker) bonds which makes this slice indistinguishable from a real F face. The classical PBC method is missing a physically acceptable justification to neglect weak bonds for the prediction of facets. The obvious reason why on real crystals rarely facets or layer growth mechanisms are found which do not correspond to F faces is that weakly connected faces have low roughening temperatures, in practice usually below the crystallization temperature. Stated alternatively, the distinction between F, S and K faces is that the first have a high, the latter two a low roughening temperature ($T_R = 0$ for S and K faces when only "strongest bonds" are taken into account). We thus see that the notion of the roughening transition is in a sense underlying the predictions of the classical PBC theory.

In this section it is shown that at present network models are the appropriate instruments to discuss crystal growth. The most important results of the theoretical study of these models in recent years have been obtained in the field of the roughening transition. On one hand the theory on this subject

1.2 The network model for crystal-fluid systems

still has to be extended beyond the tetragonal solid on solid model (Kossel crystal) on which the results discussed above have been obtained. An important point would be the influence of long range interactions in ionic crystals. On the other hand it is a challenge for crystal growth experimentalists now and in future to find crystal growth situations in which the roughening transition can be studied, i.e. in which an F face loses its facet character. Such experiments are reported in sect. 2.1. Before they can be fully appreciated a quantitative estimate of the model parameters must be obtained for the given experiment. The next section describes a method to obtain such estimations.

1.3 THE VALUES OF THE MODEL PARAMETERS

In this section we discuss possible methods to obtain reasonable estimates for the values of model parameters in a given experimental situation and effects that might modify them. From the foregoing sections it is clear that the important parameters to determine the roughness of a certain (hkl) face are the interruption energies ϕ [uvw] of the PBC's parallel to the (hkl) plane and the way in which these are interconnected. As we have seen, this involves the replacement of half a solid-solid and half a fluid-fluid contact by one solid-fluid contact, in fact of the weakest solid-solid contact of the PBC which should be interrupted. Formally this can be written as:

$$\phi = - \phi(\text{bisection})/2 - \phi(\text{cohesion})/2 + \phi(\text{adhesion})$$

where, as before, the energies are potential energies, the first one positive, the latter three negative. Bisection is done in vacuum, cohesion refers to the mother phase and adhesion is between the interrupted PBC and the mother phase. We denote the PBC interruption energy as ϕ [uvw], although in general different PBC's may exist parallel to the same [uvw] direction. The ϕ [uvw] for which [uvw] is parallel to the (hkl) plane determine the roughness of the (hkl) face. The other basic parameter is the supersaturation. In this section we shall not discuss this quantity further but rather restrict ourselves to interface quantities, since the supersaturation is a bulk quantity whose determination is usually less problematic. For a discussion of the case of different supersaturations for different particles see sect.4.4.

In general there may be several different effects on the interruption energy ϕ [uvw]. Here we mention some of the most important ones:

- 1) bond energy between crystal particles,
- 2) cohesion of the mother phase (including the mother phase interaction with and the mutual interaction of the crystal particles which are taken up by the mother phase),
- 3) adhesion of the mother phase to the interrupted PBC,
- 4) deviation from stoichiometry at the end of the PBC,
- 5) lattice distortion and bond reconstruction at the crystal surface.

The first two effects do not depend on the interface and may be

1.3 The values of the model parameters

called bulk effects therefore. The last three depend not only on the PBC which is interrupted, but on the whole (hkl) face under consideration. In general these interface effects are not independent, e.g. the adhesion properties will vary with the stoichiometry of the PBC end.

For $T > 0$ temperature effects can not be neglected. Each of the energy effects mentioned above has an entropy effect as counterpart:

- 1) internal entropy of crystal particles,
- 2) internal and configurational entropy of mother phase particles,
- 3) loss of configurational entropy of mother phase particles which are adsorbed to the crystal surface,
- 4) mixing entropy of crystal particles at the interface,
- 5) partial release of degrees of freedom of crystal particles at the interface.

Again the first two effects are bulk effects and the last three interface effects.

As a matter of fact we are interested in the interface quantity $\phi[uvw]$. In most cases, however, much more is known about bulk properties. Recipes, therefore, to estimate $\phi[uvw]$ attempt to express ϕ in terms of bulk quantities. This is possible only if somehow an ad hoc assumption is made of a relation between bulk phases and interface (in the absence of precise knowledge of interface properties). We now proceed to show examples of such assumptions, the assumptions of complete and equivalent wetting.

A widely used recipe is historically due to Jackson [16]. It is useful to sum the $\phi[uvw]$ of those PBC's which have to be interrupted in order to cut a growth unit out of the (hkl) slice. In the case of different growth units take the average. The resulting quantity, divided by kT , was termed $\alpha(hkl)$ and is conveniently written in the form:

$$\alpha(hkl) = \xi(hkl) L / (kT)$$

Here ξ is the ratio of the slice energy to the total bond energy of the crystal, and L is the differential heat of formation (all per stoichiometric unit) in equilibrium. The value of α gives an impression of the values of the $\phi[uvw]$ of the PBC's in the slice and hence of the character of the (hkl) face. The roughening transition occurs at a temperature for which α is of the order of the number of connected neighbours of a growth unit in the slice. A more logical definition of ξ would be the ratio of α and $\alpha + f$. Here f is the interface free energy per growth unit,

$$f(hkl) = \sigma(hkl) \times M(hkl) / N$$

where N is the number of growth units per unit cell, and σ and M are, as before, the interface free energy and the mesh area. This usage of ξ is an application of a rather general approximation

$$f(hkl)/(kT) + \alpha(hkl) = \text{constant}$$

which is a generalization of the statement of Hartman that the crystallization energy is the sum of the attachment and the slice

1.3 The values of the model parameters

energy. Often ξ is approximated using bisection energies only.

The essential difficulty with the use of this recipe is not the interpretation of α or the evaluation of ξ , for which suitable modifications can be given in particular cases. The fundamental problem is that α is an interface property whereas ξ and L refer to bulk phases. It is not a priori clear (neither true) that a direct relation should exist between interface and bulk properties.

An experimental example which shows dramatically the weakness of Jackson's recipe when interface effects play an important role is provided by the growth of easily soluble salts from solution. It may happen that the differential heat of dissolution for equilibrium solutions is negative. This would lead to a negative α value and hence the crystal could not even exist in the solution.

The question naturally arises under what conditions the recipe of Jackson does work. First of all the effects 4) and 5) must be negligible. The other important restriction is the assumption of complete wetting. This can be expressed as the assumption that dividing the mother phase in two parts requires the same amount of energy per unit area as separation of the mother phase from the crystal:

$$\phi(\text{cohesion}) = \phi(\text{adhesion})$$

Then the interruption energy is of the form

$$\phi[\text{uvw}] = \phi(\text{cohesion})/2 - \phi(\text{bisection})/2$$

Since crystallization can be seen as the replacement of mother phase by crystal, and since in equilibrium $\Delta E = T \Delta S = L$, it follows that the heat of crystallization L equals the sum of the interruption energies $\phi[\text{uvw}]$ for those PBC's which have to be bisected in order to cut a growth unit out of the crystal. The expression of Jackson now follows immediately.

From this argument it is easily seen why Jackson's recipe did not work in the example of the easily soluble salts. In those systems the main contribution to the adhesion energy will be the hydration of the crystal surface, whereas the separation energy of the mother phase is hardly influenced by the "iceberg" formation around dissolved ions. Thus complete wetting seems a too crude approximation. The same can alternatively be seen from the point of view of entropy. The total entropy change L/T during the crystallization process involves not only the disordering of the crystal particles but also the ordering of solvent particles which form the "iceberg" around the solute particles. Most of this "iceberg" is still present at the interface and hence this contribution to L/T should not be taken into account, at least not for the estimation of the $\phi[\text{uvw}]$ or the $\alpha(\text{hkl})$.

Thus, in order to be able to describe interfaces of easily soluble salts there is a need to generalize Jackson's recipe, even in cases where effects 4) and 5) are negligible. We found that this can be done simply by replacing the assumption of complete wetting by the assumption of equivalent wetting. This is defined as:

1.3 The values of the model parameters

- 1) mother phase particles adhere with the same strength to the end of an interrupted PBC, independent of whether the interruption is at the interface or at the surface of a single dissolved crystal particle.
- 2) the increase of internal entropy of a crystal particle from its value in the crystal to the value in the mother phase is proportional to the sum of the $\phi[uvw]$ of those PBC's around the particle which are already interrupted.

This assumption again enables us to relate the interface quantity ϕ to bulk quantities. Indeed, replacing a particle from its position in the crystal lattice to the mother phase PBC's are interrupted. The energy increase (sum of the $\phi[uvw]$ of the PBC's surrounding the particle) must in equilibrium be compensated by an entropy increase. Let us call this entropy increase the disordering entropy S_{dis} . Two main contributions can be distinguished. First, the configurational part, the entropy difference between particles confined to their position in the crystal lattice and the same particles which can move more or less freely in the mother phase. Second, the internal part, due to the release in the mother phase of some degrees of freedom which are frozen in the crystal. The expression

$$\alpha(hkl) = \xi(hkl) \cdot S_{dis}/k$$

is therefore the proposed generalization of Jackson's recipe.

The assumption of equivalent wetting was first applied in sects. 2.1 and 2.2, although this terminology was not used before. In these papers the chaos model was used to estimate the disordering entropy. Here the "icebergs" in the solution do not feel each other and the crystal particles have the whole unit cell at their disposal. During dissolution three rotational degrees of freedom are released and the following expression for α was obtained:

$$\alpha(hkl) = \xi(hkl) \cdot (2.5 - \ln(X_s \text{ eq}))$$

Note that the replacement of $X_s \text{ eq}$, the ratio of the particle densities in the solution and in the crystal, by a ratio of activities will not improve the estimation of α since the activity coefficients are mainly determined by the formation energy of the icebergs and this energy is already accounted for by the assumption of equivalent wetting.

Using this expression it was possible to explain the experiments of Bourne and Davey [17], who grew urotropine from different solutions. Growing from an aqueous solution they found linear growth kinetics, growing from methanol a layer growth mechanism. This behaviour has to be expected above and below the roughening temperature respectively. Indeed substitution of the solubilities in the above expression gave values which are consistent with this observation. For a more detailed description see sect. 2.1.

One might ask under which conditions Jackson's recipe and our generalized recipe lead to the same result. From the derivations it follows that this is the case when, during crystalliza-

1.3 The values of the model parameters

tion, the only entropy change of the combined crystal-mother phase system is due to ordering of the crystal particles. This is, at least to first approximation true for growth from simple melts (where $X_s \text{ eq}$ is close to unity), and for ideal solutions and perfect gas mixtures (where $X_s \text{ eq} \ll 1$). As explained above, the generalized recipe applies moreover in some cases where a strong crystal-solvent interaction is present.

It is important to stress once more the special property of both Jackson's and the generalized recipe, that they relate the inter phase quantity α to bulk quantities (ξ , L , S_{dis}). The validity of the assumptions of complete or equivalent wetting must be seen as a lucky coincidence. For each particular crystal growth situation it must be reconsidered whether such an assumption is reasonable before either of the recipes is applied.

Let us shortly discuss some effects which violate the wetting assumptions. If such an effect becomes important a new recipe has to be developed for the estimation of the $\phi[\text{uvw}]$ or the $\alpha(\text{hkl})$.

1) Surface reconstruction.

This occurs frequently on the surfaces of crystals growing from the vapour. At the surface the bisection of a PBC is partially compensated by the strengthening of some bonds parallel to the (hkl) plane. α increases and the interface free energy $f(\text{hkl})$ decreases.

2) Surface enrichment.

An important effect for metal alloys. The crystal particles near the surface are rearranged in such a way that less strong bonds and more weak bonds are broken than from the bulk structure had to be expected. Both α and f decrease.

3) Specific adsorption, of impurities or mother phase particles.

Since bisection of all PBC's is partially compensated both α and f decrease. Often adsorption acts as surface poisoning, decreasing the speed of the crystal growth process. An example of the opposite may occur in the chemical vapour deposition (CVD) of CuInS_2 , where presumably a liquid layer of CuI is formed on the (112) face, such that that the fast VLS (vapour-liquid-solid) mechanism operates there.

4) Clustering of crystal particles in the mother phase.

This may be association or complex formation in a solution, chemical compounds in a vapour phase etc, as long as they do not occur in the same form and with the same probability in the interface. Analyzing this situation in the same way as our generalized recipe was obtained, it follows that less interface energy is involved in the removal of the crystal particle from the crystal, hence less disordering entropy is necessary to compensate. Both α and f increase.

5) Partial incorporation of large molecules.

An example is the growth of polymer chains from the melt. The main contribution to the disordering entropy comes from the partial release of many degrees of freedom of a polymer molecule. If the mother phase flows, velocity gradients will reduce its entropy which causes its supersaturation. The

1.3 The values of the model parameters

internal entropy of the partially released polymer molecules will vary over the interface, such that α can not give more than rough information on the interface structure.

6) Partial discharge of adsorbed ions.

In electrochemical experiments the metal ions in the solution must ultimately be neutralized at the electrode surface. Metal ions at the surface will be in an intermediate state. Hence their interaction with water molecules will be less than for dissolved particles. Both α and f increase.

In this section we discussed two simple recipes to estimate the factors $\alpha(hkl)$ which could as well be used to estimate the interruption energies $\phi[uvw]$ of PBC's in the $[uvw]$ direction. It was shown that they apply to systems in which a special relation is valid between interface and bulk properties: the assumptions of complete or of equivalent wetting. In that case precise knowledge of the thermodynamics and the statistical mechanics of the bulk phases is sufficient to determine the interface character. If no such assumption can be made, moreover precise knowledge of the interface is necessary.

1.4 FACETING

In the preceding sections we encountered frequently the property of crystals to form facets. In this context we must distinguish the equilibrium and growth form. An appropriate method to study faceting are sphere experiments. A crystal is polished to a spherical shape and placed in an equilibrium or supersaturated mother phase. After some time facets appear, perpendicular to some $[hkl]$ directions. In general not all of them are equally large, and, continuing the experiment, some of them may disappear, as it were buried under the larger ones. Ultimately a stationary shape is reached and to this shape we refer as equilibrium or growth form respectively.

Thus there are two aspects of the phenomenon of faceting. First, the a priori possibility to form (hkl) facets, and, second, the actual occurrence of those facets on the equilibrium and growth forms. The analysis of these aspects is based on the Wulff theorem, for a simple derivation we refer to a survey paper by Toshev [18]. It is shown that the equilibrium form can be constructed, if the interface free energies of all (hkl) planar interfaces are known, as follows. Take an arbitrary point P as the origin of three dimensional space, and construct a polar plot of the interface free energy σ , i.e. cut rays in the direction $[hkl]$ at a length proportional to the free energy $\sigma(hkl)$ of the (hkl) face. Draw planes through these points, perpendicular to the rays. The inner envelope of these planes is the equilibrium form. This construction is the geometrical formulation of the solution of the following problem:

Find, for a given crystal volume and for given orientation dependence of the interface free energy the shape of the crystal with minimal total interface free energy.

The growth form can be found analogously, using the normal growth rate instead of the interface free energy. Often these polar

1.4 Faceting

plots are referred to as Wulff plot and growth plot respectively.

A priori no relation exists between the Wulff plot and the growth plot. As a matter of fact, the second depends on the particular growth mechanism. In general, however, the growth rate will decrease if α increases. As a working hypothesis Hartman [6] proposes to assume that for given temperature and supersaturation the relative growth rates of different faces are proportional to the attachment energies, although "a justification is hard to give". If the hypothesis is valid, the Wulff plot and the growth plot are directly related because $\sigma(hkl)$ is the attachment energy divided by the mesh area. Differences of the growth and the equilibrium form are then the result of different mesh areas for different orientations.

Before discussing this point in more detail we study when the Wulff or growth plot lead to facets. It has been shown by Burton, Cabrera and Frank [4] that a facet, i.e. a finite, geometrically flat region, appears with the (hkl) orientation in a sphere experiment if the Wulff or growth plot has a cusp for the $[hkl]$ ray. A cusp can be visualized as a point-bottomed dip. Analytically, the edge free energy has a singularity at the (hkl) orientation, which is such that, close to the cusp, it varies linearly with the misorientation respective to (hkl) . The question of the relation between facets and F faces can thus be reformulated as a question about the relation between F faces and cusps in the polar plots.

Consider the Wulff plot first. We have seen that the roughening transition is characterized by the vanishing of the edge free energy of monolayer steps. Take the F face whose normal \underline{n} is parallel to the vector $[hkl]$. A small misorientation \underline{dn} is obtained by the creation of parallel monolayer steps, in a direction \underline{s} perpendicular to \underline{dn} . Let \underline{dr} be a vector in the (hkl) plane which connects successive steps. Let \underline{d} define the step orientation in such a way that, at $T=0$, the stepped interface would be created by the translation of the strips between steps over the vector \underline{d} , starting with the flat F face. Note that the interplanar distance $d(hkl)$ is the inner product $\underline{d} \cdot \underline{n}$ of \underline{d} and \underline{n} . Moreover let $f(\underline{n})$ be the interface free energy of the (hkl) face, and $f(\underline{n}, \underline{s}, \underline{d})$ the edge free energy of the monolayer step. From these interface free energies we have to compute the interface free energy $f(\underline{n} + \underline{dn})$ of the misoriented face. All of these free energies are defined per unit area. Since $|\underline{d} \times \underline{s}|$ is proportional to the area of the step, $|\underline{dr} \times \underline{s}|$ of the strip between steps, and $|(\underline{d} + \underline{dr}) \times \underline{s}|$ of the misoriented face between the steps, it follows that

$$\begin{aligned} df &= f(\underline{n} + \underline{dn}) - f(\underline{n}) = \\ &= f(\underline{n}, \underline{s}, \underline{d}) \cdot |\underline{d} \times \underline{s}| / |(\underline{d} + \underline{dr}) \times \underline{s}| \end{aligned}$$

On the other hand, using that \underline{n} is the unit vector in the direction $\underline{dr} \times \underline{s}$ and $\underline{n} + \underline{dn}$ the unit vector in the direction $(\underline{d} + \underline{dr}) \times \underline{s}$ one obtains for the absolute value dn of \underline{dn} , to lowest order in $|\underline{d}|/|\underline{dr}|$,

$$dn = \{ |\underline{d} \times \underline{s}| / |\underline{dr} \times \underline{s}| \} |\sin \phi|$$

1.4 Faceting

where ϕ is the angle between \underline{n} and the unit vector perpendicular to the step edge (i.e. in the direction $\underline{d} \times \underline{s}$). Upon combining the above two equations the following relation is found

$$df = f(\underline{n}, \underline{s}, \underline{d}) \cdot |\sin \phi| \cdot dn \cdot$$

The angle ϕ is different from zero (in many cases ϕ will be an almost right angle). A cusp for a certain direction in the Wulff plot corresponds to positive changes of f for any (small) deviation from this direction. The expression we obtained thus shows that this is the case if, and only if, all edge free energies are positive. Since this is exactly the characteristic of an F face below its roughening temperature, we have established the 1-1 correspondence between facets on the equilibrium form and F faces below their roughening temperature.

Next we proceed to obtain analogous information about the growth plots. As before we restrict ourselves to dislocation free crystals. The first important thing to note is that the advance velocity of monolayer steps is roughly proportional to the supersaturation and varies smoothly with step orientation. The growth of an F face below its roughening temperature takes place by two dimensional nucleation, a mechanism which is studied in detail in sects. 4.1 and 4.2. The growth rate decreases rapidly with decreasing supersaturation: the logarithm of the growth rate is inversely proportional to the supersaturation (which is given as $\Delta\mu/(kT)$, $\Delta\mu$ being the difference in chemical potential of growth units in the mother phase and in the crystal) The proportionality constant is, apart from a numerical constant, minus the square of the edge free energy. The value of the numerical constant is usually close to 1, and is discussed by Van Leeuwen and Bennema [19]. When the F face becomes slightly misoriented, steps necessarily appear with a density proportional to the misorientation dn . These steps will at low enough values of dn and of $\Delta\mu$, hardly interact with the steps produced before by the nucleation process. The difference in growth rate between the actual and the misoriented face is thus proportional to dn which means that a cusp in the growth plot is present. Above the roughening temperature the edge free energy vanishes, a lot of steps are present on the F face itself and the introduction of some additional steps due to misorientation has negligible influence on the growth rate, such that the cusp disappears. Monte Carlo simulations which we carried out on a special purpose computer [sect. 4.1] confirmed this qualitative arguments.

It can be observed that the present reasoning leads to the same facets on growth and equilibrium sphere experiments. Their relative importance and thus their occurrence on the (final) equilibrium or growth form are not necessarily the same. It is conceivable, e.g., that on an F face with a high α factor and low interface free energy, the interface processes (surface diffusion etc.) are fast, thus leading to a large growth rate. In such a case the cusp in the Wulff plot would be deep and in the growth plot shallow, such that this facet might appear on the equilibrium form but disappear on the growth form.

The appropriate method to obtain a growth plot for per-

1.4 Faceting

fect, faceted crystals is, therefore, to take the growth rate expression for the mechanism of two dimensional nucleation.

The actual growth mechanism, however, of F faces is usually by means of growth spirals, i.e. steps emerging from a screw dislocation. Due to these spirals growth hillocks are formed on top of F faces. Consequently the exact F face orientation does not appear on real crystals. For the growth plot this means that the cusps are replaced by smooth dips in the pseudo F face orientation. The faceting of the crystals is thus less pronounced, and a direct microscopical observation may be necessary to determine the F face character of the facet. It is shown by Burton, Cabrera and Frank [4], and in a more fundamental way in sects 4.5 and 4.6 that in the spiral growth regime the growth rates are given by

$$R(hkl) = R_{WF} (\Delta\mu/\Delta\mu^*(hkl)) \tanh (\Delta\mu^*(hkl)/\Delta\mu)$$

where R_{WF} is the maximal or Wilson Frenkel growth rate and $\Delta\mu^*$ is a scaling factor for the supersaturation $\Delta\mu$. $\Delta\mu^*$ is proportional to the edge free energy and inversely proportional to the mean free path of growth units on the surface. The orientation dependent factor approaches unity for large supersaturations. In that case both the growth plot and the growth form would be spherical.

In the opposite case of small supersaturations the orientational factor is inversely proportional to $\Delta\mu^*$. In order to get a rough idea of the growth plot we might assume the following

- 1) the edge free energy is proportional to α ,
- 2) the activation energy for surface diffusion is about one fourth of the interface free energy [4],
- 3) the sum of $\alpha(hkl)$ and $f(hkl)$ is constant [sect. 1.2].

Combining these assumptions we find that the growth rate is proportional to

$$1/\Delta\mu^* \propto \{\exp(-\alpha/8)\} / \alpha$$

and it is this relation which could replace Hartmans working assumption that the growth rate is proportional to the attachment energy. The exponential part is due to the mean free path of growth units, which is proportional to the square root of the surface diffusion constant. Note that for small α values the growth rate is inversely proportional to α , for large α values an exponential fall off is obtained. Thus both the growth rate and the interface free energy decrease with decreasing α . The formula above shows that the growth rate decreases faster, in general faster than with Hartmans working hypothesis too. Therefore the growth form will be poorer (contain less facets) than the equilibrium form, even though the same a priori facets appear in a sphere experiment.

1.5 SUMMARY OF THE REPRINTED PAPERS

Since september 1974 I have worked in a laboratory in which crystal growth is studied both experimentally and theoretically. The next chapters of this thesis reflect the work done till februari 1979. The theory of crystal growth has made con-

siderable progress in the last five years. Therefore the point of view of the earliest papers would have been slightly modified if they had been written today, especially where surface roughening is involved. Nevertheless these articles still seem to have their value and are reproduced here.

It will be noted that in many papers Monte Carlo simulations play a central role. Indeed they turn out to be a most powerful tool to obtain qualitative and quantitative information about network models. In ch.2 two survey papers are given which illustrate this point. They both show how such simulations can be set up, on the basis of statistical mechanics for lattice models. The first paper (2.1) continues with the determination of the basic parameters α and $\Delta\mu$ for growth from solution (this part is developed further in sect.1.3) and concludes with a comparison with experimentally observed growth kinetics. The second paper summarizes and compares most of the Monte Carlo simulations which have been reported in the literature in 1972-1979.

Ch.3 is devoted to the theory of the roughening transition in equilibrium systems (see also 1.2). A practical method to estimate roughening temperatures for several lattices is described in 3.1. It is, however, not yet clear whether the formulation of interface localization which underlies this method, can be justified from a fundamental point of view. A step towards the discovery that the roughening transition is a textural transition was 3.2, where the edge free energy was identified with the inverse of the spin-spin correlation length in the planar XY model.

In Ch.4 kinetic results are reported. Extensive simulations carried out on a special purpose computer are reported in 4.1. The Monte Carlo data were used to study the transition from nucleation to normal growth, not only close to equilibrium, but also, below the roughening temperature at a finite $\Delta\mu$ value. In 4.2 the nucleation and growth of small clusters, just below the transition temperature, was studied. The spreading rate of small supercritical clusters was shown to deviate from the behaviour at lower temperatures. In 4.3 an example is given of the direct use of numerical methods (in this case the solution of a set of differential equations) for the interpretation of the evaporation of KCl in a molecular beam experiment. The regular structure of a two component crystal may be destroyed if the crystal is grown too fast. An example of this dynamic disordering is studied in 4.4. So far the papers used models on an atomic scale. It is of principal importance, however, for real crystal growth to study the crystal surface on a larger (say micron) scale as well. Far enough below the roughening temperature the distribution of growth units over the surface may be considered as a differentiable diffusion field in the presence of differentiable, curved boundaries (the steps). In 4.5 and 4.6 the diffusion problem for a steadily rotating growth spiral is treated in a fundamental, new way.

The adsorption of particles on a crystalline substrate is the subject of ch.5. The Monte Carlo simulation technique was used to interpret experimental situations for which network

Summary of the reprinted papers

models existed. Direct calculations were too complicated to lead to reliable results in some interesting parameter ranges. In 5.1 the film roughness in the initial adsorption stage is studied in dependence on the impingement rate, the temperature and the relative strength of the film-film and the film-substrate bonds. A deeper understanding of the difference between island and layer growth was obtained. In 5.2 the random walk of small crystallites is studied with a Monte Carlo technique which was not yet applied in the field of crystal growth. In 5.3 a misfit ratio (difference of the lattice units of film and substrate, divided by the average of the two) of the order of unity led to so-called $1/n$ adsorption. The critical behaviour of such a two dimensional system is a research object, both in experimental and in theoretical physics. The Monte Carlo simulation led to an adsorption isotherm which virtually coincides with the experimental isotherm of the electrochemical adsorption of Pb and Tl on mono crystalline Ag substrates.

REFERENCES

1. R.F. Sekerka in "Crystal growth, an introduction", (North Holland, Amsterdam, 1973)403.
2. A.A. Chernov, Sov. Phys. Cryst. 8(1963)63 and 16(1971)734, and J. Crystal Growth 24/25(1974)11.
3. J.S. Langer and H. Mueller Krumbhaar, J. Crystal Growth 42(1977)11.
4. W.K. Burton, N. Cabrera and F.C. Frank, Phil. Trans. Roy. Soc. 243(1951)299.
5. G.H. Gilmer and P. Bennema, J. Appl. Phys. 43(1972)1347.
6. P. Hartman, see [1] p. 367.
7. J.D. Weeks, G.H. Gilmer and H.J. Leamy, Phys. Rev. Lett. 31(1973)549.
8. D.E. Temkin in "Crystallization processes" (Cons. Bureau, New York, 1966)15.
9. C. van Leeuwen, Thesis (Delft, 1977)ch.3.
10. H.J. Leamy and G.H. Gilmer, J. Crystal Growth 24/25(1974)499.
11. R.H. Swendsen, Phys. Rev. B13(1977)5421. H. Mueller-Krumbhaar, T.W. Burkhardt and D.M. Kroll, J. Crystal Growth 38(1977)13.
12. H. van Beyeren, Phys. Rev. Lett. 38(1977)933.
13. H.J.F. Knops, Phys. Rev. Lett. 39(1977)766.
14. J. v. Jose, L.P. Kadanoff, S. Kirkpatrick and D.R. Nelson, Phys. Rev. B16(1977)1217.
15. R.H. Swendsen, Phys. Rev. B17(1978)3710.
16. K.A. Jackson, in "Liquid metals and solidification" (Am. Soc. for Metals, Cleveland, 1958).
17. J.R. Bourne and R.J. Davey, J. Crystal Growth 36(1976)278.
18. S. Toshev, see [1], p. 328.
19. C.van Leeuwen and P. Bennema, Surf. Sci. 51(1975)109.

CRYSTAL GROWTH FROM SOLUTION DEVELOPMENT IN COMPUTER SIMULATION

P BENNEMA and J P VAN DER EERDEN

RIM Laboratory of Solid State Chemistry Faculty of Science, Catholic University Toernooiveld, Nijmegen, The Netherlands

It is shown in this paper that progress has been made in the understanding of crystal growth mechanisms of organic crystals growing from organic solutions or aqueous solution

The main part of this paper is devoted to the statistical mechanical background of the simulations. It is shown that it follows from the same formalism from which the transition probabilities of the computer simulations are derived that (i) crystal growth from solution is an allowed interpretation of the simulations (ii) expressions for the surface energy factor α and the driving force for crystallization $\Delta\mu/kT$ can be derived for a real system

1 Introduction

In a previous survey paper presented during the ICCG 4 Conference in Tokyo, three years ago [1], it was shown that, in the subfield of crystal growth from solution (out of the whole field of crystal growth), generally applicable crystal growth models can be adapted to growth from solution. In addition, it was shown that in crystal growth from solution, a set of loosely coupled complementary crystal growth models ought to be confronted with a set of coupled crystal growth and characterization experiments

In fig 1 a scheme is presented with static and dynamic models, which are suited to be confronted with a whole set of complementary experiments [1] (See also fig 1 in ref [2]) The scheme speaks for itself and is similar to the scheme presented before [1] We only mention that morphology is defined as the subsistence of crystal growth in which the order of morphological importance of crystal faces on the crystal growth form is described from the viewpoint of the classical morphological theory [3] and the Hartman-Perdok theory [4]

In the last three years elapsed since the Tokyo Conference real progress has been made concerning (i) The interpretation of new data of measured rates of growth in dependence of the supersaturation of organic (and metal organic) crystals growing from aqueous or organic solutions with the aid of statistical, thermodynamic and computer simulation studies

on one hand and the BCF and two-dimensional nucleation models on the other hand

(ii) The role of hydrodynamics in the kinetics of crystal growth from solution concerning (a) the influence of the flow velocity on the crystal growth rate (see ref [2]), (b) the influence of the hydrodynamical regime around a crystal on the formation of fluid inclusions (see ref [2]), (c) the stability of growth forms and the formation of dendrites in relation to spiral growth and two-dimensional nucleation (iii) Preliminary interpretation with the aid of the BCF theory of new measurements of rates versus supersaturation data of slightly soluble salts

The subject (i) will be discussed briefly. The subjects (ii) and (iii) will not be discussed in this paper. We just mention that papers on the subjects (ii) (b), (ii) (c) and (iii) will be presented during this conference (see refs [5], [6] and [7] respectively), and a paper on the role of hydrodynamics will be presented elsewhere [8]

One of the most intriguing problems of the last three years was raised by Bourne and Davey [9,10]. This problem concerns the interpretation of rate versus supersaturation data of hexamethylene tetramine (HMT) crystal growing from an aqueous and an ethyl-alcohol solution. These authors found a more or less linear R (rate) versus σ (relative supersaturation) curve for growth from an aqueous solution and a BCF like curve for growth from an alcoholic solution. These results were explained with the aid of the com-

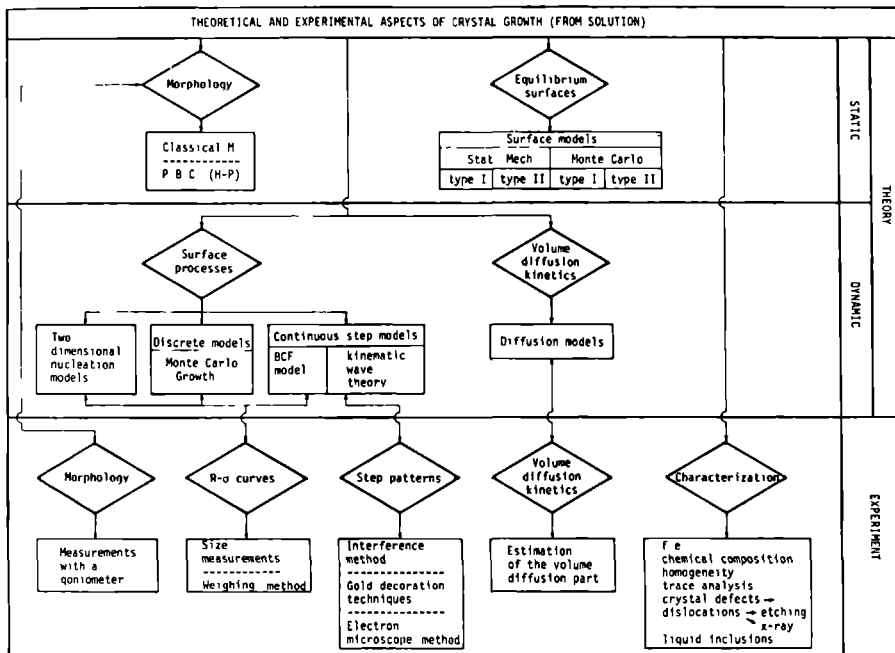


Fig. 1. Survey of crystal growth models and experimental techniques

puter simulations of the crystal growth process carried out by Gilmer and Bennema [11] (see also ref. [12] and refs. [13-18]). Since a lot of quite interesting detailed problems arise upon applying computer simulation experiments - based on cell or Ising like models - to growth from solution, the largest part of this paper will be devoted to an investigation of the statistical mechanical and thermodynamical background of the computer simulations and to their applicability to growth from solution. It will be shown in section 2 that: (i) crystal growth from solution is an allowed interpretation of the computer simulations, (ii) from the same formalism from which the creation and annihilation probabilities are derived, the proper expressions for calculating the α factor and $\Delta\mu/kT$ for a real solid solvent system can be obtained.

The structure of this paper then is as follows after the introduction in section 1, the background of the

computer simulations and the applicability to growth from solution is investigated in section 2 and interpreted kinetical data of organic crystals are reviewed briefly in section 3.

2. Statistical mechanical backgrounds of computer simulations and its implications for growth from solution

2.1. Roughening temperature

One of the most important results of recent computer simulation studies is the "discovery" and development of the concept of roughening temperature [11-22].

From the point of view of crystal growth kinetics the roughening temperature can be considered as the temperature above which continuous growth occurs

(the rate of growth being proportional to the driving force of crystallization $\Delta\mu$) and below which a layer growth mechanism occurs (the rate of growth being proportional to $(\Delta\mu)^2$ for a spiral growth mechanism or to $\exp(-C/\Delta\mu)$ for a nucleation mechanism)

The concept of a roughening temperature was treated by Burton, Cabrera and Frank [23], where they considered the interface solid-vapor as a two-dimensional phase in which – according to Onsager [24] – a phase transition occurs. This phase transition was defined as the roughening temperature. Applying the mean field approximation to the same two-dimensional phase Jackson [25] introduced a recipe to calculate the critical α factor and a criterium for the roughening temperature. This recipe was applied in a successful way to growth from the melt.

In recent years, it was found that also for a multi-layer SOS (solid on solid) interface model a kind of roughening temperature occurs. This whole problem is now being reinvestigated using both powerful theoretical methods developed by theoreticians in the field of critical phenomena and Monte Carlo simulations [19–22]. There is now very strong evidence that in a SOS interface of a Kossel crystal a roughening temperature occurs, which differs very little from the roughening temperature defined by BCF [23].

We note that the roughening temperature can be either expressed with the aid of α , which will be defined below in subsection 2.7, which is a factor characterizing the bond strength of the surface divided by the temperature or by some critical dimensionless temperature which is proportional to the temperature divided by the bond strength [27]. In a forthcoming survey paper on computer simulations [26], we will introduce this last convention and use as a unit of temperature the exact transition temperature expressed as temperature over bond strength of the two-dimensional phase [24].

2.2 Probability of a configuration in a canonical ensemble

The probability $P(\Psi_j)$ for the occurrence of an arbitrary surface configuration Ψ_j is given by

$$P(\Psi_j) = Q^{-1} \exp\left\{ \left[\sum_p \beta(-N_{pp}\phi_{pp} + N_p F_p) + \sum_{p \neq q} \left(\frac{1}{2} \beta N_{pq} \phi_{pq} \right) \right] \right\} \quad (1)$$

Here $\beta = 1/kT$, N_{pq} is the number of pq bonds where $p, q = s(\text{solid}), f(\text{fluid}),$ or $g(\text{gas})$. N_p is the number of cells. $-\phi_{ss}$ is potential energy of a solid-solid nearest neighbor interaction, $-\phi_{ff}$ is the average potential energy of interaction between the average contents of two neighboring fluid cells. For reasons which will become obvious we add a gas phase to the system on top of the fluid. The gas is assumed not to be in contact with the solid. Therefore, ϕ_{fg} bonds need not be taken into consideration. F_p is the internal free energy of a p cell, which as a consequence of the cell or Ising approximation is supposed to be equal for each of the different types of s, f and g cells and independent of the bonds. It is formally given by

$$F_p = -kT \ln \int \exp[-\beta F_p(\xi)] d^l \xi_p, \quad (2)$$

where the integration is carried out over all degrees of freedom ξ of an isolated p cell. Q is the partition function given by

$$Q = \sum_{\Psi_j} \exp\{\beta E(\Psi_j)\}, \quad (3)$$

where the summation is over all possible energies corresponding to the configurations Ψ_j , keeping the number of solid, fluid and gaseous cells constant together with the atoms and molecules within it.

We assume that each of the phases solid, fluid and gas are completely homogeneous and that within these phases all cells (and their contents) are in equilibrium with each other. We apply the concepts of equilibrium statistics and thermodynamics to these phases having in mind the possibility of absence of equilibrium between the solute and solid particles. In what follows we will use the partition function of a canonical ensemble if the number of cells and their contents remain constant. If the number of cells and particles changes, we will use the partition function of the grand canonical ensemble.

2.3 Broken bond convention

In order to simplify eq. (1) we will introduce the so-called broken bond convention. Applying this to the simple cubic Kossel crystal with only first neighbor interactions we obtain the following relation between the number of cells of type p and the num-

ber of pp and pq bonds or “contacts:”

$$3 N_p = N_{pp} + \frac{1}{2} \sum_q N_{pq}. \quad (4)$$

If there were only a one-dimensional crystal with a system of bonds in only one direction it is easily seen that, using periodic boundary conditions the factor 3 in the left hand side of eq. (4) must be replaced by unity. For three symmetrically equivalent directions of interaction the factor 3 needs to be introduced. It is easy to see that eq. (4) can be generalized for any structure, containing different growth units and different types of bonds corresponding to different pairs of interactions. Upon substituting N_{pp} , using eq. (4), into eq. (1) we obtain:

$$P(\Psi_j) = Q^{-1} \exp[-\omega N_{sf} - \beta \sum_p N_p (F_p - 3\phi_{pp})] \quad (5)$$

where

$$\omega = [\frac{1}{2}(\phi_{ss} + \phi_{ff}) - \phi_{sf}] \beta, \quad (6)$$

and again $p = s, f, g; \phi_{fg} = 0$.

2.4. Chemical potentials of cells; solids and solvent particles

The “thermodynamic potential of a p cell”, μ_p , can be formally defined by

$$\begin{aligned} \mu_p &= \left(\frac{\partial F}{\partial N_p} \right)_{V, T, N_{q \neq p}} \\ &= \frac{\partial}{\partial N_p} \left[-\frac{1}{\beta} \ln \sum_{\Psi_j} \exp -\beta E(\Psi_j) \right], \end{aligned} \quad (7)$$

where $E(\Psi_j)$ is given by the term between brackets of eq. (5). It follows from eq. (7) that

$$\mu_p = F_p - 3\phi_{pp}, \quad (8)$$

where for the time being we assume that the number of solid–fluid bonds, which mainly occur on the surface, is not influenced by N_p . We come back to this question in subsection 2.5. It can be seen from eq. (8) that “the chemical potential of a cell” is given by (i) the internal free energy of a cell and (ii) the bond energy of a p cell in the p phase ($p = s, f, g$). Substituting eq. (8) into eq. (5) gives:

$$P(\Psi_j) = Q^{-1} \exp(-\omega N_{sf} - \beta \sum_p N_p \mu_p). \quad (9)$$

In order to check the applicability of the simulations to growth from solution we change from the “thermodynamical potential of a cell” to the thermodynamical potential of atoms or molecules – to be called particles in what follows – in the solid state and particles in the fluid state – to be called solution. The solution will be considered as a binary mixture consisting of solute and solvent particles. (The limitation to one type of solvent particles is not necessary.)

It is clarifying in this connection to compare three different types of cell models, which are used in this section.

In fig. 2a the solid–fluid lattice model is presented using the solid on solid (SOS) condition, which excludes overhangs and vacancies of one phase in the other. The cells are either in a solid (black) state or a fluid (white) state. If we allow the cells of the fluid state (having the same size and shape as the solid cells) to be an average mixture of solute and solvent particles we change from a solid–fluid (or black–white) model to a what will be called “grey sea model,” where the grey sea refers to the solution. In subsection 2.8, we will again use another model, where we dissolve in a reversible way solid particles (black cells) in a saturated solution and allow the black cells to move and rotate freely in the solution. This will be called the “chaos model”.

We will assume for simplicity – this is again not a necessary condition – that there is a one to one cor-

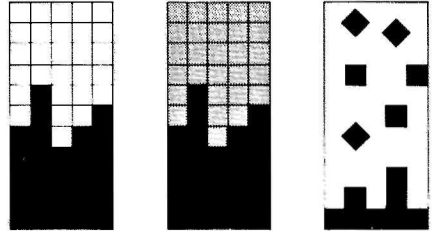


Fig. 2. (a) Solid–fluid model with energies ϕ_{ss} , ϕ_{ff} and ϕ_{sf} bonds between solid–solid, fluid–fluid and solid–fluid pairs of neighboring cells. (b) The “grey sea” model with fluid cells having the average composition of x_s solute and $1 - x_s$, solvent molecules. The “chemical potential of a cell” is given by eq. (11), the average energy between fluid cells being determined by eqs. (38) and (39). (c) The “chaos model”. The solute particles are allowed to move and rotate freely through the solution.

response between the contents of a solid cell and the solid particles, which makes

$$\mu_s(\text{cell}) = \mu_s(\text{solid particle}), \quad (10)$$

and we will not distinguish the two μ_s 's in what follows

For the solution we write using the idea of the grey sea model

$$\mu_f(\text{cell}) = x_s \mu_s^f + (1 - x_s) \mu_f^f, \quad (11)$$

where x_s is the fraction of solute particles in the solution and consequently, $(1 - x_s)$ is the fraction of solvent particles. μ_s^f is the thermodynamical potential of a solute particle and μ_f^f of a solvent particle

We write

$$\mu_s^f = \mu_{s, st}^f + kT \ln x_s \quad (11a)$$

$$\mu_f^f = \mu_{f, st}^f + kT \ln(1 - x_s), \quad (11b)$$

where the $\mu_{ps, t}^f$'s are constants defined with reference to a standard state. The expressions (11a,b) hold for ideal (dilute) solutions. For non ideal solutions activity coefficients must be introduced. Upon substituting eqs (11a,b) into eq (11) the expression for an ideal mixture is obtained. This is due to the fact that the thermodynamical potentials are assumed to be additive.

The concept of a "chemical potential of a fluid cell" consisting of fractions of μ 's from solvent and solute is somewhat artificial, which is inherent to the use of the cell concept in the fluid phase. It can be justified, however, since the "thermodynamic potential of a fluid cell" is nothing else than the free energy of a homogeneous solution with a volume V divided by N_f , the number of cells in the fluid phase (solution) (see eq (7)). The solute and solvent particles may wander freely through the solution and are not confined in a cell. This concept of freely moving particles will be used explicitly in section 2.7 when the concept of communal entropy is introduced. There the chaos model will be used.

The basic assumption behind a cell description in the grey sea model is that one may calculate the free energy, interaction energy between cells in the fluid state and the solid state etc. using the average content of the cells. That the solution is homogeneous down to cells, with dimensions of a few tens of an \AA^3 , may be justified if it is taken into consideration that the

exchange kinetics of solute and solid particles progresses much slower than the diffusion processes in the solution. So the crystal surface may only "see" homogeneous fluid cells. These fluid cells are transformed in solid cells and vice versa (see ref. [12]).

Upon substituting eq (11) into eq (9) we find

$$P(\Psi_j) = Q^{-1} \exp[N_{st} \omega - \beta N_s \mu_s - \beta x_s N_f \mu_s^f - \beta(1 - x_s) N_f \mu_f^f - \beta N_g \mu_g] \quad (12)$$

2.5 Transition probabilities

In order to show that the kinetical coefficients for creating and annihilating growth units on the surface used in the computer simulations [11,12] can be derived from the formalism, and to make the character of the driving force more explicit, we will first introduce the condition of conservation of solid and solute particles in the system under consideration. Since $x_s N_f$ is the number of solute particles in the system, the conservation condition is given by

$$N_s + x_s N_f = C, \quad (13)$$

where the constant C is the total number of solid and solute particles. Upon replacing N_f using eq (13) and substituting this in turn in the third term of the expression between brackets of eq (12), we find

$$P(\Psi_j) = Q^{-1} \exp[N_{st} \omega + \beta N_s \Delta \mu - \beta C \mu_s^f - \beta(1 - x_s) N_f \mu_f^f - \beta N_g \mu_g], \quad (14)$$

where

$$\Delta \mu = \mu_s^f - \mu_s \quad (15)$$

In order to derive the relations between transition probabilities used in the computer simulation, we will compare the probability of configuration $\Psi_j(N_s, N_f, N_g)$ with the probability of a configuration $\Psi_k(N_s + 1, N_f', N_g')$ having one more solid cell and having the corresponding different numbers of fluid and gas cells N_f' and N_g' respectively. The probabilities of these two terms are terms of the partition function of a grand canonical ensemble with varying numbers of cells and particles in the different phases. This partition function is given by

$$\Xi = \sum_{\Psi_j} \exp\{-\beta E[\Psi_j(N_s, N_f, N_g)]\} \quad (16)$$

Since we want to compare the probabilities of configurations within a grand canonical ensemble, we will replace probabilities given by eq (14) by probabilities of the same form as eq (14), but divided by Ξ instead of Q . The probability for the configuration $\Psi_k(N_s+1, N_f', N_g')$ is given by

$$P\{\Psi_k(N_s+1, N_f', N_g')\} = \Xi^{-1} \exp[-(N_{sf} + \Delta N_{sf}) \omega + \beta(N_s+1) \Delta\mu - \beta C \mu_s^f - \beta(1-x_s)(N_f - 1/x_s) \mu_f^f - \beta(N_g + v) \mu_g], \quad (17)$$

where ΔN_{sf} is the increase in the number of sf bonds as compared to N_{sf} in Ψ_j and $\Delta\mu$ is given by eq (15). In what follows we will assume that if one solid cell is formed, $1/x_s$ fluid cells are transformed into one solid cell and that $1/x_s - 1$ fluid cells are transformed into v gas cells. The reverse will also be assumed to be valid. If we assume such a transformation and in addition that the following "equilibrium" condition holds between the solvent particles and the gas cells

$$(1/x_s - 1) \mu_f^f = v \mu_g$$

Eq (17) can be rewritten giving

$$P\{\Psi_k(N_s+1, N_f - 1/x_s, N_g + v)\} = \Xi^{-1} \exp[-(N_{sf} + \Delta N_{sf}) \omega + \beta(N_s+1) \Delta\mu + \beta C \mu_s^f - \beta(1-x_s) N_f \mu_f^f - \beta N_g \mu_g] \quad (17a)$$

As a matter of fact, we assume that the crystallization or dissolution process which is simulated occurs in a crystallizer in which the thermodynamical potential of the solute particles and hence the super or undersaturation is kept constant by "evaporating" or "condensing" solvent from or into the solution from the gas reservoir (or any other reservoir).

Applying the principle of microscopic reversibility – we assume that this principle also holds for non equilibrium – we write

$$P(\Psi_k) p(\Psi_k \rightarrow \Psi_j) = P(\Psi_j) p(\Psi_j \rightarrow \Psi_k), \quad (18)$$

where $p(\Psi_k \rightarrow \Psi_j)$ and $p(\Psi_j \rightarrow \Psi_k)$ are the transition probabilities per unit time for the change from state Ψ_k to Ψ_j , and vice versa respectively $p(\Psi_j \rightarrow \Psi_k)$

is the transition probability for creating or condensing a growth unit and $p(\Psi_k \rightarrow \Psi_j)$ for annihilating or evaporating it. Substituting eq (17a) and eq (14) into eq (18) (somewhat modified for the grand canonical ensemble), we find

$$p(\Psi_j \rightarrow \Psi_k) / p(\Psi_k \rightarrow \Psi_j) = P(\Psi_k) / P(\Psi_j) = \exp(-\Delta N_{sf} \omega + \beta \Delta\mu) \quad (19)$$

We have neglected that from a theoretical point of view there is a slight difference between the chemical potential $\Delta\mu(N_s)$ of a canonical ensemble existing of N_s solid cells and the same quantity of a canonical ensemble of $N_s + 1$ solid cells. Substituting the eq (14) into eq (3) and differentiating the result with respect to N_s one gets

$$\Delta\mu(N_s) = \Delta\mu + \sum_{\Psi_j} \left(\frac{\partial N_{sf}}{\partial N_s} \right) \exp(-N_{sf} \omega) \times \left[\sum_{\Psi_j} \exp(-N_{sf} \omega) \right]^{-1} = \Delta\mu + \omega \left\langle \frac{\partial N_{sf}}{\partial N_s} \right\rangle,$$

where the expression between brackets means the average of the derivative of N_{sf} .

It is generally assumed that $\Delta\mu(N_s) = \Delta\mu$, which means that

- (i) ϕ_{sf} bonds only (or mainly) occur on the interface, this will always be the case if the SOS condition (i.e., the solid on solid condition which excludes overhangs and vacancies in solid and solution) is used
- (ii) The average number of sf bonds in the interface does not change if solid cells are added to the surface
- (iii) That the μ 's are bulk properties which are independent of the interface. This means that the number of particles, which are either in the bulk of the solution or solid are large as compared to the particles in the surface

We note that it is a consequence of the Ising like character of the simulation models that the contents of a cell are either in a solid or a fluid state. (In fact, the surface cells have a content of a solid cell or a fluid cell.) Only the bonds ϕ_{sf} determine whether the cells are in a solid or a fluid state.

2 6 Transition probabilities for Kossel like crystals

Upon using eq (19) for a Kossel crystal introducing the SOS condition where the blocks on the (001) surface have $i = 0$ to 4 or five possibilities – i refers to the number of lateral solid cells – we find

$$\Delta N_{\text{eff}} = 2(i - 2), \tag{20}$$

which gives the following mutual relations between the five creation and annihilation probabilities

$$p(\Psi_j \rightarrow \Psi_k) = k_i^+, \quad p(\Psi_k \rightarrow \Psi_j) = k_i, \\ k_i^+/k_i = \exp[2(i - 2) \omega + \beta \Delta \mu] \tag{21}$$

It can be seen that for $i = 2$ and equilibrium ($\Delta \mu = 0$) $k_2^+ = k_2$. This shows the particular property of the kink site (repeatable step, or in German Halbkristall lage), introduced in the thirties by Kossel and employed by Stranski and Kaishev, that the chances of creation and annihilation of a solid unit are equally probable. In the derivation given by Gilmer and Bennema [12], eq (21) was obtained as the result of three presuppositions

- (i) The principle of microscopic reversibility applied for equilibrium
- (ii) The special property of a kink $k_2^+ = k_2$
- (iii) In case of non equilibrium it was assumed that the chances for creation are $\exp(\Delta \mu/kT)$ higher than for annihilation

Eq (21) is now obtained as a result of (i) simple statistical mechanical arguments, (ii) the principle of microscopic reversibility which is supposed to be also valid for non equilibrium situations. This is justified because for fluctuations giving rise to local deviations for non equilibrium the principle of microscopic reversibility is also supposed to hold. Whether $\Delta \mu$ occurs due to fluctuations or is imposed by a crystal lizer does not make any difference. In case the cubic symmetry of the (001) face is reduced so that the X and Y directions are not equal we must distinguish ω_x and ω_y ,

$$\omega_x = \frac{\{1/2(\phi_{ss} + \phi_{ff}) - \phi_{sf}\}_x}{kT},$$

and the same for ω_y . We then find the following relations between the creation and annihilation coefficients

$$k_{ij}^+/k_{ij} = \exp[2(i - 1) \omega_x + 2(j - 1) \omega_y + \beta \Delta \mu], \tag{21a}$$

where i and j run from 0 to 2. Eq (21a) was used in recent computer simulations of an "orthorhombic Kossel crystal" with the aid of a special purpose computer [15].

If the SOS condition in eq (21) is abandoned, then the factor 2 must be replaced by 3 and in eq (21a) a term $2(k - 1) \omega_z$ must be added (assuming $\omega_z \neq \omega_x$ and ω_y), where again k runs from 0 to 2.

It follows from the formalism presented above that the computer simulations carried out so far for cell like or Ising like solid fluid models allow for an interpretation which corresponds to growth from solution. For a system, which consists of one type of solid particles and a binary solution consisting of solute and solvent particles the following independent parameters determine the simulations (here specified for a Kossel crystal)

$$\alpha = 4 \frac{1}{2} (\phi_{ss} + \phi_{ff}) - \phi_{sf} / kT = 4\omega/kT, \tag{22}$$

and

$$\beta^1 = \Delta \mu / kT = (\mu_s^f - \mu_{s,eq}^f) / kT \tag{15a}$$

Since it is assumed that the solid phase is in equilibrium, we may assume that the thermodynamic potential of the solute μ_s^f equals the corresponding potential of the solid μ_s . This gives eq (15a) from eq (15).

We note that the interpretation from the point of view of solution growth is certainly not the only allowed one. First of all we may consider the solution also as a flux or a vapor. Electrocrystallization from a solution is also a possible interpretation.

If we take $x_s = 1$, it can be seen from eq (11) that the fraction of solvent particles becomes zero, so that the fluid cells only contain one type of particle. The difference in fluid and solid cells can then either be interpreted as spin up, spin down or solid atoms being in phase 1 and the same (solid) atoms being in phase 2, where phase 2 may be considered as a melt or a solid. This interpretation is somewhat artificial, however, since it is difficult to see how the same particles having the same volume can belong to different phases.

2 7 Calculation of the α factor for a real solid-solution system

Equation (22) can be rewritten in the following

way

$$\alpha = \frac{2}{3}(L^1 - 6\Delta\phi_{sf})/kT \quad (23)$$

where

$$L^1 = 3\phi_{ss} - 3\phi_{ff}, \quad (24)$$

and

$$\Delta\phi_{sf} = \phi_{sf} - \phi_{ff} \quad (25)$$

Only if the condition of “complete wetting” is introduced, i e , $\phi_{sf} = \phi_{ff}$ and $\Delta\phi_{sf} = 0$ do we obtain Jackson’s α factor [27]

$$\alpha = \xi L^1/kT, \quad (22b)$$

where ξ is the surface anisotropy factor defining the number of bonds within a slice over the number of bonds in the crystal (i e , the crystallization energy in reference to vacuum) and L^1 is the “heat of dissolution” if a solid cell is transformed in a fluid cell. If the interaction between the solid cell and the fluid cell is stronger than the interaction between fluid cells the real α becomes less than Jackson’s α and in the reverse case the real α becomes higher than Jackson’s α .

The argument given above can be easily generalized to an arbitrary face (hkl) of an arbitrary structure

$$\alpha_{hkl} = \sum_r \left[\frac{1}{2}(\phi_{ss} + \phi_{ff}) - \phi_{sf} \right]_r^{\text{slice}} / kT, \quad (26)$$

where r is the distance between two pairs of cells, which characterize a set of ϕ_{ss} , ϕ_{ff} and ϕ_{sf} bonds. If, as shown before [27], we introduce the assumption that

$$\frac{F_{ss}^{\text{slice}}}{E_{ss}} = \frac{F_{ff}^{\text{slice}}}{E_{ff}} = \frac{F_{sf}^{\text{slice}}}{E_{sf}},$$

where

$$F_{pq}^{\text{slice}} = \sum_r \phi_{pq}^{\text{slice}}$$

with $p, q = s, f$, the slice energy of the face (hkl) having a thickness d_{hkl} , the interplanar distance as used in the Hartman Perdok theory [4], (see also ref [27]) and

$$E_{pq} = \sum_r \phi_{pq},$$

where the summation is now over all pairs of interaction, so that F_{pq} can be considered as the crystallization energy of the solid phase from vacuum, the crystallization energy of an ff crystal and the “crystallization energy” of a solid cell in the kink of an ff crystal (or the crystallization energy of a fluid cell in the kink of a solid crystal) respectively, we find from eq (26)

$$\alpha = \xi(L^1 - \Delta\phi^1)/kT, \quad (23a)$$

where

$$\xi = E^{\text{slice}}/E_{ss}, \quad (26)$$

$$L^1 = \sum_r (\phi_{ss} - \phi_{ff})_r, \quad (24a)$$

$$\Delta\phi^1 = \sum_r 2(\phi_{sf} - \phi_{ff})_r \quad (25a)$$

ξ and L^1 have the same significance as given above

In order to change from the heat of dissolution of cells to the heat of dissolution of solute particles we will introduce a somewhat different cell model, which was called the “chaos model” (see fig 2c). Within this model we will transform in a reversible way 1 mol of solid particles (cells) into 1 mol of solute molecules dissolved in an infinite large reservoir of saturated solution. Upon dissolving the solid particles in such a reservoir the solution itself does not change, only the bond energy and the internal free energy of the solid particles changes due to this transformation. This is the only relevant change for crystal growth from solution and the only change, which is taken into consideration in computer simulation models of the crystal growth process. We cannot simply take the heat of melt or dissolution to calculate α with the aid of eq (22b) (Among others, the heat of dissolution released when solid particles dissolve in a *saturated* solution is probably not known.) We, therefore, will try in what follows to work out a recipe to calculate a relevant “heat of dissolution” from the saturation concentration using the chaos model. This will be called L'' .

The thermodynamical potential of a solute particle in reference to vacuum ($\mu_v = 0$) is given by [28]

$$\begin{aligned} \mu_s^f &= F/N_f = -kT \ln Q_f \\ &= (-kT/N) \ln(V^N/N_f^f F_s^{fN}) - (6\phi_{sf}^f - 3\phi_{ff}^f), \quad (28) \end{aligned}$$

where V is the volume of the saturated solution, N_f the number of solute particles and F_s^f the free energy of a solute particle in a fluid "cell" having a volume

$$v_f = V/N_f, \quad (29)$$

and ϕ_{sf}^f is the potential energy of a bond of a solute particle in a saturated solution. We assume that the solute particles can freely move through the solution $-\phi_{ff}^f$ is the potential energy of a solvent-solvent pair (see also section 2.8). Since the solute particles are supposed to move very fast through the solution, they are indistinguishable, hence the factor N_f is added to eq (28). Upon applying the Stirling formula $\ln N_f! = N_f \ln N_f - N_f$ we find

$$\mu_s^f = -kT \ln \frac{v_f}{F_s^f} - kT - (6\phi_{sf}^f - 3\phi_{ff}^f) \quad (30)$$

The extra kT term is due to the communal entropy resulting from the $N_f!$ term [28]. For the thermodynamical potential of a solid particle, which is confined in one cell (since the time of making diffusion jumps within the solid is very high as compared to the times of the exchange kinetics and diffusion in the solution) we write (in reference to $\mu_v = 0$)

$$\mu_s = -kT \ln Q_s = -kT \ln \left(\frac{v_s}{F_s} \right) - 3\phi_{ss} \quad (31)$$

Here no communal entropy term occurs since the particles within the solid are distinguishable. v_s is the volume of a solid cell and F_s the internal free energy of a solid cell.

For equilibrium $\mu_s^f = \mu_s$, so that

$$L'' = 3\phi_{ss} + 3\phi_{ff}^f - 6\phi_{sf}^f \\ = -kT \ln(v_s/v_f) - kT \ln(F_s^f/F_s) + kT \quad (32)$$

$1/v_f$ and $1/v_s$ represent the number of solute and solid particles per unit volume in the solution phase and the solid phase N_s and N_s respectively. We then can write

$$v_s/v_f = N_s^f/N_s = N_s^f v_s / N_s v_s = x_{s,eq}, \quad (33)$$

where $N_s^f v_s$ is the part of the unit volume ($= N_s v_s = 1$) of fluid occupied by solute particles, assuming that the "molecular volumes" of solute and solvent particles, equal v_s . This makes x_s of eq (33) equivalent to eqs (11) and (38) (section 2.8).

If we use the picture of one solid or solvent particle in an infinite deep square potential well it follows from statistical mechanics that

$$F_s^f = F_s = h^3 / (2\pi m k T)^{3/2}, \quad (34)$$

which means that the second hand term of eq (32) is zero (m is the mass of the particle, h Planck's constant). For simple molecules, we may assume that the vibrational entropy for solvent and solute are equal. Also the entropies due to the movement of the center of gravity (see eq (34)) may be equal (except for the volumes v_f and v_s which are taken care of in eq (32)). However, the molecules in the solution may more or less rotate freely as compared to the molecules in the crystal. In that case F_s/F_s^f equals

$$F_s/F_s^f = (\pi^{1/2} e^{3/2} / \sigma') (T^3 / \theta_A \theta_B \theta_C)^{1/2}, \quad (35)$$

where $\theta_{A,B,C}$ are characteristic temperatures for rotation corresponding to three moments of inertia, of the molecule, σ' is a symmetry number close to unity. Assuming that $T \approx \theta_A \approx \theta_B \approx \theta_C$, $\pi^{1/2} / \sigma' \approx 1$ we then find $\ln F_s/F_s^f \approx 3/2$ (e is the base of the natural logarithm). We assumed that the solute molecules move freely in the solution, which also may not be true. On the other hand, $\theta_{A,B,C}$ may be (much) smaller than the temperature of the solution T .

With so many uncertainties it is necessary to study the thermodynamics of each solution in more detail, but for the time being we will write for eq (32) using eq (33) and considering eqs (34), (35)

$$L'' = kT(-\ln x_{s,eq} + \Delta f_{fs}), \quad (36)$$

where

$$1 < \Delta f_{fs} < 2.5 \quad (37)$$

is due to the difference in internal free energies of solute and solid particles. For a saturated solution $x_{s,eq}$ and Δf_{fs} can in principle be determined experimentally.

2.8 Comparison of heat of dissolution of chaos model and solid fluid model

Since we presuppose a solution which can be partitioned in (cubic) blocks with a fraction of x_s solute and $(1 - x_s)$ solvent particles the bond energies ϕ_{ff} between neighboring fluid cells can be written as a

consequence of the grey sea model (fig 2b, subsection 2.4) using a mean field approximation

$$\phi_{ff}(\text{cells}) = x_s^2 \phi_{ss}^f + 2x_s(1 - x_s) \phi_{sf}^f + (1 - x_s)^2 \phi_{ff}^f, \quad (38)$$

$\phi_{ss}^f (= \phi_{ss})$ is the average interaction energy of two solute particles (in neighboring cells) and ϕ_{sf}^f and ϕ_{ff}^f the corresponding solute-solvent and solvent-solvent interaction energies

Using the same considerations we find directly for the ϕ_{sf} bonds between cells

$$\phi_{sf} = x_s \phi_{ss}^f + (1 - x_s) \phi_{sf}^f \quad (39)$$

Upon substituting these values in the value of α given by eq (22) we find for the (001) face of a Kossel crystal

$$\alpha = (1 - x_{s \text{ eq}})^2 \alpha^f, \quad (40)$$

where α^f is given by

$$\alpha^f = 4 \left(\frac{1}{2} \phi_{ss}^f + \frac{1}{2} \phi_{sf}^f - \phi_{sf}^f \right), \quad (41)$$

which can be rewritten as

$$\alpha^f = (2/3) L''/kT \quad (42)$$

Upon substituting for L'' the expression given by eq (36) we find

$$\alpha = \xi (1 - x_{s \text{ eq}})^2 (-\ln x_{s \text{ eq}} + \Delta f_{sf}), \quad (23b)$$

where for the (001) face of a Kossel crystal

$$\xi = 2/3$$

It follows from eq (23b) and the presuppositions of average bonds between a solid and fluid and fluid and fluid cells, which are expressed in bonds between solute and solvent particles that in the α factor a "heat of dissolution" L'' for the transformation of solid particle in a solute particle in a saturated solution can be used provided a correction for the concentration is used. Eq (23b) gives the relation between α - used in the computer simulations - and the solubility $x_{s \text{ eq}}$ and ξ

It is interesting to note that eq (23b) has the implication the lower the saturation concentration the higher α . It is very worthwhile to check in future research the validity of eq (23b) (Sometimes it seems to hold [9,10])

2.9 Interpretation of supersaturation

Since the chemical potential μ_s^f can be given by

$$\mu_s^f = \mu_{s \text{ st}}^f + kT \ln \gamma x_s, \quad (43)$$

where $\mu_{s \text{ st}}^f$ refers to a standard state and γ is an activity coefficient (due to the mutual interaction of solute particles). We have chosen here for the concentration x_s the fraction of solute molecules or the molar fraction $\mu_{s \text{ st}}^f$ and γ have values, which correspond to this particular choice. The concentration can be expressed in different units, but then γ and $\mu_{s \text{ st}}^f$ must be adjusted to this choice of the units.

Upon substituting eq (43) into eq (15a) we obtain

$$\Delta\mu/kT = \ln[\gamma x_s / (\gamma x_s)_{\text{eq}}] \quad (15b)$$

If we assume (i) $\gamma \approx \gamma_{\text{eq}}$ and (ii) the supersaturation is small, we find by writing $x_s = x_{s \text{ eq}} + \Delta x_s$ and $\sigma = \Delta x_s / x_{\text{eq}}$, where σ is the relative supersaturation

$$\Delta\mu/kT \approx \sigma, \quad (15c)$$

It follows from this section that the most general expression for the driving force for crystallization is given by eq (15b). This means that in principle the activity coefficients must be known by measuring and/or calculating them for super- or under-saturated solutions. In most cases γ values are not available from literature. For dilute solutions γ is close to unity and condition (i) may be fulfilled.

It follows from this section that only if conditions (i) and (ii) are fulfilled the driving force for crystallization becomes equal to the relative supersaturation σ . In experiments for growth from solution, this quantity is usually chosen as the driving force for crystallization.

Upon comparing driving forces reported by different authors in the literature one must check how the concentrations are expressed, because different ways of expressing concentrations may lead to different values of σ . This is demonstrated by Mullin, in his book on industrial crystallization, who showed that for the same supersaturated aqueous solution of sucrose (characterized by the same $\Delta\mu/kT$), σ varied from 8 to 18%, depending on how the concentration was expressed [29].

3 Growth kinetics of organic crystals

3.1 Growth of HMT/hexamethylenetetramine from aqueous and alcoholic solution, calculation of α

As mentioned in the introduction and in section 2.1, Bourne and Davey [9,10] found linear growth kinetics for growth from an aqueous and a BCF like growth law for growth from an alcoholic solution. The authors tried three different ways to calculate α (i) Using eq (26) (subsection 2.7), taking $\Delta\phi_{sf}' = 0$ and for $\xi = 1/2$ which corresponds to the (110) face of the HMT body centered structure (instead of $\xi = 2/3$ for a Kossel crystal) B and D found that the recipe eq (22b) failed for the aqueous solution because L is reported to be negative. For an alcohol solution, however, B and D found

$$\alpha_{alc} = 3.2$$

Since the roughening temperature occurs at $\alpha \approx 2.95$, it is suggested that for alcohol the surface "temperature" is close to the roughening temperature [30]

(ii) From thermodynamic data by adding the entropies of fusion, and mixing. We believe that this calculation is incorrect, the obtained values of $\alpha = 0.9$ for an aqueous and $\alpha = 5.4$ for an alcoholic solution probably have no meaning

(iii) From the surface free energy by correlating the "real" heat of dissolution L with the measured surface free energy (obtained from nucleation data) using the expression

$$F = L/2a^2b,$$

where a^2 is the surface area and b is defined in the following way, using the concepts of the Hartman-Perdok theory [4]

$$\xi = F_{ss}/E^{slie}$$

Recalling, that

$$f^{att} + f^{slie} = F_{ss},$$

we find $b = 3$ for a (001) face of a Kossel crystal and $b = 2$ for the (011) face of a bcc crystal. Using measured data for an aqueous solution and data reported

in the literature for F the following α values were obtained

$$\alpha_{aq} = 0.1, \quad \alpha_{alc} = 5.2$$

(iv) In this connection it is interesting to try the recipe given by eq (23b) assuming $\Delta f_{sf} = 2$. Using $x_s = 0.100$ for an aqueous solution and $x_s = 0.0110$ for an alcoholic solution we then find

$$\alpha_{aq} = 0.35, \quad \alpha_{alc} = 2.84,$$

If we take $\Delta f_{sf} = 2.5$ we find

$$\alpha_{aq} = 0.65, \quad \alpha_{alc} = 3.08$$

With so many uncertainties in the calculations it is suggested that for an aqueous solution due to the strong interaction between the HMT molecules and water, which also makes $x_{s,eq}$ high - α is much lower than α for an alcoholic solution and that in the first case growth takes place above and in the second case slightly below the roughening temperatures. This seems to be consistent with the linear and non-linear growth kinetics.

One intriguing problem, however, remains unsolved. It is to be expected that if a crystal face grows far enough above the roughening temperature, it will grow without facets. It is a well known fact, however, that the HMT crystals grow as beautiful rhombododecahedra from an aqueous solution. It follows from the computer simulations [10-16] that even above the roughening temperature the maximal linear Wilson-Frenkel law is not reached (This depends also on the surface diffusion). If the "temperature" is slightly above the roughening temperature (or α slightly lower than 2.95) a certain anisotropy obviously occurs and the crystal obviously does not grow like a sphere. This anisotropy does not imply, however, that no visible roughening should occur. It is interesting to note in this connection that Bourne and Davey found a different type of layer growth for growth from an aqueous solution as compared to growth from an alcoholic solution [31]. Crystals growing from an alcoholic solution developed better glittering faces and showed much less tendency for the formation of solvent inclusions. In future long runs on a large special purpose computer will be car-

ried out to investigate growth and dissolution above and below the roughening temperature in order to investigate this problem (work in progress).

We note that the obtained (R, σ) curves were carefully interpreted by B and D with the whole body of available growth models, after correcting for volume diffusion. The authors arrived at the conclusion that the maximal W-F law is not reached for water and that for growth from an alcoholic solution a coupled volume and BCF surface diffusion process occurs as described by the theory of Gilmer, Ghez and Cabrera [32] (see also refs. [33] and [34]). This is the first example of such a coupled process reported in the literature.

3.2. Growth of paraffin crystals growing from organic solutions

In the last years very important work has been carried out concerning the growth kinetics of paraffin crystals growing from organic solutions by scientists of the "Laboratoire des Mécanismes de Croissance Cristalline" in Marseille-Aix headed by Professor Kern, Drs Boistelle, Simon, Aquillano, Grassi, Dousoulin, Madsen and others [35-39].

The following remarks can be made:

(i) Grey sea and/or chaos models of the ideal solute-solvent solutions are applied (see subsection 2.4) with great success. ϕ_{ff}^* and ϕ_{bb}^* bonds of "orthorhombic cells" are equal. Calculations carried out by B and D of $C_{36}H_{74}$ paraffins show that the α values are very high ($\alpha \approx 30$). This also follows from calculations using eq. (41) in subsection 2.8.

(ii) Simon et al. [35,36] and Grassi [37] found for slow moving side faces of $C_{36}H_{74}$ paraffin crystals that the (R, σ) curves could be described in a satisfactory way with the aid of the two-dimensional birth and spread model. The calculated edge free energies were in good agreement with the energy obtained from the experimental growth rate versus supersaturation measurements.

(iii) Boistelle et al. [38] and Doussoulin [39] found for the fast growing side faces of $C_{28}H_{58}$ paraffin crystals a parabolic law $R = C\sigma^2$. As a result of an extensive and complete analysis where the chaos model (without rotation) was employed together with a consideration of all possible growth mechanisms the authors arrived at the conclusion that a BCF mech-

anism in which surface diffusion plays a certain role gave a consistent interpretation of the measured (R, σ) curves and all other available thermodynamic data. (iv) Recently the kinetics of the top face (001) on which spirals were observed and which grow with a parabolic BCF law was investigated, together with the formation of double layers and twinning [39].

It would be quite interesting to compare the results of recent computer simulations of anisotropic crystals [15,16] with the experimental data of the Marseille group.

3.3. Growth of metal organic crystals

At the end of this section we want to mention that recently extensive research has been carried out on $(C_2H_5(NH_3)_2)CuCl_4$ and isomorphous compounds concerning [40].

(i) The rate of growth in dependence of the supersaturation of the side faces of these crystals. It was found that side faces either grow very fast with, what may be considered as a second linear BCF law [27], or much slower with a BCF like law, with a large influence of volume diffusion.

(ii) The occurrence of kinematic waves on the (001) faces and other surface phenomena among others with a laser interference microscope.

(iii) The interpretation of the morphology with the aid of the Hartman-Perdok theory [41].

(iv) The crystal perfection, with the aid of among others Lang topography.

4. Conclusion

A few examples were given, which show that in the last three years since ICCG-4 real progress has been made in understanding crystal growth mechanisms for growth from solution of organic crystals.

It was shown that computer simulations allow for an interpretation for growth from solution and that α and $\Delta\mu/kT$ can be derived from the formalism which determine the rules of the simulation.

Acknowledgements

We want to thank Dr. R. Janssen-van Rosmalen for her help to make fig. 1 and Dr. G.H. Gilmer for dis-

Discussing the subject of section 2 and critical reading of the manuscript. We also want to thank Dr. A.A. Chernov for his critical reading of the manuscript.

References

- [1] P. Bennema, *J. Crystal Growth* 24/25 (1974) 76
- [2] R. Janssen van Rosmalen, Thesis, Technical University Delft (1977)
- [3] I.C. Philips, *An Introduction to Crystallography* (Wiley, New York) Ch. XIII
- [4] P. Hartman, in *Crystal Growth: An Introduction*, Ed. P. Hartman (North Holland, Amsterdam, 1973) p. 367
- [5] R. Janssen van Rosmalen and P. Bennema, *J. Crystal Growth* 42 (1977) 224
- [6] T. Kuroda, T. Iwasawa and A. Ookawa, *J. Crystal Growth* 42 (1977) 41
- [7] P. Bennema, G. Brouwer and G.M. van Rosmalen, presented at ICCG 5
- [8] R. Janssen van Rosmalen and P. Bennema, presented at Manchester, 1977
- [9] J.R. Bourne and R.J. Davey, *J. Crystal Growth* 36 (1976) 278
- [10] J.R. Bourne and R.J. Davey, *J. Crystal Growth* 36 (1976) 287
- [11] G.M. Gilmer and P. Bennema, *J. Crystal Growth* 13/14 (1972)
- [12] G.M. Gilmer and P. Bennema, *J. Appl. Phys.* 43 (1972) 1347
- [13] S.W.H. de Haan, V.J.A. Mecussen, B.P. Th. Veltman, P. Bennema, C. van Leeuwen and G.H. Gilmer, *J. Crystal Growth* 24/25 (1974) 491
- [14] G.H. Gilmer, *J. Crystal Growth* 35 (1976) 15
- [15] J.P. van der Eerden, C. van Leeuwen, P. Bennema, W.L. van der Kruk and B.P. Th. Veltman, *J. Appl. Phys.* 48 (1977) 2124
- [16] C. van Leeuwen, Thesis, Technical University, Delft (1977)
- [17] G.H. Gilmer and K.A. Jackson, in *Crystal Growth and Materials*, Eds. F. Kaldis and H.J. Scheel (North-Holland, Amsterdam, 1977) p. 79
- [18] G.H. Gilmer, *J. Crystal Growth* 42 (1977) 000
- [19] H.J. Leamy, G.H. Gilmer and K.A. Jackson, in *Surface Physics of Materials*, Ed. J.M. Blakeley (Academic Press, New York, 1975) p. 121
- [20] H. Müller-Krumhhaar, in *Crystal Growth and Materials*, Eds. F. Kaldis and H.J. Scheel (North-Holland, Amsterdam, 1977) p. 115
- [21] R.H. Swendsen, *Phys. Rev. B* 15 (1977) 5421
- [22] H.J. Leamy and G.H. Gilmer, *J. Crystal Growth* 24/25 (1974) 499
- [23] W.K. Burton, N. Cabrera and I.C. Frank, *Phil. Mag.* 243 (1951) 299
- [24] L. Onsager, *Phys. Rev.* 65 (1944)
- [25] K.A. Jackson, in *Liquid Metals and Solidification* (ASM, 1958) p. 174
- [26] J.P. van der Eerden, P. Bennema and T.A. Cherepanova, in *Progress in Crystal Growth and Assessment* (Pergamon, Oxford, 1977)
- [27] P. Bennema and G.H. Gilmer, in *Crystal Growth, An Introduction*, Ed. P. Hartman (North-Holland, Amsterdam, 1973) p. 282
- [28] T.H. Hill, *An Introduction to Statistical Thermodynamics* (Addison-Wesley, 1962) ch. 9, 16
- [29] J.W. Mullin, *Crystallization*, 2nd ed. (Butterworths, London, 1972)
- [30] J.P. van der Eerden, *Phys. Rev. B* 13 (1976) 4942
- [31] J.R. Bourne and R.J. Davey, *J. Crystal Growth* 39 (1977) 267
- [32] G.H. Gilmer, R. Ghez and N. Cabrera, *J. Crystal Growth* 8 (1971) 79
- [33] R. Janssen van Rosmalen, P. Bennema and J. Garside, *J. Crystal Growth* 29 (1975) 342
- [34] J. Garside, R. Janssen van Rosmalen and P. Bennema, *J. Crystal Growth* 29 (1975) 353
- [35] B. Simon, A.G. Grassi and R. Boistelle, *J. Crystal Growth* 26 (1974) 77
- [36] B. Simon, A.G. Grassi and R. Boistelle, *J. Crystal Growth* 26 (1974) 90
- [37] A.G. Grassi, Thesis, University of Marseille-Aix (1974)
- [38] R. Boistelle and A. Doussoulin, *J. Crystal Growth* 33 (1976) 335
- [39] A. Doussoulin, Thesis, University of Marseille-Aix (1975)
- [40] I.H. Mischgofsky, Thesis, Technical University of Delft (1977)
- [41] H.J. Human, P. Bennema, I.H. Mischgofsky and C. Woensdrecht, to be published

SURVEY OF MONTE CARLO SIMULATIONS OF CRYSTAL SURFACES AND CRYSTAL GROWTH

J. P. van der Eerden and P. Bennema

RIM Laboratory of Solid State Chemistry, Faculty of Science, Catholic University,

Toernooiveld, Nijmegen, The Netherland

and

T. A. Cherepanova

Computing Centre Latvian State University, Boulevard Raina 29, Riga USSR

During the Summerschool in Erice one of us (P.B.) presented a series of five lectures in which a survey of crystal growth theories and a comparison with experiments was given.

In this chapter we only will give an updated survey on computer simulations, which are relevant for crystal growth since surveys on the other subjects are published elsewhere.

Thanks to an exchange program between the Soviet Union and the Netherlands Mrs. Dr. T. A. Cherepanova spent a year in Delft, which enabled us to present this joint survey paper.

LIST OF FREQUENTLY USED SYMBOLS

$A(\theta, X_g)$	probability that a particle reaches an active site on the surface,
$A_{st}(\theta, X_g)$	probability that a particle reaches an active site on a step,
$A_o(\theta)$	= $A(\theta, 0)$ density of active sites,
α	as subscript: refers to a type of particle,
β	= $1/kT$ (k Boltzmann's constant, T absolute temperature),
ch	subscript, referring to the chaos model (Section 10),
γ_o	specific edge free energy of a nucleus,
E	interaction energy (enthalpy) of the system, see eq.(5),
E_{bb}	broken bond energy (enthalpy) see eq. (8),
G, G^p	free enthalpy of the system, of a p -cell,
ϕ_r^{pq}	potential energy of a p - and q - cell which are r apart,

$\phi_{\vec{r}}^{PQ}$	$= \phi_{\vec{r}}^{PQ} - \frac{1}{2}\phi_{\vec{r}}^{PP} - \frac{1}{2}\phi_{\vec{r}}^{QQ}$, generalized interaction energy,
f^s	superscript, referring to a fluid cell,
H	Hamiltonian (in Section 2), or enthalpy (elsewhere),
I	normalized nucleation rate,
k^+, k^-	attachment and detachment frequencies for single cells,
L	surface enthalpy of an isolated solid cell, see eq. (26) and Section 10,
L_J	heat of melting, evaporation or dissolution, see eqs. (46) and (47),
LP	lattice enthalpy of a pure P -phase, see eq. (9),
μ^P, μ_{eq}^P	actual and equilibrium chemical potential of a P -cell,
n^P	number of P -cells in the system,
$n_{\vec{r}}^{PQ}$	number of P - and Q -cells which are \vec{r} apart,
$P(\Psi)$	probability of a state Ψ ,
$F(\Psi \rightarrow \Psi')$	transition frequency from Ψ to Ψ' ,
P, q	as a superscript, running parameters for the type of a cell,
R	growth rate, as a subscript it refers to the roughening transition,
R_n	n -th pseudo-random number, $R_n \in (0, 1)$,
\vec{r}	vector of the crystal lattice with positive coordinates,
r^σ	interface roughness,
s	superscript, referring to a solid cell,
σ	relative supersaturation, as a superscript it refers to the interface,
θ	dimensionless temperature, see eq. (26),
v	velocity of a monatomic surface step,
χ_s	mean surface diffusion distance,
	ratio of lateral to total binding energy of a crystal cell, see Section 10
Ψ	state of the system, configuration of cells.

1 INTRODUCTION

In this survey we give a survey of the role of Monte Carlo (MC) simulations in the science of crystal growth. Characteristic for MC simulation is its stochastic nature: random numbers will determine whether and how a system changes its state. This should be done according to transition probabilities which are determined from a model of the physical system of interest. Fluctuations are automatically included, in contrast to most other theories which are deterministic and give, therefore, only the average time development.

As MC simulations are now a tool which is used in a wide variety of fields, ranging from mathematics ("experimental mathematics") to industrial management, we shall restrict ourselves with respect to the systems which we want to discuss

Firstly we assume that the changes in the system (e.g. particles attaching to the crystal) take place so fast that intermediate states can be neglected. Therefore we restrict ourselves to discrete simulation, i.e. simulation of a system with a discrete set of states.

Secondly we intend to describe crystals, growing from some surrounding phase which

may be fluid or gaseous. This allows us to define a lattice with the crystal symmetry, whose cells are either solid or belong to the ambient phase. We shall not go into detail concerning the ambient phase. We assume that it is homogeneous and that the concept of the chemical potential of a particle which is going to join the crystal can be used.

The aim of simulation is to describe the time development of a system when the probabilities of some "elementary events" are known. In our case three types of elementary events come into consideration: addition (also called attachment, condensation or creation), subtraction (detachment, evaporation, dissolution or annihilation) and migration (diffusion) of single solid cells.

Discrete Monte Carlo simulation has a number of different aspects and can therefore be used for several purposes

- (i) It can be seen as an ideal experiment with a simple, perfectly known system. Several effects can be studied independently, e.g. nucleation, growth spirals, surface diffusion, temperature, crystal structure etc.
- (ii) It solves the master equation of the system (which governs its time evolution), numerically. Usually both high and low temperature approximations fail close to transition temperatures, such that MC simulations may be the only possibility which is left
- (iii) In addition to (ii) it can be used to show that the results of analytical theories are often applicable, even when their presuppositions are already valid. Their domain of validity is, in such a way, checked and even extended
- (iv) Simulation of a concrete physical experiment may give a better insight to the relevant atomic processes and may stimulate further experimental investigations and the development of new ideas and models.
- (v) Observation of a fluctuating system may reveal unexpected effects which may have general implications. The no man's land between theory and experiment can be reduced.

On the other hand there are some limitations

- (i) Simulations do not give insight by themselves and are therefore useful only if they are accompanied by thorough interpretations.
- (ii) Because long computational times are invariably necessary, it is impossible to study complicated systems (e.g. large X_S or low T) long. Even a special purpose computer (a hardware model, constructed for crystal growth simulations only) can only partly overcome this difficulty.

The organisation of this survey will be as follows. In Section 2 we give a statistical mechanical description of the system which will lead to expressions for the energy and the chemical potentials of the different particles. With the help of the principle of microscopic reversibility, relations between transition probabilities are derived. Complete understanding of this is not strictly necessary for reading the rest of the chapter. Section 3 contains a survey of the simulations which will be discussed and the definition of a standard temperature θ , which will be used to compare different systems. In Sections 4-7 we discuss equilibrium aspects and different growth mechanisms, Section 8 concentrates upon film growth on a substrate, and Section 9 deals with two-component crystals. Discussion of results, implications for experiments and open questions are briefly commented on in Section 10. Definitions of frequently occurring symbols and quantities are given above.

2 ELEMENTARY TRANSITION PROBABILITIES

In this section we develop a generalized lattice gas model which can be used to describe a system containing a crystal phase and a completely homogeneous fluid phase. The lattice is defined by the symmetry of the crystal. It may contain solid cells of

different types, containing one or more particles each, as shown in Fig. 1. The fluid phase can be interpreted as melt, solution or vapor, in which gradients in temperature, density etc. can be neglected. In this section we will use the terminology of growth from the solution. When we discuss, however, the work of other authors we shall use their interpretation.

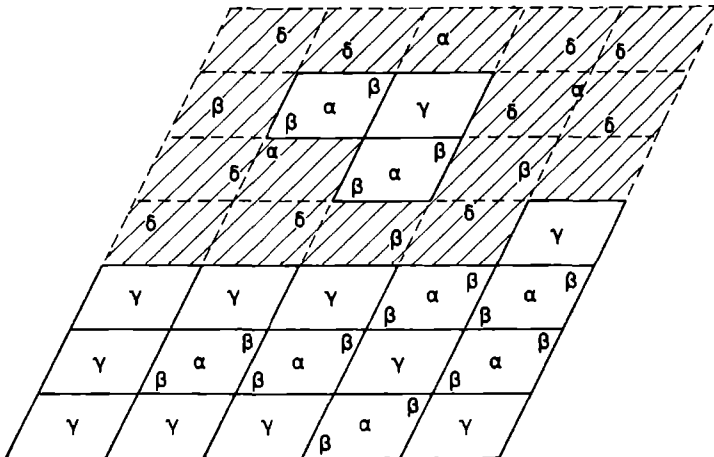


Fig. 1. Example of an interface: two types of solid cells, containing α , β and γ particles, the fluid cells also contain δ particles.

In Section 1 we noted that we consider here discrete simulations. This means that, at each moment, the system is completely described by the distribution Ψ of solid and fluid cells over the lattice which we imagine to be extended to the fluid phase as well. We are interested in the time evolution of the system as a whole. The Monte Carlo simulations are a way of studying this evolution. The elementary transition probabilities $p(\Psi \rightarrow \Psi')$ that the system changes its configuration from Ψ to Ψ' in a certain time interval τ are chosen in such a way that at most one (for condensation and dissolution) or two (surface diffusion) cells change their type.

We shall derive the elementary transition probabilities $p(\Psi \rightarrow \Psi')$ from the equilibrium probability $P(\Psi)$ using the principle of microscopic reversibility. The use of these $p(\Psi \rightarrow \Psi')$ for non equilibrium as well, is justified by the regression axiom of Onsager (1,2) which states that the way in which the system goes to its equilibrium state is independent of how the actual state is reached. For our case this means that the system will behave the same under the influence of a non equilibrium chemical potential, whether it is caused by spontaneous fluctuations around equilibrium, or by external influences.

For $P(\Psi)$ we shall use the Boltzmann distribution (3). If H is the Hamiltonian of the system then $H(\Psi(\xi))$ is the energy if Ψ is the configuration of cells and $\{\xi\}$

denotes the other degrees of freedom (impulses and relative coordinates of the particles belonging to each cell). The following expression then holds for P .

$$P(\Psi) \sim \int d\{\xi\} \exp - \beta [H(\Psi, \{\xi\}) - \sum_p \mu_{eq}^p N^p(\Psi)], \quad (1)$$

where the integration is over all $\{\xi\}$ which are compatible with Ψ , and the summation is over all types of cells. The probability distribution P will be normalizable only for finite systems. We shall not worry about finiteness in this section, but simply assume that we have a finite system which is so large that we can regard it as if the thermodynamic limit has been reached. The free enthalpy of the system is then, at a pressure P_0 ,

$$G(P_0, T, \{N^p\}) = -kT \ln \sum_{\Psi} \{N^p\} P(\Psi) \exp - \beta \mu_{eq}^p N^p(\Psi), \quad (2)$$

where the summation is over Ψ with N^p p -cells.

We assume moreover that $H(\Psi, \{\xi\})$ can be written as the sum of interactions $E(\Psi)$ between the cells and internal parts $H_i(\{\xi\})$ for each cell i separately. In that case we can define the internal free enthalpy G^p of a p -cell by

$$G^p = -kT \ln \int_p d\{\xi\} \exp - \beta H_i(\{\xi\})_p \quad (3)$$

where the integration is over all degrees of freedom of an isolated p -cell and the integrand is the factor of eq. (1) which refers to a given p -cell. Upon inserting eq. (3) in eq. (1) we find:

$$P(\Psi) \sim \exp - \beta [E(\Psi) + \sum_p N^p(\Psi) (G^p - \mu_{eq}^p)] . \quad (4)$$

The interaction energy E is given by contributions $\phi_{\vec{r}}^{pq}$ which depend on the types of cells in a pair and on their relative positions:

$$E(\Psi) = \frac{1}{2} \sum_{p \neq q} \sum_{\vec{r}} \phi_{\vec{r}}^{pq} N_{\vec{r}}^{pq}(\Psi) + \sum_p \sum_{\vec{r}} \phi_{\vec{r}}^{pp} N_{\vec{r}}^{pp}(\Psi) , \quad (5)$$

where the summations are over all types of cells and over all \vec{r} . In this expression we can easily take into account that the $N_{\vec{r}}^{pq}$ are not independent: if at a position \vec{r}_1 a p -cell is present then at $\vec{r}_1 + \vec{r}$ a cell is present which is either again of type p or of a different type q . Therefore:

$$N_{\vec{r}}^p = N_{\vec{r}}^{pp} + \frac{1}{2} \sum_{q \neq p} N_{\vec{r}}^{pq}, \text{ for all } p, \vec{r} . \quad (6)$$

Equation (6) can be used to eliminate the $N_{\vec{r}}^{pp}$ from eq. (5) and we find:

$$E = E_{bb} + \sum_p N_{\vec{r}}^p L_{\vec{r}}^p . \quad (7)$$

Here E_{bb} is the so-called broken bond energy, as it involves only interactions between different cells:

$$E_{bb} = \frac{1}{2} \sum_{p \neq q} \sum_{\vec{r}} (\phi_{\vec{r}}^{pq} - \frac{1}{2} \phi_{\vec{r}}^{pp} - \frac{1}{2} \phi_{\vec{r}}^{qq}) N_{\vec{r}}^{pq} \equiv \frac{1}{2} \sum_{p \neq q} \sum_{\vec{r}} \phi_{\vec{r}}^{pq} N_{\vec{r}}^{pq} \quad (8)$$

and $L_{\vec{r}}^p$ is the lattice enthalpy of a pure phase, containing only p -cells:

$$L_{\vec{r}}^p = \sum_{\vec{r}} \phi_{\vec{r}}^{pp} . \quad (9)$$

Expression (7) can also be interpreted as follows. The second term is the energy of the system if all cells are combined in pure p -phases and the first term gives a

correction $\sum_{\vec{r}, \vec{r}'} \Delta \psi^{pq}$ for each exchange of cells between the p - and q -phase which is necessary to reach the actual configuration Ψ . It may be instructive to see that for a simple cubic, one-component crystal with nearest neighbour interactions only, eq (7) reduces to

$$E = \phi N^S f + 3N^S \phi^{SS} + 3N^f \phi^{ff}, \quad \phi = \phi^{Sf} - \frac{1}{2} \phi^{SS} - \frac{1}{2} \phi^{ff}. \quad (10)$$

The next step to simplify eq. (4) is to make the role of the chemical potential, and therewith the role of the supersaturation, more explicit. By definition the chemical potential of a p -cell is

$$\mu^p \equiv \partial G / \partial N^p = \langle \partial H / \partial N^p \rangle. \quad (11)$$

The second equality follows from eqs. (1) and (2), $\langle \dots \rangle$ denotes the ensemble average, and for any configuration Ψ we mean with $\frac{\partial H}{\partial N^p}$ (ψ) the average decrease in H if one p -cell is removed from the system. If we now use eqs. (2), (3) and (7) we find an explicit form for eq.(11):

$$\mu^p = G^p + L_o^p + \langle \psi_{bb}^p / \partial N^p \rangle, \quad (12)$$

which can be used to rewrite eq. (4):

$$P \sim \exp - \beta [F_{bb} + \gamma \sum_p N^p (\mu^p - \mu_{eq}^p - \langle \psi_{bb}^p / \partial N^p \rangle)]. \quad (13)$$

Finally, we can use the fact that a configuration is completely determined, as soon as the configuration of solid cells is given. Indeed, N^p can be eliminated from eq. (13) which then reads:

$$P \sim \exp - \beta [E_{bb} - \gamma \sum_{p \neq f} B^p \psi^p], \quad (14)$$

where B^p is a constant whose interpretation depends on the simulated system. We mention however, that the interpretation does not affect the simulations themselves. There are two, principally different ways to carry out the elimination of N^p and therefore to interpret B^p .

The first, and at first sight most natural approach is to assume that the total number of cells $\sum N^p$ in the system is constant. This implies that one p -cell will be transformed into one fluid cell, and therefore $\mu_{eq}^f = \mu_{eq}^p$. The following result is then found from eqs. (13) and (14):

$$B^p = \mu^f - \mu^p + \langle \psi_{bb}^p / \partial N^p \rangle \quad (15)$$

This approach is useful in magnetic Ising models, but for crystal growth it has an important disadvantage. In general the number of particles is not conserved if one solid cell (which contains an integer number of particles) is transformed into one fluid cell (containing a concentration of particles which may be quite different).

Therefore we propose an approach which is based in the conservation of particles, rather than of cells. Let C_α^p be the number of α -particles in one p -cell. then the total number of α -particles is constant if $\sum C_\alpha^p N^p$ is constant. Dissolution of a p -cell means in this interpretation that α -particles go from a p -cell to the fluid phase, and therefore $\mu_{eq}^f = \mu_\alpha^p$ eq. In general we define the contribution Q_α^p of α -particles to a quantity ψ^p for a p -cell, in such a way that

$$\psi^p = \sum_\alpha C_\alpha^p Q_\alpha^p \quad (16)$$

Using this equation to decompose ν^P , ν_{eq}^P and $\langle \partial E_{\text{bb}} / \partial N^P \rangle$ in contributions of the different type of particles, and applying the condition that $\Sigma C_{\alpha}^P N^P$ is constant we get the following interpretation of B^P from eqs. (13) and (14):

$$B^P = \Sigma_{\alpha} C_{\alpha}^P (\nu_{\alpha}^f - \nu_{\alpha}^P + \langle \partial E_{\text{bb}} / \partial N^P \rangle_{\alpha}) \equiv \Sigma_{\alpha} C_{\alpha}^P (\Delta \nu_{\alpha}^P + \langle \partial E_{\text{bb}} / \partial N^P \rangle_{\alpha}) \quad (17)$$

where $\Delta \nu_{\alpha}^P$ is the supersaturation of α -particles in the solution, respective to their situation in a p -cell.

In order to reach the object of this section, we use the principle of microscopic reversibility

$$P(\Psi)p(\Psi \rightarrow \Psi') = P(\Psi')p(\Psi' \rightarrow \Psi) , \text{ all } \Psi, \Psi' \quad (18)$$

to obtain a relation between the probability of a certain process and of the inverse one:

$$\frac{P(\Psi \rightarrow \Psi')}{P(\Psi' \rightarrow \Psi)} = \exp\{ -\beta[E_{\text{bb}}(\Psi') - E_{\text{bb}}(\Psi) - \Sigma_{p \neq f} B^p (N^p(\Psi') - N^p(\Psi))] \} \quad (19)$$

Obviously, this relation is not sufficient to determine all transition probabilities. A further choice has to be made, inspired by considerations about the physical system of interest. Often the frequency with which particles are attached to the crystal is chosen proportional to $\exp \beta \Delta \mu$ and independent of the subsequent bonding. The probability of a surface diffusion jump is taken proportional to the detachment frequency from the present site and to the equilibrium attachment frequency.

Such assumptions lead to expressions for the detachment frequencies because the ratio k^+/K^- of the attachment and detachment frequencies is given by eq. (19). For some characteristic cases we shall give this expression in an explicit form. The interactions in a simple cubic lattice are combined into the parameter ϕ given in eq. (10), so

$$k^+/k^- = \exp[\beta(\Delta \mu - l\phi)] . \quad (20)$$

Here l is the decrease in the number of solid-fluid (sf) neighbours upon detachment, and related to the number i of broken solid-solid bonds by $l = 6 - 2i$. Upon introducing the solid on solid (SOS) restriction (i.e. solid cells are allowed only above other solid cells) we get the so-called Kossel crystal. There only the number i' of lateral bonds changes, and again (20) holds with $i = 4 - 2i'$. The same is true for the SOS (100) face of a f.f.c. structure and for the unrestricted (111) face we again have eq. (20) but now $l = 12 - 2i'$. The Kossel crystal becomes orthorhombic if the lateral bonds are different and

$$k^+/k^- = \exp[\beta(\Delta \mu - l_x \phi_x - l_y \phi_y)] . \quad (21)$$

The growth of a film on a substrate can be simulated by eq. (20) for the second and higher layers of the film, and by a multiplication of the detachment frequency for atoms from the substrate with $\exp \beta \Delta \phi$, where $\Delta \phi = \phi$ (film-vapor) + ϕ (film-substrate) - ϕ (substrate-vapor). For a two component (a,b) crystal with one particle per cell we get

$$k^{+a}/k^{-a} = \exp \beta (\Delta \mu^a + \gamma^a \phi^{ab} - l^{ab} \phi^{ab} - l^{af} \phi^{af} - l^{bf} \phi^{bf}) . \quad (22)$$

These, or similar, expressions are used in most of the investigations which we are going to discuss.

A slightly different derivation of eq. (20) has been given by Gilmer and Bennema

(4). They first gave an expression for equilibrium, using the principle of microscopic reversibility, the Boltzmann distribution for closed systems and the concept of a kink site (halb Kristallage) where attachment and detachment should be equally likely, i.e. $l=0$ in eq (20) Non-equilibrium expressions are then introduced using expressions inspired by the absolute rate theory of Eyring

Finally we want to mention some general restrictions. As stated in the beginning of this section the system should be quite large in order to be justified in using a thermodynamic description. Concerning the boundary conditions, two cases can be distinguished. If a solid on solid restriction is preferred then periodic boundary conditions in the lateral directions (i.e. parallel to the interface) are chosen, and the height of each column can in principle vary from $-\infty$ to $+\infty$. In an unrestricted model either a minimal and a maximal height is chosen where the layer is completely solid or fluid, respectively, or periodic boundaries are also applied in the vertical direction.

3 SUMMARY OF MC RESEARCH

Monte Carlo simulations in the field of crystal growth have been proved very useful in the study of equilibrium surface properties and growth mechanisms like normal growth, nucleation growth, spiral growth etc. The first simulations were carried out by Chernov (5,6) and Binsbergen (7,8) between 1966 and 1971. After 1971 the number of people involved with simulations increased rapidly and Table 1, which collects all investigations which have to our knowledge been reported since 1971 (including surveys of refs (5-8) in refs (9) and (10) gives a complete picture of the present state of the investigations.

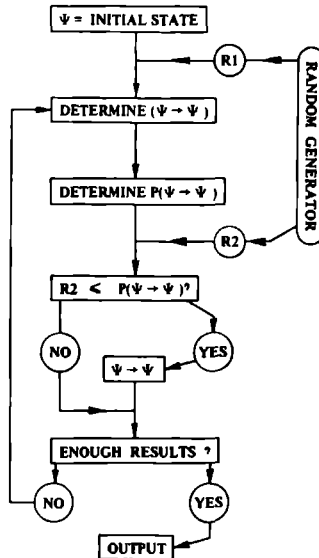


Fig. 2. Flow diagram for Monte Carlo simulations.

Before discussing this list in detail we make a few general remarks. In Fig. (2) a general design for a simulation programme is shown. First an initial state Ψ is given, then one or more random numbers $R1$ are used to determine a process (attach-

Table 1. Survey of the simulations

Crystal structure	Main subject	Temperature θ	el. processes	Ref.
Kossel (100)	roughness	0.7-3.5	+ -	11
Kossel (100)	melt growth	1.2, 10.6	+ -	12
Kossel (100)	melt growth	1.2, 10.6	+ -	13
Kossel (100)	nucleation theory	?	+ -	10
Kossel (100)	growth mechanisms	0.88-1.41	+ - j	14
Kossel (100)	nucleation	0.88	+ - j	15
Kossel (100)	dynamics of roughening	0.71-1.23	+ -	16
sc (100)	unrestricted model	1.00-2.00	(+, -)	17
sc (3dim)	dynamics of phase transition	> 1.8	+ -	18
Kossel (100)	evaporation, Morse potential	0.15	- j	19
Kossel (100)	octupole interactions	0.59-1.76	+ -	20
orthorhombic (100)	equilibrium surface	0.59-1.76	+ -	21
Kossel (100)	special purpose computer	0.78-1.41	+ -	22
orthorhombic (100)	growth mechanisms	0.78-1.18	+ -	23
fcc (100)	growth and evaporation	0.88-1.41	+ -	24
fcc (111)	equilibrium surface	1.43-2.82	+ -	25
bcc (001)	Lennard Jones interactions	0.06-0.08	+	26
spherical	Ostwald ripening	\approx 1.0	+ -	27
Kossel (100)/steps (10)	nucleation/step growth	0.88-1.41	+ -	4
Kossel (100)/steps (10)	nucleation/step growth	0.88-1.41	+ -	28
Kossel (100)/steps (10)	step dynamics	0.80	+ - j	29
Kossel (100)/steps (10)	roughening transition	0.71-1.23	+ -	30
Kossel (100)/steps (10)	step structure	0.88-1.41	+ -	31
Kossel (100)/spiral	spiral shape	0.35, 0.88	+ -	32
Kossel (100)/spiral	nucleation/spiral growth	0.18-1.26	+ - j	33
binary chain	kink growth mixed crystals	0.88-1.26	+ -	9
binary Kossel	growth of metal alloy	4.41	+ -	34
binary Kossel	pseudo ionic interaction	1.76	+ -	35
Kossel film	adsorption isotherm	1.0-2.0	+ - j	36
Kossel film	electrical conductivity	\approx 0.0	+	37
Kossel film	nucleation	0.10-0.16	+ - j	38
Kossel film	island/layer growth	0.68	+ -	39

ment, detachment, diffusion jump). A next random number determines whether the process is really carried out and the cycle is again initiated. Output in the form of growth rates, surface structure etc. is given after a certain number of cycles or events has been carried out.

A sequence ($R_1, R_2 \dots$) of random (more precisely pseudo-random) numbers can be obtained conveniently by the following procedure.

$$R_{n+1} = I_{n+1}/I_{\max} \quad (23)$$

$$I_{n+1} = I_n I_0 \pmod{I_{\max}} \quad (24)$$

Here I_{\max} is the largest integer number which can be represented in the computer, I_0 is an arbitrary number which is chosen in such a way that two successive numbers become independent. Indeed, it can be shown that the correlation coefficient

$$\frac{\langle R_{n+1} R_n \rangle - \langle R_{n+1} \rangle \langle R_n \rangle}{\langle R_{n+1} \rangle \langle R_n \rangle} = \frac{1}{3I_0} - \frac{1}{I_{\max}} - \frac{I_0}{I_{\max}} \quad (25)$$

which vanishes for $I_0 \approx \sqrt{I_{\max}}/3$. Since the cycle length of this generator is $\frac{1}{2} I_{\max} = 2^{30}$ for IBM 370/55 many different R_n are generated. In practice it turns out that this very simple generator is good enough for all purposes.

It can be noted that interactions and temperatures do not occur separately in the simulation, but only as ratios. There is, however, in the literature no consistency in the use of such ratios to characterize the range of temperatures and interactions which is considered. For didactical reasons we think it is best to use a temperature representation. Therefore we shall choose such a ratio (denoted by θ) with the following properties: (i) for a given system θ is proportional to T , (ii) different systems at the same temperature and with the same average potential energy between two cells have the same θ ; (iii) θ is scaled in such a way that the critical temperature of a two dimensional square Ising system with nearest neighbour interactions $\theta_c = 1$.

Point (ii) is inspired by the assumption that a system with complicate interactions can, to some extent, be approximated by a system with nearest neighbour interactions only, which are such that the total lattice energy is the same. We refer to θ as standard temperature from now on.

Let L be the difference in enthalpy per solid cell, to be obtained from eq (10), between one state in which all solid cells are so far away from each other that they have no mutual interaction any more, and another state where these cells are combined in a completely solid crystal. Then we define θ by

$$\theta = 0.88138 \ s kT/L \quad (26)$$

where s is the number of nearest neighbours in the lattice. For convenience of the reader we give in Table 2 and Fig. 3 the relation of θ with the interaction parameters $\omega, \epsilon, \alpha, \gamma$ and L/kT which are used by other authors.

Turning next to the list in Table 1 we see that most attention is given to the (100) face of a Kossel crystal (i.e. a simple cubic lattice with the SOS restriction),

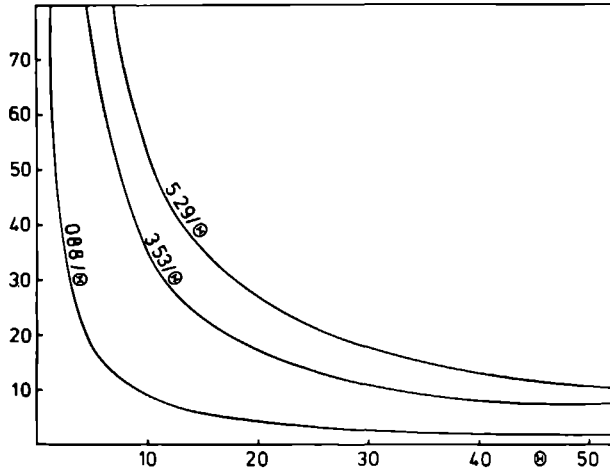


Fig. 3. Standard temperature vs interaction parameters of other authors (see also Table 2).

both with and without surface steps. The surface structure (4,11,12,13,16,17,20,21, 24,25,26) and growth mechanisms (4,10,14,15,22,23,24,28,33,34,35,38,39) are studied in dependence of temperature. Special attention has been given to the transition from normal growth to some mode of step growth (11,14,16,23,24,30,39). A dynamic approach to the critical phenomena occurring at this transition (16) and at the critical temperature of the three-dimensional Ising model (18) revealed a number of similarities. Steps generated by high index faces or by screw dislocations have

Table 2. Relation of θ with interaction parameters of other authors

parameter	$\omega = \phi/kT$	$\epsilon \equiv j = \phi$	$\alpha \equiv \gamma = \xi L/kT'$	L/kT
Ref.	5,6,11-14,21, 23,28,31	4,7-10,16-18,24,26,27 29,30,32,34	1,15,19,20 22	2,3,25,33
Kossel (100)	0.88/0	1.76/0	3.53/0	5.29/0
f.c.c. (100)	0.88/0	1.76/0	3.53/0	10.58/0
f.c.c. (111)	0.88/0	1.76/0	5.29/0	10.58/0
b.c.c. (100)	0.88/0	1.76/0	3.53/0	7.05/0

been studied concerning their structure (31,32), their contribution to be overall growth rate (4,15,28,33), the influence of elementary processes (29) and their edge energy (30). The effect of different types of solid cells and the corresponding order-disorder transition are discussed in refs (9,34,35,38). Growth of a film is simulated by choosing different particles below a certain level (i.e. the substrate) which are not allowed to take part in the elementary processes (36-39).

As mentioned in Section 2 the elementary processes are attachment, detachment and surface migration of solid cells, they are denoted by +, - and j respectively in

Table 1. Equation (19) states that each elementary process should be accompanied with a reverse one. Sometimes however, the reverse process is so unlikely that it is omitted (19,37). In ref. (17) attachment and detachment always occur simultaneously. In ref. (26) vapour molecules have a Maxwell-Boltzmann distributed kinetic energy. If they hit the crystal they will stay there if the gain in bond energy is larger.

Among other computer simulations which are of interest for crystal growth we mention especially free energy computations of small molecular clusters (40,41) and the growth of a thin polymer film on a rough substrate (42).

4. EQUILIBRIUM

A characteristic property of surfaces which is intensively studied, is their roughness r^σ , defined as the interface contribution to the total number of solid-fluid neighbours, per surface particle. For a solid on solid model this is the total number of such pairs, for unrestricted models one has to correct for solvent inclusions and solid islands in the bulk phases.

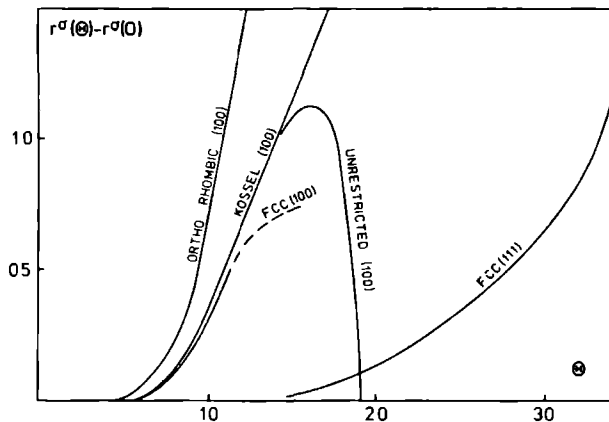


Fig. 4. Interface roughness as function of temperature for different crystal structures: orthorhombic (21), Kossel (11), unrestricted (17), f.c.c. (100) (24) and f.c.c. (111) (25).

The surface enthalpy E^σ and free enthalpy G^σ are closely related to r^σ . For example, for a simple cubic crystal with generalized interaction strength ϕ we have from eq. (10):

$$E^\sigma = \phi r^\sigma \tag{27}$$

$$G^\sigma = \frac{1}{T} \int_0^T E^\sigma dT = \phi \int_0^T \frac{r^\sigma}{T} dT \tag{28}$$

for a simple cubic crystal one can use eq. (27) again if from r^σ and E^σ the contribution at $T=0$ (i.e. a completely flat surface) is subtracted. Equations (27) and (28) give

then the contribution of lateral broken bonds. For more complicated systems one has to take into account that different ϕ_{xy}^{pq} exist.

In Fig. 4 the variation of r^σ with temperature is shown for different crystal structures. The Kossel (100) (11) and f.c.c. (100) (24) faces have the same lateral structure, a square lattice with isotropic nearest neighbour interactions. Therefore their r^σ are similar at low temperatures. At higher temperatures, however, the difference becomes more important, mainly because the SOS condition for the f.c.c. (100) is a much stronger restriction than for the Kossel (100) face).

Also the unrestricted sc (100) face (17) is equivalent with the Kossel (100) face at low temperatures. Upon increasing the temperature, however, the solid and fluid phases become less and less distinguishable until, at the critical temperature $\theta_c^{3D} = 2.00$ of the three dimensional Ising model, the interface vanishes and $r^\sigma \equiv 0$.

The orthorhombic crystal (21) has, at the same temperature θ , stronger bonds in one lateral direction (weaker ones in the other) than in the Kossel crystal (here $\phi_x/\phi_y = 3$), which leads to many sf neighbours parallel to the weak interactions. Therefore in Fig. 5 long shaped clusters, oriented parallel to the strong interactions can be seen. Low temperature expansion of several physical quantities can be obtained from eq. (14) by collecting the configurations with the same (small) broken bond energies in one term (43). The first term corresponds to an empty surface, the second to monomers, the third to dimers etc. For example, when only three terms are considered, one obtains for r^σ the following expression:

$$r^\sigma = 8 \exp(-2\beta(\phi_x + \phi_y)) [1 + 3 \exp(-2\beta\phi_x) + 3 \exp(-2\beta\phi_y)] \quad (29)$$

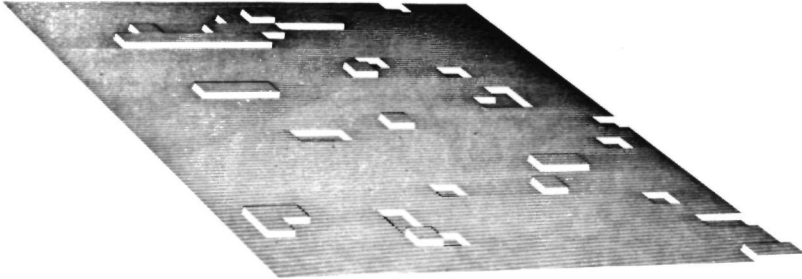


Fig. 5. Example of the interface of an orthorhombic structure at $\theta = 0.8$ (21).

Due to the convex shape of the exponential function the roughness is in the orthorhombic case ($\phi_x \neq \phi_y$) higher than for the Kossel crystal at the same temperature θ (i.e. at the same $\phi_x + \phi_y$).

The f.c.c. (111) face (25), finally, has a triangular structure, such that cells are more strongly bound in the lateral direction, which is also reflected in the higher critical temperature $\theta_c^{2D} = 2.07$ of the two - dimensional triangular Ising model and a much smaller roughness.

The roughness of a face is of major importance for the growth mechanism. Roughly speaking, normal growth takes place on rough surfaces, on smooth surfaces steps have to be generated (high index faces, nucleation, growth spiral). Therefore the roughening transition from "smooth" to "rough" faces has received much interest. We summarize the development in the ideas and understanding of the roughening transition.

Burton *et al.* (44) suggested that the first order phase transition in a two dimensional Ising model (which is equivalent to a one layer surface model) would have a general equivalent for n -layer models (with $n \rightarrow \infty$). Namely, there would exist a transition temperature θ_R below which the adatoms present on the surface tend to be collected in large, flat clusters, thus leaving the surface with a small roughness. Moreover they suggested that θ_R was the temperature at which the surface energy has a point of inflection. Consequently, they computed this inflection point for several n -layer models ($n=1,2,4$) in the Bethe approximation. They found $\theta_R = 1.10$.

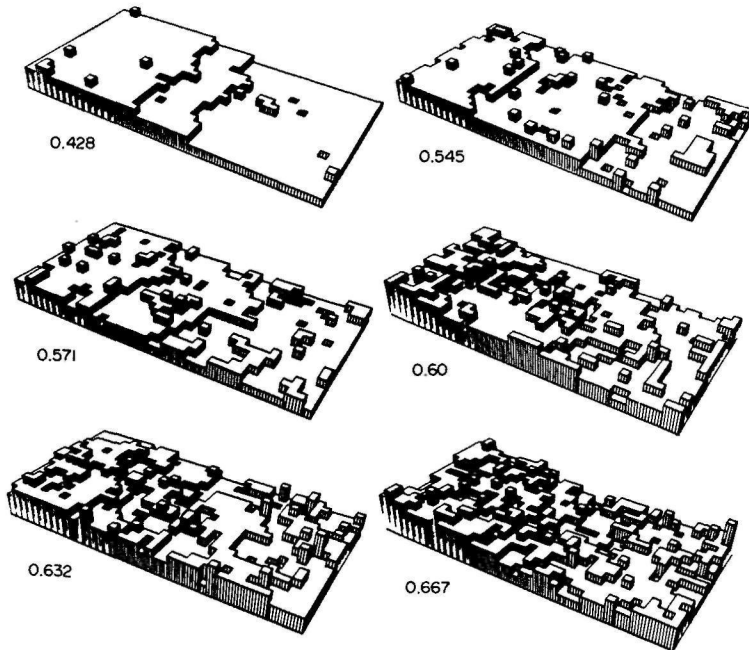


Fig. 6. Interface structure at different temperatures (43), showing the "disappearing" of a (10) step at temperatures above θ_R on a Kossel (100) face. Temperature θ (left to right, top to bottom): 0.75, 0.96, 1.01, 1.06, 1.11 and 1.18.

Using the same analogy with the two-dimensional Ising model, Leamy and Gilmer supposed that at θ_R the excess edge energy and free energy of a surface step would vanish and their Monte Carlo simulations (13) indicated $\theta_R = 1.11$. From their series of stepped surfaces at increasing temperature, shown in Fig. 6, it is seen that at high temperatures the steps are almost indistinguishable from the rest of the surface.

Recently, however, it was shown by more precise Monte Carlo investigations (45) that the excess edge energy does not vanish completely at $\theta=1.13$, but seems to decrease smoothly. Low temperature series up to ninth order (eq. (29)), is only up to third order indicate (43) that the interface slope, width and the fourth moment of the height may diverge at $\theta=1.08$, 1.15 and 1.16, respectively. If it is accepted that the interface "diverges" at and above θ_R then these temperatures also estimate θ_R . Clearly, more terms are necessary to give a definite answer for the problem.

As the static considerations mentioned so far are not able to determine θ_R satisfactorily, it becomes somewhat doubtful whether they give a correct insight in the roughening transition. Swendsen (18) then studied the dynamic aspect, determining relaxation times τ_E^I and $\tau_{h_2}^I$, which estimate the average time that fluctuations in surface energy and height persist. It should be expected that the relaxation times are small both below θ_R (because there is a strong tendency to make the surface flat) and above θ_R (where the surface is not rigid and fluctuations damp quickly), and as a consequence they will show a maximum at θ_R . Such a behaviour is indeed found, but the unexpected thing is that with this method θ_R may coincide with $\theta_S^D \approx 1$, namely $\theta_R = 1.01 \pm 0.04$. A strong dependence of the relaxation times on the system size is found at $\theta \approx \theta_R$, which reflects the importance of long wavelength perturbations of the surface.

In conclusion we may say that, although there is still no definite solution of the roughening problem, there exists a transition from flat to rough surfaces at a temperature, close to the critical temperature of the Ising model $\theta_c \approx 1$. As atomically smooth surfaces will lead to macroscopic facets and a crystal, we expect that the equilibrium form of a crystal will be faceted below θ_R and rounded off or even isotropic above θ_R . Two difficulties from an experimental point of view should be noted. Firstly, very often the growth form of a crystal, especially close to θ_R , will be quite different from the equilibrium form. Secondly, the wavelengths of the spontaneous oscillation of the crystal surface at $\theta \approx \theta_R$ may be so large that they exceed the crystal size, such that it still looks faceted.

The study of a monatomic step (31) at temperatures varying from $\theta = 0.6$ to 0.9 also revealed long wavelength undulations which will be visible in electron microscope observations. A transition to faceted step shapes should not be expected (and was not found) because the one - dimensional Ising models do not possess a phase transition except at $\theta = 0$. It was shown that the overhang density varied from 1 to 10%, therefore the exact theory for overhangless steps (43,44) is valid for $\theta \leq 0.9 \theta_R$.

We want to remark that from eq. (14) a symmetry property for one component crystals in equilibrium can be derived, which is used sometimes (4,24) to check the correctness of a simulation program. Namely, the probability $P(\Psi)$ of a given configuration Ψ is equal to $P(\tilde{\Psi})$ where $\tilde{\Psi}$ is the configuration in which the solid and fluid cells of Ψ are interchanged.

A simple consequence (holding also for multicomponent crystals) is that the equilibrium surface concentrations of adunits and vacancies should be equal, as they involve the same number of solid-fluid neighbours.

Because equilibrium is principally determined by thermodynamics it has to be expected that the static quantities mentioned above (n^0 , E^0 , F^0 , θ_R and symmetry) are not

influenced by the choice of elementary events. In particular we expect no influence of surface diffusion. Evidently, the kinetics may, and probably will, influence the dynamic quantities like the relaxation times τ_E^I and τ_{h2}^I for fluctuations

Ostwald ripening is a process which controls the growth and dissolution of small crystalline particles in equilibrium with a solution. As the surface of a small particle is more curved than that of a large one, the smaller particles will, on the average, dissolve and the larger ones grow. This process has been considered, assuming that the crystals are spherical and that evaporation of atoms from a flat surface is unlikely. These conditions will be satisfied at temperatures close to θ_R . It was found that in the case of two or four crystallines with a total of 100 particles, the deviation from a deterministic theory, consisting in the solution of a set of differential equations is small.

5 NORMAL GROWTH

Other current names for this growth mechanism are continuous growth and liquid-like growth. It takes place on relatively rough surfaces and a characteristic feature is that the growth rate R depends linearly on the supersaturation for small supersaturation. Throughout this paper we define R as the number of layers added to the crystal per unit time and we normalize it usually by dividing R by the frequency k^+ of attachment.

It can readily be shown (4) that, if the surface of a mono-component crystal retains its equilibrium structure then

$$R/k^+ = 1 - \exp(-\beta\Delta\mu) \quad (30)$$

This equation is known as the maximal or Wilson-Frenkel law. The linear behaviour for small $\beta\Delta\mu$ is immediately found from a Taylor expansion of the exponential function. In Figs. 7 and 8 it is seen that we have linear growth curves for $\theta \lesssim \theta_R - 10$ but they are below the maximal law eq. (30).

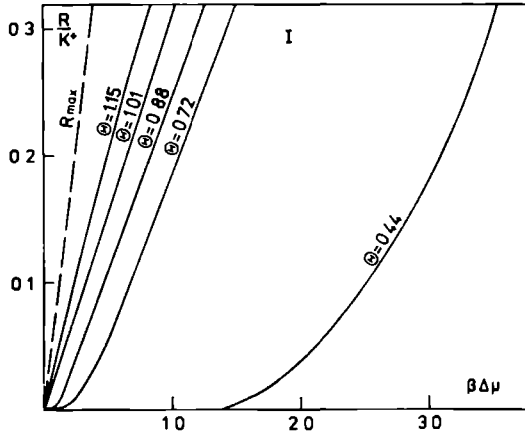


Fig. 7. Growth rate of a Kossel (100) face at different temperatures (4,33) for $\theta < \theta_R$ a "nucleation dip" at low supersaturation $\beta\Delta\mu$ is seen. The symbol I denotes the standard deviation.

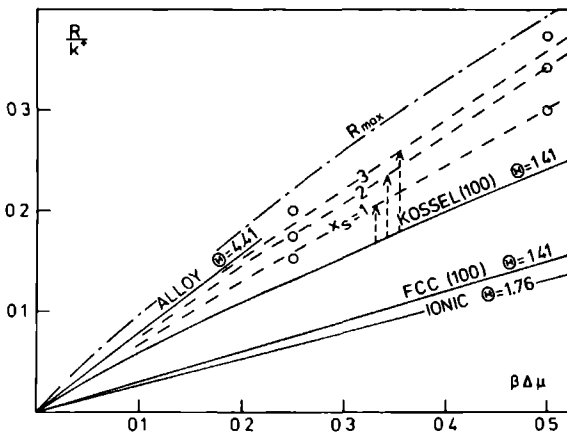


Fig. 8. The influence of surface diffusion and of the crystal structure on the normal growth rate. The dashed curves are computed with eq. (32). The open circles and solid curves are measured. Kossel: ref. (4), f.c.c.: ref. (24), ionic: ref. (35) and alloy: ref. (34).

It is clear that the surface cannot retain its equilibrium structure during all stages of growth, unless it is very rough. In Fig. 4 it can be seen that at θ_R the roughness is ~ 0.3 which is considerably below e.g. the maximal roughness 2.0 per layer, so the surface structure will still play an important role.

The right hand side of eq. (30) is exactly the rate of growth of a kink site (German: halb Kristallage), i.e. a site at which addition or subtraction of a solid cell does not change the broken bond energy ϵ_{bb} (for a Kossel crystal this means that the number of solid-fluid neighbours remains constant). Figures 5 and 6 suggest that eq. (30) should be modified into

$$R/k^* = A(\theta, X_g)(1 - \exp[-\beta \Delta \mu]) \quad (31)$$

and we propose the following interpretation of the proportionality constant A :

$$A(\theta, X_g) = A_0(\theta) \frac{1 + X_g^2}{1 + X_g^2 A_0(\theta)} \quad (32)$$

The first factor describes the growth rate when surface diffusion is absent and we see that it increases from 0.4 at the roughening temperature $\theta = 1$, to 1.0 if $\theta \rightarrow \infty$. We suppose that it is proportional to the contribution of sites which are suitable for growth. Let us call these generalizations of kink sites, active sites, then A_0 should be the concentration of active sites on the surface (which is considerably larger than the concentration of kink sites (4)).

The effect of surface diffusion is that an atom which was not deposited on an active site may still reach it by surface migration. This effect can, for $\theta > \theta_R$ easily be

computed since the active sites are randomly distributed over the (rough) surface. In that case, the probability P_N that an active site is reached at the N -th jump is A_0 (the probability that the $N+1$ st position is active) multiplied with $(1-A_0)^N$ (the probability that all preceding sites were not active). Then the probability w_M that a particle reaches an active site in, at most, M jumps is

$$w_M = \sum_{N=0}^M P_N = \sum_{N=0}^M A_0 (1-A_0)^N = 1 - (1-A_0)^{M+1} \quad (33)$$

where a finite geometric series is summed. If B_0 is the probability that an adatom evaporates then the probability q_M that it makes M jumps is $B_0(1-B_0)^M$. The average diffusion distance X_S is related to B_0 by the general property of random walks

$$\chi_s^2 = \langle M \rangle = \sum_{M=0}^{\infty} M B_0 (1-B_0)^M = (1-B_0)/B_0 + B_0 = (1+\chi_s^2)^{-1}. \quad (34)$$

The probability A can be found from q_M and w_M by

$$A = \sum_{M=0}^{\infty} q_M w_M = 1 - \frac{B_0(1-A_0)}{1 - (1-B_0)(1-A_0)} = \frac{A_0}{A_0 + B_0 - A_0 B_0} \quad (35)$$

where two geometrical series have been summed. Upon inserting the expression (34) for B_0 into eq. (35) results eq. (32).

It can be noted that this equation satisfies the intuitively expected limitation behaviour: (i) eq (32) reduces to the maximal law $A=1$ if the rate is maximal for $X_S = 0$ (i.e. if $A_0=1$), (ii) the same happens if $X_S \rightarrow \infty$, (iii) if $X_S = 0$ then $A=A_0$ and (iv) if no active sites would be present ($A_0 = 0$) then no growth takes place since $A=0$. In Fig. 6 it is seen that eq. (35) predicts the influence of surface diffusion within the accuracy of the measurements, which is also the case for the measurements in ref. (9) which are not shown here.

An analytical theory to determine the normal growth rate in the absence of surface diffusion (i.e. a theory to determine A_0) is the mean field theory. Especially the second order version, known as the pair approximation, has been found to give fairly accurate results, refs. (23,46,47). Mean field theories are high temperature (more precisely high roughness) approximations. Therefore they can be seen as the counterparts of the low temperature expansions in the preceding section. The basic idea is to determine a set of differential equations for the time development of the probabilities $P(z)$ that the crystal has, at a given site, the height z . This set, the master equation, corresponds to the given kinetics in the actual or Monte Carlo process. An approximation which makes the numerical solution possible, is to approximate the actual detachment probability by the same probability if the cell (first order) or pair of cells (pair approximation) would have been surrounded by the average surface as determined by the $P(z)$. The form of the equations involved can be found in refs. (23,46).

For the f.c.c. (100) face growth is much slower than for the Kossel (100) face. This is again a consequence of the solid on solid condition which prohibits attachment and/or detachment at several surface sites. In such a way the number of active sites is reduced. That the ionic crystals grow slower is obviously a consequence of the fact that sites which would have been active on a Kossel (100) face (i.e. which have the desired geometry), are inactive for at least one type (+ or -) of particles, due to the particular types of cells which form the possibly active site. For example, a kink site for a+ particle contains three-particle and is hence repulsive for a-particle.

This effect also explains why the alloy, described in Section 9 and ref. (9), even at $\theta \gg \theta_P$ still does not grow according to the maximal law.

6. NUCLEATION GROWTH

The main difference between normal growth and the various types of step growth (nucleation growth, spiral growth, growth of high index faces) which we are going to discuss in this and in the next section, is that the active sites for growth which were interpreted in the preceding section are not randomly distributed over the surface any more. Indeed they are present at step edges only. Moreover, they will be more similar to the classical kink sites. On perfect faces steps are generated as the edges of large solid clusters. The number of active sites (or kinks) on a step will depend on its curvature: in a slightly supersaturated environment a straight step will always grow, a strong curved step will even tend to dissolve. A cluster whose edge is such that it is in equilibrium at the given supersaturation, is called a nucleus. Large clusters will tend to grow, smaller ones to dissolve.

The size of a nucleus obviously depends on the supersaturation, therefore the factor A in eq. (31) is now dependent on $\beta\Delta\mu$ too. Nucleation theories determine the rate I with which nuclei are formed. When attachment and detachment are the only elementary processes one finds (15) that even on relatively rough surfaces ($\theta = 0.88$) I is given quantitatively by the theoretical formula:

$$I/k^+ = \xi C_0 \sqrt{\beta\Delta\mu} \exp - \pi\beta\xi^2\gamma_0^2/\Delta\mu, \quad (36)$$

where C_0 is the concentration of adsorption sites on the surface, ξ is a shape factor varying from 1.07 for a square nucleus (at $\theta=0$) to 1 for a circular shape (at $\theta \approx 0.9$) (48), and γ_0 is the edge free enthalpy of the nucleus per unit length. The overall growth rate combines I with the spreading velocity of a supercritical growth cluster. Usually a power law dependence of the size of a cluster with time is assumed:

$$n(t) = a(t - t_0)^\alpha \quad t > t_0 \quad (37)$$

here t_0 is the time that the nucleus was formed, a and α are phenomenological parameters. The Kolmogoroff-Avrami-Vetter theory (15) gives for this case

$$R/k^+ = \frac{\alpha + 1}{\Gamma(\frac{1}{\alpha + 1})} \left(\frac{aI/k^+}{\alpha + 1} \right)^{\frac{1}{\alpha + 1}} \quad (38)$$

where Γ is the gamma function. If a constant radial velocity v of the spreading cluster is assumed ($\alpha = \pi v^2$, $\alpha = 2$) then eq. (36) reads:

$$R/k^+ = 1.137 \sqrt[3]{Iv^2}. \quad (39)$$

If, on the other hand, the spreading of a cluster is neglected ($\alpha = n_0$, the size of the nucleus, and $\alpha = 0$) we get

$$R/k^+ = I n_0. \quad (40)$$

A careful observation of Monte Carlo data in ref. (15) revealed that on relatively rough surfaces (at $\theta = 0.88$) an intermediate case $\alpha \approx 1$ occurs which leads to

$$R/k^+ = 0.789 \sqrt{I\alpha}. \quad (41)$$

If we insert eq. (36) into eq. (38), or into any of the eqs. (39-41) then the supersaturation dependence of R is found to be of the form

$$R/k^* = A_1(\beta\Delta\mu)^{A_2} \exp(-A_3\beta\gamma_0^2/\Delta\mu), \quad (42)$$

where A_1 , A_2 and A_3 are numerical constants which depend on the choice of the elementary processes and the spreading mechanism. The dependence of the second factor on $\beta\Delta\mu$ is much weaker than that of the exponential term. Therefore, upon plotting $\ln R/k^*$ versus the reciprocal of $\beta\Delta\mu$, one finds for small $\beta\Delta\mu$ a straight line with slope $A_3\beta^2\gamma_0^2$. In such a way the edge free energy γ_0 and the activation energy $\pi\zeta^2\gamma_0^2/\Delta\mu$ can be determined experimentally.

In Fig. 9 such plots are given. It should be noted immediately that one needs very accurate values for the growth rate at very small supersaturation to be able to determine the linear part of the curves and therewith to find the parameters A_1 and γ_0^2 . Unfortunately this requires much computer time, more than is usually available for such investigations. On the other hand, no definite conclusion can be drawn from measurements at high supersaturations only: the nucleation dip, present in the direct curves of Fig. 7 for $\theta < 1.0$ gives only an indication that something else than normal growth occurs for small $\Delta\mu$. A special purpose computer built in Delft, is able to simulate growth on a Kossel (100) face about 100 times faster than a fast general purpose computer like the IBM 370/55 (22,23). In Fig. 9 it is seen that in fact only the measurements on this SPC give quantitative information.

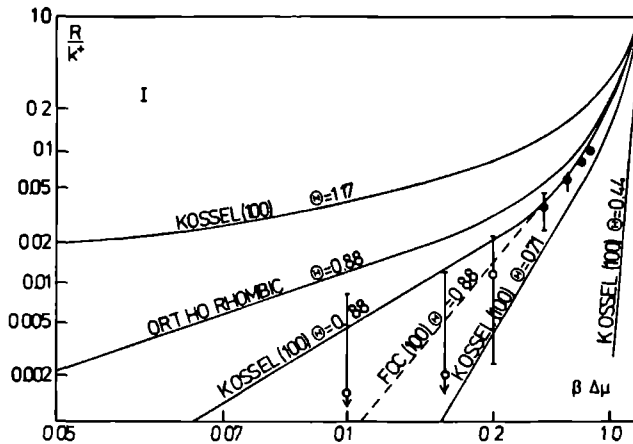


Fig. 9. Growth rates of different faces and different temperatures, the Kossel and orthorhombic crystals are from SPC measurements (23), except at $\theta = 0.44$ (33). The f.c.c. data (• and o) are from ref. (24). The scaling on the axes is linear in $\ln R$ and in $(\Delta\mu)^{-1}$.

Upon comparing the curves in Fig. 9 with theoretical predictions about the size and shape of the nucleus one finds satisfactory quantitative agreement. It turned out, however, to be impossible to discriminate between eqs. (39-41) on the basis of rate curves alone (23). Also qualitative results are reported: upon increasing the temperature, it can be seen that the edge free energy (given by the slope of the linear part of the curves) decreases until at $\theta \approx \theta_R \approx 1.0$ no linear part is found anymore, corresponding to the fact that the edge free energy is supposed to be zero for $\theta > \theta_R$. The edge free energy is smaller for an orthorhombic (100) face, there-

fore the nucleus is smaller and growth faster. The f.c.c. (100) face grows more slowly than the Kossel (100) face but, as explained before, on the basis of the measurements we cannot decide whether this is due to a larger edge free energy or to different factors A_1 and for A_2 which may be influenced by different kinetics in these two cases.

Surface diffusion changes the kinetic processes, but in principle not the size and shape of the nucleus. Therefore, the dip in the direct curve and the slope of the linear part in the $\ln R$ vs $1/\Delta\mu$ curves will remain unaltered. The other characteristic properties of the curves, however, are influenced, as they are determined by A_1 and A_2 . Especially at high supersaturation, where the surface is so rough that normal growth takes place (23), the growth rate increases considerably. Nevertheless a slight influence of surface diffusion on the nucleus itself has been reported (15). This was interpreted as a consequence of the fact that at temperatures just below θ_R quasi-equilibrium is not reached during the growth process, and therefore the nucleus has a higher edge free energy than predicted by statistical theories (48). Surface diffusion brings the system closer to equilibrium, and gives therefore a lower edge free energy.

For high supersaturations normal growth occurs again. This has led to a surprising effect for the orthorhombic (100) face. At small supersaturations it grows faster than a Kossel (100) face at the same temperature, due to a smaller nucleus (48). At high $\beta\Delta\mu$ the opposite is the case, due to an increased backflux: from surfaces with the same roughness it is easier to detach particles in the orthorhombic than in the Kossel case. This is again (like with eq. (29)) to be ascribed to the convex shape of the exponential function. The corresponding intersection point of the rate vs supersaturation curves gave an estimation for the roughening transition in the non-equilibrium case.

Finally we mention that a convenient and accurate method to determine the nuclear size is to investigate a step connecting two screw dislocations of opposite sign. As long as their distance is smaller than the diameter of the nucleus, a waiting time exists for growth. Simulations (15) of this effect showed that the continuum approximation for the edge of the nucleus or of a step (48) predict the size of a nucleus correctly if it contains more than about 50 particles (15). For smaller nuclei the basic ideas and concepts of classical nucleation theory, like edge free energy, Zeldovich fluctuation region and critical size, can be used still. However, neither a continuum approximation nor an equilibrium statistical mechanical treatment lead to quantitatively reliable results.

7. STEP GROWTH

Strictly speaking, the spreading of nuclei, discussed in the preceding section is an example of step growth, i.e. growth due to attachment of solid cells to step edges. Other examples, which will be discussed in this section, are steps generated by screw dislocations and by the inclination of a high index faces.

As a one-dimensional Ising model has no critical temperature (except $\theta = 0$) we expect that a roughening transition does not exist either and that as a consequence, step nucleation is never necessary. Therefore, we expect that the step velocity v will behave analogous to the normal growth rate eq. (31).

$$v/k^+ = A_{st}(\theta, X_g)(1 - \exp[-\beta\Delta\mu]), \quad (43)$$

where A_{st} is the probability that an active site on the step will be reached by an attached cell. If surface diffusion is absent ($X_g=0$) or the distance L between steps so large that the diffusion fields of neighbouring steps do not overlap ($L \gg X_g$), then this probability is proportional to the step density on the surface. The cor-

responding proportionality for the overall growth rate was found indeed in ref. (29). Under these conditions the following expression was derived and found to be consistent with simulation measurements (see ref (4) and Fig.(10)).

$$A_{st}(\theta, X_s) = 1 + \frac{2X_s}{1 + 4/\gamma_s} \quad (44)$$

Here the equilibrium structure for a step without overhangs was assumed during growth. Consequently there is no temperature dependence. At a temperature just below θ_p and high supersaturation ($\theta = 0.88$, $\beta\Delta\mu > 0.3$) the actual velocity is even higher than eq. (44) predicts, which is obviously due to the fact that overhangs introduce additional active sites. For lower temperatures overhangs almost disappear and eq. (44) serves as a maximal law.

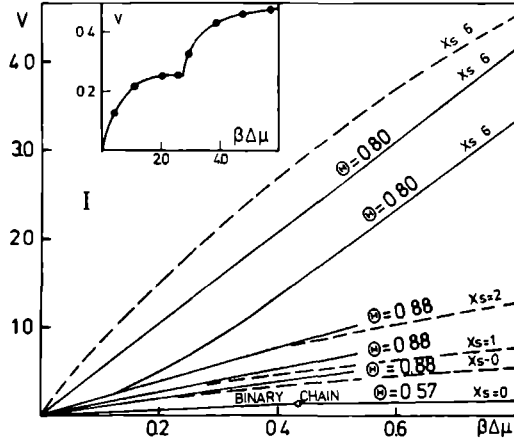


Fig. 10. Advance velocity of a monatomic step. Solid curves are measured $\theta = 0.80$ in ref (29), $\theta = 0.88$ in ref (4) and the binary chain (inset) in ref. (9). Dashed curves are computed with eq (44). At $\theta = 0.80$ adunits could enter the step from both sides (upper curve) or from the lower side only (lower curve).

When X_s is of the order of the step distance the diffusion fields overlap, a smaller area than assumed in the derivation of eq. (44) supplies adunits to each step. In this case the second term in eq. (44) should be multiplied with a factor $\tanh L/\sqrt{2}X_s$ in order to account for the disturbance of the adunit concentration in the neighbourhood of each step due to the presence of other steps at a distance L (44).

$$A_{st}(\theta, X_s) = 1 + \frac{2X_s}{1 + 4/\gamma_s} \tanh \frac{L}{\sqrt{2} X_s} \quad (45)$$

The investigations of ref. (29) showed indeed that if X_s is comparable with L , then deviations from eq. (44) in the direction of eq. (45) occur. From eq. (45) it follows that spontaneous fluctuations of step distances reduce their average velocity and consequently the overall growth rate as well, which was confirmed in the simulations.

Again in ref. (29) a suggestion of Schwoebel was investigated. Adunits were inhibited from reaching the step from the higher side. As predicted by continuum theories the step velocity decreased and a tendency of step clustering (the initial state of kinematic wave formation) was observed. The velocity of a step on a mixed crystal ($\phi^{aa} = \phi^{bb} = \frac{1}{2}\phi^{ab}$) growing from the melt has been estimated from data for the advance rate of a kink (9). In this case the supersaturation

$$\Delta\mu = L_f \Delta T / T \quad (46)$$

where L_f is the heat of fusion and $\Delta T = T_m - T$ is the difference in temperature with the melting temperature T_m . The relation between the step velocity and $\beta\Delta\mu$ was found by multiplying the advance rate of the kink with the equilibrium density of kink sites on a step. At $\theta = 0.57$ the active sites will be almost only kink sites and overhangs will be rare. It is seen that this step velocity is far below the maximal one for two reasons. First, a kink site is an active site for one type of particles only, and second, the temperature of the whole system decreases, so the step contains less kink sites. The discontinuity of the v vs $\beta\Delta\mu$ curve reflects the transition from ordered to disordered growth.

The shape of a growth spiral has been computed by continuum theories, first with isotropic step velocities both approximately (44) and exactly (49), and recently also in the anisotropic case (direction dependent velocities) (50). This shape is also investigated with Monte Carlo (32) simulations and compared with the results of the general theory in ref. (50). In accordance with the theory it is found that at high temperatures the spiral is isotropic and tends to an archimedean shape at large distances from the centre, at low temperatures the symmetry of the crystal is reflected and the spiral becomes polygonized.

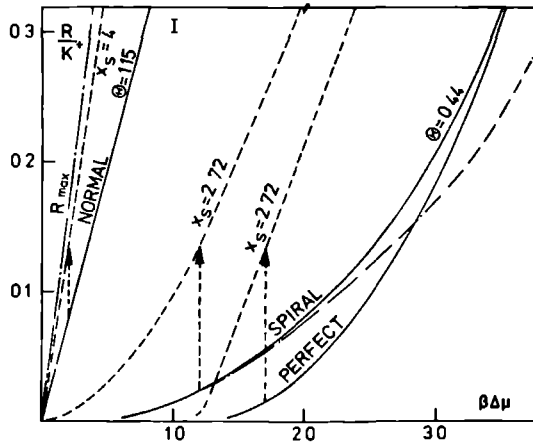


Fig. 11. The influence of surface diffusion on the three different growth mechanisms of a Kossel (100) face. Data at $\theta = 1.15$ from ref. (4), at $\theta = 0.44$ from ref. (33).

The distance Δr between the arms of the spiral is proportional to the radius of the nucleus (and therefore inversely proportional to $\beta\Delta\mu$), the proportionality constant being 18.98 for high temperatures, 8.0 for low temperatures. The change over between

these values occurs simultaneously with the change from isotropic to polygonized spirals between $\theta \approx 0.1$ and $\theta \approx 0.88$. It was shown indeed that the product $\beta \Delta \mu$ is constant up till supersaturations which are so large that the size of the nucleus is of the order of magnitude of the lattice constant. As the advance velocity of a step is supposed to be linear in $\Delta \mu$ (eq. (43)), the overall growth rate, being the product of step density and step velocity should be quadratic in $\beta \Delta \mu$. This second prediction is also valid over the same range of $\Delta \mu$. It should be mentioned, however, that in these simulations attachments and detachments were allowed at the spiral only, so nucleation between spiral steps was automatically inhibited. This will be a reasonable approximation at small supersaturations and at long surface diffusion distances, but not so long that the distance between the arms is exceeded since that would lead to a decrease in R/k^+ and eventually to a linear law (51).

The competitive effect of spiral growth and nucleation growth is considered in ref. (33). In Fig. 11 it is seen that at low supersaturations spiral growth is dominant, whereas, upon increasing $\Delta \mu$, nucleation is enhanced and at large supersaturation the surface is so rough that no distinction can be made between the perfect and imperfect surfaces any more. As it should be expected for the rather smooth surfaces at $\theta = 0.44$, well below θ_p , there is a large influence of surface diffusion.

8. THIN FILM GROWTH

In this field some simulations have been carried out to investigate different experimental facts. The substrate is assumed to be at least smooth and to have an interaction with the atoms which are going to be deposited, which is different from the mutual interaction between deposit atoms. An equilibrium adsorption layer is formed if the environment is undersaturated for the film material. The concentration of particles in the adsorption layer as function of the supersaturation (i.e. vapour pressure) is commonly called adsorption isotherm. In ref. (36) they have been measured for a simple cubic deposit material, condensing in a square lattice with nearest and next nearest neighbour interactions (computed with the Van der Waals-London potential). The temperature if the film varied from $\theta = 1.0$ to 2.0 and the interaction with the substrate was kept constant at $\frac{1}{2} kT$. The Langmuir adsorption isotherm neglects lateral interactions of the film particles. The effect of such interactions is taken into account by Fowler and Guggenheim (52) in the mean field approximation, and by Honig (53) in third order cluster variance approximation. It was shown that the first theory agreed qualitatively, the second one even quantitatively over its range of temperatures.

The simplest case of film growth is to assume that atoms are deposited stay on the substrate and do not migrate. This case was considered in ref. (37) which was intended to explain the behaviour of the electric resistance of a metal film on an insulating substrate. It was shown that a statistical description of this system could be given which is exact in the limit of large systems. The simulations (on a 60 x 60 lattice) agreed closely with this theory and also qualitatively with experiments.

If lateral interactions are included, a nucleation growth mechanism will operate in the adsorption layer if $\theta < \theta_p$. This was studied in ref. (38) for $\theta = 0.10, 0.13, 0.16$, and including surface diffusion ($X_g = 5.6, 3.9, 3.0$). The values of the interaction parameters were taken from estimations for the deposition of silver on sodium chloride. The large deviations from the theory of Zinsmeister for two-dimensional nucleation if $X_g \gg 1$ show that the contribution of direct attachment from the surrounding phase to the clusters cannot be disregarded under these conditions.

The influence of supersaturation on the shape of a growing film was studied in ref. (39) for $\theta = 0.68$, omitting surface diffusion, and with a substrate-deposit inter-

action which is smaller than or equal to the mutual interaction deposit particles. At small supersaturation, nucleation is necessary in all layers and most difficulty in the adsorption layer, therefore many particles will attach on top of growing clusters before they touch each other. Consequently, the film will be rough. At high supersaturation nucleation is not necessary any more and a relatively smooth film will develop. The results of the simulations were found to be in quantitative agreement with the theory of Kashchiev for layer growth (54).

Under the same conditions the movement of clusters of particles has received experimental interest (55). A recent simulation of one of the possible mechanisms for this movement (morphological changes) revealed (56) that the existing theory was unable to predict quantitatively the mobility of small clusters (up to at least 20 particles). Indeed, the influence of stable cluster-cores is dominant and plays a central role in an improved description (56).

9. TWO COMPONENT CRYSTALS

In this section we describe briefly some very recent results in the simulation of the growth of two-component crystals. Until now, three cases have been considered: (1) Chernov (9) studied attractive interactions between all solid cells, the strongest between different ones ($\phi^{aa} = \phi^{bb} = \frac{1}{2}\phi^{ab}$), (11) in Riga (34, 56) again only attractive interactions were assumed, but now the b - b bonds are emphasized ($\phi^{aa} = \phi^{ab} = \frac{3}{5}\phi^{bb}$), and (111) in Delft (35) pseudo-ionic interactions are used ($\phi^{aa} = \phi^{bb} = -\phi^{ab} > 0$). In case (1) the surface of the crystal was artificially kept completely flat except for one monatomic step, containing one kink site, in (11) and (111) the solid on solid restriction was used. These restrictions are, at the temperatures θ which are considered, clearly unphysical. Therefore the relevance of these simulations is assured only if an additional overall force towards the centre of the crystal can be assumed to replace the actual long range interactions in the physical crystal (it was shown in (35) that such an interaction does not change the expression (eq (22) for the transition frequencies). In cases (1) and (11) the supersaturation was caused by a decrease in temperature of the system, growth from the melt ($\Delta\mu^D = L^D\Delta T/T^m$) with possibly different heats of melting L^D for a and b particles, and in case (111) the $\Delta\mu^D$ were changed independently (growth from solution).

The major difference between one- and two-component crystals obviously lies in the structure of the solid phase. Therefore special attention has been paid to structural transitions since Chernov (9) argued that the building up of the crystal phase is a cooperative process, such that a kinetic phase transition should be anticipated. Indeed a transition from a regular NaCl structure at small supersaturation to a disordered structure at high supersaturation was found in cases (1) and (111). This led to a cusp in the growth rate vs $\Delta\mu$ curve (see Fig 10) and to the formation of domains with an internal regular structure (Fig 12). It can be considered as a remarkable result that the tendency to form a regular structure is so strong that only very high supersaturations can destroy such a structure. The additional long range Coulomb interaction, which plays a very important role in physical situations will even amplify this tendency. This result seems to agree with experimental findings. For example, the needle shaped crystals of gypsum ($\text{CaSO}_4 \cdot 2\text{H}_2\text{O}$) - which grow almost only at their rough (so $\theta > \theta_R$ and/or very high $\Delta\mu$ there) end faces - never show irregularities in the alternating structure of positive and negative ions. Thus we see that both for the partly ionic - case (1) - and for the completely ionic - case (111) - types of interaction a NaCl structure arises such that the concentration of a and b particles in the crystal will be equal.

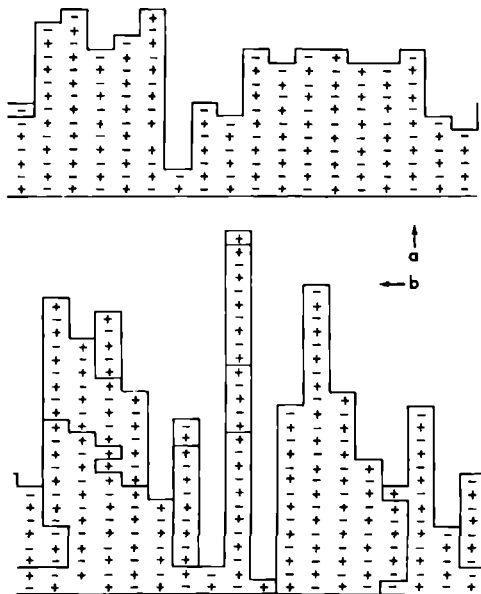


Fig. 12 The structure of a two-component crystal with pseudo-ionic nearest neighbour interactions (a) grown at low and at moderate supersaturations, (b) grown at very high supersaturation, and $\Delta\mu^+ > \Delta\mu^-$.

For the non-ionic interactions - case (11) - this is not necessarily the case. Here decreasing the growth rate will lead to increasing sizes of domains containing merely *b*-particles. Therefore, there is no direct correlation between the number of *a* and *b* particles in the crystal, and the crystal composition will be determined by the properties of the melt. A convenient way to represent such a relation is to use phase diagrams as in Figs. 13 and 14. In order to obtain the fluidus curves it was assumed that the attachment frequencies k^{+a} and k^{+b} were proportional to the concentrations of *a* and *b* particles, respectively in the melt. When the heats of melting L^a and L^b are equal (therefore $k_{eq}^{+a} = k_{eq}^{+b}$ as well) a monotonic increase of the solidus and liquidus is found from the temperature at which a pure *a*-crystal is formed, to the temperature at which a pure *b*-crystal is formed. In the equilibrium diagram ($R=0$) these temperatures are the melting temperatures θ_a of *a*- and θ_b of *b*-crystals, respectively. If, however, $L^a \neq L^b$ (as should be expected when *a* and *b* particles interact differently with the crystal) the diagrams are more complicated. They show at each temperature θ a coinciding minimum for the solidus and the fluidus. At that temperature (the eutectic temperature) both phases have the same (eutectic) composition, such that the melt can crystallize completely into a homogeneous crystal. The results indicate moreover that this kinetic eutectic composition is nearly independent of the growth rate (or undercooling), so it will not differ much from the equilibrium eutectic composition.

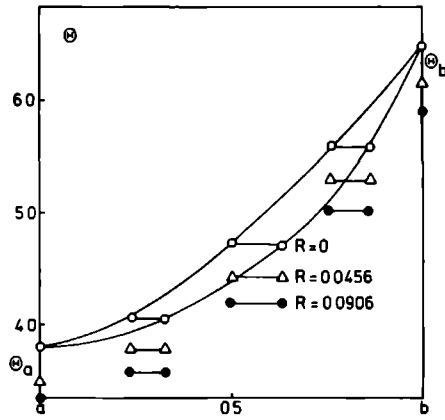


Fig. 13. Equilibrium and kinetic phase diagrams for an alloy (case iii Section 9), with equal heats of melting $L_j^a = L_j^b = kT$. The upper line (fluidus) gives the concentration in the melt, the lower one (solidus) in the crystal.

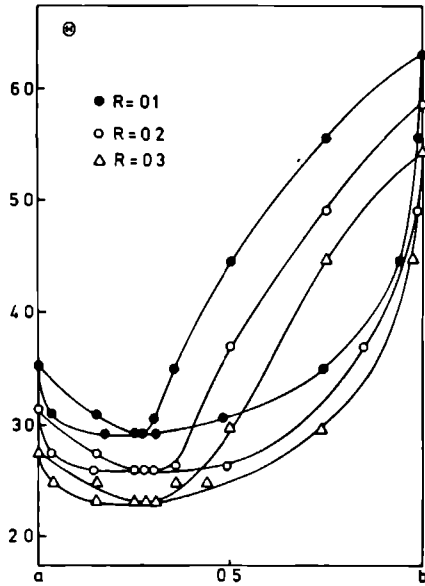


Fig. 14. Kinetic phase diagrams (case iii Section 9) with different heats of melting $L_j^a = L_j^b/3 = kT$.

10. RELATION WITH EXPERIMENTS

In order to be able to compare experiments and simulations, one should relate temperature, interactions and supersaturations of the complicated experimental system with those of the simplified simulation model. Let us first consider the temperature and interactions, i.e. the determination of the standard temperature θ for a physical system. As a first attempt Jackson (57) defined for each face (hkl) a factor $\alpha_J(\text{hkl})$:

$$\alpha_J = \xi_J \beta L_J, \quad (47)$$

where the geometrical factor ξ_J is the ratio of the energy of the bonds parallel to the (hkl) face and the total bond energy, and L_J is the differential heat of melting, dissolution or evaporation. Bennema and Gilmer (58) proposed to use another parameter α which is more closely connected with the simulations

$$\alpha = 2 \beta \sum_{\vec{r}} (\text{hkl}) \phi_{\vec{r}} = \beta L (\text{hkl}) \equiv \xi \beta L. \quad (48)$$

Here $L(\text{hkl})$ is the broken bond enthalpy of the (hkl) face, often referred to as "slice energy". The geometrical factor $\xi = L(\text{hkl})/L$ can be estimated with the Hartman-Perdok theory (59). Clearly, this expression can be used if $L = L_J$, which is true if solid-fluid and fluid-fluid interactions can be neglected (e.g., ideal gas, perfect solution). Otherwise $L = L_J$ only if (i) complete wetting ($\phi_{\vec{r}}^{\text{sf}} = \phi_{\vec{r}}^{\text{ff}}$) is assumed, and (ii) ξ_J is equal to an analogous factor for fluid-fluid interactions.

Let us consider solution growth, then both assumptions will be often invalid, such that $L \neq L_J$. Convincing examples of this statement are found in cases where L_J is negative. A general recipe to estimate L has been developed recently (60,61) on the basis of what we called "chaos model". Here the fluid part of the lattice gas model of Section 2 is replaced by a homogeneous solvent in which solute particles are randomly distributed (no lattice restrictions). Moreover, these solvent particles have the same surface characteristics as the crystal particles. In equilibrium the enthalpy and entropy increases when a crystal cell dissolves, compensate each other.

The entropy contribution is given by

$$\Delta S_{\text{ch}} = \chi k - k \ln C_s^f + S_s^f - S^s. \quad (49)$$

Here χk is the entropy due to the absence of lattice restrictions for the solute ($\chi = 1$ for an isotropic particle, additional terms $\approx \frac{1}{2}k$ arise from each additional degree of freedom of the solute particle (62)). We used the notation of eq. (16) to denote C_s^f for the fraction of the solution cells which is occupied by solute particles. Experimentally C_s^f can be found from the molarities m_f of the solute and m_s of the crystal particles (in mol/cm³), or from the densities C_f and C_s in (g/cm³). Namely $C_s^f = m_f/m_s = C_f/C_s$. The last two terms describe the difference in internal entropy of solute and crystal particles.

The enthalpy increase, on the other hand, is given by

$$\Delta H_{\text{ch}} = L_{\text{ch}} + H_s^f - H^s - z e_0 \phi L_J. \quad (50)$$

Here L_{ch} is the surface enthalpy of a solute particle, $H_s^f - H^s$ is the difference in internal enthalpy of solute and crystal particles and the last term gives, for electrocrystallization, the potential energy increased of an ion of charge $z e_0$ when the solution has a Galvani potential ϕ respective to the metal (63).

Combining eqs (49) and (50) with the equilibrium condition $\Delta H = T\Delta S$ we get

$$\beta L_{ch} = \chi - \ln C_s^f + \beta(G^s - G_s^f) + \beta Z e_0 \phi . \quad (51)$$

Often this expression can be simplified. When the particles are hardly deformed in the crystal we have $G^s \approx G_s^f$. For non electrolytic solutions $\phi=0$, so

$$\beta L_{ch} = \chi - \ln(C_s^f)_{eq} . \quad (52)$$

This means that L_{ch} is given by the solubility. For electrolytic solutions an equilibrium Galvani potential ϕ exists for all ion concentrations, given by (63):

$$\phi = \phi_{st} + \frac{kT}{Ze_0} \ln C_s^f . \quad (53)$$

In the 'Nernst equation', the standard potential ϕ_{st} is known to be almost independent of the specific solution. Combination of eqs (51) and (53) gives:

$$\beta L_{ch} = \chi + \beta Z e_0 \phi_{st} . \quad (54)$$

It is important to note that it follows from this equation the L_{ch} is characteristic for a given metal. Unfortunately, till now it is impossible to measure Galvani potentials directly, but an indirect determination with one of the methods we mention below can be used for other cases as well.

The surface enthalpy L of the generalized lattice gas can be found from L_{ch} if we conceive the fluid phase as a statistical average of the solvent-solute mixture in the chaos model (60):

$$L = (1 - C_s^f)^2 L_{ch} \quad (55)$$

which value can then be used in eq. (26) to find θ or eq. (48) for α .

Equation (50) implies that L_{ch} is the surface contribution to L_J . Therefore we can substitute L_J for L_{ch} in eq (55) and then in eq (48) only if $\phi=0$ and internal changes are negligible

Let us consider, as an illustration, the work of Bourne and Davey (59) who studied the growth of a hexamethylene tetramine (HMT) crystal from aqueous and ethanolic solutions. They found a normal growth mechanism in the first case and spiral growth or nucleation growth in the latter case. Comparing this result with the simulations of Gilmer and Bennema (4), they expected that θ was above and below the roughening temperature, respectively. As the heat of solution of HMT in water is negative it was clear that the recipe of Jackson, eq. (47) was useless in their case. Consequently they attempted to estimate ΔS from data about the activity of HMT in the two solutions. They found $3.5 \text{ cal.mol}^{-1} \text{ }^\circ\text{K}$ for the aqueous and $21.2 \text{ cal.mol}^{-1} \text{ }^\circ\text{K}$ for the ethanolic solution, which leads to $\theta = 4.0$ and 0.66 , respectively (HMT has a b.c.c. structure, therefore $s=8$).

Their results however, probably have no physical meaning since a complete computation should still give $T\Delta S = L_J < 0$. Using, therefore, solubilities (with $\chi = 2.5$) in eq (53) we get for aqueous solution $C_s^f = 0.39$, $\alpha = 0.65$ and $\theta = 5.45$ and for the ethanolic one $C_s^f = 0.0199$, $\alpha = 3.08$ and $\theta = 1.14$. These results are in agreement with the observed growth mechanism since for a b.c.c. (100) face the roughening temperature is about $\theta_R = 1.20$ ($\alpha_R = 2.95$) (65).

It can be noted that a direct estimation or computation of ΔS to determine θ is often cumbersome, or even impossible because the fluid chemistry (activities) should be well known. Approximations can be obtained in different ways. One way is to go back to the proposal of Jackson, using $L \approx T\Delta S$ which will be good for growth from

the vapour phase, from a perfect solution or from a melt where differences in molar volume can be neglected. An alternative way is to use surface free enthalpies G^σ , obtained from homogeneous nucleation rates. It may be expected that below the roughening temperature $G^\sigma \approx H^\sigma \approx \xi L$, such that

$$\theta \approx 0.88 \xi s kT/H^\sigma \quad \theta < 0.8 \theta_R \quad (56)$$

an ξs will be approximately equal to the number of lateral nearest neighbours. Bourne and Davey also investigated this possibility and found that eq. (56) gave about the same θ for ethanolic solution ($\theta = 0.68$) but a much larger value ($\theta = 47$) for the aqueous one. This shows that the restriction in eq. (56) with respect to θ is essential.

Another example can be taken from electrocrystallization. The nucleation experiments of Budevski *et al.* (66) show that the edge free energy of a two-dimensional nucleus on (100) surfaces of Silver-monocrystals is 2.1×10^{-6} erg cm^{-1} . Since the nearest neighbour distance for Ag is 2.89×10^{-8} cm and the edges of the nucleus were along (110) directions we can estimate $\alpha \approx 4.9$ and $\theta \approx 0.60$. In view of eq. (54) we can consider these values as reasonable estimates for all (almost) ideal electrolytic solutions with Ag electrodes.

From these two examples we expect that the parameters of solution growth systems are such that interesting comparison of simulations and experiments will be possible in future.

Turning next to the supersaturation $\Delta\mu/kT$ we can distinguish several cases. First we consider mono-component crystals. For growth from the vapour the driving force is given by deviations of the partial vapour pressure p from the equilibrium value p_{eq} :

$$\frac{\Delta\mu}{kT} = \ln \frac{p}{p_{eq}} \approx \frac{p-p_{eq}}{p_{eq}}, \quad (57)$$

where the last equality is an approximation for small $\Delta\mu/kT$. For solutions, the activity a plays the role of the partial pressure:

$$\frac{\Delta\mu}{kT} = \ln \frac{a}{a_{eq}} = \ln \frac{f c}{f_{eq} c_{eq}} \approx \frac{c-c_{eq}}{c_{eq}} \equiv \sigma, \quad (58)$$

where f and c are the activity coefficient and the solute concentration, respectively. In principle many different units are suitable for the concentrations (e.g. gcm^{-3} , gg^{-1} , mol mol^{-1} etc.). It is convenient to make the choice that makes the activity a as well as possible proportional to c (i.e. $f \approx \text{constant}$). Only then can $\Delta\mu/kT$ be approximated by the relative supersaturation σ for small $\Delta\mu/kT$. For electrolytic condensation the over-voltage $\Delta\phi$ is the driving force:

$$\Delta\mu = z e_0 \Delta\phi, \quad (59)$$

where $z e_0$ is the electric charge of the ions. For growth from the melt, finally we repeat eq. (46)

$$\Delta\mu = L_j \Delta T / T^m. \quad (60)$$

For the growth of two-component crystals it is seen from eq. (22) that two different driving forces $\Delta\mu^a$ and $\Delta\mu^b$ have to be given. For growth from the melt and electrolytic solution this is achieved by a straight forward generalization of eqs (59) and (60), namely the introduction of heats of melting L_j^a and L_j^b and different charges z^a and z^b . For the other cases there seems to exist some arbitrariness because it is well known that different combinations of solute concentrations will result in

an equilibrium system as soon as their ion products are equal. Consequently there are different combinations (μ^a, μ^b) which lead to equilibrium, therefore $\Delta\mu^a$ and $\Delta\mu^b$ are not ambiguously determined, and it seems that eq (22) cannot be used. This difficulty is only apparent because $\Delta\mu^a$ and $\Delta\mu^b$ alone are not sufficient to determine the kinetic model completely, also the ratio $\lambda_{eq}^{+a}/\lambda_{eq}^{+b}$ has to be given, and to each equilibrium crystal structure belongs one value of this ratio, namely the ratio of dissolution frequencies of a and b particles from a kink site.

After the correspondence between the characteristic parameters of the simulation and the experimental system has been established, the two systems can be compared and the simulation results can be used to elucidate experimental results. One possibility which we mentioned already is to compare growth rate, and, in particular, growth mechanisms, which show an encouraging agreement. Also the study of step patterns of growth spirals and etch pits are open to study both for experiments and simulations. A fruitful cooperation in this field may be expected, especially if the simulations can be modified in such a way that lower temperatures (say $0 < 0.5$) and longer surface diffusion distances (say at least ten lattice sites) are allowed. A third field of interest are the structural changes in a two-component crystal, induced by the kinetics. Not only the order-disorder transition in alloys is of importance but also point defects (vacancies, impurities) in a one-component crystal can be easily included. An obvious omission in the crystal structures which have been simulated, is the diamond structure. This is probably due to larger programming difficulties but nevertheless a certain effort in this direction seems worthwhile to overcome these problems.

Finally it seems useful to investigate the roughening transition further, especially a fast special purpose computer can possibly help to complete our understanding of this phenomenon such that ultimately it can be used to be confronted with experiments as well.

At this moment, the basic technical problems about Monte Carlo simulations seem to be solved and it may be expected and hoped that in the future MC simulation will not remain restricted to theoreticians but will become useful to experimentalists as well.

REFERENCES

1. L. Onsager, *Phys. Rev.* 37, 405 (1931), *Phys. Rev.* 38, 2265 (1931).
2. S.R. de Groot and P. Mazur, *Non-equilibrium Thermodynamics*, North-Holland, Amsterdam (1962).
3. T.L. Hill, In: *Statistical Thermodynamics*, Addison Wesley, Reading, Mass. (1960)
4. G.H. Gilmer and P. Bennema, *J. appl. Phys.* 43, 1347 (1972).
5. A.A. Chernov, *Proc. Int. Conference on Crystal Growth*, Boston, Ed. H. Steffen Peiser, 25 (1966).
6. A.A. Chernov and J. Lewis, *J. Phys. Chem. Solids* 23, 2185 (1967).
7. F.L. Binsbergen, *Kolloid u. Z. Polym* 237, 289 (1970).
8. F.L. Binsbergen, *Kolloid u. Z. Polym* 238, 389 (1970).
9. A.A. Chernov, *Soviet Phys. Usp.* 13, 101 (1970).
10. F.L. Binsbergen, *J. Cryst. Growth* 13/14, 44 (1972).
11. H.J. Leamy and K.A. Jackson, *J. appl. Phys.* 42, 2121 (1971).
12. V.V. Solov'ev and V.T. Borisov, *Soviet Phys. Dokl.* 17, 8 (1972).

13. V.V. Solov'ev and V.T. Borisov, *Soviet Phys. Crystallogr.* 17, 814 (1973).
14. P. Bennema, J. Boon, C. van Leeuwen and G.H. Gilmer, *Krist. Tech.* 8, 69 (1973).
15. C. van Leeuwen and J.P. van der Eerden, *Surf. Sci.* 64, 237 (1977).
16. R.H. Swendsen, *Phys. Rev. B* 15, 542 (1977).
17. H.J. Leamy, G.H. Gilmer, K.A. Jackson and P. Bennema, *Phys. Rev. Lett.* 30, 601 (1973).
18. H. Müller-Krumbhaar and K. Binder, *J. Stat. Phys.* 8, 1 (1973).
19. C.S. Kohl and M.B. Ives, *J. Cryst. Growth* 16, 123 (1972).
20. C. van Leeuwen, *J. Cryst. Growth* 19, 133 (1973).
21. D.J. van Dijk, C. van Leeuwen and P. Bennema, *J. Cryst. Growth* 23, 81 (1974).
22. S.W.H. de Haan, V.J.A. Meeussen, B.P.Th. Veltman, P. Bennema, C. van Leeuwen and G.H. Gilmer, *J. Cryst. Growth* 24/25, 491 (1974).
23. J.P. van der Eerden, C. van Leeuwen, P. Bennema, W.L. van der Kruk and B.P.Th. Veltman, *J. appl. Phys.* 48, 2124 (1977).
24. U. Bertocci, *J. Cryst. Growth* 26, 219 (1974).
25. V.O. Esin, V.J. Daniluk, J.M. Plishkin and G.L. Podchinenova, *Soviet Phys. Crystallogr.* 18, 578 (1974).
26. B.N.F. Eddleston, Thesis, M.I.T. (September 1966).
27. I. Hors'ak and S.J. Shrivaneek, *Ber. Bunsenges. Phys. Chem.* 77, 336 (1973).
28. G.H. Gilmer and P. Bennema, *J. Cryst. Growth* 13/14, 148 (1972).
29. C. van Leeuwen, R. van Rosmalen and P. Bennema, *Surf. Sci.* 44, 213 (1974).
30. H.J. Leamy and G.H. Gilmer, *J. Cryst. Growth* 24/25, 499 (1974).
31. C. van Leeuwen and F.H. Mischgofsky, *J. appl. Phys.* 46, 1075 (1975).
32. R.H. Swendsen, P.J. Kortman, D.P. Landau and H. Müller-Krumbhaar, *J. Cryst. Growth* 35, 73 (1976).
33. G.H. Gilmer, *J. Cryst. Growth* 35, 15 (1976).
34. T.A. Cherepanova, A.V. Shirin and V.T. Borisov, In: *Industrial Crystallization*, Ed. J.W. Mullin, Plenum, New York (1976).
35. T.A. Cherepanova, J.P. van der Eerden and P. Bennema, to be published in *J. Crystal Growth* (1978)
36. F.F. Abraham and G.H. White, *J. appl. Phys.* 41, 1841 (1970).
37. J.J. Coutts and B. Hopewell, *Thin Solid Films* 9, 37 (1972).
38. A.C. Adams and K.A. Jackson, *J. Crystal Growth* 13/14, 144 (1972).
39. D. Kashchiev, J.P. van der Eerden and C. van Leeuwen, *J. Cryst. Growth* 40, 47 (1977).
40. A. Bonnissent and B. Mutaftschiev, *J. Cryst. Growth* 24/25, 503 (1974).
41. F.F. Abraham, *J. Chem. Phys.* 61, 1221 (1974).
42. D. Hinze and H.-U. Poll, *Thin Solid Films* 21, 1 (1974).
43. H.J. Leamy, G.H. Gilmer and K.A. Jackson, In: *Surface Physics*, Ed. J.H. Blakeley (1976).
44. W.K. Burton, N. Cabrera and F.C. Frank, *Philos. Mag.* 243, 299 (1951).
45. Müller-Krumbhaar, *Proc. E.C.G.C.1*, Zurich (1976).
46. G.H. Gilmer, H.J. Leamy and K.A. Jackson, *J. Cryst. Growth* 24/25, 495 (1975).

47. J.P. van der Eerden, R. Kalf and C. van Leeuwen, *J. Cryst. Growth* 35, 241 (1976).
48. C. van Leeuwen and P. Bennema, *Surf. Sci.* 51, 109 (1975).
49. N. Cabrera and M.M. Levine, *Phil. Mag.* 1, 450 (1956).
50. H. Müller-Krumbhaar, T.W. Burkhardt and D. M. Kroll, unpublished.
51. P. Bennema, J. Boon, C. van Leeuwen and G.H. Gilmer, *Krist. Tech.* 8, 659 (1973).
52. R.H. Fowler and E.A. Guggenheim, In: *Statistical Thermodynamics*, Cambridge, New York (1939).
53. J.M. Honig, In: *The Solid Gas Interface*, Ed. E.A. Flood, Dekker, New York, 371 (1967).
54. D. Kashchiev, *J. Cryst. Growth* 40, 29 (1977).
55. J.P. van der Eerden, D. Kashchiev and P. Bennema, *J. Cryst. Growth* 42, 31 (1977).
56. T.A. Cherepanova, V.F. Kiselev and V.T. Borisov, unpublished.
57. K.A. Jackson, In: *Liquid Metals and Solidification*, Am. Soc. for Metals, Cleveland (1958).
58. P. Bennema and G.H. Gilmer, In: *Crystal Growth: an Introduction*, Ed. P. Hartman, North-Holland, Amsterdam (1973).
59. P. Hartman, In: *Crystal Growth: an Introduction*, see ref (58).
60. P. Bennema and J.P. van der Eerden, *J. Cryst. Growth* 42 201 (1977).
61. J.P. van der Eerden and P. Bennema, *Proc. ISE 28 Druzhba-Varna*, p. 12 (1977).
62. T.L. Hill, *Statistical Mechanics*, McGraw Hill, New York (1956).
63. K.J. Vetter, *Electrochemical Kinetics*, Academic Press, New York (1967).
64. J.R. Bourne and R.J. Davey, *J. Cryst. Growth* 36, 278 (1976).
65. J.P. van der Eerden, *Phys. Rev. B* 13, 492 (1976).
66. E. Budevski, W. Bostanoff, T. Vitanoff, Z. Stoinoff, A. Kotzewa and R. Kaischew, *Phys. Status Solidi*, 13, 577 (1965).

Roughening transition in mean-field and pair approximation of Ising models

J. P. van der Eerden

Laboratory of Physical Chemistry, University of Technology, Delft, The Netherlands

(Received 3 November 1975)

It is shown that the macroscopic phenomena of the roughening transition in an Ising interface model can be connected with a property, corresponding to a second-order phase transition, of the local thermodynamic potential for interfaces with an even symmetry. Using this connection a method is developed to evaluate the roughening temperature in first- and second-order mean-field approximations of a simple-cubic crystal. These values are compared with Monte Carlo results and with values found from the fundamental assumption that thermodynamic quantities such as the specific heat should have singularities at the transition temperature. It turns out that the second-order results are very accurate. Finally then, the method is generalized to give results for fcc, bcc, and hexagonal structures.

I INTRODUCTION

Below its critical temperature an Ising system has two possible bulk phases. An interface model describes the system if the two bulk phases are simultaneously present. At very low temperatures such a two-phase system will contain both phases separated by an almost flat surface. At higher temperatures this surface will become more and more rough until at the critical temperature the two phases become identical and the surface is no longer present.

At a certain temperature T_R below the critical temperature the surface becomes so rough that there is no longer any tendency to form surfaces that are oriented along crystallographic directions. We shall call this temperature the roughening temperature and the corresponding phenomenon the roughening transition of the Ising model.

In the following we select from the possible applications of the Ising model the solid-fluid lattice model, i.e., each cell of the lattice is either solid or fluid. This interpretation is very useful for the science of the growth and structure of crystal surfaces because it describes various systems such as crystal-melt, crystal-vapor, or crystal-solution. Also, the roughening temperature is probably best visualized with the morphology of a crystal: Below the roughening temperature a crystal is bounded by low-index areas that are almost flat on atomic scale, above T_R the whole surface becomes rough and the edges between the originally flat regions become rounded off. The growth mechanism at low supersaturation also changes at T_R . Below T_R the crystal grows by attachment of new atoms to step edges (i.e., nucleation or dislocation growth), above T_R these steps are hardly recognizable because small and large clusters are present all over the surface. From this reasoning it is clear that different

roughening temperatures belong to each surface orientation. The roughening temperature of the crystal is the highest of these temperatures.

The idea, however, of a roughening transition is general and applies also to other Ising-type models such as the magnetic Ising model and the binary systems used in metallurgy.

Although these macroscopic phenomena are quite clear and generally accepted it turns out to be rather difficult to relate them to quantities in the microscopic statistical-mechanical theory.

Burton, Cabrera, and Frank¹ pointed out that at the transition some thermodynamic quantities exhibit singularities. They found in 1951 that the roughness versus temperature curve has a point of inflection and the specific heat, therefore, has a maximum. Temkin² found the same in his model in 1966. They associated this point with the roughening transition but neither of them proves directly that it is really related to the morphological change mentioned above.

Leamy, Gilmer, and Jackson³ relate the roughening temperature with Monte Carlo data by looking for a temperature where the excess edge energy of a step vanishes. In this way they determine the critical temperature for phase separation in a layer. On the other hand they associate the roughening transition with what they call a divergence of the interface. Above the roughening temperature the surface is free to move up and down, therefore the interface width will become infinite at T_R . This divergence, however, is of long-range type and therefore it is not surprising that such a behavior is not found in static-mean-field-type models, as was proved recently by Weeks and Gilmer.^{4,5} Their conclusion, however, that these models possess no roughening transition is premature.

To overcome these difficulties we make a new start. We shall define a local potential function

depending on the concentration of the central layer between the two phases only (by minimizing the model grand potential function with respect to all other independent variables). Below T_R this function will have certain maxima and minima, indicating that some concentration profiles (namely, those who lead to flat surfaces) are favorable while others are not, and that, therefore, flat surfaces probably occur in the interface. At and above T_R the function will be constant and therefore the interface is free to move.

Using this criterion we give a method for computing the roughening temperatures in mean-field approximations of Ising models. In such a way we have succeeded in constructing a logical connection between the macroscopic definition and a theoretically and numerically accessible method for computing T_R .

Two types of lattice models are frequently used, the solid-on-solid (SOS) model, where each solid cell is situated above another solid cell (crystal science), and the unrestricted (unr) model, where each distribution of solid cells over the lattice is allowed (metallurgy, magnetism). The roughening temperatures of the first- (MFA, mean-field approximation) and second- (pair) order approximations for these two types of model are given. The assumption that the two types are equivalent up to the roughening temperature is confirmed. Possible generalizations of the method could be other crystal symmetries and longer-range interactions.

II EXPRESSIONS FOR THE GRAND POTENTIAL

The state of a simple-cubic crystal is described by the distribution of solid and fluid cells over the cubic lattice. We number the lattice layers perpendicular to the z axis with the parameter i and use the following variables for an approximate (mean-field-type) description of the system: N_i^p number of cells of type p in layer i , $N_i^{p\alpha}$ number of cells of type p that have a cell of type q as their neighbor in the positive α direction, p -S (solid) or F (fluid), $\alpha = x, y$ or z .

An example of the use of the variables is given in Fig. 1. From simple geometric arguments it can be seen that it is possible to express these dependent variables in terms of the independent variables N_i^S and $N_i^{SF\alpha}$ (N is number of cells in a layer)

$$N_i^F = N - N_i^S, \quad (1)$$

$$N_i^{FS\alpha} = N_i^{SF\alpha}, \quad (2)$$

$$N_i^{FF\alpha} = N_i^F - N_i^{SF\alpha}, \quad (3)$$

$$N_i^{SS\alpha} = N_i^S - N_i^{SF\alpha}, \quad (4)$$

if $\alpha = x$ or y , and

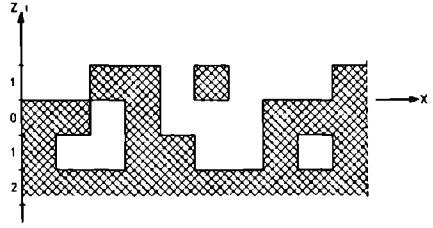


FIG 1 Example of an unrestricted interface (only x - z plane shown) $N_i^S = 4$, $N_i^{SSx} = 1$, $N_i^{SFx} = 4$, $N_i^{FSx} = 2$, $N_i^{SFFx} = 3$, $N_i^{FSSx} = 3$, $N = 10$

$$N_i^{FS\alpha} = N_i^{SF\alpha} + N_{i+1}^S - N_i^S, \quad (5)$$

$$N_i^{FF\alpha} = N_i^F - N_i^{SF\alpha}, \quad (6)$$

$$N_i^{SS\alpha} = N_i^S - N_i^{SF\alpha}. \quad (7)$$

In general there are nonzero interactions $\phi^{p\alpha}$ between cells of both types. We shall restrict ourselves to nearest-neighbor interactions dependent on the direction α and on the types p and q of cells whose interaction is considered. In such a case it is useful to define a generalized interaction parameter $\tilde{\omega} = (\omega^x, \omega^y, \omega^z)$,⁶ thus establishing the equivalence of a solid-fluid lattice model and a lattice gas model (each cell of the lattice is either empty or occupied), where only interactions between the occupied cells are considered

$$\omega^\alpha = (1/2kT)(\phi^{SS\alpha} + \phi^{FF\alpha} - 2\phi^{SF\alpha}). \quad (8)$$

The total interaction energy E can be simplified,

$$\frac{E}{kT} = -2 \sum_{i=-\infty}^{\infty} \sum_{\alpha} \omega^\alpha N_i^{SS\alpha}, \quad (9)$$

and the equilibrium value of the chemical potential is the opposite of the interaction energy per cell of a totally solid lattice,³

$$\mu_e/kT = -2\omega^x - 2\omega^y - 2\omega^z. \quad (10)$$

From straightforward combinatorial computations the entropy S of the system is found to be⁷

$$\frac{S}{k} = \sum_{i=-\infty}^{\infty} \ln \binom{N}{N_i^S} \prod_{\alpha} \left[\frac{\binom{N_i^S}{N_i^{SS\alpha}} \binom{N_i^F}{N_i^{FF\alpha}}}{\binom{N_i^S}{N_i^{SF\alpha}}} \right]. \quad (11)$$

The proper potential function for this open system at constant temperature is the grand potential, and divided by NkT it is given by

$$\Omega = \frac{E}{NkT} + \frac{S}{Nk} - \frac{\mu_e}{NkT} \sum_{i=-\infty}^{\infty} N_i^S. \quad (12)$$

In the following we will use concentrations $C_i^p = N_i^p/N$, $C_i^{pa} = N_i^{pa}/N$, which leads to the following expressions for the grand potential in the

cases we want to consider

The unrestricted pair formula is found by substituting (4) and (7)-(11) in (12).

$$\Omega_{\text{unr}}^{\text{pair}} = \sum_{i=-\infty}^{\infty} \left(\sum_{\alpha=x}^y 2\omega^\alpha C_i^{S\alpha} - 5C_i^S \ln C_i^S - 5C_i^F \ln C_i^F + \sum_{\alpha=x}^y \sum_{p,q=S}^F C_i^{pa} \ln C_i^{pa} \right). \quad (13)$$

The SOS restriction is built in by substituting $C_i^{F\alpha} = 0$ in (5) and (13)

$$\Omega_{\text{SOS}}^{\text{pair}} = 2\omega^x + \sum_{i=-\infty}^{\infty} \left(2\omega^x C_i^{F\alpha} + 2\omega^y C_i^{S\alpha} - 4C_i^S \ln C_i^S - 4C_i^F \ln C_i^F + \sum_{\alpha=x}^y \sum_{p,q=S}^F C_i^{pa} \ln C_i^{pa} \right) + (C_i^S - C_{i+1}^S) \ln(C_i^S - C_{i+1}^S). \quad (14)$$

Substituting $C_i^{pa} = C_i^p C_i^a$ if $\alpha = x$ or y and $C_i^{pa} = C_i^p C_{i+1}^a$ in (13) we get the mean-field expression⁸

$$\Omega_{\text{unr}}^{\text{MFA}} = \sum_{i=-\infty}^{\infty} [2(\omega^x + \omega^y) C_i^S C_i^F + 2\omega^x C_i^S C_{i+1}^F + C_i^S \ln C_i^S + C_i^F \ln C_i^F]. \quad (15)$$

Finally the SOS-MFA expression² is again found from (14) by $C_i^{pa} = C_i^p C_i^a$

$$\Omega_{\text{SOS}}^{\text{MFA}} = 2\omega^x + \sum_{i=-\infty}^{\infty} [2(\omega^x + \omega^y) C_i^S C_i^F + (C_i^S - C_{i+1}^S) \ln(C_i^S - C_{i+1}^S)]. \quad (16)$$

In the SOS-type models the first term $2\omega^x$ results from the boundary condition $C_{-\infty} = 0$ and $C_{-\infty} = 1$. Therefore, it has no influence on the structure of the surface (therefore, neither on the roughening temperature) This is the consequence of the SOS restriction in which the bulk phases contain either only solid or only fluid cells. Such phases are only relevant for physical application at $T=0$, and we have to realize that these models are in themselves interface models. The functions given in (14) and (16) are, therefore, surface quantities. The term, then, enables us to estimate a limiting temperature below which the model can be used. If the total expression (14) or (16) becomes negative the surface tension also becomes negative, therefore, the temperature at which this happens is referred to as the critical temperature of the model.⁹

III DERIVATION OF THE MICROSCOPIC CRITERION

The equilibrium values of the variables we define are those for which the grand potential is minimal. Taking, therefore, the first-order partial derivatives equal to zero gives for each model a set of equations for the independent variables which have to be solved

pair-unr

$$5 \ln \frac{C_i^F}{C_i^S} + \ln \frac{C_i^{Sx}}{C_i^{F\alpha}} \frac{C_i^{Ssy}}{C_i^{F\beta}} + \ln \frac{C_{i-1}^{Sx}}{C_{i-1}^{F\alpha}} \frac{C_{i-1}^{F\beta}}{C_{i-1}^{Sx}} = 0, \quad (17a)$$

$$C_i^{S\alpha} C_i^{F\beta} = e^{-2\omega^\alpha} C_i^{S\alpha} C_i^{F\beta}, \quad (17b)$$

pair-SOS

$$4 \ln \frac{C_i^F}{C_i^S} + \ln \frac{C_i^{Sx}}{C_i^{F\alpha}} \frac{C_i^{Ssy}}{C_i^{F\beta}} + \ln \frac{C_i^S - C_{i+1}^S}{C_{i-1}^S - C_i^S} = 0, \quad (17c)$$

$$C_i^{S\alpha} = e^{-2\omega^\alpha} C_i^{S\alpha} C_i^{F\beta}, \quad (17d)$$

MFA-unr

$$2(\omega^x + \omega^y)(1 - 2C_i) + 2\omega^x(1 - C_{i+1} - C_{i-1}) - \ln(C_i^F/C_i^S); \quad (17e)$$

MFA-SOS

$$2(\omega^x + \omega^y)(1 - 2C_i) + \ln \frac{C_i^S - C_{i+1}^S}{C_{i-1}^S - C_i^S}. \quad (17f)$$

From these equations it can be seen that two types of solution are possible ($\bar{S} = F, \bar{F} = S$)

odd solution

$$C_i^S - C_{i-1}^F, C_i^{pa} = C_{i-1}^{\bar{p}\alpha} \quad \text{if } \alpha = x \text{ or } y, C_i^{pa} = C_{i-1}^{\bar{p}\beta}, \quad (18a)$$

even solution

$$C_i^S = C_{i-1}^F, C_i^{pa} = C_{i-1}^{\bar{p}\alpha} \quad \text{if } \alpha = x \text{ or } y, C_i^{pa} = C_{i-1}^{\bar{p}\beta}. \quad (18b)$$

Thus the solutions possess a mirror symmetry leading to either an atom-center boundary (odd solution) or an interstitial-center boundary (even solution) as they were named by Kikuchi and Cabn¹⁰

In the atom-center boundary the central layer is half filled, therefore, the roughness of the

interface will be high, whereas the interstitial-center boundary corresponds to a more flat surface. So the crystal will have flat surfaces if the even solution has a lower potential than the odd solution. At low temperatures this condition will be fulfilled (at $T=0$ the interface is given by $C_{-i}=1, C_{i+1}=0, i \geq 0$, which is an example of an interstitial-center boundary) The roughening temperature is thus the temperature where the grand potential of the interstitial boundary becomes equal to the grand potential of the atom-center boundary. At temperatures below T_R the even solution corresponds to a minimum in the potential, the odd solution to a saddle point.

Upon minimizing Ω with respect to all independent variables except the concentration C_0 of the central layer [i.e., solving all the equations (17) except the one derived from $\partial\Omega/\partial C_0=0$] these other variables are expressed in terms of C_0 . Substituting these values back in the expressions for the grand potential (13)–(16) one defines a probability function for C_0

$$\Omega_T^*(C_0) \equiv \Omega(T, C_0, C_i(C_0), C_i^{SF\alpha}(C_0)) - \Omega_{\text{even}}(T), \quad (19)$$

where Ω_{even} is the grand potential of the even solution. The shape of this probability function below T_R is given schematically in Fig 2. When C_0 is equal to any concentration of the even solution all the other concentrations will be such that an interstitial-center boundary is formed, so these values lead to minima in Ω_T^* . On the other hand when C_0 equals one of the concentrations of the even solution an atom-center boundary will result and these values correspond to maxima in Ω_T^* . When T rises towards T_R the difference between the minimal and maximal value will shrink down until at $T \geq T_R$ the function is constant

$$\Omega_T^*(C_0) = 0 \text{ if } T \geq T_R \quad (20)$$

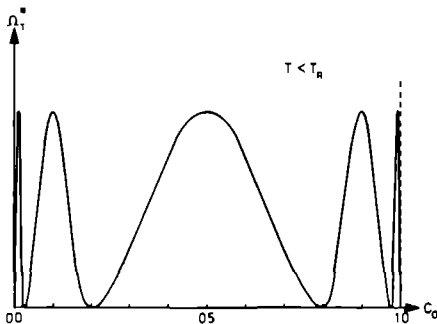


FIG 2 Unconstrained local thermodynamic potential

To get a criterion which is more accessible for numerical calculation of the roughening temperature we go one step further. Again we minimize Ω with respect to all variables except C_0 , but now subject to the constraint that the boundary should be of the atom-center type for all concentrations except for C_0

$$\bar{\Omega}_T(C_0) = \Omega(T, C_0, C_i(C_0), C_i^{SF\alpha}(C_0)) - \Omega_{\text{even}}(T), \quad (21)$$

$$C_i + C_{-i} = 1 \text{ if } i \neq 0.$$

The shape of this potential function is given in Fig. 3. For $T < T_R$ the function has two minima corresponding to configurations where the even solution is best imitated [$C_{-1} - C_0 \approx (C_0 - C_1)_{\text{even}}$ or $C_0 - C_1 \approx (C_0 - C_1)_{\text{even}}$, these layers give the main contribution to the potential]. At $C_0 = \frac{1}{2}$ a relative maximum is present and the whole boundary is of the atom-center type. At temperatures above T_R the interface is by the symmetry restriction forced towards the atom-center boundary, so then $C_0 = \frac{1}{2}$ is a minimum. We now have a simple criterion for the roughening temperature

$$\bar{\Omega}_T^*(\frac{1}{2}) = 0 \quad (22)$$

This property of $\bar{\Omega}$ can easily be transformed into a property for the total grand potential Ω giving.

$$\begin{aligned} \bar{\Omega}_T^*(\frac{1}{2}) &= \frac{\partial^2 \Omega}{\partial C_0^2} + \sum_{i \neq 0, \alpha} \frac{\partial^2 \Omega}{\partial C_0 \partial C_i^{SF\alpha}} \frac{dC_i^{SF\alpha}}{dC_0} \\ &+ \sum_{i \neq 0} \frac{\partial^2 \Omega}{\partial C_0 \partial C_i} \frac{dC_i}{dC_0} = 0, \end{aligned} \quad (23)$$

and the dependence of the C_i and $C_i^{SF\alpha}$ on C_0 is given by the solution of the Eqs. (17) under the symmetry constraint. The partial derivatives have to be computed for the odd solution.

The method of finding the roughening temperature is (i) derive the minimization Eqs. (17), (11) compute $(dC_i/dC_0)_{C_0=1/2}$ and $(dC_i^{SF\alpha}/dC_0)_{C_0=1/2}$ from

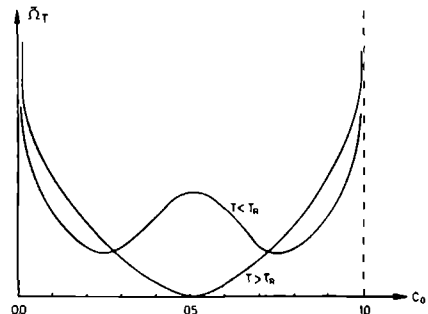


FIG 3 Evenly constrained local thermodynamic potential

these equations; (iii) solve from the minimization Eqs. (17) and the roughening Eq. (23) the interface profile ($\dots, C_{-1}, C_0, C_1, \dots$); (iv) determine the temperature T_R for which this is a physical interface.

IV APPLICATION TO THE MODELS

The first step of the method has already been carried out, so now we will look at the second. Because of the symmetry constraint we have

$$\frac{dC_i}{dC_0} + \frac{dC_{-i}}{dC_0} = 0, \quad i=1, 2, \dots \quad (24)$$

This property makes the last term in (23) zero, so in the MFA models only the first term survives. From the second term only the horizontal pairs in the zeroth layer and the vertical pairs in the zero and minus one layer are nonzero in the expression. For horizontal pairs the equation $\partial\Omega/\partial C_0^{SF\alpha} = 0$ can be solved easily, giving in the case that $C_0 = \frac{1}{2}$:

$$C_0^{S\alpha} = C_0^{F\alpha} = C_0^{SF\alpha} e^{\omega^\alpha} = \frac{1}{2}(1 + e^{-\omega^\alpha})^{-1}, \quad \alpha = x \text{ or } y$$

$$\frac{dC_0^{SF\alpha}}{dC_0} = 0, \quad \alpha = x \text{ or } y. \quad (25)$$

Finally from the equation $\partial\Omega/\partial C_i^{SF\alpha} = 0$ one derives:

$$\frac{dC_i^{SF\alpha}}{dC_i} = - \frac{dC_{i-1}^{SF\alpha}}{dC_{i-1}}$$

$$= \left(\frac{1}{C_i^{FS\alpha}} + \frac{1}{C_i^{SS\alpha}} \right) \left(\frac{1}{C_i^{FS\alpha}} + \frac{1}{C_i^{SS\alpha}} + \frac{1}{C_i^{SF\alpha}} + \frac{1}{C_i^{FF\alpha}} \right)^{-1}. \quad (26)$$

Applying this and the symmetry constraint to layers zero and minus one gives

$$\frac{dC_0^{SF\alpha}}{dC_0} + \frac{dC_{-1}^{SF\alpha}}{dC_0} = 0. \quad (27)$$

The roughening equations then are

pair-unr:

$$-12 + 4e^{-\omega^x} + 4e^{-\omega^y} + 4C_1^S C_1^F (C_0^{FSx} C_0^{FFx} + C_0^{SSx} C_0^{SFx})^{-1} = 0; \quad (28a)$$

pair-SOS:

$$-8 + 4e^{-\omega^x} + 4e^{-\omega^y} + 2(\frac{1}{2} - C_1)^{-1} = 0; \quad (28b)$$

MFA-unr:

$$4 - 4\omega^x - 4\omega^y = 0; \quad (28c)$$

MFA-SOS:

$$-4\omega^x - 4\omega^y + 2(\frac{1}{2} - C_1)^{-1} = 0. \quad (28d)$$

The roughening temperature for the mean-field unrestricted model is directly found from (28c)

$$T_R = (1/2k)(\phi^{SSx} + \phi^{SSy} + \phi^{FFx} + \phi^{FFy} - 2\phi^{SFx} - 2\phi^{SFy})$$

$$= \phi/k, \quad (29)$$

where we defined the average interaction strength ϕ by the last equality. From now on we shall only consider the isotropic case $\omega^x = \omega^y = \omega$ (anisotropic results will be given in a paper about the Monte Carlo simulation of such systems¹¹) and use this definition of ϕ . For the SOS models Eq. (28) can be seen as an equation for C_1 . In the pair-unr model Eq. (28) together with $\partial\Omega/\partial C_0^{SF\alpha} = 0$ forms a set of two equations in the two unknowns, C_1 and $C_0^{SF\alpha}$. So in all cases C_0 and C_1 are known for each temperature and the structure of the set of equations (17) is such that the whole concentration profile is found easily by a numerical procedure. This profile, however, will only be physically relevant if it meets the proper concentration boundary conditions. This will happen for only one temperature (Figs. 4 and 5), which is therefore the roughening temperature.

V RESULTS AND DISCUSSION

Table I gives the critical temperature, the roughening temperature as computed with our method, the temperature where the roughness curve has a point of inflection, and the two-dimensional critical temperature. The first thing to mention is that the roughening temperature is predicted very accurately in the pair approximation.

The next important remark is that the roughening temperature agrees within the given accuracy of the transition temperature computed from the roughness curve. This also holds when the interface is restricted to a finite number of layers (this can be achieved by replacing the proper boundary condition $C_{-n} = C_{\text{bulk}}$ by $C_i = C_{\text{bulk}}$ for i greater than a certain number n). Therefore it seems legitimate to identify the two transitions, although a rigorous proof of this statement has not yet been found. On comparing then the two ways to compute the transition temperature our method has not only the advantage of the clear correspondence between the macroscopic and microscopic phenomena but also requires less effort to compute the temperature to a great accuracy.

Often the critical temperature of the two-dimensional lattice is used as an estimate for the roughening temperature. This estimate is based on the idea that below the roughening temperature the interface mainly consists of only one layer. The roughening equations for a one layer interface (constructed by the boundary condition $C_{-1}^S = C_{-1}^F = 0$) are indeed the equations for the critical temperature of the two-dimensional lattice! From the table it is seen that this estimate leads to a 12%

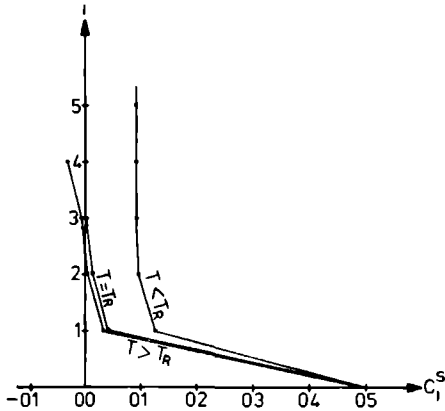


FIG. 4 SOS profiles, evaluated from Eq (28b).

lower transition temperature indicating that the third dimension tends to stabilize the surface. Note, however, that in the mean-field-type approximations (to the same order) this order is reversed. This effect should be mainly attributed to the fact, however, that the two-dimensional critical temperature is not very well approximated even in the pair model.

From Table II the convergence from the unr model to the SOS model can be seen in the pair

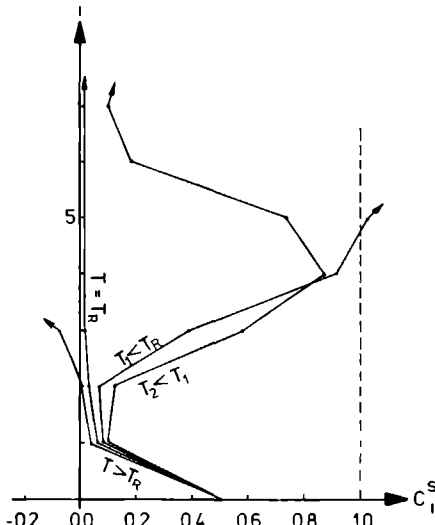


FIG. 5 unr profiles, evaluated from Eq (28a)

TABLE I. Transition temperature in several models

	kT_c/ϕ	kT_R/ϕ	kT_{inf}/ϕ	kT_c^{2-dim}/ϕ
MFA-unr	1.5	1.0		1.0
MFA-SOS	1.11 ^a	0.855	0.82 ± 0.05 ^f	1.0
Pair-unr	1.235 ^b	0.676		0.719 ^b
Pair-SOS		0.649	0.64 ± 0.02 ^g	0.719 ^h
Exact unr	1.136 ^c	~ 0.6 ^d		0.568 ^h
Exact SOS	1.02 ^a	0.64 ± 0.02 ^e		0.568 ^h

^a Comment, see below Eq (16), values from Ref. 9.

^b Exact formula e g. in Ref. 12.

^c Monte Carlo result in Ref. 13.

^d Low temperature expansion in Ref. 4.

^e Monte Carlo result in Ref. 3, low temperature expansion: $T_R \approx 0.62$.

^f Value given in Ref. 2.

^g Recalculation from the Bethe method in Ref. 1 which is equivalent to the pair-SOS model.

^h Exact formula from Onsagers method (Ref. 14).

approximation. This behavior corresponds of course to the well-known fact that the SOS model is equivalent to a unr model with infinite vertical interactions. The only 4% difference in T_R justifies the use of SOS models for temperatures below T_R .

The whole method can easily be generalized to more complicated bond structures. If there are h directions for the horizontal bonds and v for the vertical ones the pair equations in (17) and (28) are modified into

pair-unr:

$$(2h + 2v - 1) \ln \frac{C_i^F}{C_i^S} + \sum_{\alpha} \ln \frac{C_i^{SS\alpha}}{C_i^{FF\alpha}} + \sum_{\beta} \ln \frac{C_i^{SS\beta} C_{i-1}^{FF\beta}}{C_{i-1}^{SS\beta} C_i^{FF\beta}} = 0, \quad (17a')$$

$$C_i^{SF\alpha^2} = e^{-2\omega^{\alpha}} C_i^{SS\alpha} C_i^{FF\alpha}, \quad (17b')$$

$$C_i^{SF\beta} C_i^{FF\beta} = e^{-2\omega^{\beta}} C_i^{SS\beta} C_i^{FF\beta},$$

 TABLE II. Dependence of T_R on the bond strength in the vertical direction.

ω^v/ω^x	kT_R/ϕ^v
1.0	0.676
2.0	0.655
3.0	0.651
4.0	0.650
5.0	0.649
∞	0.649

$$-4(2h+v-1)+4 \sum_{\alpha} e^{-\omega^{\alpha}}$$

$$+4C_1^S C_1^F \sum_{\beta} (C_0^{FS\beta} C_0^{FF\beta} + C_0^{SS\beta} C_0^{SF\beta})^{-1} = 0; \quad (28a')$$

pair-SOS:

$$(2h+v-1) \ln \frac{C_1^F}{C_1^S} + \sum_{\alpha} \ln \frac{C_1^{SS\alpha}}{C_1^{FF\alpha}} + \nu \ln \frac{C_1^S - C_{1+1}^S}{C_{1-1}^S - C_1^S} = 0, \quad (17c')$$

$$C_1^{SF\alpha^2} = e^{-2\omega^{\alpha}} C_1^{SS\alpha} C_1^{FF\alpha}, \quad (17d')$$

$$-4(h+v-1)+4 \sum_{\alpha} e^{-\omega^{\alpha}} + 2\nu(\frac{1}{2} - C_1^S)^{-1} = 0, \quad (28b')$$

where β runs over all vertical pairs and α over all horizontal ones. With these equations we evaluated the results of Table III, again assuming all ω to be equal. From Table III we see that in general the horizontal structure determines T_R mainly and that the stabilization from the third dimension is the largest at the addition of the first vertical bond. In view of this result (and also on intuitive grounds) we assume that growth below the roughening transition (nucleation and spiral growth) will also depend mainly on horizontal bond structures. Another tendency which is shown in the table is

TABLE III. Roughening temperature in several structures.

Type	n	ν	kT_R^{unr}/ϕ	kT_R^{SOS}/ϕ
Square	2	0	0.568	
(100) sc	2	1	0.676	0.649
(110) bcc	2	2	0.679	0.664
(100) fcc	2	4	0.694	0.692
Triangular	3	0	0.910	
(100) hex ^a	3	1	1.178	1.095
(100) hex ^a	3	2	1.179	1.122
(111) fcc ^a	3	3	1.182	1.148

^a Triangular layers can be packed in different ways to form one, two, or three nearest-neighbor bonds per atom between layers.

the closer correspondence between unrestricted and solid on solid models if the number of vertical bonds increases. This is another consequence of the fact that the SOS model is a limiting case of the unr model, as we mentioned above.

ACKNOWLEDGMENT

The author wishes to thank ir. C. van Leeuwen for many helpful discussions.

¹W. K. Burton, N. Cabrera, and F. C. Frank, *Philos Mag.* **243**, 299 (1951).

²D. E. Temkin, in *Crystallization Processes*, edited by N. N. Sirota *et al.* (Plenum, New York, 1966), p. 15.

³H. J. Leamy, G. H. Gilmer, and K. A. Jackson, in *Surface Physics*, edited by J. M. Blakeley (Academic, New York, 1975).

⁴J. D. Weeks and G. H. Gilmer (unpublished) (unr model)

⁵J. D. Weeks and G. H. Gilmer (unpublished) (SOS model).

⁶C. van Leeuwen and P. Bennema, *Surf. Sci.* **51**, 109 (1975).

⁷R. Kikuchi, *J. Chem. Phys.* **47**, 1647 (1967).

⁸C. van Leeuwen, P. Bennema, and D. J. van Dijk, *Acta Metall.* **22**, 687 (1974)

⁹C. van Leeuwen, *J. Cryst Growth* **19**, 133 (1973).

¹⁰R. Kikuchi and J. W. Cabin, *J. Phys Chem. Solids* **23**, 137 (1962).

¹¹J. P. van der Eerden, C. van Leeuwen, P. Bennema, W. van der Kruk, and B. P. Th. Veltman (unpublished).

¹²R. Kikuchi, *J. Chem. Phys.* **57**, 4633 (1972).

¹³H. J. Leamy, G. H. Gilmer, and K. A. Jackson, *Phys. Rev. Lett.* **30**, 601 (1973)

¹⁴L. Onsager, *Phys. Rev.* **65**, 117 (1944)

CORRELATIONS IN THE XY MODEL AND SCREW DISLOCATIONS IN THE SOLID-ON-SOLID MODEL

J P van der LERDEN

RIM Instituut voor Vaste Stof Chemie Universiteit Nijmegen, Nijmegen, The Netherlands

and

H J F KNOPS

Instituut voor Theoretische Fysika, Universiteit Nijmegen Nijmegen, The Netherlands

Received 28 March 1978

An exact relation is proven between the two point correlation function of the classical XY model and the free energy of a step associated with two screw dislocations on a crystal surface described by a solid on solid model. This result suggests a way to obtain the XY critical exponent η_c from Monte Carlo studies of the solid on solid model.

Recently, it has been shown [1,2] that the solid-on solid model (SOS model), used in the theory of crystal growth to describe the crystal surface, can be translated into a (classical) XY-model. Monte Carlo simulations of the SOS model [3,4] show a transition from nucleation growth at low temperatures to linear growth at high temperatures. This so-called roughening transition should then correspond to a magnetic (Standley-Kaplan) transition [5] in the XY model. It has become clear that the nature of this latter transition is rather special, there is no obvious order parameter and the critical exponents vary continuously with temperature [2,6-8] as exemplified by the asymptotic behaviour of the two point correlation function given by

$$g(r) \approx r^{-\eta(T)}, \quad T < T_c, \quad (1a)$$

$$g(r) \approx e^{-r/\xi(T)}, \quad T > T_c \quad (1b)$$

In this formula $\xi(T)$ denotes the correlation length, this length becomes infinite for $T < T_c$ and a power law decay described by the critical exponent $\eta(T)$ takes over. While most theories agree on this general picture, large differences remain in the details. In particular the renormalization theory of refs [2,8] implies an *universal* value $\eta_c = 1/4$ (i.e. the Ising value) for the

exponent $\eta(T)$ at $T = T_c$, whereas the theory advocated by Luther and Scalapino [9] predicts a non universal result for η_c and Zittarz [8] finds $\eta_c = 2$. It is therefore of interest to investigate which quantity corresponds to η_c in the models connected with the XY model. Such a correspondence was recently reported by Nelson and Kosterlitz [10] for superfluid helium films which is another system known [11] to be related with the XY-model. They showed that η_c can be obtained from a jump in the superfluid density.

In the present letter we want to establish the analogous relationship for η_c (or more generally $g(r)$) in the case of the duality transformation from the XY model to the SOS-model. Consider a XY model (defined on a square lattice) with a nearest neighbour interaction

$$-\beta \mathcal{H} \equiv H = \sum_{\langle i,j \rangle} \tilde{V}(\phi_i - \phi_j), \quad (2)$$

where V is periodic with period 2π and ϕ_i represents the angle of spin i with an arbitrary axis. Following ref [1] we introduce for every bond a new variable

$$\phi_{\langle i,j \rangle} = -\phi_{\langle j,i \rangle} \equiv \phi_i - \phi_j \quad (3)$$

A description of the model in terms of these variables would increase the number of degrees of freedom from

N to $2N$ so that one should take into account N constraints which can be expressed by demanding that for every elementary square

$$\phi_{(i,j)} + \phi_{(i,k)} + \phi_{(k,l)} + \phi_{(i,l)} = \text{mod}(2\pi), \quad (4)$$

where i, j, k and l are the corners of the square. This constraint is fulfilled if we introduce for every elementary square a factor

$$(2\pi)^{-1} \sum_{n_j} \exp [in_j (\phi_{(i,j)} + \phi_{(i,k)} + \phi_{(k,l)} + \phi_{(i,l)})], \quad (5)$$

in the partition sum. The integers n_j may be associated to the centers of the squares (numbered by j') which form the dual lattice. The partition sum of the XY model may be transformed by integrating over the decoupled variables $\phi_{(i,j)}$ to a partition sum over the variables n_j

$$Z_{XY}(\tilde{V}) = \sum_{\{n_j\}} \exp \sum_{(i,j)} V(n_i - n_j) = Z_{\text{SOS}}(V), \quad (6)$$

where the interaction V is related to \tilde{V} by a simple Fourier transform as

$$\exp V(n) = (2\pi)^{-1} \int_0^{2\pi} d\phi \exp [\tilde{V}(\phi) + in\phi] \quad (7)$$

Formula (6), which was already obtained in ref [1], expresses the partition function of an XY model with interaction \tilde{V} as the partition sum of an SOS model, defined on the dual lattice, with an interaction V (the integers n_j represent the number of atoms at the site j' above a reference layer for the crystal surface). It should be noted that the relation between V and \tilde{V} is such that the high temperature region of the SOS model is mapped into the low temperature region of the XY model and vice versa. Consider now the XY -correlation function for two spins at sites 0 and n (with a distance r), defined by

$$g(r) = \langle \cos(\phi_0 - \phi_n) \rangle_{XY} \quad (8)$$

In order to apply the same transformation as used above we write the difference $\phi_0 - \phi_n$ as a sum over the variables $\phi_{(i,j)}$ along a path K connecting the sites 0 and n

$$\phi_0 - \phi_n = \sum_{(i,j) \in K} \phi_{(i,j)} \quad (9)$$

The correlation function $g(r)$ can therefore be expressed

as

$$g(r) = \left\langle \exp \left(i \sum_{(i,j) \in K} \phi_{(i,j)} \right) \right\rangle_{XY} = Z_{XY}^{-1}(\tilde{V}) \int \prod_i d\phi_i \times \exp \left[\sum_{(i,j)} \tilde{V}(\phi_{(i,j)}) + i \sum_{(i,j) \in K} \phi_{(i,j)} \right] \quad (10)$$

It is clear from this formula that the problem, when expressed in terms of the variables $\phi_{(i,j)}$, again factorises. Integration over $\phi_{(i,j)}$, taking into account the constraint (4), transforms the numerator of eq (10) into a partition sum of a modified SOS model

$$g(r) = Z_{\text{SOS}}(V, r) / Z_{\text{SOS}}(V) \quad (11)$$

In this formula $Z_{\text{SOS}}(V, r)$ represents the partition sum of an SOS model with an interaction given by $V(n)$ for bonds (which are now located on the dual lattice) that are not intersected by the path K , while bonds that are intersected contribute $V(n+1)$ to the interaction (the sign depends on the orientation of bond direction and path direction). The partition sum of such a model does only depend on the distance of the end points of the path. A path K can be moved to a path K' by a shift in all SOS-spins located within the closed contour $K+K'$.

Some reflection shows that the interaction defined above is precisely the appropriate interaction for an SOS model with two screw dislocations (of Burgers vector $+1$ and -1 , see fig 1) at a distance r . On real crystals such paired dislocations occur when the crystal surface intersects a dislocation loop perpendicularly. The dislocations have to be connected by a step of minimum length r . Its free energy $\gamma(r)$ (per unit length)

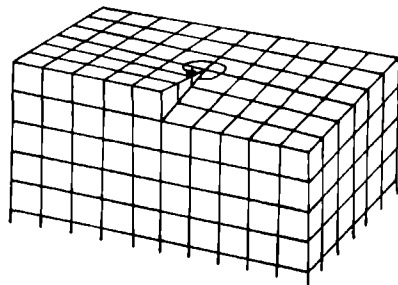


Fig 1 Schematic drawing of a step emerging from a screw dislocation with Burgers vector $+1$

is given by

$$\beta\gamma(r) \equiv \Gamma(r) = -r^{-1} \ln(Z_{\text{SOS}}(V, r)/Z_{\text{SOS}}(V)) \quad (12)$$

From eq (11) we conclude that this step free energy is related with the correlation function of the XY model by

$$\Gamma(r) = -r^{-1} \ln g(r) \quad (13)$$

The step free energy $\gamma \equiv \gamma(\infty)$ plays a central role in crystal growth theories. It is defined as the excess free energy (per unit length) of an infinitely long step relative to a surface without steps. If a driving force $\Delta\mu > 0$ is present the crystal tends to grow but only aggregates of particles which are larger than a critical nucleus are more likely to grow than to disappear. A theorem due to Wulff [12] shows that the diameter of that nucleus is given by $d = 2\gamma/\Delta\mu$. If $\gamma \neq 0$ then $d \neq 0$ and a (nucleation) barrier exists for growth. The transition from nucleation growth at temperatures $T < T_R$ to linear (barrierless) growth at $T > T_R$ should be related to the vanishing of γ for $T > T_R$. Note that for $T > T_R$ not only the step free energy $\gamma = 0$ but the step entropy ($= \partial\gamma/\partial T$) and step energy ($= \partial\Gamma/\partial\beta$) vanish as well.

Indeed, Monte Carlo simulations of Leamy and Gilmer [13] and of Swendsen [4] indicate that the step energy of a step extending over the whole surface, vanishes above T_R . Since temperatures above the roughening temperature correspond with temperatures in the XY model below T_c one can test this prediction by using eq (1a) for $g(r)$ in eq (13), yielding

$$\Gamma(r) = \eta(T) \ln(r)/r \quad (T > T_R) \quad (14)$$

One concludes that $\Gamma(r) \rightarrow 0$ as $r \rightarrow \infty$ and that $\eta(T)$ (and in particular η) can be obtained from the way in which $\Gamma(r)$ vanishes as $r \rightarrow \infty$. On the basis of his Monte Carlo data Swendsen [4] was already led to the conclusion that $\Gamma(r)$ vanishes slower than $1/r$. Work is in progress to obtain $\eta(T)$ from eq (14) by Monte Carlo calculations of $\Gamma(r)$ on a special purpose computer.

When $T < T_R$ the step free energy does no longer vanish as $r \rightarrow \infty$. From eq (1b) we conclude that its

value equals the inverse correlation length

$$\Gamma \equiv \Gamma(\infty) = 1/\xi(T) \quad (T < T_R) \quad (15)$$

The step free energy $\Gamma(\infty)$ has been calculated exactly by van Beijeren [14] for a special SOS model that could be transformed into a six-vertex model. He finds that when T approaches T_R (from below) the step (free) energy vanishes as

$$\Gamma \simeq \exp(-\alpha|T - T_R|^{-1/2}) \quad (16)$$

This result agrees precisely with the prediction of Kosterlitz [7] that the correlation length of the XY model should diverge, when T_c is approached (from above), as

$$\xi(T) \simeq \exp(\beta|T - T_c|^{-1/2}) \quad (17)$$

The authors wish to thank Dr P. Bennema for stimulating discussions.

References

- [1] H. J. F. Knops, Phys Rev Lett 39 (1977) 766
- [2] J. v. José, L. P. Kadanoff, S. Kirkpatrick and D. R. Nelson, Phys Rev B16 (1977) 1217
- [3] G. H. Gilmer and P. Bennema, J Appl Phys 43 (1972) 1347, J. P. van der Gerden, C. van Leeuwen, P. Bennema, W. L. van der Kruk and B. P. Th. Veltman, J Appl Phys 48 (1977) 2124
- [4] R. H. Swendsen, Phys Rev B15 (1977) 5421
- [5] H. E. Stanley and T. A. Kaplan, Phys Rev Lett 17 (1966) 913
- [6] V. L. Berezinskiĭ, Zh Eksp Teor Fiz 59 (1970) 907, Sov Phys JETP 32 (1971) 493
- [7] J. M. Kosterlitz, J Phys C7 (1974) 1046
- [8] J. Zittartz, Z Phys 23B (1976) 55, 63
- [9] A. Luther and D. J. Scalapino, Phys Rev B16 (1977) 1153
- [10] D. R. Nelson and J. M. Kosterlitz, Phys Rev Lett 39 (1977) 1201
- [11] J. M. Kosterlitz and D. J. Thouless, J Phys C6 (1973) 1181
- [12] W. K. Burton, N. Cabrera and F. C. Frank, Phil Mag 243 (1951) 299
- [13] H. J. Leamy and G. H. Gilmer, J Crystal Growth 24/25 (1974) 499
- [14] H. van Beijeren, Phys Rev Lett 38 (1977) 993

Crystal growth: A comparison of Monte Carlo simulation nucleation and normal growth theories

J. P. van der Eerden, C. van Leeuwen, and P. Bennema

Laboratory of Physical Chemistry, Delft University of Technology, Delft, Netherlands

W. L. van der Kruk and B. P. Th. Veltman

Department of Physics, Delft University of Technology, Delft, Netherlands

(Received 30 July 1976, accepted for publication 14 December 1976)

We simulated the growth of a (001) Kossel crystal surface on a special-purpose computer. Different nearest-neighbor bond energies in the two lateral directions of our solid-on-solid model were possible (anisotropy). The values which we obtained for the growth rate are much more accurate than previous results on a general-purpose computer. The supersaturation dependence of the growth rate was compared with predictions of mean field and nucleation theories and it was shown that the latter, if properly adjusted, apply even for relatively rough surfaces. The anisotropy dependence of the growth rate was used to determine the transition from step growth to continuous growth.

PACS numbers 61.50.Cj, 82.60.Nh, 82.65.Dp

I. INTRODUCTION

In this paper we will describe a crystal-solution system in the solid-fluid lattice model. This means that a lattice, corresponding to the symmetry of the crystal, is defined. A point of this lattice corresponds to a unit cell and can be either solid (S) or fluid (F). The model implies that we ignore gradual changes from solid to fluid and also the internal structure of a unit cell. The model can also be used for approximate descriptions of growth from the vapor and from the melt. Moreover, it can be shown to be equivalent with the three-dimensional Ising model with spins equal to $\pm \frac{1}{2}$ as described, e.g., by Hill.¹

The configuration of the system is given by the distribution of solid cells over the lattice. Therefore, we define a vector $S = (S_1, S_2, \dots)$ where $S_i = 0$ or 1 if the i th cell is solid or fluid, respectively, and i runs over all cells of the system. Alternatively, the configuration of the system can be given by the distribution of clusters of solid cells over the lattice. Binder *et al.*² used this description to study the critical properties of the system.

The time evolution of the system is given by the transition probabilities $p(S \rightarrow S')$. Here $p(S \rightarrow S')$ is the probability that the system will be found at time $t + \tau$ in configuration S' if it was in configuration S at time t . It can be noted that (i) the transition probabilities are assumed to be independent of time and of previous states and (ii) the existence of a characteristic time τ is assumed. The first assumption means that we consider the time evolution as a Markov process. The characteristic time τ is chosen so small that, on the average, the configuration of the system will not change during this interval (because only discrete changes in the configuration are allowed such a change that will take a finite time). Given the transition probabilities $p(S \rightarrow S')$, the time-dependent probabilities $p_i(S)$ (to find the system at time t in configuration S) satisfy

$$p_{i+1}(S) = \sum_{S'} p_i(S') p(S' \rightarrow S). \quad (1)$$

We are particularly interested in the behavior of the system under nonequilibrium kinetics, i.e., crystal growth and dissolution. Burton, Cabrera, and Frank³ developed a theory for crystals whose surfaces are so flat that the movement of step edges determines the growth rate completely. For rougher surfaces this theory is not applicable and, therefore, Monte Carlo simulations were carried out, e.g., by Gilmer and Bennema.⁴ In this paper we extend these measurements and some more physical interpretations are given.

We restrict ourselves to the simulation of a lattice of cells in which each cell has four horizontal and two vertical neighbors. We consider only (possibly different) horizontal interactions between neighboring cells and adopt the solid-on-solid condition (or, equivalently, assume that the vertical interactions are infinitely strong). The lattice is then equivalent to a cubic one, and, therefore, we will refer to the system as a Kossel crystal.

The object of our investigations is (i) to find the growth rate of a Kossel crystal for different temperatures and supersaturations and to study the effect of anisotropy in the nearest-neighbor interaction energies and (ii) to compare these results with predictions of nucleation theories and mean field type theories and connect them with the notion of a roughening transition in the interface.

For (i) we performed Monte Carlo simulations on a hardware model especially built for this purpose and, therefore, generating new configurations about 200 times faster than the IBM 370/55 general-purpose computer. We shall refer to these computations by SPC (special-purpose computer). Concerning (ii), we were interested especially in the ranges of validity of these theories. Classical nucleation theories assume large nuclei (> 100 particles) on flat crystal surfaces. Mean field theories, on the other hand, assume rough surfaces. The Monte Carlo technique provides the only way to describe intermediate cases.

II. EXACT THEORY AND MONTE CARLO METHOD

In equilibrium the probabilities $p_i(S)$ are given in the

grand canonical ensemble (because we assume constant temperature, volume, and equilibrium concentrations in the solution, but the number of solid particles may vary,

$$p_i(S) \sim \exp[-(1/kT)\{E(S) - \mu_s^s N^s(S) - \mu_s^f N^f(S)\}], \quad (2)$$

where $E(S)$ is the total interaction energy in the system, $N^s(S)$ and $N^f(S)$ are the numbers of solid and fluid cells, respectively, and μ_s^s and μ_s^f are the corresponding chemical potentials, in which the internal partition functions are contained.⁵ We denote by $N^{\beta\alpha}$ the number of cell pairs of type α containing in one cell a particle of type β (S or F) and in the other a particle of type q (S or F), and by $-\phi^{\beta\alpha}$, the corresponding potential energy. The energy is then given by

$$E = -\frac{1}{2} \sum_{\beta, \alpha, \alpha'} \phi^{\beta\alpha} N^{\beta\alpha} + \sum_{\beta} N^{\beta} A^{\beta}, \quad (3)$$

where A^{β} is the internal free energy of a β cell.

Introducing periodic boundary conditions we have the following geometrical relations:

$$\frac{1}{2} N^{S^S} = N^S - N^{S^F} = N^F - N^{F^F}, \quad (4)$$

$$N^S + N^F = \text{const.}, \quad (5)$$

and it is possible to rewrite Eq. (2) as follows:

$$p_i(S) \sim \exp \left[-\frac{1}{kT} \left(\sum_{\alpha} N^{S^F\alpha} \left(\frac{1}{2} \phi^{S^S\alpha} + \frac{1}{2} \phi^{F^F\alpha} - \phi^{S^F\alpha} \right) - N^S [\mu_s^S - \mu_s^F + \sum_{\alpha} (\psi^{S^S\alpha} - \phi^{F^F\alpha}) - A^S + A^F] \right) \right] \\ = \exp \left[- \left(\sum_{\alpha} N^{S^F\alpha} \omega^{\alpha} - \beta N^S \right) \right], \quad (6)$$

where we defined dimensionless interaction parameters ω^{α} and the parameter β to which we shall refer as supersaturation for reasons which will become clear later on.

To derive formulas for the transition probabilities $p(S \rightarrow S')$ we assume microscopic reversibility

$$p_i(S) p(S \rightarrow S') = p_i(S') p(S' \rightarrow S) \quad (7)$$

which expresses the fact that the system will go as many times from state S to state S' as reverse. This leads to the following expression:

$$\frac{p(S \rightarrow S')}{p(S' \rightarrow S)} = \exp \left(\beta \Delta N^S - \sum_{\alpha} \omega^{\alpha} \Delta N^{S^F\alpha} \right), \quad (8)$$

where ΔN^S and $\Delta N^{S^F\alpha}$ are the differences in number of solid particles and solid-fluid pairs between the states S and S' .

Strictly speaking, we derived Eq. (8) only for equilibrium, but we shall assume that it also holds for nonequilibrium, i. e., for supersaturation and undersaturation. The actual values of the chemical potentials μ_s^s and μ_s^f are given by the energies in the solid and liquid phase, respectively, as given in Eq. (3),

$$\mu_s^{\beta} = \left(\frac{\partial E}{\partial N^{\beta}} \right)^{\text{const.}} = A^{\beta} - \sum_{\alpha} \phi^{\beta\alpha}. \quad (9)$$

Combining this expression with the equilibrium con-

dition $\mu_s^s = \mu_s^f$ and the definition Eq. (6) of β , we find

$$\beta = (1/kT)(\mu_s^f - \mu_s^s), \quad (10)$$

which explains why we call β the supersaturation.

We see from Eq. (6) that for $\beta=0$, the probability of a configuration S is equal to the probability of the inverse configuration (where each solid cell is replaced by a fluid one and reverse). This is precisely the *a priori* condition which Leamy *et al.*⁵ use for equilibrium. Another consequence is that equilibrium surfaces will contain, on the average, as many isolated adcells as isolated vacancies on the interface.

Further on we restrict ourselves to a Kossel crystal, i. e., a simple cubic lattice in which the solid cells are restricted to be present only above (i. e., in the z direction) other solid cells. The interactions are of the nearest-neighbor type only but may be direction dependent. Because the number of solid-fluid pairs in the z direction is constant, the system has three independent parameters $\bar{\omega}$, δ , and β , where

$$\bar{\omega} = \frac{1}{2}(\omega^x + \omega^y) \quad (11)$$

gives the average interaction and δ the anisotropy,

$$\delta = \omega^x / \omega^y. \quad (12)$$

In this model we are free to choose expressions for the transition probabilities as long as they satisfy Eq. (8). We describe processes in which single solid cells are added to and subtracted from the crystal, and, moreover, we assume that the probability p^* to add a cell is independent from the local configuration at the site where it is added. These processes neglect any structure in the fluid phase (like clustering, diffusion fields, etc.) and are, therefore, appropriate only for homogeneous solutions and vapor. The probability $p_{i,j}^*$ to subtract a cell from the crystal if it has i neighbors in the x direction and j in the y direction contains the structural information

$$p^* = \nu \exp \beta, \quad (13)$$

$$p_{i,j}^* = \nu \exp[2\omega^x(i-1) + 2\omega^y(j-1)], \quad (14)$$

where ν is a characteristic frequency for the material in consideration. These probabilities, then, can be used directly for a Monte Carlo simulation. A two-dimensional lattice specifies the height of the column of solid cells at a given site. First, one of these columns is chosen at random, then a cell is added or subtracted with a probability given by Eqs. (13) and (14). However, in the SPC the columns were not chosen at random but in a certain order. For a more precise description see the Appendix and Ref. 6. This procedure introduces some correlation between subsequent events, but this effect was suppressed by neglecting at random about 60% of all columns (also see the Appendix). A statistical test showed no significant difference between simulations performed on the SPC and on the general-purpose computer where columns were chosen at random.

If we want to compare the growth rate R (height increase per unit time) of a physical experiment with the simulation results, it is necessary to have estima-

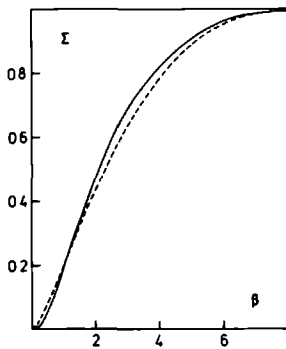


FIG. 1. The supersaturation dependence of the stick fraction. At a sufficiently low temperature, here $\bar{\omega} = 1.125$, both isotropic ($\delta = 1$, solid curve) and anisotropic ($\delta = 0.2$, dashed curve) systems show a nucleation depression. For low supersaturation the isotropic system grows slower, whereas for high supersaturation it grows faster than the anisotropic system. The curves in Figs. 1–3 are smoothed results of simulation experiments with the hardware model.

tions for the frequency ν . However, in this paper we will only give values for the stick fraction Σ (number of layers added to the crystal per addition per column). This means that we use the average time between two additions to the same column as unit time. The stick fraction Σ is related to the growth rate R , but not uniquely. e.g., for vapor growth and growth from dilute solutions the relation will be approximately^{4,7}

$$R = (d\Sigma/\tau) \exp\beta, \quad (15)$$

where d is the distance between successive layers and τ is the average time between additions to the same column in equilibrium.

III. QUALITATIVE INTERPRETATION OF GROWTH CURVES

In Figs. 1–3 results are shown of Monte Carlo simulations on the SPC in the case of growth for three dif-

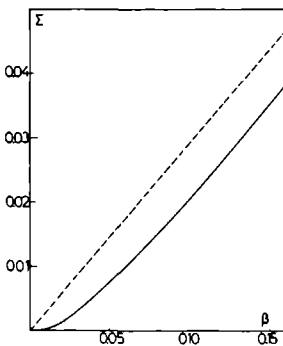


FIG. 2. For $\bar{\omega} = 0.875$ the growth curve of the isotropic system shows a nucleation depression, whereas the growth curve of the anisotropic system does not. ($\delta = 0.2$, dashed curve, $\delta = 1$, solid curve.)

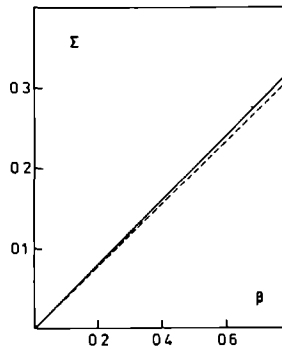


FIG. 3. At high temperature both isotropic and anisotropic growth curves show no nucleation depression anymore ($\bar{\omega} = 0.75$, dashed curve, $\delta = 0.2$; solid curve, $\delta = 1$).

ferent temperatures (i.e., three different values of the average interaction parameter $\bar{\omega}$). At the lowest temperature ($\bar{\omega} = 1.125$, see Fig. 1) we see that both for the isotropic and the anisotropic case the growth curves show a nucleation depression at small supersaturations ($\beta < 1.0$). In the region of the depression the anisotropic crystal grows faster than the isotropic one. At higher supersaturations, on the other hand, the isotropic crystal grows faster, until at very high supersaturation the stick fraction approaches its maximal value of unity for both cases.

In Fig. 2 the behavior at a higher temperature ($\bar{\omega} = 0.875$) is shown. It can be seen that the anisotropic growth curve shows no nucleation depression anymore, and we can still distinguish a region ($\beta < 0.65$) where the anisotropic crystal grows faster and another ($\beta > 0.65$) where the isotropic grows faster (not shown).

In Fig. 3, finally, we see that at a still higher temperature ($\bar{\omega} = 0.75$) the nucleation depression has disappeared for both curves and that the isotropic crystal grows faster for all supersaturations.

We can explain this behavior with the notion of two different growth mechanisms, a nucleation mechanism for flat surfaces and a continuous (or normal) growth mechanism for rough surfaces. In this context we use the adjectives rough and flat as corresponding to surfaces above and below the roughening supersaturation

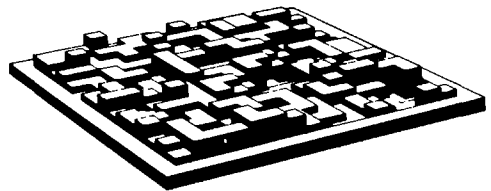


FIG. 4. The interface of a growing crystal becomes rough even below the roughening temperature (here, $\bar{\omega} = 1.125$ and $\delta = 1.0$) when the supersaturation is sufficiently high (here, $\beta = 3.0$).

β^* , respectively. In Fig. 4 an example of a rough surface generated during the simulation is shown.

In the nucleation regime the growth is limited by the nucleation time lag² (the average time necessary for the formation of a nucleus), and it is shown³ that this time lag is shorter in the anisotropic case because there the activation free energy for the formation of a nucleus is smaller.

In the continuous regime the growth is determined by the concentrations $c_{i,j}$ of cells with i and j solid neighbors in the x and y directions, respectively. The impingement rate J^* is not affected by anisotropy. If we assume that the concentrations $c_{i,j}$ are only slightly affected by the interactions and in particular that they are independent of anisotropy, then the difference ΔJ^* between the backfluxes in the anisotropic and the isotropic case is found from Eq. (14),

$$J_{an}^* - J_{is}^* = \nu c_{0,1} [\exp(-2\omega^x) + \exp(-2\omega^y) - 2 \exp(-2\omega)] + \nu c_{1,2} [\exp(2\omega^x) + \exp(2\omega^y) - 2 \exp(2\omega)]. \quad (16)$$

Due to the convex nature of the exponential function, this contribution is always positive and because

$$\Sigma_{an} - \Sigma_{is} = (J^* - J_{an}^*)/J^* - (J^* - J_{is}^*)/J^*, \quad (17)$$

the stick fraction is larger in the isotropic case than in the anisotropic one.

Another qualitative difference between the two growth mechanisms follows from the shape of the growth curves: the continuous growth curve is linear for small β , whereas the nucleation curve shows a depression.

Using these two criteria, we see that Figs. 1–3 show a transition from a nucleation mechanism at low temperatures (Fig. 1) to a normal growth mechanism at high temperatures (Fig. 3), and also that this transition takes place at a higher temperature in the isotropic case than in the anisotropic case (Fig. 2). The dependence of the roughening temperature on the anisotropy can be derived theoretically using a local thermodynamic potential as outlined in Ref. 9. The results of this method are given in Fig. 5. They indeed show a higher transition temperature in the isotropic case. At temperatures below the roughening temperature the growth mechanism will change from nucleation at small β to continuous at a value β^* of the supersaturation. An estimate of this transition value is the point where the isotropic and anisotropic curves intersect (in general there will be different intersection points for different anisotropies, and we take for β^* the limit of these points for $\delta \rightarrow 1$). In Fig. 6 we show the dependence of β^* on $\bar{\omega}$, using also other measurements on the SPC

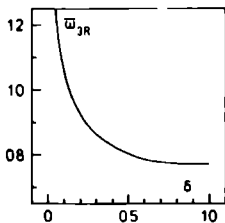


FIG. 5. The anisotropy δ dependence of the roughening temperature $\bar{\omega}_{JR}$ according to the method outlined in Ref. 9.

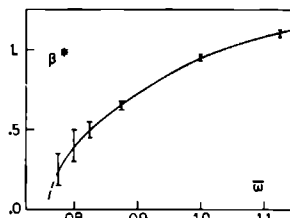


FIG. 6. The temperature dependence of the value β^* of the supersaturation for which the isotropic and anisotropic stick-fraction intersect. β^* estimates the transition from nucleation growth to continuous growth.

which are not presented here. The value of $\bar{\omega}$ for which $\beta^* = 0$ agrees with the transition value $\omega_R = 0.78$, which was also found in other theoretical⁹ and simulation¹⁰ investigations.

IV. APPROXIMATE QUANTITATIVE THEORIES

Usually we are not interested in the precise structure of the interface, but in some concentrations, if we want to describe rough surfaces we use the concentrations $c_{i,j}$ in Eq. (16). For flat surfaces we are interested in the concentrations $c_{n,s}$ of clusters of solid particles with a given size n and shape s on the surface.

In principle, the time development of these quantities is given by the basic equation (1) with the transition probabilities in Eqs. (13) and (14). However, approximate expressions are found if we divide the set of all possible configurations of the interface in classes of configurations in which the concentrations are equal. Equation (1) should then be replaced by an equation for these classes. In this way we will derive expressions for time evolutions on rough and on relatively flat surfaces. The first type of equations we shall refer to as mean field theories (in particular, we use the second-order theory, the pair approximation) and the second type as nucleation theories, although there is no principal difference between them.

A. Pair approximation

The pair approximation describes the time evolution of pairs of neighboring columns. The central variables are the concentrations $p^x(ij)$ and $p^y(ij)$ of pairs of columns with height i and j and being neighbors in the x and the y direction, respectively. Other structural information can be found from these variables. For example, the concentration $c_{0,0}$ of adatoms is given by

$$c_{0,0} = \sum_{i=0}^{\infty} \left(\sum_{j=0}^{i-1} p^x(ij) \right)^2 \sum_{k=0}^{i-1} p^y(ik)^2. \quad (18)$$

and the average height $\langle i \rangle$ can be expressed as

$$\langle i \rangle = \sum_{ij=0}^{\infty} i p^x(ij) = \sum_{ij=0}^{\infty} i p^y(ij) \quad (19)$$

The time evolution of p^x is given by

$$\frac{d}{dt} p^x(ij) = p^x [p^x(i-1j) + p^x(ij-1) - 2p^x(ij)]$$

$$\begin{aligned}
& + \rho_{0,0} [\rho^x(i+1) \xi^x(i+1) \xi^y(i+1)^2 \lambda^x(i+1-j) \\
& + \rho^x(ij+1) \xi^x(j+1) \xi^y(j+1)^2 \lambda^x(i-j-1) \\
& - \rho^x(ij) [\xi^x(i) \xi^y(i)^2 \lambda^x(i-j) \\
& + \xi^x(j) \xi^y(j)^2 \lambda^x(j-i)], \quad (20)
\end{aligned}$$

where

$$\begin{aligned}
\lambda^x(i-j) &= 1 \text{ if } i > j, \\
&= \exp(-2\omega^x) \text{ if } i \leq j, \quad (21)
\end{aligned}$$

$$\xi^x(i) = \sum_{j=-\infty}^{\infty} \rho^x(ij) \lambda^x(i-j). \quad (22)$$

The terms in Eq. (20) involve exchanges of cells on top of one of the two columns in the pair we consider. The interactions within the pair are given exactly with help of the factor λ^x , which gives a contribution $\exp(-2\omega^x)$ to the probability if a bond should be broken. The interactions with the three other neighbors are approximated by average contributions ξ^x and ξ^y . Differential equations for the pairs in the y direction are obtained by replacing x by y and reverse in Eqs. (20)–(22). The same equations were obtained by Gilmer¹¹ for the case of an isotropic crystal. We solved the set [Eq. (20)] of coupled differential equations numerically, using columns of height 1, 2, ..., 20 and periodic boundary conditions. From the solution, the stick fraction is easily found,

$$\Sigma = \frac{1}{\rho^*} \frac{d}{dt} \langle i \rangle = \frac{1}{\rho^*} \sum_{ij=-\infty}^{\infty} i \frac{d}{dt} \rho^x(ij). \quad (23)$$

In Fig. 7 we compare this stick fraction with Monte Carlo results and we find excellent agreement for the growth of rough surfaces. Even the intersection of the isotropic and anisotropic growth curves is represented. This result expresses that the pair approximation is able to describe the onset of long-range correlation phenomena (like nucleation). The pair approximation, however, shows no further growth if the nucleus contains more than two cells (according to the statistical thermodynamical computations in Ref. 8).

The Σ -vs.-height curves, given in Fig. 8, also show an analogy with the nucleation mechanism. For supersaturations below the transition value β^* , these curves

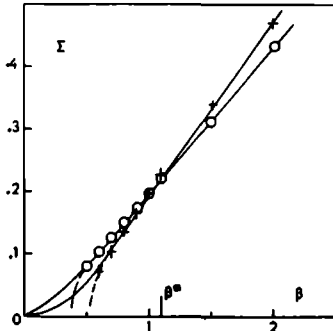


FIG. 7. Comparison of Monte Carlo stick fractions (solid curves) with data obtained from the pair approximation model $\bar{n} = 1.125$; +, pair model $\delta = 1$; \circ , pair model $\delta = 0.2$.

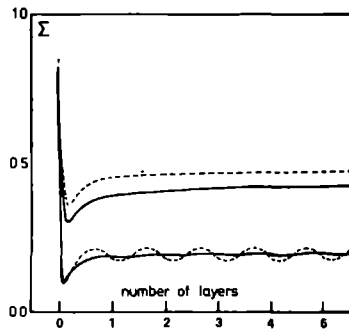


FIG. 8. The height dependence of the stick fraction Σ as obtained in the pair approximation. All curves $\bar{n} = 1.125$; solid curves, $\delta = 0.2$; dashed curves, $\delta = 1$. When $\beta = 2.0$, i. e., $\beta > \beta^*$ the isotropic system grows faster than the anisotropic one (upper curves). When $\beta = \beta^*$ ($\beta = 1.0$ for the lower curves), the average stick fractions are almost the same but a difference in time-dependent behavior can be seen.

show a minimum when a layer is about filled (and therefore relatively flat) and a maximum when the layer is about half-filled (and relatively rough). The amplitude of this oscillation diminishes strongly above β^* .

It can be mentioned that analogous investigations for evaporation (i. e., negative values of β) showed a good correspondence with experimental data obtained from molecular-beam experiments on NaCl crystal surfaces.¹²

B. Nucleation theories

In nucleation theories the state of the interface is given by the concentrations $c_{n,s}$. They are useful if these concentrations are small. In general, the clusters can grow and dissolve by addition and subtraction of single atoms or of other clusters. The latter two processes are generally (an exception was given in Ref. 2) omitted. To obtain formula (28) for the stick fraction to a growing crystal, we recall briefly the arguments of the classical nucleation theory. For a more explicit derivation and a discussion about some physical parameters we refer to Ref. 13.

A further simplification is made by averaging over all possible shapes s of clusters with size n . Under these conditions a steady-state nucleation rate I will be reached, given by¹³

$$I/\rho^* = \xi_2^{-1} c_1 \sqrt{\beta} \exp(-\pi\gamma_0^3/\xi_2^3\beta), \quad (24)$$

where ξ_2 is the shape factor

$$\xi_2 = 2\sqrt{\pi} (\sqrt{n_0}/e_0), \quad (25)$$

involving the number n_0 of atoms in the nucleus and its perimeter e_0 , c_1 is the concentration of adatoms ($c_1 = c_{0,0}$), and γ_0 is the specific edge free energy of the nucleus.

Because it was shown in Ref. 13 that supercritical clusters spread with constant velocity μ at temperature $\omega = 1.0$, we shall assume the same dependence

for all our measurements. The stick fraction is then given by

$$\Sigma = 0.798 [(l/\rho^*) (u/\rho^*)]^{1/2} . \quad (26)$$

The growth velocity u turned out to be proportional to β^2 ,

$$u = u_0 \beta^2, \quad (27)$$

so we get the following expression for Σ

$$\Sigma = 0.798 \xi_2^{-1/2} (c_1 u_0)^{1/2} \beta^{5/4} \exp(-\pi \gamma_0^2 / 2 \xi_2^2 \beta). \quad (28)$$

Using for ξ_2 the expressions given in Ref. 8 we find the parameters $c_1 u_0$ and γ_0 from a least-squares fit of our measurements to Eq. (28). The results are given in Table I. An example of fitted curves is shown in Fig. 9. It should be noted that the functional dependence of Σ on β is mainly determined by the factor in the exponent, therefore, γ_0 is found rather accurately, but the preexponential factor $(c_1 u_0)^{1/2}$ only up to a factor of about 2. The same inaccuracy, however, is found in physical experiments. It should be noted that Eq. (28) deviates from the usual expression at two different points (i) the exponent of β is usually $\frac{5}{4}$ and (ii) the exponential part usually is of the form $\frac{\pi}{2} \gamma_0^2 / 3 \xi_2^2 \beta$. This more common formula was used to fit the first measurements on the SPC.⁶ The reason for the discrepancy is in Eq. (26) where one uses a cubic root and Eq. (27) where other dependences on the supersaturation are possible. Our equation improves slightly the fitting procedure (somewhat smaller standard deviations) but was chosen mainly because the separate measurements in Ref. 13 strongly indicated this choice.

To get an idea of the consistency of our treatment, we can compare the value of γ_0 of Table I with the one measured directly in Ref. 13 $\gamma_0 = 0.52 \pm 0.05$ for $\beta = 1.0$ and $\delta = 1.0$.

As mentioned in Ref. 13, the value of γ_0 found from direct measurement is higher than the thermodynamical value because it is determined from the production rate of clusters which are very likely to grow, whereas it should in principle be found from the nucleation rate (a nucleus is a cluster with equal probability to grow or to dissolve).

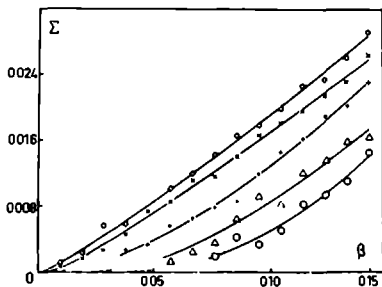


FIG. 9 The solid lines give the results of fitting the data obtained with the hardware model with the nuclear formula [Eq. (28)]. For all curves $\bar{\omega} = 1.0$, \circ , $\delta = 1$, Δ , $\delta = 0.5$, $+$, $\delta = 0.3$, \times , $\delta = 0.25$, and \diamond , $\delta = 0.2$. To account for the small matrix size we did not fit data points in the regions when the curves are dashed.

TABLE I. Preexponential factor $c_1 u_0$ and specific edge free energy of the nucleus under different growth conditions.

$\bar{\omega}$	δ	$c_1 u_0^a$	γ_0^a	γ_0^b	γ_0^c
0.875	1.0	0.028	0.188	...	0.10
	0.5	0.090	0.068	...	
	0.3	0.132	0.042	...	
	0.25	0.083	0.010	...	
	0.2	0.085	0.015	...	
1.0	1.0	0.589	0.336	0.23	0.27
	0.5	0.112	0.234	0.15	
	0.3	0.207	0.078	0.058	
	0.25	0.065	0.016	...	
	0.2	0.051	0.025	...	
1.125	1.0	0.138	0.551	0.45	
	0.5	0.182	0.489	0.35	
	0.3	0.047	0.281	0.24	
	0.25	0.037	0.193	0.16	
	0.2	0.035	0.125	0.099	

^a From fitting with Eq. (28).

^b From statistical mechanical computations, Ref. 8.

^c From measurement on vicinal surfaces Ref. 11.

Gilmer and Leamy measured¹⁰ the roughness of vicinal surfaces, and it is possible to extract values for γ_0 from their measurements. These results together with theoretical values found from Wulff's theorem and statistical thermodynamics⁸ are also shown in Table I. Both these computations have a static nature and we see that they agree rather close, especially at lower temperatures. The values, however, found from fitting growth curves or from direct measurements are of dynamic nature and are larger in general.

Turning next to the preexponential factor $(c_1 u_0)^{1/2}$, we see already from the values given in Table I that only those corresponding to relatively high values of $\bar{\omega}$ show a significant trend. This corresponds to the fact that one of the basic assumptions for the derivation of Eq. (24) (the growth of clusters takes place mainly by addition and subtraction of single cells) is not valid anymore. Therefore, we have some confidence in the values for $\bar{\omega} = 1.0$ and $\bar{\omega} = 1.125$ only. Now, $c_1 u_0$ is about 2.5 times smaller for $\bar{\omega} = 1.0$ than it is for $\bar{\omega} = 1.125$. This will be caused by a smaller adatom concentration (low-temperature series expansion predicts a factor of 1.65) and a smaller spreading velocity $u_0 \beta^2$. Finally, it can be mentioned that the preexponential factor found from direct measurements¹³ agrees in order of magnitude with the value given in Table I.

APPENDIX: THE SPECIAL PURPOSE COMPUTER

The SPC is able to carry out the simulations about 200 times faster than a general-purpose computer like the IBM 370/55. An important reason for this gain in time is that many operations occur parallel in the SPC. Moreover, the operating costs per unit of time are 100 times less.

The hardware model representing the 20×20 horizontal lattice describing the surface of a crystal has

been built up by integrated circuits. The height of the crystal at each position is stored in a shift register containing 400 four-bit binary numbers (four bits are sufficient to describe the maximal roughness of the crystal). With a shift register a fast change in the crystal surface can be obtained without the complication of proper addressing in random access memories. Shift registers can be "folded" to fill any two- or three-dimensional configuration. The four nearest neighbors of the n th position are found at positions $n-1$, $n+1$, $n-20$, and $n+20$. In such a way we introduce pseudoperiodic boundary conditions, see also Ref. 6. The way in which positions are chosen successively introduces some correlation between events on neighboring positions. To suppress this effect, all transition probabilities are multiplied with a factor smaller than 1, we took 0.4, and as a consequence 60% of the whole random-number field will never cause an event. The SPC is coupled to an IBM 1130 general-purpose computer which computes the transition probabilities. These probabilities are then stored in memories in the SPC.

The crystal-growth process is simulated as follows: first the number of neighbors of the n th cell is determined, the corresponding transition probabilities are compared with a random number, and it is decided in the usual way whether a transition takes place. Next, the shift register shifts one position and the whole pro-

cedure is repeated. The number of creations and annihilations are counted in two counters of the SPC. After having treated about 65 000 surface positions, these two numbers are transmitted to the IBM 1130 which computes the stick fraction. For each $\sum(\beta)$ point this sequence was repeated 2000 times.

- ¹T. L. Hill, *Statistical Mechanics* (McGraw-Hill, New York, 1956).
- ²K. Binder and H. Müller Krumbhaar, *Phys. Rev.* **B 9**, 2328 (1974).
- ³W. K. Burton, N. Cabrera, and F. C. Frank, *Philos. Trans. R. Soc. London A* **243**, 299 (1951).
- ⁴G. H. Gilmer and P. Bennema, *J. Appl. Phys.* **43**, 1347 (1972).
- ⁵H. J. Leamy, G. H. Gilmer, and K. A. Jackson, *Surface Physics of Materials*, edited by J. M. Blakeley (Academic, New York, 1975), p. 121.
- ⁶S. W. H. de Haan, V. J. A. Meeussen, B. P. Veltman, P. Bennema, C. van Leeuwen, and G. H. Gilmer, *J. Cryst. Growth* **24/25**, 491 (1974).
- ⁷P. Bennema and C. van Leeuwen, *J. Cryst. Growth* **31**, 3 (1975).
- ⁸C. van Leeuwen, *J. Cryst. Growth* **10**, 133 (1973).
- ⁹J. P. van der Eerden, *Phys. Rev. B* **13**, 4942 (1976).
- ¹⁰H. J. Leamy and G. H. Gilmer, *J. Cryst. Growth* **24/25**, 499 (1974).
- ¹¹G. H. Gilmer, H. J. Leamy, and K. A. Jackson, *J. Cryst. Growth* **24/25**, 495 (1974).
- ¹²J. P. van der Eerden, R. Kalf, and C. van Leeuwen, *J. Cryst. Growth* **35**, 241 (1976).
- ¹³C. van Leeuwen and J. P. van der Eerden, *Surf. Sci.* (to be published).

NUCLEATION GROWTH PROCESSES A MONTE CARLO SIMULATION

C VAN LEEUWEN and J P VAN DER EERDEN *

Laboratory of Physical Chemistry, Delft University of Technology, Delft, The Netherlands

Received 24 June 1976, manuscript received in final form 9 November 1976

We simulated the growth of a (001) Kossel crystal surface under nucleation growth conditions using the Monte Carlo technique. We obtained data for the nucleation rate, the spreading rate of supercritical clusters and the size of the clusters at the initial moment of spreading. These results are confronted with classical nucleation and nucleus theories. It was found that the small clusters in our simulations do not grow with a constant radial velocity, but proportional to their number of growth regions. It is shown that the diameter of the nucleus can be determined very well by simulating the ledge between two screw dislocations of opposite sign.

1 Introduction

At low temperatures the surface of a perfect crystal in equilibrium with a surrounding phase (vapour or solution) is almost flat, only a small concentration of adatoms and vacancies being present. If a small supersaturation is built up around the crystal, the number of adatoms will increase and the number of vacancies decrease. Also the larger number of adatoms will rearrange themselves and tend to form larger clusters. During this process nuclei will be formed: clusters with equal probability to grow and to dissolve. Larger clusters are more likely to grow (supercritical clusters) and smaller ones are more likely to dissolve (embryos).

At this point it should be noted that a general theoretical consideration of the kinetics of the nucleation process [1] revealed that the fluctuations of clusters whose size is rather close to the critical one n_0 (i.e. clusters in the so-called Zeldovich fluctuation region) show almost no tendency to grow or to dissolve. The largest cluster in the Zeldovich region we shall call growth cluster and we denote its size by n_+ , its formation time by τ_+ . Larger clusters will show a clear tendency to grow.

From this definition it follows that for kinetic effects, such as spreading of clusters and overall growth rate of the crystal, the growth clusters play the most important role. On the other hand, thermodynamic considerations will describe properties of the nucleus. By convention, throughout this paper we will use the subscript 0 for the nucleus and the subscript + for the growth cluster.

* Present address: RIM Laboratory of Solid State Chemistry, Catholic University of Nijmegen, Nijmegen, The Netherlands

A steady state production of nuclei will be reached if many nuclei are formed before one atomic layer is filled and, moreover, the concentration of supercritical clusters is small during the process. In this case the time τ between the formations of two nuclei is given by a Poisson probability distribution function P [2]:

$$P(\tau) = (1/\tau_0) \exp(-\tau/\tau_0) . \quad (1)$$

Here τ_0 is the average nucleation time. This time is related to the nucleation rate per unit area I and the total area A of the crystal surface by

$$\tau_0 = (IA)^{-1} . \quad (2)$$

In the simulation we study only the birth and spreading of the first few growth clusters. Therefore we measure the formation time of the first growth cluster instead of the time interval between two successive formations. In our case, however, the transient effects are negligible, such that we may assume that we have a Poisson process from the first beginning, and that the first formation time is equal to its time constant.

Another important parameter is the spreading velocity u of supercritical clusters, which is usually assumed to be related with the advance velocity of a straight step and the curvature of the edge of the supercritical cluster (eq. (34) in ref. [3]).

In 35 Monte Carlo experiments we investigated the supersaturation dependence of the number n_+ of particles in the growth cluster, the formation time τ_+ and the spreading velocity u . Comparisons between the properties of the nucleus and the growth cluster are given throughout the text. In 10 other experiments we investigated the influence of surface diffusion qualitatively.

Finally following a suggestion of Burton, Cabrera and Frank [3], we related the diameter of the nucleus with the metastable behaviour of a monatomic step on the surface, which connects two screw dislocations of opposite sign and with Burgers vectors 1 and -1 .

All experiments were carried out at a constant temperature which was only 22% below the roughening temperature [4]. The simulations can be seen as a test on the validity of the classical nucleation theories in the limit of small nuclei on relatively rough surfaces. Another reason for our investigations is the need of independent measurements of the processes during growth: nucleation, spreading of supercritical clusters and their coalescence in the final stage of filling a layer. These results can be combined to give an overall growth rate of the crystal, as measured, e.g. on a special purpose computer [5,6] built in Delft.

2. Simulation of the growth process

We use the same transition probabilities for addition, subtraction and diffusion of particles in the interface as Gilmer and Bennema [7]. All the experiments are carried out at a temperature T given by:

$$\omega = \phi/2kT = 1 , \quad (3)$$

where ω is the dimensionless energy parameter associated with a solid–fluid nearest neighbour bond [8], and ϕ is the standard bond energy. This temperature is far enough below the roughening temperature [4],

$$kT_R/\phi = 0.649 , \tag{4}$$

to show nucleation effects and not too low to remain within reasonable computation times. At this temperature measurable nucleation effects were found if the supersaturation parameter,

$$\beta = \Delta\mu/kT , \tag{5}$$

was chosen between 0.10 and 0.15, which corresponds to relative supersaturations between 10.5% and 16.2% for perfect solutions. In this region the nucleation times are so long that on the surfaces we used (with areas of 18×18 , 21×21 , 28×28 and 38×38 unit cells) usually no second nucleus is formed during the growth of the first supercritical cluster.

We applied periodic boundary conditions. This will affect the behaviour of the surface if one or more clusters are present whose size is of the order of magnitude of the total surface. Therefore, we usually stopped the simulation when 50% of the new layer was formed.

The time development of the number of particles in the largest cluster present on the surface, and of the total number of particles (coverage) is shown in fig. 1. The three stages of the nucleation process are readily visible. First the coverage increases from an initial value to the value in the metastable state, corresponding to the imposed supersaturation. This period corresponds to the transient time τ_t , after

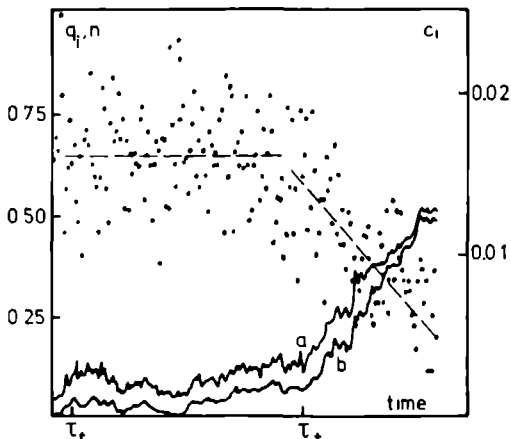


Fig. 1. Time development of the relative size n of the largest cluster relative to the total surface (b) and the coverage q_i (a). After a transient time τ_t a constant coverage remains till τ_+ . In this period the adunit concentration c_1 is about constant (dots, dashed line). This graph is typical for nucleation growth in our experiments: $\omega = 1.0$ $\beta = 0.12$, 40×10 matrix.

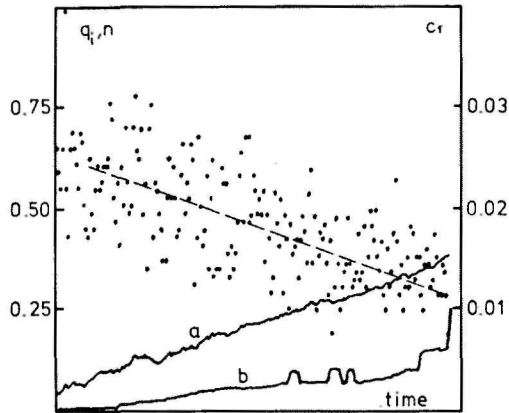


Fig. 2. Time development of the relative size n of the largest cluster (curve b) and the coverage q_i (curve a) under continuous growth conditions: $\omega = 1.0$, $\beta = 0.5$, 40×40 matrix.

which on a large surface steady state nucleation would take place. Then, during the metastable period, the number of particles in the largest cluster grows steadily till finally, at time τ_+ , this cluster becomes supercritical and starts growing rapidly. An unexpected feature of these curves is the linear time dependence of the area of a supercritical cluster, which contradicts the usual assumption that growth is proportional to the perimeter of the cluster.

Increasing the supersaturation, the nucleation time decreases until at a transition value β^* the growth gets a continuous character (normal growth). An example is shown in fig. 2. The largest cluster curve remains far below the coverage curve, indicating that many clusters are formed at the same time. Finally, all these clusters coalesce and the layer is filled.

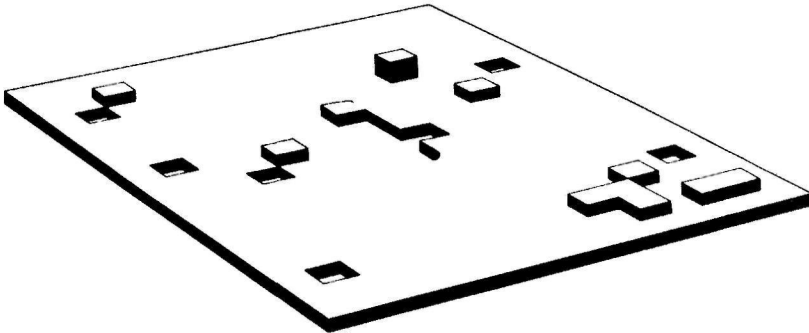


Fig. 3. Surface obtained after 100 creations per site for $\omega = 1$ and $\beta = 0.07$. The distance between the screw dislocations is $d = 5$. Initially, the surface was flat and the edge straight. Clearly, the nucleation barrier has not yet been passed.

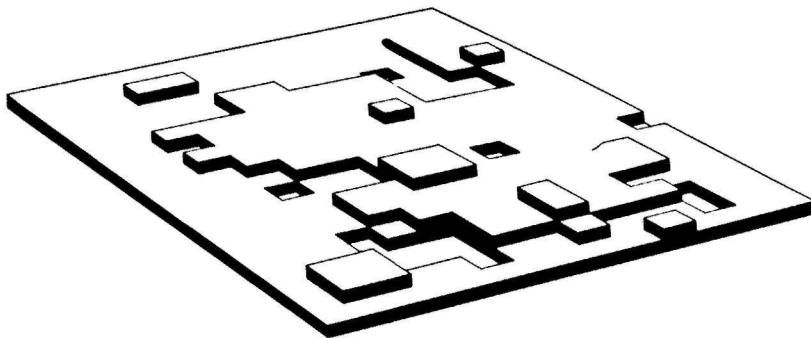


Fig. 4. Surface obtained after 100 creations per site for $\omega = 1$ and $\beta = 0.07$. The distance between the screw dislocations is $d = 12$. Initially, the surface was flat and the edge straight. A considerable spreading of the ledge as compared to fig. 3 can be seen.

As mentioned in the introduction we also measured the nucleation process of a ledge connecting two screw dislocations. We introduced the dislocations (opposite sign, Burgers vector 1 and -1 , no strain at the center) by defining neighbours of the cells surrounding the dislocations in a proper way. In figs. 3 and 4 dislocations on the surface are shown with distances smaller and larger than the diameter of the nucleus, respectively. The figures illustrate that after elapsing of the same physical time the initially straight ledge grows immediately only, when the distance between the two dislocations exceeds a critical value. It turned out to be possible to determine the diameter of the nucleus with this method more accurately in less computation time.

For the interpretation of the simulation results we shall use the average number of collisions of particles onto the area of one unit cell as time parameter. Usually [6] this parameter is proportional to the physical time.

3. The size of the nucleus and the growth cluster

The number n_+ of particles in the growth cluster is estimated directly as the size of the largest cluster at the moment τ_+ (see fig. 1). The Wulff theorem and the Gibbs–Thomson formula [3,9] predict $n_0\beta^2$ to be constant. In fig. 5 we give n_+ versus β^{-2} . The proportionality constant found is

$$n_+\beta^2 = 0.39 \pm 0.07 . \quad (6)$$

The introduction of surface diffusion gives only a minor deviation from eq. (6), which is in agreement with the thermostatic character of the fluctuation region. The tendency that n_+ is smaller if there is surface diffusion indicated that diffusion brings the system closer to thermostatic equilibrium.

The diameter of the nucleus can be found from the behaviour of a step connect-

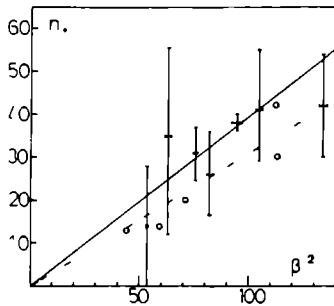


Fig 5 The number of particles n^+ in the growth cluster in dependence of β^{-2} $\omega = 1$, (+) without surface diffusion, (o) with surface diffusion, $x_s = 1$ [7]

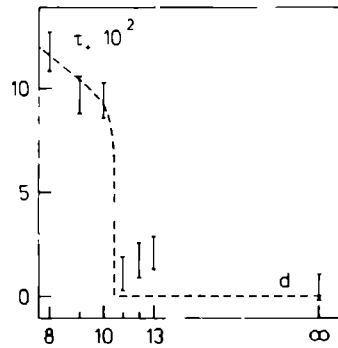


Fig 6 A step between two screw dislocations of opposite sign starts growing almost immediately when the distance d between the dislocations exceeds a critical value, $\omega = 1$, $\beta = 0.0488$, growth kinetics as discussed in ref [19] to keep β constant The horizontal scale is linear in d^{-1}

ing two screw dislocations of opposite sign Such a system will have a time lag for growth only if the distance between the dislocations is smaller than the diameter of the nucleus [3] Fig 6 gives this time lag for $\beta = 0.05$ and the critical diameter is $d_0 = 10.5 \pm 0.5$ At $\omega = 1.0$ the nucleus is assumed to be almost circular [9] and we find

$$n_0 \beta^2 = 0.21 \pm 0.02, \quad (7)$$

which agrees with the value 0.20 given by Wulff's theorem [9] The value β^* for which each particle is a nucleus is found from (7)

$$n_0(\beta^*) = 1 \rightarrow \beta^* = 0.45 \pm 0.03 \quad (8)$$

To confront the transition value for β with the results of our nucleation measurements we put $n_+ = 2$ in eq (6) as the size of the growth cluster is two when the size of the nucleus is unity The result,

$$\beta^* = 0.44 \pm 0.04, \quad (9)$$

is in agreement with the value obtained above (eq (8)) Both are smaller than the supersaturation $\beta = 0.9$, which corresponds to the change over from nucleation growth to continuous growth as detected from measurements on the special purpose computer [6] However, determining this transition involves taking a limit, and a necessary approximation tends to overestimate this transition value

Finally we can remark, that we find that the number of particles in a growth cluster is almost twice the number in the nucleus This same factor was also estimated in the theoretical consideration about the kinetics of the process [1]

4. The nucleation rate

In fig. 1, the time which the crystal surface needs to reach the metastable structure is much shorter than the nucleation time. This is the case for all our experiments. We can therefore neglect the transient time and assume that the probability of a nucleation time τ is given by eq. (1). Although the surface is so small that in general not more than one or two nuclei are formed, the average nucleation time τ_0 is related to the steady state nucleation rate by eq. (2).

In general a nucleus is built up by reactions between all types of clusters which are present on the surface. Although it will turn out that additions of clusters to other clusters are important for the spreading of clusters we shall assume that the main contribution to the growth of clusters comes from the addition of single atoms to the clusters. This assumption is justified a posteriori because the effect of clusters is mainly to induce new growth regions (see section 5), where again single atoms are added.

Defining c_n as the concentration of clusters containing n particles, the steady state nucleation rate is given by

$$I = p_n^+ c_n - p_{n+1}^- c_{n+1}, \quad n = 1, 2, \dots, \quad (10)$$

where p_n^+ and p_n^- are the probabilities that one atom is added to or subtracted from a cluster of n particles.

The set of linear equations for the c_n , eq. (10), can be solved [10] if the transition probabilities p_n^+ and p_n^- are given. These transition probabilities should at least satisfy the condition

$$p_n^+ / p_{n+1}^- = \exp[\Delta G(n) - \Delta G(n+1)], \quad (11)$$

where $\Delta G(n)$ is the increase in Gibbs free energy (in units of kT) of the system when n particles from the ambient phase form an n -cluster on the surface, i.e. $\Delta G(1) = 0$. To solve the set (10) we multiply the n -th equation with a factor

$$\frac{\exp[\Delta G(n) - \Delta G(1)]}{p_n^+} = \frac{p_2^- \dots p_n^-}{p_1^+ \dots p_n^+}. \quad (12)$$

Summing all resulting equations gives for the boundary condition $c_\infty = 0$:

$$I \left\{ \sum_{n=1}^{\infty} 1 / [p_n^+ \exp(-\Delta G(n))] \right\} = c_1. \quad (13)$$

When $\Delta G(n)$ has a maximum for $n = n_0$, the n_0 -th term gives the major contribution to the sum in eq. (13). Combining the contributions of all other terms in one factor Z , the Zeldovich factor, one gets:

$$I = Z p_{n_0}^+ c_1 \exp(-\Delta G(n_0)). \quad (14)$$

In most cases n_0 is so large that ΔG can be conceived as a differentiable function.

Frenkel [11] was the first to show that under this condition the Zeldovich factor is given by

$$Z^2 = - \frac{1}{2\pi} \left. \frac{\partial^2 \Delta G}{\partial n^2} \right|_{n=n_0} \quad (15)$$

So far the reasoning is general for two- and three-dimensional nucleation. For two-dimensional nucleation eq. (15) can be written as [10,12]

$$Z^2 = \Delta G(n_0)/4\pi n_0^2. \quad (16)$$

Upon specifying a model for nucleus formation we assume $p_{n_0}^+$ to be proportional to the perimeter e_0 of the nucleus and to the creation probability k^+ of single atoms:

$$p_{n_0}^+ = k^+ e_0. \quad (17)$$

Assuming the usual [3] parabolic dependence of ΔG on \sqrt{n} , we find a relation between the free energy and the size of the nucleus

$$\Delta G(n_0) = \beta n_0. \quad (18)$$

The Gibbs–Thompson relation [9] connects the specific edge free energy γ_0 of the nucleus with its dimensions:

$$2n_0\beta = e_0\gamma_0. \quad (19)$$

Combining eqs. (14)–(19) we find the following expression for the nucleation rate:

$$I/k^+ = (1/\xi_2) c_1 \sqrt{\beta} \exp(-\pi\gamma_0^2/\beta\xi_2^2), \quad (20)$$

where we used the shape factor

$$\xi_2 = 2\sqrt{\pi n_0}/e_0, \quad (21)$$

which was introduced in ref. [9]. The nucleation time is now found from (2):

$$A\tau_0 = (\xi_2/c_1) \beta^{-1/2} \exp(\pi\gamma_0^2/\beta\xi_2^2). \quad (22)$$

$A\tau_0$ is the total number of creations necessary to form a nucleus, independent of the size of the system. This corresponds to the fact that the physical time interval between the appearance of nuclei is inversely proportional to the size of the system. Since in the steady state I is independent of n (cf. eq. (10)), it follows that $\tau_+ = \tau_0$.

We measured the number N^+ of creations to form the first growth cluster for several system sizes. The results are presented in fig. 7. To interpret these data we assume that N^+ has the same β dependence as $A\tau_0$, i.e.

$$N^+ = (\beta^{-1/2}/c_1) \exp(\pi\gamma_0^2/\beta). \quad (23)$$

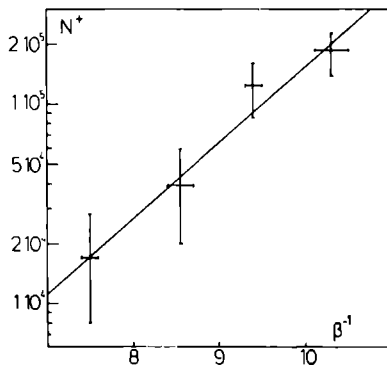


Fig. 7. The β^{-1} dependence of the number of creations required to form a growth cluster, i.e. to reach τ_+ in fig. 1: $\omega = 1$.

Note that we put $\xi_2 = 1$. This is a good approximation when $\omega = 1$ [9]. We find $\gamma_+ = 0.52 \pm 0.05$,

$$(24)$$

$$c_1 = 0.12 \pm 0.15.$$

$$(25)$$

The monomer concentration can only be found in order of magnitude because it follows from an extrapolation of the curve in fig. 7 and depends very sensitively on the slope of this curve. Nevertheless, the order of magnitude is correct. The value of γ_+ is considerably larger than the specific edge free energy $\gamma_0 = 0.22$, computed [9] for the nucleus. The measurements of the overall growth rate, carried out on the special purpose computer [6] also indicate a higher value of γ_0 than the theoretical one, but lower than the value γ_+ we found here. This result indicates that the growth cluster has a more rough periphery than the nucleus. This is not unexpected because the nucleus is in the Zeldovich fluctuation region and has therefore time to get the equilibrium shape (i.e. to reach thermodynamic equilibrium with the surrounding interface). The growth cluster, on the other hand, has a growth shape.

5. The spreading of a supercritical cluster

As stated in section 4 a supercritical cluster grows mainly by the addition of single atoms. If, during this process the cluster would have a constant shape, then the number of particles in the cluster would increase quadratically in time. However, in our measurements we always find a linear dependence:

$$n(t) = n_+ + u(t - \tau) \quad \text{for } t > \tau, \quad (26)$$

where τ is the observed nucleation time and u the spreading velocity. Moreover, the observed values of u show a very large scatter if one assumes that u depends on β only (see fig. 8).

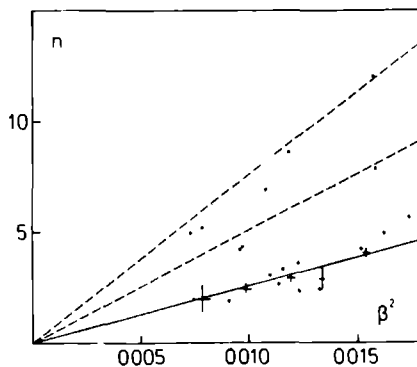


Fig 8 The area increase of a growing cluster per time unit \dot{n} appears to be proportional to β^2 . The three proportionality constants are interpreted as being due to the number of growth regions. The dots correspond to the overall slope in figures like fig 1, 2 and 10. $\omega = 1$. Points marked with a cross resulted as averages after division of data by 1, 2 or 3.

A more thorough inspection of these measurements suggests that they can be divided in groups with a considerably smaller scatter. Indeed, assuming equidistant levels u , $2u$ and $3u$ gives a decrease of the standard deviation per point from 71% to 30%. Of course, other probability distributions of the spreading velocities would

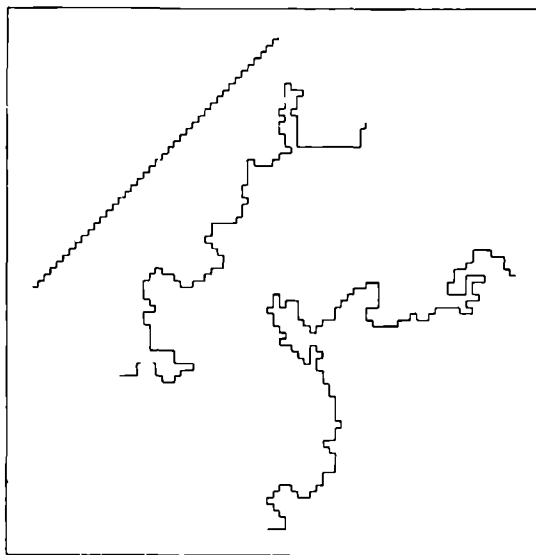


Fig 9 The time development of an initially "straight" $\langle 11 \rangle$ step, which is constrained by the boundary conditions on a 40×60 matrix. $\omega = 1$, $\beta = 0.1$. Step patterns after 100 and 200 creations per site show the tendency to facet during growth.

also show a decrease in the standard deviation with this procedure, but e.g. a Gaussian or a uniform distribution would give a decrease to only 59% or 60% respectively

Both these observations are in contradiction with the classical assumptions. Therefore, we propose the following alternative. The advance velocity of any curved edge is controlled by two different mechanisms: (i) the edge tends to form facets and (ii) the growth takes place mainly in concave parts of the step (growth regions). The first assumption is supported by the behaviour of a step which was originally straight, along the (11) direction. The tendency to form facets is clearly visible in fig. 9.

If the tendency to form facets is also present on the edge of supercritical clusters, it is clear that usually only a few concave parts can be present, due to the small dimensions of the clusters. In view of assumption (ii) we can associate now the growth levels with the presence of one, two or three growth regions on the edge of the cluster.

Also a third observation which cannot be understood by the classical treatment is now easily explained. In fig. 10 we show the growth of two supercritical clusters where discontinuities in the spreading velocity are seen. One cluster first grows rapidly, then very slowly (disappearance of a growth region) and after some time it starts growing again (appearance of a new growth region). The other cluster first grows by a certain spreading velocity and at a certain time this velocity increases abruptly with a factor 2 (addition of a new growth region).

Finally, it should be noted that growth regions will become filled up after some time. However, addition of other relatively small clusters will in general induce faceting and therefore add one or two new growth regions.

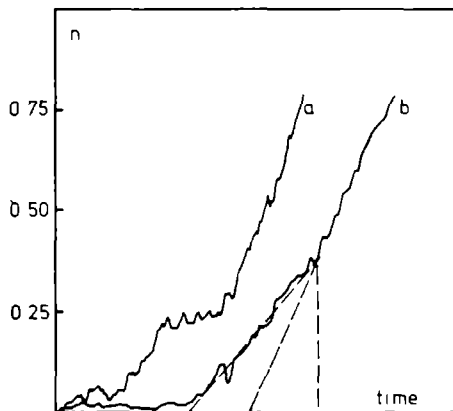


Fig. 10 Time evolution of the size (n) of the largest cluster. It can be seen that spreading may stop for a while (curve a: disappearance of the growth region) or that the spreading rate increases by a factor 2 (curve b: appearance of a second growth region). (a) $\omega = 1$, $\beta = 0.125$, 40×40 matrix, (b) $\omega = 1$, $\beta = 0.1$, 40×40 matrix.

In the case of surface diffusion we find qualitatively the same behaviour, but all levels are about a factor 5.4 higher (for $x_s = 1$)

6. The growth rate

In the previous sections we obtained numerical data for the rate of nucleus formation and the spreading velocity of supercritical clusters. Here we will compare these data with the average (overall) growth rates obtained from Monte Carlo simulation experiments with a hardware model [6]. Kolmogoroff [13] and Avrami [14] considered the problem of covering a flat surface by spreading of point-nuclei ($n_+ = 0$), formed with a rate $I(t)$ (per unit area), also accounting for coalescence in the advantage stages of the process. In the Russian translation of his book, Vetter [15] showed that this theory can be extended to a multi-layer model. Generalizing his approach, we assume that at the moment t the coverage of the n -th layer is $q_n(t)$, satisfying

$$q_n(t) \geq q_{n+1}(t) \quad (\text{solid on solid condition}), \quad (27)$$

and

$$q_\infty(t) = 1 \quad \text{and} \quad q_0(t) = 0. \quad (28)$$

The $\{q_n(t)\}$ satisfy a set of coupled equations

$$q_{n+1}(t) - q_{n+1}(0) = [q_n(0) - q_{n+1}(0)] F(t, 0) + \int_0^t \frac{\partial q_n}{\partial \tau} F(t, \tau) d\tau, \quad (29)$$

where

$$F(t, \tau) \equiv 1 - \exp\left[-\int_\tau^t I(t') A(t' - \tau) dt'\right]. \quad (30)$$

In the Avrami–Kolmogoroff equation (eq. (30)), $A(t' - \tau)$ is the area covered at t' by spreading of a free growing cluster formed at τ . Hence eq. (29) reads: the coverage of the $(n + 1)$ -th layer at t with respect to its coverage at $t = 0$ is due to covering already existing – but not covered – area at $t = 0$ and in addition due to covering area formed in the n -th layer during the interval $(0, t)$.

Summation of all equations (29), using the boundary condition eq. (28) and the definition of the growth rate $R(t)$

$$R(t) = \sum_n \partial q_n / \partial t, \quad (31)$$

immediately gives

$$\int_0^t R(\tau) [1 - F(t, \tau)] d\tau = F(t, 0). \quad (32)$$

If the process physically converges in time to a steady state growth rate R , then R can be found from eq. (32) since the integrand is only sufficiently large if τ is close to t :

$$\lim_{t \rightarrow \infty} R \int_0^t \{1 - F(t, \tau)\} d\tau = 1. \quad (33)$$

Upon assuming a stationary nucleation process and some powerlaw for the spreading of a supercritical cluster, i.e.,

$$I(t')A(t' - \tau) = Ia(t' - \tau)^m, \quad (34)$$

with a and $m \geq 0$ constants, eq. (33) becomes:

$$R_m = \frac{m+1}{\Gamma[1/(m+1)]} \left(\frac{aI}{m+1} \right)^{1/(m+1)}, \quad (35)$$

where Γ denotes the gamma function. The exponent m distinguishes different types of growth kinetics: $m = 0$ layers are filled by deposition of nuclei of size $n_0 = a$, which do not grow (poly-nuclear model [16]). This is in conflict with the assumption of point-nuclei and indeed the same result is obtained as in a model disregarding coalescence [17]. The steady state growth rate is given by

$$R_0 = In_0. \quad (36)$$

$m = 1$ the area of point-nuclei increases linearly with time, i.e. cf. eq. (26)

$$\frac{dn}{dt} = u. \quad (37)$$

This gives

$$R_1 = 0.789 (Iu)^{1/2}. \quad (38)$$

$m = 2$ this case was also found by Stoyanov [18] who used another approach. The area of point-nuclei increases quadratically with time. This corresponds to the classical case of spreading of (circular) nuclei with a constant radial velocity v . The steady state growth rate in this case becomes

$$R_2 = 1.137 (Iv^2)^{1/3}. \quad (39)$$

By relating the separately determined constants I and a obtained above with the overall growth rate obtained before [6], we can determine the type of growth kinetics, independent from any specific assumption about the supersaturation dependence of the nucleation rate and the constant a .

It is seen in table 1 that for low supersaturations the power $m = 1$ gives the best correspondance. At higher supersaturations, however, this power law predicts a too high growth rate. We interpret this as follows. At low supersaturations there is a strong tendency to form faceted clusters because the average length of facets is at

Table 1

Determination of the growth mechanism ($m = 0, 1$ or 2) by comparing R_m , as calculated from our data, with the overall growth rate R obtained with the SPC, clearly, $m = 1$ gives the best correspondence

β	0 10	0 11	0 12	0 13	0 14	0 15
$10^3 I/k^+$	0 0065	0 0147	0 0278	0 0500	0 0800	0 111
n_0	39	33	27	23	20	17
R_0/k^+	0 00025	0 00049	0 00075	0 0012	0 0016	0 0019
u/k^+	4 0	5 0	6 2	7 8	9 6	12 0
R_1/k^+	0 0041	0 0068	0 011	0 016	0 022	0 029
v^2/k^{+2}	0 0054	0 0080	0 014	0 022	0 034	0 051
R_2/k^+	0 00037	0 00055	0 00083	0 00116	0 0016	0 0021
R/k^+	0 0034	0 0051	0 0082	0 0093	0 0110	0 0144

least of the order of the linear dimensions of the clusters, and the spreading velocity is so small that these facets remain present on the growing cluster. At high supersaturations, however, the spreading is so fast that a constant average shape results.

Acknowledgement

The authors wish to express their gratitude to Dr D Kashchiev for many clarifying discussions.

References

- [1] J B Zeldovich, *Acta Physicochim URSS* 18 (1943) 1
- [2] S Toshev, A Milchev and S Stoyanov, *J Crystal Growth* 13/14 (1972) 123
- [3] W K Burton, N Cabrera and G C Frank, *Phil Trans Roy Soc (London)* A243 (1951) 299
- [4] J P van der Eerden, *Phys Rev* B13 (1976) 4942
- [5] S W H de Haan, V J A Meeussen, B P Veltman, P Bennema, C van Leeuwen and G H Gilmer, *J Crystal Growth* 24/25 (1974) 491
- [6] J P van der Eerden, C van Leeuwen, P Bennema, W L van der Kruk and B P Veltman, *J Appl Phys*, to be published
- [7] G H Gilmer and P Bennema, *J Appl Phys* 43 (1972) 1347
- [8] C van Leeuwen, *J Crystal Growth* 19 (1973) 133
- [9] C van Leeuwen and P Bennema, *Surface Sci* 51 (1975) 109
- [10] A C Zettlemoyer, *Nucleation* (Dekker, New York, 1969)
- [11] J I Irenkel, *Kinetic Theory of Liquids* (Dover, New York, 1955)
- [12] J P Hurth *Acta Met* 7 (1959) 755
- [13] A N Kolmogoroff, *Bull Acad Sci URSS (Sci Math Nat)* 3 (1937) 355
- [14] M Avrami, *J Chem Phys* 7 (1939) 1103, 8 (1940) 212, 9 (1941) 177
- [15] K Vetter, *Elektrochimische Kinetika* (Khimiya, Moscow, 1967) p 348
- [16] M O'Hara and R C Reid, *Modelling Crystal Growth Rates from Solution* (Prentice Hall, London, 1973)
- [17] W B Hillig, *Acta Met* 14 (1966) 1868
- [18] S Stoyanov, *Commun Dept Chem Bulg Acad Sci* 3 (1970) 491
- [19] C van Leeuwen, R Janssen van Rosmalen and P Bennema, *Surface Sci* 44 (1974) 213

EVAPORATION AT HIGH UNDERPRESSURE CONFRONTATION OF THEORY AND EXPERIMENT

J P VAN DER EERDEN, R L KALF and C VAN LEEUWEN

Laboratory of Physical Chemistry, Delft University of Technology, Delft, The Netherlands

Received 15 May 1976

A pair approximation model was used to describe the kinetics of an evaporating crystal. Relaxation effects were induced by suddenly suppressing the incident flux of particles towards the surface.

It was pointed out [1] that the molecular beam method is one of the most convenient possibilities to compare theory and experiment in crystal science. The purpose of the model computations described in this paper is to study the behaviour of evaporating crystals at high underpressure and to test the relevance of the pair approximation model for evaporation. We particularly wanted to study the relaxation effects, which occur when the condensation on a surface in equilibrium is suddenly suppressed. From the experiments of Dabringhaus and Meyer [2–4] we expect to find that the growth rate versus time curves show a damped oscillating behaviour.

Dabringhaus and Meyer used the molecular beam method to study these effects. A crystal is placed in a heated holder in a vacuum chamber. Then the crystal is brought in equilibrium by inserting particles of the same chemical composition on the surface. When this molecular flux is suddenly dropped to zero free evaporation takes place. The flux from the crystal is recorded to give the evaporation rate.

To simulate these experiments we used the pair approximation model. For a simple cubic lattice with nearest neighbour interaction this pair approximation model consists of a set of coupled differential equations, describing the changes on the crystal surface. We exclude overhangs, thus allowing the surface configuration to be specified by the number of atoms in each column. The influence of neighbouring columns on the evaporation probability is given by a second-order approximation. The model is described in detail by Gilmer, Leamy and Jackson [5]. Comparison of Monte

Carlo simulations of crystal growth shows in general an excellent agreement with the results of the pair approximation if the surface is relatively rough [6]. Additional measurements for evaporation (unpublished data) show the same tendency. Especially, for the temperatures we are dealing with in this paper, the pair approximation describes the processes on the crystal surfaces accurately.

The behaviour at the crystal surface is controlled by the transition probabilities. For adatoms we have a creation probability k^+ and an annihilation probability k^- . For other surface atoms the annihilation probability depends on the number of bonds with neighbours. These transition probabilities can be calculated from two parameters: (i) $\beta = \Delta\mu/kT$, where $\Delta\mu$ is the difference in chemical potential induced by the supersaturation, and (ii) an energy parameter ω . The lattice energy in our model is given by $6kT\omega$ and we will equate this to the experimental heat of evaporation, even for ionic crystals like potassium chloride. From these parameters the transition probabilities can be calculated using the formulas

$$k^+ = 1/[1 + \exp(4\omega - \beta)], \quad (1)$$

$$k^- = 1/[1 + \exp(\beta - 4\omega)] \quad (2)$$

These are the normalized transition probabilities given by Gilmer and Bennema [7].

At small underpressure the evaporation rate varies periodically, each period corresponding to the evaporation of one atomic layer. If the underpressure in-

creases the amplitude of this oscillation decreases, whereas at very high underpressures the oscillations damp out completely.

We also measured the thickness of the interface, i.e. the standard deviation in the height of the surface. At small values of $|\beta|$ the thickness of the interface oscillates with the same frequency as and in the same phase with the growth rate, while at high values of $|\beta|$ the thickness of the interface increases steadily. At high interface thicknesses the surface is very rough and more layers are growing at the same time. The growth of one layer is not necessarily in phase with the growth of others, which explains why no oscillations are found. The main difference is that in case of evaporation oscillations occur at higher values of $|\beta|$, because at negative β terraces are formed (cf. fig. 1).

All computations were carried out at $\omega = 0.875$ and $\omega = 1.000$, which for potassium chloride corresponds to temperatures of 600 and 500°C, respectively. The experiments were carried out at temperatures ranging from 400 till 300°C. Our computations were performed at somewhat higher temperatures to save computation time.

Both the experiment and the simulation can be divided into three parts: We started with a completely flat surface at equilibrium pressure until the equilibrium structure was reached. At time t_1 the creation probability k^+ was suddenly suppressed to $k^+ = Sk_{eq}^+$, where S is the saturation ratio. After the evaporation of a few monolayers a steady state evaporation rate was reached. Finally, at time t_2 , the creation probability was changed to k_{eq}^+ again.

As will be shown below, eq. (4), the physical evaporation coefficient α is proportional to the ratio Σ of the

number of evaporated atoms and the number of atoms evaporating from a kink site, both per unit time. The latter number equals the number of creations at equilibrium and therefore is independent of the saturation ratio.

Immediately after the creation probability is dropped, rapid evaporation occurs, because at first all the isolated adatoms evaporate (cf. figs. 2 and 3). Then we have a very flat surface and thus very slow evaporation. During the evaporation of the first atomic layer the surface roughness increases until this layer is completely evaporated and the surface again is rather flat and therefore evaporation is slow. Nevertheless, the amplitude of the oscillation decreases, because the surface will never be as flat as at the start of the evaporation. After some cycles a steady state value of the amplitude is reached. At very high undersaturation the amplitude converges to zero. Fig. 4 shows that the decrease in the amplitude of the physical evaporation coefficient depends linearly on the saturation ratio S . The mean value of α is almost independent of S . In fig. 4 the effect of temperature changes is shown. At the lower temperature the steady state amplitude is higher. Also the critical saturation ratio, below which no oscillations are found, will be lower at lower temperatures. This could be expected, since the surface is flatter at lower temperatures.

After the creation probability is changed to k_{eq}^+ , during a short period of time the crystal grows rapidly. Thereafter the growth rate returns to its equilibrium value. The height of the growth peak depends on the configuration of the interface: the rougher the surface, the higher the growth peak. On a very rough surface many holes can be filled up, while on a flat surface less

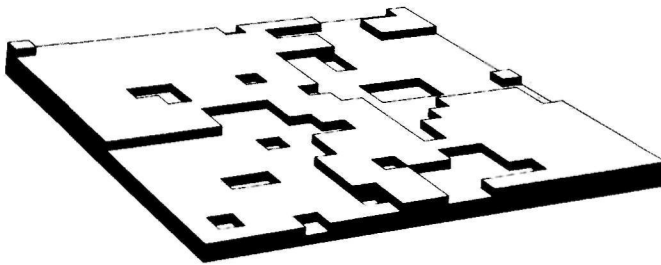


Fig. 1. Structure of the surface after the evaporation into vacuum of six atomic layers in a Monte Carlo simulation ($\omega = 1.0$).

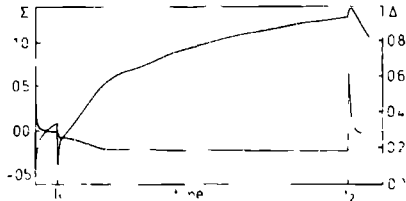


Fig. 2. Stick fraction (curve a) and interface thickness (curve b) versus time (arbitrary units), at high underpressure ($\omega = 0.875$ and $S = 0.0001$).

holes are present. For the same reason the growth peak is higher at lower saturation ratios.

Dabringhaus and Meyer defined the evaporation coefficient by

$$\alpha = -\Delta / (j_{on} - j_{on,eq}), \quad (3)$$

where Δ is the fraction of the incident molecules that remains on the surface, j_{on} is the flux onto the surface and $j_{on,eq}$ is the flux onto the surface to reach equilibrium. Using the definitions α can be related to Σ by the formula

$$\alpha = \Sigma / (S - 1). \quad (4)$$

The incident beam can be regulated by a shutter, which corresponds to a change in the creation probability in our model. If we compare the results of our computations with the result from Dabringhaus and Meyer's experiments, we see that, apart from the growth peak after the shutter is opened again, there is a good qualitative agreement. However, there are three quantitative differences:

(a) The relaxation time in the molecular beam experi-

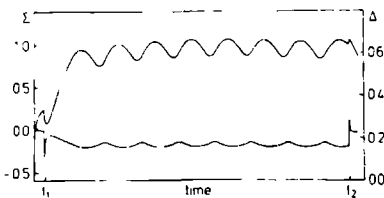


Fig. 3. Stick fraction (curve a) and interface thickness (curve b) versus time at intermediate underpressure ($\omega = 0.875$ and $S = 0.2$).

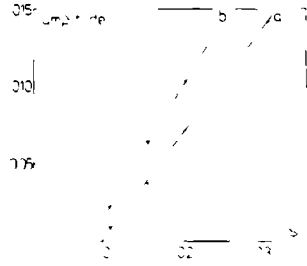


Fig. 4. Steady state amplitude of α versus the saturation ratio at two different temperatures, (a) $\omega = 0.875$ and (b) $\omega = 1.000$.

ments is longer. This is because at the lower temperatures in the experiments the surface is more flat. This means that it takes a longer time for the surface to roughen up. Also in our simulations we found a longer relaxation time at the lower temperature.

(b) The experimental oscillations have a larger amplitude. This is partially due to the influence of lower temperatures in the experiments. This is in agreement with our simulations (cf. fig. 4). This effect is amplified by the back stress effect [8,9]. The adatoms on the surface probably have a large mean diffusion distance [10]. Therefore it is difficult to form a new hole nucleus when the first layer has not yet evaporated, because the adatoms can easily fill up a newly formed hole.

(c) The oscillation does not damp completely in the experiments. The oscillations would damp if several atomic layers were evaporating at the same time. The back stress effect tends to keep all parts of the surface in phase. Also a small remaining vapour pressure would stabilize the oscillations.

Therefore we have carried out some simulations at saturation ratios not equal to zero (i.e. corresponding to a small remaining vapour pressure). Under these conditions we found that the oscillation does not damp completely (cf. fig. 3). In fig. 5 we see that the amplitude decreases to a steady state value at higher saturation ratios, but the amplitude decreases steadily to zero at $S = 0$.

After the shutter is opened again, corresponding to changing $k^+ = Sk_{eq}^+$ to $k^+ = k_{eq}^+$ Dabringhaus and Meyer find no growth peak. This may be attributed to a flatter surface at lower temperatures, too.

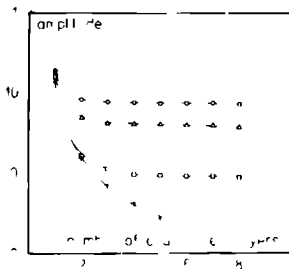


Fig 5 The amplitude of Σ versus the number of evaporated layers for various underpressures; $\omega = 0.875$ and (a) $S = 0.20$, (b) $S = 0.15$, (c) $S = 0.10$, and (d) $S = 0.00$

From the molecular beam experiments, our model computations and the surface structure from Monte Carlo simulation (cf fig 1) we expect the evaporation mechanism to be the spreading of holes (German Lochkeimbildung). A few holes (negative nuclei) are formed and on the edges of these nuclei evaporation takes place. The nuclei grow and eventually form several large holes. If one atomic layer has evaporated the process starts anew. At high underpressure in the first holes new nuclei can be formed, which is one reason why the oscillation damps out. Another reason for the damping of the oscillation is that the nuclei are not necessarily formed at the same time. At low underpressure a new nucleus is formed after one complete atomic layer has evaporated. However a relaxation effect can be observed at all underpressures. This is because the first vigorous evaporation is from the adatoms always present on an equilibrium surface. The first atomic layer

always evaporates at a slower rate, because the surface is very flat after the first vigorous evaporation, while after the evaporation of one atomic layer it is somewhat rough, except perhaps at very low underpressure. Even at very high undersaturation evaporation still takes place by spreading of holes. Contrary to evaporation, no nucleation has been observed on growing crystals at high overpressure. This is because it is easier to create an adatom on, than a vacancy in a flat surface.

The authors wish to thank Dr P Bennema for carefully reading the manuscript.

References

- [1] P Bennema and C van Leeuwen, *J Crystal Growth* 31 (1975) 3
- [2] H Dabringhaus and H J Meyer, *J Crystal Growth* 16 (1972) 17
- [3] H Dabringhaus and H J Meyer, *J Crystal Growth* 16 (1972) 31
- [4] H Dabringhaus and H J Meyer, *J Crystal Growth* 30 (1975) 225
- [5] G H Gilmer, H J Leamy and K A Jackson, *J Crystal Growth* 24/25 (1974) 495
- [6] J P van der Eerden, C van Leeuwen, P Bennema, W van der Kruk and B P Th Veltman to be published
- [7] G H Gilmer and P Bennema, *J Appl Phys* 43 (1972) 1347
- [8] N Cabrera and R V Coleman, in *The Art and Science of Growing Crystals* (Wiley New York, 1963) p 3
- [9] T Surek, J P Hirth and G M Pound, *J Crystal Growth* 18 (1973) 20
- [10] H Betge, K W Keller and E Ziegler, *J Crystal Growth* 3/4 (1968) 184

FAST GROWTH OF ORDERED AB CRYSTALS: A MONTE CARLO SIMULATION FOR IONIC CRYSTAL GROWTH

T.A. CHEREPANOVA

Computer Centre, Latvian State University, Riga, USSR

and

J.P. VAN DER EERDEN and P. BENNEMA

RIM Laboratory of Solid State Chemistry, Catholic University, Toernooiveld, Nijmegen, The Netherlands

Received 8 March 1978; manuscript received in final form 2 June 1978

We allow the cells of a Kossel crystal in contact with a fluid phase (F) to be of two different types, + or -. The model is determined by: (i) three energy parameters for the (+, -), (+, F) and (-, F) nearest neighbours, (ii) two supersaturation parameters in the solution, and (iii) two equilibrium frequencies for the attachment of new particles to the crystal. From physical experiments it is known that ionic crystals retain internally a regular (NaCl-like) structure, even if their surfaces are rough, which we found indeed. Different attachment frequencies will give rise to an excess number of one type of particles only at the surface. We investigated the supersaturation dependence of short and long range order parameters. At very high supersaturations the regularity of the crystal phase diminishes by the formation of small internally regular domains.

1. Introduction

During the last five years considerable progress has been made in the development of theories for crystal surfaces and crystal growth of Ising like models, employing Monte Carlo methods [1–12]. Crystal growth theories, developed for monocomponent crystals, have been applied even to such complicated systems as ionic crystals growing from the solution [13], both theoretically [14–16] and to explain experiments [17,18].

Chernov and Lewis [19–21] studied binary chain growth, which corresponds to step growth where exchanges of particles (attachment or detachment) take place at kink sites only. They showed that at small exchange frequencies the resulting crystal structure is regular whereas at larger frequencies it is disordered.

Cherepanova, Borisov, Shirin and Kiselev [22–27] removed the restriction of kink exchange and gave a more general description of the model which is applicable to growth from the melt. For the case of attrac-

tive interactions between all particles they obtained equilibrium and kinetic phase diagrams, and they studied interface properties (width, energy, roughness and atomic structure). They described quantitatively the degree of ordering in the crystal phase and in the interface with correlation functions and a short range order parameter.

Recently we derived [28,29] the transition probabilities for a multicomponent lattice gas. Here we obtain analogous results for a two component tetragonal crystal. Our purpose is to obtain qualitative and quantitative results for the growth and internal order of SOS crystals with nearest neighbour pseudo ionic interactions. Although equilibrium phase diagrams for such systems are not available our results show clearly that for our choice of interaction strength we are in a region where the crystal phase is well ordered in equilibrium, and this order can be broken only by very large supersaturations.

It is to be expected that our results apply qualitatively to the growth from solution of tetragonal ionic crystals with strong bonds in the growth direction.

Macroscopically this implies [30] that we consider the top faces of needle shaped crystals

2 The model

The model which we use belongs to a class of lattice gas models for crystal growth. We consider a cubic lattice of cells which may be fluid (f) or, if they are solid, of type a or b. As usual we adopt the solid on solid (SOS) restriction, such that an f cell is never below an a or b cell. The fluid phase is assumed to be completely homogeneous and each f cell represent its average. Although this is not essential, we assume that a and b cells contain only one particle.

The parameters of our model are nearest neighbour interaction ϕ^{pq} between two cells of type p and q (throughout this paper p and q are a, b or f) and two supersaturations $\Delta\mu_f^a$ and $\Delta\mu_f^b$. These are the deviations of the chemical potentials μ_f^a and μ_f^b of solvent a and b particles from that equilibrium solution where the attachment frequencies of both types are equal. We return to the question of different equilibrium solutions in the next section. It is well known [29] that the interactions ϕ^{pq} occur only in combinations ω^{ab} , ω^{af} and ω^{bf} , defined by

$$\omega^{pq} = \beta(\phi^{pq} - \frac{1}{2}\phi^{pp} - \frac{1}{2}\phi^{qq}), \quad (1)$$

where $\beta = 1/kT$ scales the energy. The total broken bond energy

$$\beta E^{bb} = N^{ab}\omega^{ab} + N^{af}\omega^{af} + N^{bf}\omega^{bf}, \quad (2)$$

where N^{pq} is the total number of neighbouring p and q cells in the system. Since the crystal contains no fluid cells all af and bf pairs are to be ascribed to be surface, ab pairs, however, are present inside the crystal as well. The contribution of these pairs to E^{bb} is conveniently described with parameters γ^a and γ^b (N^p is the number of p cells)

$$\gamma^p = \langle \partial N^{ab} / \partial N^p \rangle, \quad (3)$$

where $\langle \rangle$ denotes the ensemble average, to which only the bulk phase can contribute. The value of γ^p may vary between 0 for completely separated a and b phases and 3 for a completely ordered (NaCl) structure.

Using the thus defined parameters and the principle of microscopical reversibility, the general theory

gives us a relation between the frequencies k^{+p} and k^{-p} of attachment and detachment of p particles

$$k^{+p}/k^{-p} = \exp[\beta\Delta\mu_f^p - (I^{ab} - \gamma_{eq}^p)\omega^{ab} - I^{af}\omega^{af} - I^{bf}\omega^{bf}], \quad (4)$$

where I^{pq} is the decrease of the number of pq bonds during the detachment, and γ_{eq}^p is the value of γ^p in the equilibrium solution.

Let us discuss shortly some consequences of eq (4). When a and b particles are equal, eq (1) implies that $\omega^{ab} = 0$ and $\omega^{af} = \omega^{bf}$ such that eq (4) reduces to the well known relation for a 1 component crystal. If the crystal retains the equilibrium structure during growth then I^{ab} will be γ_{eq}^p on the average such that $\Delta\mu_f^p$ is the supersaturation $\Delta\mu^p$ which is felt by the particles (since $\langle k^{+p}/k^{-p} \rangle \equiv \exp \beta\Delta\mu^p$ and $\langle I^{af} \rangle = \langle I^{bf} \rangle = 0$). If the growing crystal, however, has a different structure, i.e. $\langle I^{ab} \rangle = \gamma^p \neq \gamma_{eq}^p$ then the definition of $\Delta\mu^p$, given above gives

$$\beta\Delta\mu^p = \beta\Delta\mu_f^p + (\gamma_{eq}^p - \gamma^p)\omega^{ab} \quad (5)$$

We may interpret $\Delta\mu^p$ as the effective supersaturation. We see that if the ordering in the growing crystal is less than in the equilibrium crystal then $\Delta\mu^p$ is smaller than the "applied" supersaturation $\Delta\mu_f^p$. Indeed, if $\omega^{ab} > 0$ then a and b phases tend to separate. Thus γ_{eq} is small and less order means $\gamma > \gamma_{eq} \approx 0$. If, on the other hand $\omega^{ab} < 0$ the crystal tends to an NaCl structure and less order means $\gamma < \gamma_{eq} \approx 3$. In the usual way [5,29] we have carried out Monte Carlo simulations for a model in which attachment and detachment of single particles are the only allowed processes.

As usual we assume that the attachment of a particle is not influenced by its future neighbours but only by the supersaturation $\Delta\mu_f^p$

$$k^{+p} = \frac{1}{2}\nu \exp \beta\Delta\mu_f^p, \quad (6)$$

and hence the detachment frequency is given by

$$k^{-p} = \frac{1}{2}\nu \exp[(I^{ab} - \gamma_{eq}^p)\omega^{ab} + I^{af}\omega^{af} + I^{bf}\omega^{bf}] \quad (7)$$

Here ν is the equilibrium attachment frequency for any type of particle.

From these two equations we see that the following parameters are necessary to carry out the simulations: (i) the three energy parameters ω^{ab} , ω^{af} and ω^{bf} , (ii) two supersaturation parameters $\Delta\mu_f^a$ and $\Delta\mu_f^b$ which

are chosen relative to a standard equilibrium state where $k^{+a} = k^{+b} = \frac{1}{2} \nu$. The constant ν fixes the time scale and does not enter the simulations itself but is necessary to relate dynamical results of the simulation model with physical systems, γ_{eq} is found self consistently with eq (3)

3. Physical relevance of the simulations

Our simplified model of the fluid phase allows in principle an interpretation as solution, melt or vapour. We omit, however, surface diffusion of crystal particles and to keep the fluid phase homogeneous, the volume diffusion has to be much faster than the integration of cells into the crystal. Therefore we think that our results may apply to growth from solution and possibly from melt. Of course, the neglect of more than nearest neighbour interactions (except an overall interaction to maintain the SOS condition) is also a major simplification.

We have chosen ion like interactions

$$\phi^{af} = \phi^{bf} = \phi^{ff} = 0, \quad \phi^{aa} = \phi^{bb} = -\phi^{ab} = kT, \quad (8)$$

or

$$\omega^{ab} = 4\omega^{af} = 4\omega^{bf} = -2, \quad (8a)$$

and equal characteristic frequencies for a and b particles

$$k_{eq}^{+a} = k_{eq}^{+b} = \nu \quad (9)$$

From the simulation results which we will present in section 4 it will be clear that under these conditions the equilibrium crystal structure is of the NaCl type so that we may take $\gamma_{eq}^a = \gamma_{eq}^b = 3$.

It turns out that the interface is very rough so that the solid on solid restriction is only justified if we may assume additional strong homopolar bonds in the vertical direction. Fortunately, such interactions, provided that they are equal between aa, ab and bb, particles do not change the basic kinetic equation eq. (4). As a matter of fact, if we would have allowed direction and distance dependent interaction energies ϕ_r^{pq} between pairs of cells which can be connected by a vector r , then eq (4) would have read [28]

$$\frac{k^{+p}}{k^{-p}} = \exp \left[\frac{\Delta\mu^p}{kT} \right]$$

$$- \sum_r \left[(I_r^{ab} - \gamma_r^p) \omega_r^{ab} - I_r^{af} \omega_r^{af} - I_r^{bf} \omega_r^{bf} \right], \quad (10)$$

where the subscripts r refer to analogous variables used previously. If we now add a homopolar vertical interaction ϕ to the isotopic ones in eq (1) we get

$$\phi_x^{pq} = \phi_y^{pq} = \phi_z^{pq} + \phi, \quad p, q = a \text{ or } b \quad (11)$$

Hence ω_z^{ab} is not affected but $\phi/2kT$ is subtracted from ω_z^{af} and ω_z^{bf} . However, due to the SOS restriction,

$$I_z^{af} + I_z^{bf} = 0 \quad (12)$$

Therefore eq (10) is in this case equal to eq (4) and the isotropic SOS model is apparently equivalent with a SOS model with additional strong vertical interactions, and such a model is in turn equivalent to an unrestricted model with strong vertical interactions. On the basis of the Hartman-Perdok theory [30] it is to be expected that such interactions lead to needle shaped crystal habits. A physical realization of our model may be, therefore, the top faces of gypsum crystals, where faceting disappears during growth from a highly supersaturated gel [31].

We define dimensionless growth rates R^p for p-particles as the number of p-cells which is added to the crystal per unit time (for which we chose the average time ν^{-1} between successive attachments of cells in equilibrium) and per side

$$R^p = \frac{N^{+p} - N^{-p}}{N^{+a} + N^{+b}} \left(\frac{1}{2} \exp \beta \Delta\mu_a^p + \frac{1}{2} \exp \beta \Delta\mu_b^p \right), \quad (13)$$

where N^{+p} and N^{-p} are the number of attached and dissolved p-particles during the simulation experiment. R^p is related to the growth rate V^p in m/sec and the lattice constant a by

$$R^p = V^p / \nu a \quad (14)$$

If the growth is stationary, the interface energy will be constant in time which, in view of eq (2), means

$$\langle I_{int}^{ab} \rangle_p \omega^{ab} + \langle I_{int}^{af} \rangle_p \omega^{af} + \langle I_{int}^{bf} \rangle_p \omega^{bf} = 0, \quad (15)$$

where $\langle \dots \rangle_p$ denotes the average over all exchanges (attachments and dissolutions) of p-particles. The total number of broken ab bonds is

$$\langle I_{int}^{ab} \rangle_p = \gamma^p + \langle I_{int}^{ab} \rangle_p, \quad (16)$$

therefore γ^p can be determined from the numbers of bonds broken during exchanges

$$\gamma^p \omega^{ab} = \langle l^{ab} \rangle_p \omega^{ab} + \langle l^{af} \rangle_p \omega^{af} + \langle l^{bf} \rangle_p \omega^{bf} \quad (17)$$

A geometrical argument [29] can be used to replace l^{af} and l^{bf} in eq (7) by l^{aa} and l^{bb} . In that case eq (4) would have been

$$\frac{k^{-p}}{k^{-p}} = \exp[\beta \Delta \mu_f^p + \gamma_{eq}^p \omega^{ab} + (2l^{pp} - 6) \omega^{pf} - l^{ab}(\omega^{ab} - \omega^{af} - \omega^{bf})], \quad (18)$$

where $k^{-p} = k^{-p}(l^{ab}, l^{pp})$ involves only solid solid bonds. This expression determines 2 attachment and 40 dissolution frequencies and was used in the simulations.

It can be noted that we can choose such interactions that the system reduces to 1-component crystal fluid. Indeed, if we choose $\phi^{aa} = \phi^{ab} = \phi^{bb}$ then $\omega^{ab} = 0$, $\omega^{af} = \omega^{bf} = \omega$, $\Delta \mu_f^p = \Delta \mu$ and eq (4) is the kinetic equation used e.g. by Gilmer and Bennema [4,5].

For growth from solution the driving force $\Delta G = \Delta \mu_f^a + \Delta \mu_f^b$ is given by the activities a^a and a^b of solvent particles. Indeed, equilibrium results if the product of a^a and a^b equals the solubility product I .

$$\beta \Delta \mu_f^a + \beta \Delta \mu_f^b = \ln[a^a a^b / (a^a a^b)_{eq}] = \ln(a^a a^b / I) \quad (19)$$

In order to find another relation for the $\Delta \mu_f^a$ and $\Delta \mu_f^b$ we employ the special equilibrium solution which we chose as a standard. Namely, we chose that solution for which both $\Delta G = 0$ and $k^{+a} = k^{+b}$. This led us to eq (6) and so

$$\beta \Delta \mu_f^a - \beta \Delta \mu_f^b = \ln(k^{+a}/k^{+b}) \approx \ln(v^a a^a / v^b a^b), \quad (20)$$

where v^a and v^b are the drift velocities of a and b particles respectively, quantities which are accessible to experimental determination. Upon combining eqs (19) and (20) we find

$$\beta \Delta \mu_f^a = \ln(a^a / \sqrt{I}) + \frac{1}{2} \ln(v^a / v^b), \quad (21)$$

$$\beta \Delta \mu_f^b = \ln(a^b / \sqrt{I}) + \frac{1}{2} \ln(v^b / v^a) \quad (22)$$

So we see that the splitting of the driving force (19) by the choice of a standard solution into parts for a and for b particles involves not only activities (first term in eqs (21) and (22)), but the relative mobilities as well.

In the case of growth from the melt the system is brought from the melting temperature T_{eq} to a lower temperature $T = T_{eq} - \Delta T$ which induces a supersaturation $\Delta \mu_f^p$, given by

$$\frac{\Delta \mu_f^p}{kT} = \frac{L^p \Delta T}{kT T} = \left[\frac{3(\phi^{ff} - \phi^{pp})}{kT} \gamma_{eq}^p \omega^{ab} \right] \frac{\Delta T}{T}, \quad (23)$$

where L^p is the heat of melting for a p particle. Eq (23), combined with the assumption of complete wetting ($\phi^{pf} = \phi^{ff}$) leads to the transition probabilities used in refs [22–25].

4 Simulation results

As mentioned in section 3, we used 10n like interactions for the simulations and equal equilibrium attachment probabilities for the two types of particles, whence we use the notation “+” and “-” for the solid particles. We studied the influence of the supersaturations $\Delta \mu^+$ and $\Delta \mu^-$ at constant temperature (i.e. constant ω^{+-} and $\omega^{+f} = \omega^{-f}$). We used a lattice of cells with periodic boundary conditions in the two lateral (x,y) directions, such that we got a surface of 18×18 lattice units. The height $k(r)$ of the crystal at r (a vector lying in the x-y plane whose length is measured in lattice units) could vary from 1 to 80. We used a flat ordered crystal face as starting configuration. Data of the first few layers were not used in order to avoid possible influence of the initial state.

The structure of the crystal/fluid interface is described with the correlation function $g(\Delta r)$ of the crystal heights at equal time, as suggested in ref [22].

$$g(\Delta r) = \frac{\langle \tilde{k}(r) \tilde{k}(r + \Delta r) \rangle}{\langle \tilde{k}(r) \rangle \langle \tilde{k}(r) \rangle} = \frac{\sum [k(r) - \langle k \rangle] [k(r + \Delta r) - \langle k \rangle]}{[k(r) - \langle k \rangle] [k(r) - \langle k \rangle]} \quad (24)$$

Here $\langle \rangle$ is the average over the surface, $k(r)$ is the deviation of k from the average value $\langle k \rangle$, the summation is over the $18(18 - \Delta r)$ lattice positions r which are such that both r and $r + \Delta r$ are within the system. In fig 1 we show the correlation function for $\Delta \mu_f^+ = \Delta \mu_f^- = 1.7 kT$ as an example, the vector Δr was chosen along the two coordinate axes. It is seen that the correlation length is very small, less than two lat-

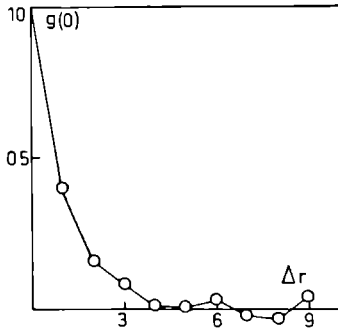


Fig 1 Normalized correlation function of the surface height

tice units, therefore only very small clusters are present and the surface is very rough (like for a metal–melt interface) Nevertheless, for $\Delta\mu_f^+ = \Delta\mu_f^-$ we always find after some transition time a stable interface and constant growth rate

As it should be expected, we have found that the distribution of + and – cells over the surface is disordered Moreover, different supersaturations result in different surface concentrations of + and – cells, e.g. for $\Delta\mu_f^+ = 0.7 kT$ and $\Delta\mu_f^- = 1.7 kT$ we found a considerable surface enrichment of – particles (2.5 times as much – as + particles) In physical experiments this effect could easily lead to the development of double layers in the crystal–fluid interface

The surface properties which we mentioned above, do not show any qualitative difference when we vary the supersaturations $\Delta\mu_f^+$ and $\Delta\mu_f^-$ within the range where the interface is stable At the same time, however, the volume properties which we discuss next do show a distinct difference at high and at low supersaturations.

An example of the crystal phase at low supersaturations is shown in figs 2 and 3 Although the surface is rough the volume has a completely regular structure, of the NaCl type, even if the two supersaturations $\Delta\mu_f^+$ and $\Delta\mu_f^-$ are considerably different

Increasing the supersaturation leads to a breakdown of this ordered structure by the formation of domains which have internally still a regular structure but these structures do not match at the domain boundaries, as shown in figs 4 and 5 The average size of these domains can be found from a correlation

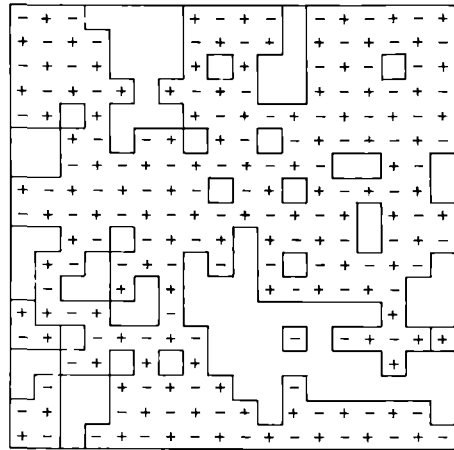


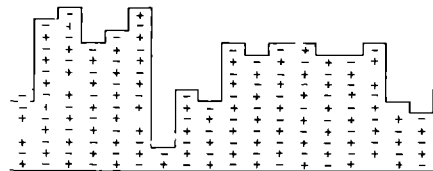
Fig 2 Horizontal cross section of the crystal solution interface, showing the distribution of +, – and fluid (empty) cells, for small supersaturations $\Delta\mu_f^+ = 0.7 kT$, $\Delta\mu_f^- = 1.7 kT$ The solid part is almost completely regular

function within each layer In this way we found that the domain size decreases smoothly with increasing supersaturation

Numerically, the degree of ordering of the solid phase can also be described with the short range order parameter as defined by Chernov and Lewis [20]

$$\eta^+ = (\frac{1}{2}\Lambda^+ / N^{ss} N^+ N^- / N^{s^2}) / (N^+ N^- / N^{s^2}), \quad (25)$$

where N^s and N^{ss} are the number of solid cells and solid–solid neighbours respectively For the NaCl structure $\eta^{+-} = 1$ whereas $\eta^{+-} = 0$ for a random mixed crystal phase In fig. 6 the supersaturation



$$\begin{aligned} \Delta\mu^+ &= 0.7 kT \\ \Delta\mu^- &= 1.7 kT \\ \frac{C_{surt}^+}{C_{surt}} &= 0.44 \end{aligned}$$

Fig 3 Vertical cross-section under the same conditions as fig 2 The regular crystal structure is again clearly visible

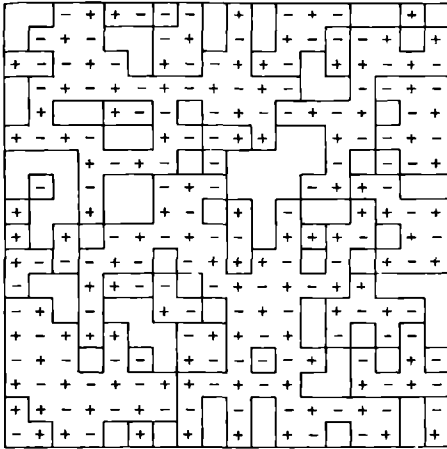


Fig. 4 Horizontal cross section at higher supersaturation $\Delta\mu_1^+ = \Delta\mu_1^- = 3.2 kT$. The solid phase is now divided in many domains which have a regular internal structure. In this example the domain size, i.e. the correlation length of the regular structure, is 4–5 lattice units.

dependence of η^{+-} is shown for $\Delta\mu_1^+ = \Delta\mu_1^-$. Averages and standard deviations were obtained from measurements in each layer separately. It follows immediately that for small supersaturations the crystal has a regular structure, whereas for $\Delta\mu_1^+ = \Delta\mu_1^- \geq 2.0 kT$ deviations become more frequent until at $\Delta\mu_1^+ =$

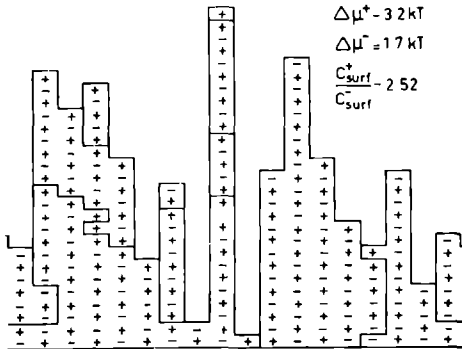


Fig. 5 Vertical cross section at $\Delta\mu_1^+ = 3.2 kT$, $\Delta\mu_1^- = 1.7 kT$. Again the domain structure is seen.

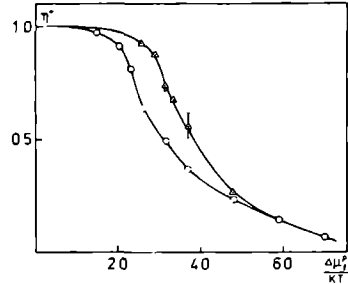


Fig. 6 Dependence of the short range order parameter η^{+-} on supersaturation ($\Delta\mu_1^+ = \Delta\mu_1^-$), showing the change from regular ($\eta^{+-} = 1.0$) to disordered ($\eta^{+-} = 0.0$) structure of the crystal phase. The curves with \circ and \triangle refer to our and to the "kink exchange" kinetics of Chernoc and Lewis [20] see also section 5. Here and in the following figs. standard deviations are indicated by symbols if they exceed the size of the indicator symbols or the line thickness.

$\Delta\mu_1^- \approx 6.0 kT$ the cells are almost completely mixed.

As mentioned in section 2 deviations of the solid phase from its equilibrium structure lead to a decrease of the effective supersaturation which is determined by the factors γ^+ and γ^- in eq. (5). In fig. 7 we show the supersaturation dependence of $\gamma^+ = \gamma^-$ for $\Delta\mu_1^+ = \Delta\mu_1^-$, and how this influences the dependence of the total supersaturation $\Delta\mu^P$ on the supersaturation of the solution $\Delta\mu_1^P$. For small supersaturations γ has the value for a regular structure ($\gamma =$

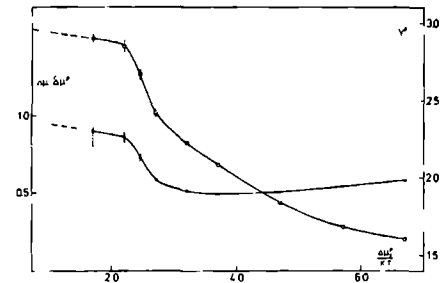


Fig. 7 Dependence of the structure parameter $\gamma^+ = \gamma^-$ (circles) and $\Delta\mu^P / \Delta\mu_1^P$ (dots) on supersaturation ($\Delta\mu_1^+ = \Delta\mu_1^-$). γ^P changes from $\gamma = 3.0$ (ordered structure) to $\gamma = 1.5$ (random mixed structure).

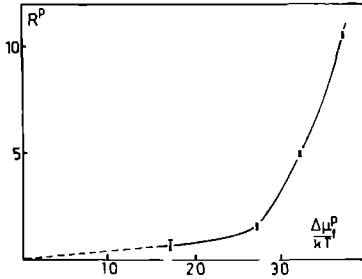


Fig 8 Growth rate for small supersaturations ($\Delta\mu_i^+ = \Delta\mu_i^-$)

$\gamma_{eq} = 3$) and therefore $\Delta\mu^P = \Delta\mu_i^P$. For $\Delta\mu_i^P > 2.0$ deviations from $\gamma = 3.0$ suddenly become important and a large part of the supersaturation of the solution is "frozen in" in the solid phase. Further increase in $\Delta\mu_i^P$ induces a gradual decrease to the value $\gamma = 1.5$ for a completely mixed phase. This decrease in γ^P leads to a reduction of the total supersaturation $\Delta\mu^P$ (which cannot exceed $1.5 \omega^{ab}$) and therefore to a minimum in $\Delta\mu^P/\Delta\mu_i^P$.

In figs 8 and 9 the growth rate is shown for equal supersaturations. It is seen that for high supersaturations the dependence is exponential (normal or liquid like growth, i.e.

$$R \approx \exp(\Delta\mu_i^P/kT) \quad 1$$

If the two supersaturations are different ($\Delta\mu_i^+ > \Delta\mu_i^-$) fig 10 shows that for small values still $R^+ = R^-$ but the growth rates are now much less than in the

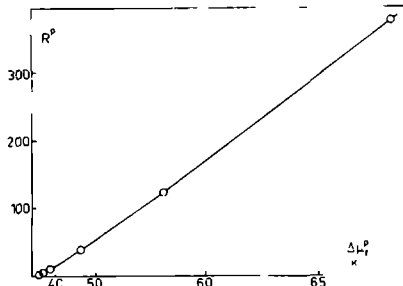


Fig 9 Growth rate for large supersaturations ($\Delta\mu_i^+ = \Delta\mu_i^-$). The horizontal scale is exponential in $\Delta\mu_i^P$, therefore linear in the activities a^P when eqs. (21) and (22) hold

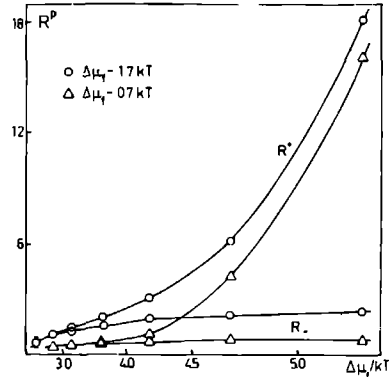


Fig 10 Dependence of R^+ and R^- on the supersaturation for positive particles if $\Delta\mu^-$ is kept constant. The horizontal scale is exponential in $\Delta\mu_i^P$ (see fig 9)

case that $\Delta\mu_i^+ = \Delta\mu_i^-$. At higher supersaturations the crystal does not grow in a stoichiometric way anymore ($R^+ > R^-$), corresponding to the formation of (positively charged) domains. At the same time, however, the simulations lose most of their physical relevance, because the interface becomes unstable and consists mainly of high columns (like the one in fig 5) at alternating positions. These "hairs" contain mostly positive particles and therefore the positions between them can be filled almost only by - particles which, however, arrive less often on the surface.

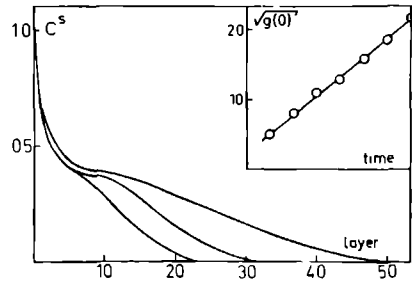


Fig 11 Dependence of the concentration of solid particles (C^s) on the layer number of an unstable interface ($\Delta\mu_i^- = 0.7 kT$, $\Delta\mu_i^+ = 5.2 kT$) at three successive times. In the inset the linear time dependence of the interface width $2[g(0)]^{1/2}$ is shown

Indeed in fig 11 it is seen that only half of the layers is filled and that the interface width increases linearly with time (independent growth of the hairs)

5 Conclusion

We found different mechanisms of crystal growth for large and relatively small supersaturations. The singularities, however, which Chernov and Lewis [20] found at the transition point for the order parameter η^{+-} , the domain size and the growth velocity are absent in our simulations. Their simulations differed at three points from ours: (i) they exchanged cells only at kink sites, (ii) they used the "melt interpretation" eq (23) and (iii) they chose non-ionic interactions ($\phi^{aa} = \phi^{bb} + \frac{1}{2} \phi^{ab}$). The triangles in fig 6 show how η^{+-} varies with their kinetics. It is seen that in this case there is more order (as expected because this method includes correlations in the kinetics), but still the dependence is not singular. Also the melt interpretation does not result in singularities. We were not able to investigate larger systems because of limitations of the available computation time. Nevertheless we suppose that upon increasing the system size curves like in figs 6 and 7 would become singular.

Even for rough surfaces, where we find a normal growth mechanism, the order of the crystal is not broken up till very high supersaturation. An analogous observation can be done on the growth of gypsum crystals from an aqueous solution [31]. Growth takes place at the top faces of long needles. Under certain circumstances these faces are not faceted such that the temperature is presumably above the roughening temperature. No indication of irregularities in these crystals has ever been found.

Acknowledgement

One of the authors (T A Cherepanova) wishes to express her gratitude to the collaborators of the Laboratory of Physical Chemistry, Delft University of Technology, where this work was carried out, for stimulating discussions.

References

- [1] H J Leamy and K A Jackson, *J Appl Phys* 42 (1971) 2121
- [2] V V Soloviev and V T Borisov, *Soviet Phys Dokl* 17 (1972) 8
- [3] V V Soloviev and V T Borisov, *Soviet Phys-Cryst* 17 (1973) 814
- [4] G H Gilmer and P Bennema, *J Crystal Growth* 13/14 (1972) 148
- [5] G H Gilmer and P Bennema, *J Appl Phys* 43 (1972) 1347
- [6] V O Esin, V J Danduk, J M Plishkin and G L Podchunova, *Soviet Phys-Cryst* 18 (1974) 578
- [7] H J Leamy and G H Gilmer, *J Crystal Growth* 24/25 (1974) 499
- [8] K Binder and H Müller Krumbhaar, *Phys Rev B* 9 (1974) 2328
- [9] H Müller Krumbhaar, *Phys Rev B* 10 (1974) 1308
- [10] U Bertocci, *J Crystal Growth* 20 (1974) 219
- [11] C van Leeuwen and I H Mischgsky, *J Appl Phys* 46 (1975) 1056
- [12] J P van der Eerden, C van Leeuwen, P Bennema, W L van der Kruk and B P Th Veltman, *J Appl Phys* 48 (1977) 2124
- [13] P Bennema, J Boon, C van Leeuwen and G H Gilmer, *Kristall und Technik* 8 (1973) 659
- [14] C van Leeuwen, *J Crystal Growth* 19 (1973) 138
- [15] V T Borisov, *Soviet Phys Dokl* 7 (1962) 50
- [16] V A Petrovski and V T Borisov, *Soviet Phys-Dokl* 17 (1972) 606
- [17] R Cadoret and M Cadoret, *J Crystal Growth* 31 (1975) 142
- [18] M Takata and A Ookawa, *J Crystal Growth* 24/25 (1974) 515
- [19] A A Chernov, in *Crystal Growth*, Ed H S Peiser (Pergamon, Oxford, 1967) p 25
- [20] A A Chernov and J Lewis, *J Phys Chem Solids* 24 (1967) 2185
- [21] A A Chernov, *Soviet Phys Usp* 13 (1970) 101
- [22] T A Cherepanova, A V Shirin and V T Borisov, *Soviet Phys Uch Zap Latv Gos Univ* 237 (1975) 40
- [23] T A Cherepanova, A V Shirin and V T Borisov, in *Industrial Crystallisation* (Plenum, New York, 1976) pp 113-121
- [24] T A Cherepanova, A V Shirin and V T Borisov, *Soviet Phys-Cryst* 22 (1977) 260
- [25] T A Cherepanova, V I Kiselev and V T Borisov, *Soviet Phys-Cryst* 23 (1978)
- [26] T A Cherepanova and V I Kiselev, *Soviet Phys-Uch Zap Latv Gos Univ* 237 (1975) 60
- [27] T A Cherepanova, *Soviet Phys Dokl* 238 (1978) 1
- [28] P Bennema and J P van der Eerden, *J Crystal Growth* 42 (1977) 201
- [29] J P van der Eerden, P Bennema and T A Cherepanova, in *Progress in Crystal Growth and Characterization*, Ed B R Pamplin (Pergamon, Oxford, 1978)
- [30] P Hartman, *Crystal Growth, an Introduction* (North-Holland, Amsterdam 1973)
- [31] G M van Rosmalen, W G J Marchle and P Bennema, *J Crystal Growth* 35 (1976) 169

On the influence of surface diffusion and
step integration kinetics on spiral growth

J.P. van der Eerden
RIM Laboratory of solid state chemistry
Catholic University of Nijmegen
Toernooiveld, Nijmegen
The Netherlands

Abstract

The results of an analytical theory for the surface diffusion problem on a surface which contains a single growth spiral are discussed. Different regimes for the spiral growth mechanism are identified and the supersaturation dependence of the growth rate and of the slope of the spiral hillock are given for each of the regimes. An implicit equation for the slope is given which replaces the, partially ad hoc, estimations of the previous back force theories. The role of tapering of the spiral hillock is discussed and it is argued that its influence is probably negligible for most experimental situations.

1 INTRODUCTION

In crystal growth theory much attention has been given to the surface diffusion of growth units. Burton, Cabrera and Frank (BCF) [1] showed that, if the growth unit concentration can be described by a continuous function c , then it satisfies the equation of the Helmholtz type, given in the next section.

BCF [1] solved this equation in the case where step integration kinetics can be neglected for parallel straight steps and for concentric circles by straight forward solution. Step integration kinetics can be characterized by a length λ^* and were studied by Chernov [2] (where $\lambda^* = 2D/\beta_{\mu}$) and by Bennema and Gilmer [3] (where $\lambda^* = 2D\tau_k/a$). Surek, Hirth and Pound [4, 5] pointed out that surface diffusion influences the nucleation rate at repeated nucleation sites (by the so-called back force effect). Upon applying these

results to the growth spiral they argued that the spiral growth rate given by BCF had to be modified in essentially the same sense as was previously conjectured by Cabrera and Coleman [6]. Müller Krumbhaar solved the case of excentric circular steps in a linearly varying supersaturation [7].

The aim of the present paper is to obtain the spiral growth rate for the surface diffusion mechanism, taking step integration kinetics into account. The essential difference with previous treatments is that at the same time surface diffusion is taken into account and the spiral is treated as a semi infinite curve, whose precise shape may vary with supersaturation, surface diffusion length, step retardation factor and edge free energy.

The paper is written in the language of growth but it is equally well applicable to dissolution (or evaporation, etching etc.). The only modification is that $\Delta\mu/kT$ is negative. It is shown in ref. [8] that a change of sign of $\Delta\mu/kT$ leads to a line reflected spiral rotating with the same frequency in the opposite sense.

The most fundamental problem which is overcome in the present analysis is to treat the spiral centre properly. It cannot be approximated by a circle, which is nevertheless done in all previous treatments. However small the diffusion length is, the end point 'feels' a diffusion field which is essentially different from that of a closed step.

2 MATHEMATICAL FORMULATION

Here we formulate the spiral problem under the following presuppositions:

- (i) The applied supersaturation $\Delta\mu$ is constant in space and time
- (ii) The discrete nature of step and surface can be neglected
- (iii) The problem is isotropic
- (iv) Stress can be neglected (for an extensive treatment see e.g. ref [9])
- (v) Step velocities are small compared to drift velocities of growth units
- (vi) Growth units frequently cross the step without being captured at kink sites.

Burton, Cabrera and Frank [1] have shown that for the concentration c of growth units on the surface, conditions (ii) - (iv) lead to

$$\lambda^2 \nabla^2 c = c - c_\infty, \quad (1)$$

where λ is the mean displacement along a given direction during the stay of a growth unit on a step free surface (erroneously λ was set equal to the

total mean displacement x_s in ref [1], whereas the correct relation is $x_s = \sqrt{2\lambda}$. On such a surface a constant (due to (i)) concentration c_∞ would result, given by

$$c_\infty = c_{eq} \exp(\Delta\mu/kT) = c_{eq} \exp(r_1/r_c) , \quad (2)$$

where c_{eq} is the equilibrium ($\Delta\mu=0$) growth unit concentration, $r_1 = \gamma a/kT$ measures γ , the edge free energy of a step (per growth unit of length a), and r_c is the radius of the (critical) nucleus [1].

Note that r_1 is the radius of the nucleus at $\Delta\mu/kT = 1$.

Apart from the Helmholtz equation (1), the presence of steps, which may be considered as immobile due to (v), imposes boundary conditions. In order to formulate these we introduce the notation $[f]$ for the difference between the value of an arbitrary function f (defined between steps) at the positive (lower), and at the negative (higher) side of the step. Then

$$[c] = 0 \quad (3)$$

$$c = c_{eq} \exp(r_1/\rho) + \lambda^* \left[\frac{\partial c}{\partial n} \right] . \quad (4)$$

hold on the step. The first condition states that the concentration varies continuously upon passing the step. This will be true if growth units cross the step frequently without being captured at kink sites (vi). This mechanism tends to suppress a possible Schwöbel effect [8] which a priori assumes independent concentration fields on both sides of the step. The second equation states that the deviation of the actual step concentration c from the stationary value $c_{eq} \exp(r_1/\rho)$ at the given radius of curvature is proportional to the step velocity v in the normal direction:

$$v = f_0 D \left[\frac{\partial c}{\partial n} \right] . \quad (5)$$

Following Bennema and Gilmer [3] we use f_0 (german Flächenbedarf) for the area occupied by a growth unit.

It is straightforward to solve this diffusion problem for a set of parallel straight steps at a mutual distance d , who turn out to move with a velocity v :

$$v = 2f_0 (D/\lambda) \mathcal{J}(c_\infty - c_{eq}) \tanh(d/2\lambda), \quad (6)$$

where the step retardation factor \mathcal{J} is given by [3]

$$1/\mathcal{J} = 1 + 2 (\lambda^*/\lambda) \tanh(d/2\lambda). \quad (7)$$

The maximal, or Wilson Frenkel, growth rate [3] R_{\max} is approached when adsorbed particles are likely to reach a step during their stay on the surface. Taking, therefore, the limit $d \rightarrow 0$ in the growth rate $R = vd(hkl)/d$ ($d(hkl)$ is the thickness of a growth layer) we find

$$R_{\max} = f_0 (D/\lambda^2) d(hkl) (c_\infty - c_{eq}) \equiv C\sigma, \quad (8)$$

where the quantity C defined in ref [3], is the equilibrium exchange flux of growth units between the surface and the mother phase, multiplied by the volume $f_0 d(hkl)$ of a growth unit, and $\sigma = \exp(\frac{\Delta\mu}{kT}) - 1$ is the relative supersaturation.

Let us now consider the case of a growth spiral, rotating with a stationary shape and an angular velocity ω . The growth rate R normal to the surface on which this spiral is located is related to ω by

$$R = \omega d(hkl)/2\pi. \quad (9)$$

The spiral curve \vec{R}_t can, at any time t , be parametrized by

$$\vec{R}_t(p) = r(p) (\cos(\theta(p) - \omega t), \sin(\theta(p) - \omega t)), \quad (10)$$

where the parameter p runs through all positive real numbers and r and θ are polar coordinates. It is a matter of straight forward differential geometry [11] to compute the normal component of the step velocity $\frac{\partial}{\partial t} \vec{R}_t(p)$. Setting this equal to eq (5) a third boundary condition is obtained:

$$f_0 d(hkl) D \frac{\partial c}{\partial n} = \omega r r' / S^2, \quad (11)$$

where primes denote derivatives with respect to p and where S is the arc length, in polar coordinates:

$$S^1 = \sqrt{(r^1)^2 + (r\theta^1)^2} \quad , \quad (12)$$

The problem is to find a curve \tilde{R}_t , a number ω , and a concentration field c such that eqs (1), (3), (4) and (11) are satisfied.

The equations are somewhat simplified by defining ϕ and ω as follows:

$$\phi = (c_\infty - c)/(c_\infty - c_{eq}) \quad (13)$$

is a function with values between 0 and 1, and ω_0 the fractional growth rate

$$\omega_0 = R/R_{\max} = \omega\lambda^2/(2\pi f_0 D(c_\infty - c_{eq})) \quad (14)$$

is a number between 0 and 1.

With these definitions eqs (1), (3), (4) and (11) are transformed into

$$\lambda^2 \nabla^2 \phi = \phi \quad , \quad (15)$$

$$[\phi] = 0 \quad , \quad (16)$$

$$\phi = 1 - \frac{1 - \exp(r_1/\rho)}{1 - \exp(r_1/r_c)} + \lambda^* \left[\frac{\partial \phi}{\partial n} \right] \approx 1 - \frac{r_c}{\rho} + \lambda^* \left[\frac{\partial \phi}{\partial n} \right] \quad , \quad (17)$$

$$\lambda^2 \left[\frac{\partial \phi}{\partial n} \right] = -2\pi\omega_0 r r^1 / S^1 \quad , \quad (18)$$

where it is understood that eq (15) holds on the surface between the steps and eqs (16) - (18) at the steps. The second equality in eq (17) follows if $r_1/r_c < 1$, which is the case on which refs [1] and [3] have concentrated. We shall, however, not use this simplification, since in many cases, e.g. growth from the vapour phase and growth from solution of slightly soluble salts large $\Delta\mu/kT$ values are involved.

At this point we stop the treatment of the problem formulated above and transfer the mathematical treatment to a separate paper [8]. Instead we use the results of that approach and discuss the physically most relevant results below, in order to avoid that the mathematical complexity would cause the loss of transparency of the present paper for readers who are mainly interested in the physics. We shall further on talk about growth since it follows immediately from eqs (10) and (15) - (16) that spirals for opposite $\Delta\mu/kT$ are symmetric and rotate with the same frequency in the opposite sense (see also ref [8]).

3 PHYSICAL IMPLICATIONS

The essential results of ref [8] can be summarized by the behaviour of the fractional growth rate ω_0 and a so-called tapering factor T, defined as the ratio of the slopes of the spiral hillock at the top and at the base. Also the different behaviour of these quantities in different parameter regimes can be studied. Here we shall discuss these results and present the consequences for the two quantities which are the most accessible to actual measurement, i.e. the growth rate and the slope of the hillock at the base. Meanwhile we compare them with the predictions of older theories.

The fractional growth rate ω_0 is related to the radius of curvature $\rho(o)$ in the centre of the spiral by

$$\omega_0 = 1 - \frac{1 - \exp(r_1/\rho(o))}{1 - \exp(\Delta\mu/kT)} \quad (19)$$

This relation has no equivalent in the older theories and could be derived with the potential theory approach [11]. It shows that, since ω_0 is, due to eq (14), always positive, $\rho(o) > r_c$ (remember $\Delta\mu/kT = 1/r_c$) and the deviation of $\rho(o)$ from r_c determines in a sense the fractional growth rate. It is seen that $\omega_0 \rightarrow 0$ if $\rho(o) \rightarrow r_c$ and $\omega_0 \rightarrow 1$ if $\rho(o) \rightarrow \infty$ faster than r_c . We shall define the back force regime as that parameter region where the relative deviation of $\rho(o)$ from r_c is large i.e. $(\rho(o) - r_c)/r_c \geq 1$.

The fractional growth rate ω_0 is not only related to $\rho(o)$ but also to the interstep distance δr far from the centre by

$$\omega_0 = \frac{2\lambda}{\delta r} \tanh \frac{\delta r}{2\lambda} \quad (20)$$

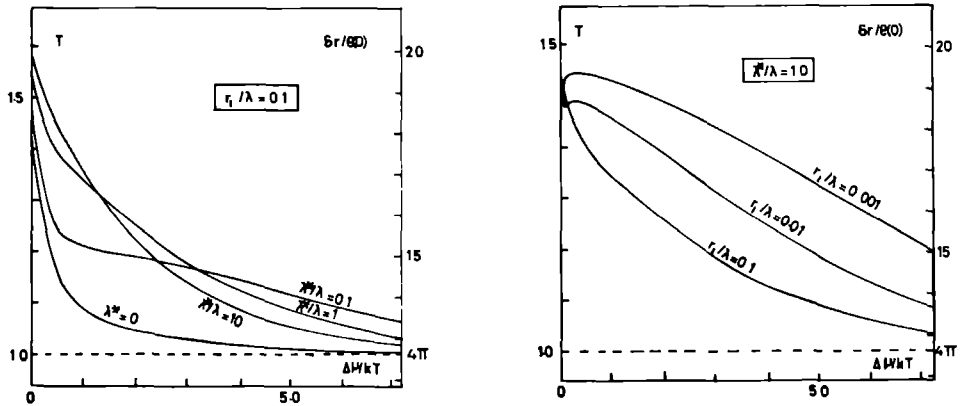
In contrast to eq (19) this relation was obtained before [1, 3], using the approximation of the spiral by straight equidistant parallel steps in that region.

The third result is the determination of the tapering factor T. As mentioned before it is the ratio of the slopes of the spiral hillock at the base and at the top. If ϕ is the angle between the tangent plane to the hillock and the crystal face we mean with slope $\tan \phi$. At the base $\tan \phi = d(hkl)/\delta r$ whereas at the top some elementary differential geometry shows

that $\text{tg } \phi = d(hk1)/(4\pi\rho(o))$. Consequently T relates δr and $\rho(o)$ by

$$T = \frac{\delta r}{4\pi\rho(o)} \quad (21)$$

For an archimedean spiral $T = 1$ and hence $T - 1$ is a measure for the deviation from archimedicity. The analysis shows that for $\Delta\mu \rightarrow 0$ the tapering factor approaches $1 + [(1 + 4\lambda^*/\lambda)/(6 + 12\lambda^*/\lambda)]^{\frac{1}{2}}$ whereas for $\Delta\mu \rightarrow \infty$ $T \rightarrow 1$ and the archimedean shape is obtained. The change over from the first to the second limiting case may be a monotonical decrease but also a maximum in between is possible. In fig (1) the supersaturation dependence of T is given for some characteristic cases.



- 1a. The tapering factor T as a function of supersaturation for $r_1/\lambda = 0.1$ and different values of λ^*/λ . This figure is the same as fig 2a of ref [10].
- 1b. The tapering factor T as a function of supersaturation for $\lambda^*/\lambda = 1.0$ and different values of r_1/λ . This figure is the same as fig 2b of ref [10].

Upon equating eqs (19) and (20) and eliminating δr by means of eq (21) an equation for $\rho(o)$ is obtained:

$$1 - \frac{1 - \exp(r_1/\rho(o))}{1 - \exp(r_1/r_c)} = \frac{\lambda}{2\pi T \rho(o)} \tanh \frac{2\pi T \rho(o)}{\lambda} \quad (22)$$

Once a value for T is substituted eq (22) is an implicit equation for $\rho(o)$. It is this equation which is the central new result of this treatment, and it will be the basis of our further investigations. Analysis of this non-linear equation shows that $\rho(o)$ differs considerably from r_c only if r_1/r_c , r_1/λ , $2\lambda^*/\lambda$ and $2\pi Tr_c/\lambda$ are all small quantities. Thus, for given (small) values of r_1/λ and λ^*/λ the back force regime extends from $r_1/r_c \approx 2\pi Tr_1/\lambda$ to $r_1/r_c \approx 1$. Outside this parameter range ω_o is given to a reasonable approximation by the right hand side of eq (22), using r_c in stead of $\rho(o)$. In the next section we discuss how this outer region can again be subdivided.

Here let us compare eq (22) with the basic equations of the classical back force theory where $\lambda^* = 0$ was considered only. Cabrera and Coleman [6] who first used the word back stress effect, and Surek, Hirth and Pound [4, 5] argued that the spiral centre feels a smaller supersaturation $\Delta\mu_o$ than the applied one $\Delta\mu$, due to the rest of the spiral step which also absorbs growth units. Since $\rho(o)$ is inversely proportional to $\Delta\mu_o$ this gives immediately an implicit equation for $\rho(o)$. Cabrera and Coleman give an expression for the resulting $\rho(o)$ in terms of the Bessel function I_o

$$1 - \frac{r_c}{\rho(o)} = I_o^{-1} \left(\frac{4\pi T \rho(o)}{\lambda} \right) \quad (22a)$$

and the more precise derivation of Surek, Hirth and Pound leads to

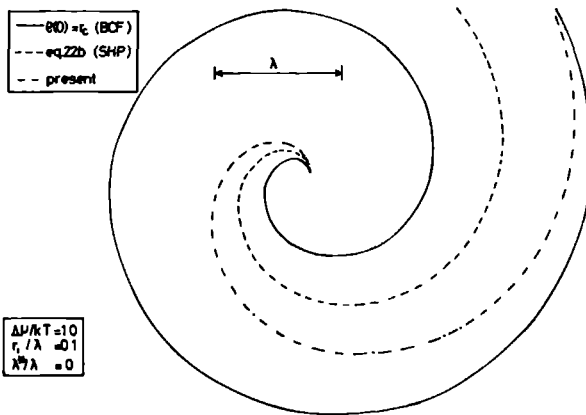
$$\frac{\exp(r_1/\rho(o)) - \exp(r_1/r_c)}{I_o(\rho(o)/\lambda)} = \frac{\exp(r_1/4\pi T \rho(o)) - \exp(r_1/r_c)}{I_o(4\pi T \rho(o)/\lambda)} \quad (22b)$$

Moreover an ad hoc estimate of T had to be made. In ref [6] the value $T = 1.51$ for the direct integration mechanism [12] was taken, in ref [4] one took $T = 1.0$. The most serious disadvantage of eqs (22a) and (22b) is that in their derivation the concentration field in the spiral centre had to be approximated by the field of one [6] or two [4] circular steps, whereas in eq (22) no such approximation had to be used. The left hand sides of eqs (22), (22a) and (22b) are similar (if $r_1/\rho(o) \ll 1$ and $r_1/r_c \ll 1$ eq (22) reduces to eq (22a) and if $r_1/4\pi T \rho(o) \approx 0$ eq (22b) coincides with eq (22)). The right hand sides of eq (22), (22a) and (22b) approach 1 and 0 if $\rho(o)/\lambda$ approaches 0 or ∞ respectively. The manner in which these limits are reached is, however, different. Indeed, to lowest order eq (22) gives for small $\rho(o)/\lambda$ $1 - 1/3 (2\pi T \rho(o)/\lambda)^2$, eq (22a) leads to $1 - (2\pi T \rho(o)/\lambda)^2$ and eq (22b) implies $1 - ((2\pi T - 1) \rho(o)/\lambda)^2$. For large $\rho(o)/\lambda$ eq (22) shows an inverse

proportionality $(2\pi T \rho(o)/\lambda)^{-1}$, whereas eqs (22a) and (22b) predict an exponential fall off, with $\sqrt{8\pi^2 T \rho(o)/\lambda} \exp - (4\pi T \rho(o)/\lambda)$ in eq (22a), and with $\sqrt{4\pi T} \exp - ((4\pi T - 1) \rho(o)/\lambda)$ in eq (22b) .

We conclude, therefore, that the present theory roughly confirms the previous back force relations but, both with respect to accuracy and to theoretical foundation, eq (22) is superior to the older basic equations. Further advantages are that the step retardation is taken into account and that the exponential function in the new expression is somewhat easier accessible to analysis than the Bessel functions I_0 in the old ones.

As an example of the influence of the present modification on the growth spirals themselves we show in fig (2) growth spirals predicted by the BCF theory ($\rho(o) = r_c$, $T = 1$), by the old back force theory, eq (22a) or eq (22b) (which virtually coincide), and by the present theory.



2. Example of the prediction of a growth spiral by different theories, the classical theory of Burton, Cabrera and Frank [1], the old back force theory [4 - 6], and the present theory.

Finally, in order to facilitate the comparison of the present theory with the classical BCF theory we can write the fractional and total growth rate in the form

$$\omega_o = \frac{\Delta\mu}{\Delta\mu^*} \tanh \frac{\Delta\mu^*}{\Delta\mu} , \quad (23)$$

$$R = C \left\{ \exp\left(\frac{\Delta\mu}{kT}\right) - 1 \right\} \frac{\Delta\mu}{\Delta\mu^*} \tanh \frac{\Delta\mu^*}{\Delta\mu}, \quad (24)$$

where we defined the characteristic value $\Delta\mu^*$ of $\Delta\mu$ by

$$\frac{\Delta\mu^*}{kT} = \frac{\Delta\mu}{kT} \cdot \frac{\delta r}{2\lambda} = \frac{2\pi T r_1}{\lambda} \frac{\rho(0)}{r_c} \quad (25)$$

In the BCF theory [3] $\Delta\mu^* = 9.5 r_1/\lambda$ is constant, here it depends on the supersaturation, both through the tapering factor (a slow variation) and through the $\rho(0)/r_c$ ratio (in the back force regime).

4 FOUR SPIRAL GROWTH REGIMES

In this section we divide the parameter space, i.e. the possible sets of $(r_1/\lambda, r_1/r_c, \lambda^*/\lambda)$ values in four parts. In each of these one physical process is rate determining. Of course, the transition from one regime to another does not occur suddenly and close to boundaries between two parts both physical processes have to be taken into account usually. For each of the regimes we give the fractional growth rate ω_0 , the total growth rate $R = C\omega_0$ and the slope of the spiral hillock $\text{tg } \phi = d(\text{hkl})/\delta r$.

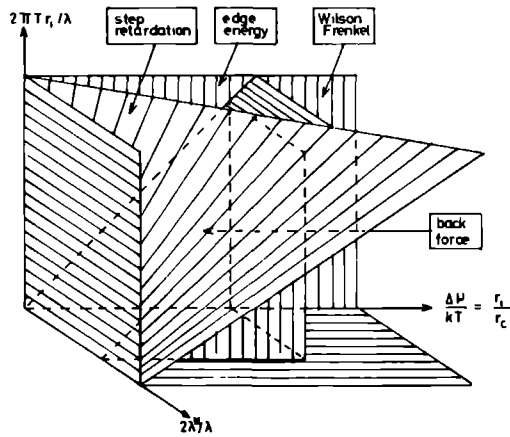
The partitioning of the parameter space is given in fig (3). We distinguish between the back force regime (the half cube), the step retardation regime (above the curved plane), the edge energy regime (the region below the curved plane and above the plane which bounds the half cube above), and the Wilson Frenkel regime (the rest of the parameter space).

In the back force regime $\rho(0)$ deviates considerably from r_c . The interstep distance d can be conveniently represented in the form

$$\frac{\delta r}{\lambda} = (A \frac{\Delta\mu}{kT})^\alpha \left(\frac{2\lambda^*}{\lambda}\right)^\beta, \quad (26)$$

where A , α and β are functions which vary only slowly through the back force regime. E.g. for $r_1/r_c \rightarrow 0$ and $\lambda^*/\lambda \ll 1/6 \sqrt{3}$ it is found that $A \approx \lambda/(48\pi T r_1)$, $\alpha = -1/3$ and $\beta = 0$, whereas for r_1/r_c larger than $4\pi T r_1 \lambda^2 (\frac{\lambda^*}{\lambda} - 1/12)^2 / \lambda^{*3}$ one obtains $A \approx \lambda/(8\pi T r_1)$, $\alpha = -1/2$, $\beta = -1/2$.

As a comparison, Cabrera and Coleman's treatment leads to constants values $A = \lambda/(16\pi T r_1)$, $\alpha = -1/3$ and β is undetermined (there only $\lambda^*/\lambda = 0$ was considered). Since the slope $\text{tg } \phi$ is inversely proportional to δr it follows



3. The partitioning of the parameter space in four regions. The curved face is given by $\delta r_c \lambda^* = \lambda^2$, the face bounding the semicube above by $\delta r_c = 2\lambda$ (with $\delta r_c \equiv 4\pi Tr_c$).

that the supersaturation dependence of the slope allows to determine the exponent α , and, conversely, if $\alpha \neq -1$ this should suggest that the experiment takes place in the back force regime. Since $r_1/r_c \leq 1$ the fractional and absolute growth rate are approximately given by

$$\omega_0 = 1 - \frac{r_c}{\varrho(0)} = 1 - 4\pi T \frac{r_1}{\lambda} A^{-\alpha} \left(\frac{\Delta\mu}{kT}\right)^{-\alpha-1} \left(\frac{2\lambda^*}{\lambda}\right)^{-\beta} \quad (27)$$

$$R \approx C\omega_0 \frac{\Delta\mu}{kT} = C \left\{ \frac{\Delta\mu}{kT} - 4\pi T \frac{r_1}{\lambda} \left(A \frac{\Delta\mu}{kT}\right)^{-\alpha} \left(\frac{2\lambda^*}{\lambda}\right)^{-\beta} \right\} \quad (28)$$

The growth rate R is thus essentially linear in $\frac{\Delta\mu}{kT}$ with a correction proportional to $\left(\frac{\Delta\mu}{kT}\right)^{-\alpha}$.

In all other regimes $\varrho(0) \approx r_c$. Formally this can be expressed by taking $A = \lambda/(4\pi Tr_1)$, $\alpha = -1$ and $\beta = 0$ in eq (26), which equation then simplifies to

$$\delta r = 4\pi Tr_c \quad (29)$$

In the step retardation regime the integration of growth units in the step is rate determining.

The regime is characterized by small ω_0 and small \mathcal{J} values. After some

reflection it turns out that this is the case if

$$\frac{\delta r \lambda^*}{\lambda^2} = \frac{4\pi T r_c \lambda^*}{\lambda^2} > 1, \quad (30)$$

which defines the region above the curved plane in fig 3. In this regime the fractional and total growth rate are given by

$$\omega_o = \frac{\lambda^2}{\lambda^* \delta r} = \frac{\lambda^2}{4\pi T r_1 \lambda^*} \cdot \frac{\Delta\mu}{kT}, \quad (31)$$

$$R = \frac{C\lambda^2}{4\pi T r_1 \lambda^*} \frac{\Delta\mu}{kT} (\exp(\frac{\Delta\mu}{kT}) - 1). \quad (32)$$

The growth rate is thus quadratic in $\frac{\Delta\mu}{kT}$ for small $\frac{\Delta\mu}{kT}$ and follows an exponential dependence at large $\frac{\Delta\mu}{kT}$. The prefactor is inversely proportional to λ^* and hence to the step relaxation time.

In the edge energy regime again $\omega_o \ll 1$ but now $\mathcal{J} \approx 1$.

This corresponds to

$$\frac{4\pi T r_c \lambda^*}{\lambda^2} < 1 \text{ and } \frac{2\pi T r_c}{\lambda} > 1, \quad (33)$$

which defines the pocket shaped region in fig 3. In this regime the fractional and total growth rates are given by

$$\omega_o = \frac{2\lambda}{\delta r} = \frac{\lambda}{2\pi T r_1} \cdot \frac{\Delta\mu}{kT}, \quad (34)$$

$$R = \frac{C\lambda}{2\pi T r_1} \frac{\Delta\mu}{kT} (\exp(\frac{\Delta\mu}{kT}) - 1). \quad (35)$$

Note that these equations have the same supersaturation dependence as the ones in the edge retardation regime, the only difference being a factor $2\lambda^*/\lambda$.

In the Wilson Frenkel regime, finally, the maximal law holds: $\omega_o \approx 1$ and this regime covers the rest of the parameter space in fig 3.

The fractional and total growth rates are given for completeness:

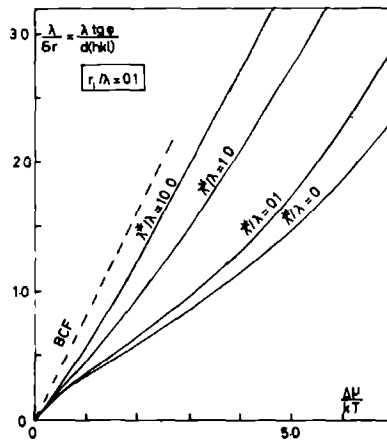
$$\omega_o = 1, \quad (36)$$

$$R = C(\exp(\frac{\Delta\mu}{kT}) - 1). \quad (37)$$

It can be noted that, strictly speaking, the linear law (linear $R - \Delta\mu$ relation), which was defined in ref [3] does not occur. The region where it would apply is divided in the back force regime, where the $R - \Delta\mu$ dependence is slower than linear, and the Wilson Frenkel regime where it is faster.

5 CONCLUSION

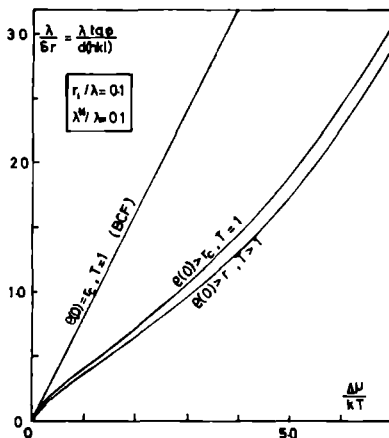
In the preceding sections we have shown how the parameter space of the spiral growth mechanism can be divided in different regions and how the slope of the spiral hillock and the fractional and absolute growth rates can be approximated roughly in the different regimes. To illustrate this further we now give some results obtained from a direct numerical solution of eq (71) in ref [18]. This equation is similar to eq (22) but now also T is expressed in terms of $\delta r/2\lambda$ through a rather involved set of equations, which we shall not reproduce here.



4. The slope $\tan \phi = d(hkl)/\delta r$ of the spiral hillock as a function of supersaturation, for $r_1/\lambda = 0.1$ and different values of λ^*/λ .

In fig 4 the slope of the spiral hillock is given for a small value of r_1/λ . For small supersaturations, where we are in the edge energy or the step retardation regime, δr varies linearly with r_c , hence $\lambda/\delta r$ linear with $\beta\Delta\mu = r_1/r_c$. The slope of this linear rise is $\lambda/(4\pi Tr_1)$, which is 40-60 %

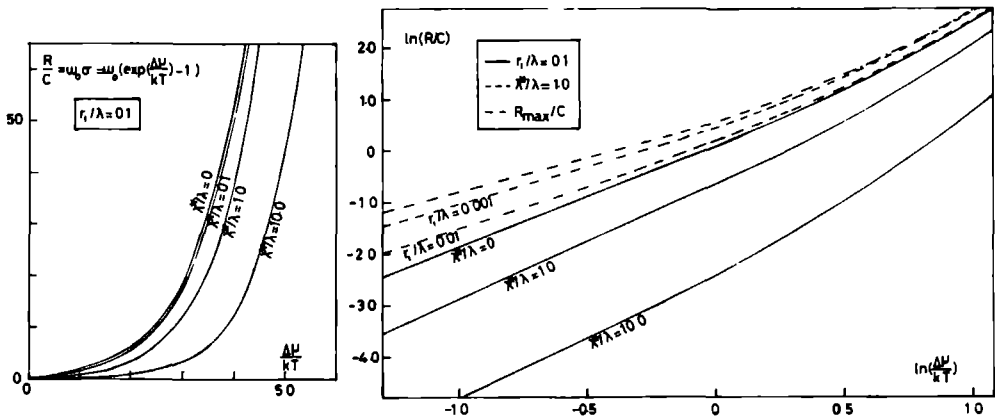
below the archimedean value $\lambda/(4\pi r_1)$, due to the higher T values (see fig 1). At higher supersaturations the back force regime is entered for $\lambda^*/\lambda \leq 1$ (see fig 3) and indeed a negative deviation from the linear relation is seen between $\beta\Delta\mu \approx 0.2$ and $\beta\Delta\mu \approx 2.0$. For still higher supersaturations the slope increases again and this reflects the influence of the Wilson Frenkel regime. Note again that these results confirm the global picture of fig. 3, whose boundaries should not be understood as very sharp.



5. The slope $\text{tg } \phi = d(hkl)/\delta r$ of the spiral hillock as a function of supersaturation, for $r_1/\lambda = 0.1$ and $\lambda^*/\lambda = 0.1$, predicted by different theories, the BCF theory [1], the present theory without tapering ($T = 1$) and the present theory with varying tapering.

In order to illustrate the use of eq (22), in the approximation $T = 1$ we compare in fig 5 the slope as predicted with eq (22) with the more sophisticated treatment in ref [1]. It is seen that the qualitative behaviour is found in this approximation, in contrast to the BCF theory which only predicts a linear dependence.

The growth rate as a function of supersaturation has the same qualitative features as in the BCF theory. First a slow, parabolic dependence of the rate on supersaturation, next, for $\Delta\mu > \Delta\mu^* \approx 2\pi Tr_1/\lambda$ (see eq (25)) a maximal law behaviour. The dependence of the absolute value of R on the step retardation coefficient λ^*/λ is clearly seen in fig 6



6. The absolute growth rate R as a function of supersaturation for $r_1/\lambda = 0.1$ and different values of λ^*/λ .
7. Double-logarithmic plot of the growth rate vs supersaturation. For large supersaturations the Wilson Frenkel law is approached, for low supersaturations a power law approximation is valid.

whereas the transition from the parabolic to the maximal law is better visualized in the double-logarithmic plot in fig 7. Note also that in these examples, and probably in many experimental cases as well, when the maximal law is reached it is already non-linear, such that a real linear $R - \Delta\mu$ law [3] does not occur.

In conclusion we may say that the present analysis leads to the following suggestions for experiments. First it turns out to be useful to measure both the slope of growth hillocks and the normal growth rate of a certain crystal face. Upon fitting the results with eq (22) (e.g. with $T = 1$ for large $\beta\Delta\mu$ or with $T = 1.5$ for small $\beta\Delta\mu$) and eq (25) relevant estimations of r_1/λ and λ^*/λ can be made. A first, simple, estimate can always be made if, for $\beta\Delta\mu \leq 2$, a slower than linear dependence of the slope on supersaturation is observed. For this indicates a back force mechanism and hence (see fig (3)) $2\lambda^*/\lambda \leq 1$ and $2\pi r_1/\lambda \leq 1$. If, on the other hand such a behaviour is absent either step integration is difficult: $2\lambda^*/\lambda > 1$ or the edge energy is relatively large $2\pi r_1/\lambda > 1$. Only if very accurate determinations of slope and growth rate are available it may be useful to go beyond eq (22) and to use the full

eq (71) of ref [10] to obtain better (supersaturation dependent) values of the tapering factor T.

REFERENCES

1. N.K. Burton, N. Cabrera and F.C. Frank, Phil. Mag. 243 (1951) 299.
2. A.A. Chernov, Sov. Phys. Usp. 4 (1961) 116.
3. P. Bennema and G.H. Gilmer in "Crystal Growth, an introduction", ed. P. Harman (North-Holland, Amsterdam, 1973) 263.
4. T. Surek, J.P. Hirth and G.M. Pound, J. Crystal Growth 18 (1973) 20.
5. T. Surek, G.M. Pound and J.P. Hirth, Surf. Science 41 (1974) 77.
6. N. Cabrera and R.V. Coleman, in "The art and science of growing crystals", Ed. J.J. Gilman (Wiley, New York, 1963) 3.
7. H. Müller Krumbhaar, J. Crystal Growth 44 (1978) 135.
8. J.P. van der Eerden, the manuscript, going herewith.
9. P. Bennema, B. van der Hoek and J.P. van der Eerden, to be published.
10. R.L. Schwoebel and E.J. Shipsey, J. Appl. Phys. 37 (1966) 3682.
11. See, e.g., K. Rektorys, "Survey of Applicable Mathematics", (M.I.T. Press, Cambridge, 1969) Ch. 9.
12. I. Stakgold, "Boundary Value Problems of Mathematical Physics" Vol II (Mac Millan, New York, 1968).
13. N. Cabrera and H.M. Levine, Phil. Mag. 1 (1956) 450.

J.P. van der Eerden
RIM Laboratory of solid state chemistry
Catholic University of Nijmegen
Toernooiveld, Nijmegen
The Netherlands

Abstract

The diffusion problem of growth units on a crystal surface which contains a single screw dislocation is studied. An exact relation is obtained between the central radius of curvature of the spiral and the interstep distance at large distances from the centre. A second, approximate, relation is obtained, using the Taylor and asymptotic expansions of an integral equation for the spiral shape, and assuming a smooth transition from the central to the outer regions of the spiral shape.

1 INTRODUCTION

In this paper the potential theory approach is discussed for the surface diffusion problem on a crystal surface containing a semi-infinite step under steady state conditions. Both the transformation of the physical system into the mathematical problem and the implications of the solution are given in a separate paper [1]. Thus we have to investigate the following problem.

Find in the two dimensional real space a curve \vec{R}

$$p \mapsto \vec{R}(p) = R(p) (\cos\theta(p), \sin\theta(p)), \quad (1)$$

a function $\phi : R_2 \rightarrow [0,1]$, and a number $\omega_0 \in (0,1)$, such that:

(i) ϕ satisfies, except on \vec{R} , the homogeneous Helmholtz equation

$$\lambda^2 \nabla^2 \phi = \phi, \quad (2)$$

(ii) ϕ is continuous at \vec{R}

$$[\phi](p) = 0, \quad (3)$$

(iii) the discontinuity of the normal derivative is related to the curve by

$$\lambda^2 \left[\frac{\partial \phi}{\partial n} \right](p) = -2\pi\omega_0 R(p) R^1(p) / S^1(p), \text{ and} \quad (4)$$

(iv) a further relation holds on the curve (g is a function to be given below):

$$\phi(\vec{R}(p)) = 1 - g(\rho(p)) + \lambda^* \left[\frac{\partial \phi}{\partial n} \right](p) \quad (5)$$

Here square brackets denote a jump: for a function f , defined on both sides of \vec{R} we have by definition

$$[f](p) \equiv \lim_{\epsilon \rightarrow 0} \{ f(\vec{R}(p) + \epsilon \vec{n}(p)) - f(\vec{R}(p) - \epsilon \vec{n}(p)) \} \quad (6)$$

where $\vec{n}(p)$ is the normal to the curve at $\vec{R}(p)$, S is the arc length:

$$S^1 = \sqrt{(R^1)^2 + (R\theta^1)^2}, \quad (7)$$

$\rho(p)$ is the radius of curvature at $R(p)$

$$\rho = (S^1)^3 / (2(R^1)^2 \theta^1 + R^2 (\theta^1)^3 + RR^1 \theta^{11} - RR^{11} \theta^1), \quad (8)$$

and quotes denote derivatives with respect to p . The constants r_c and λ^* are real and non-negative real numbers respectively.

At this point we shortly mention the physical meaning of the quantities entering the problem. The function ϕ determines the concentration of growth units between the spiral edges, λ is the mean free path of growth units during their stay on the surface, λ^* is proportional to the incorporation time for

growth units in the edge, and ω_0 is the fractional growth rate, proportional to the angular frequency of the rotating growth spiral. The function g is the correction, due to curvature, to the flux of particles which leave a step. It is given by Burton, Cabrera and Frank as

$$g(\rho) = \frac{1 - \exp(r_1/\rho)}{1 - \exp(r_1/r_c)} \quad (9)$$

where r_c and r_1 are the radii of curvature of a stationary circular step at the actual and at unit relative supersaturation respectively.

It can be noted that a circular step with radius r_c leads to the trivial solution $\phi \equiv 0$ and $\omega_0 = 0$. This circular step is precisely the critical nucleus.

Another observation which can be made is the symmetry between growth and dissolution. If the sign of the supersaturation is reversed, this leads to an opposite value of r_c . It can be checked easily that from a solution for a certain r_c value, a solution for the value $-r_c$ is obtained by a change of sign of $\theta(\rho)$ and hence of $\phi(\rho)$, i.e. a reflection in the y -axis. Both solutions have the same ω_0 .

It is also clear that if a spiral \vec{R} has been found, rotations and translations of the coordinate system give other spirals. In order to find a unique solution we, therefore, require that it satisfies

$$R(0) = \theta(0) = 0 \quad (10)$$

Another requirement which has to hold is that the radius of curvature is either positive or negative for all ρ

$$0 < \rho(\rho) < \infty \text{ or } 0 > \rho(\rho) > -\infty \text{ for all } \rho \quad (11)$$

It has been shown for a similar problem [2] that physical spirals arise if and only if eq (11) is satisfied.

The problem presumably is unsolvable by direct methods. Therefore the problem is reformulated as an integral equation in section 2, using potential theory. Subsequently an approximate numerical analysis of that equation will be carried out. In sections 3 and 4 the behaviour of the equation at small and at large distances from the origin is studied, which information is combined in section 5 in order to construct a global spiral shape.

2 POTENTIAL THEORY

Mathematical potential theory [3] starts from a fundamental solution, describing the adatom distribution on a surface containing no absorbing points except a single point where a unit flux is absorbed, i.e. the flux towards a unit area under equilibrium conditions. When the absorbing point is at \vec{r}_0 , the fundamental solution solves the following problem:

$$\lambda^2 \nabla^2 F(\vec{r}/\vec{r}_0) - F(\vec{r}/\vec{r}_0) = -\delta \frac{(\vec{r}-\vec{r}_0)}{\lambda} \quad , \quad (12a)$$

$$\lim_{r \rightarrow \infty} F(\vec{r}/\vec{r}_0) = 0 \quad , \quad (12b)$$

$$F \text{ is rotational symmetric around } r_0 \quad . \quad (12c)$$

(where δ denotes the two dimensional Dirac delta function).

The last condition reduces eq (12a) to an equation of the Bessel type for $\vec{r} \neq \vec{r}_0$. Consequently the problem is easily solved

$$F(\vec{r}/\vec{r}_0) = (2\pi)^{-1} K_0(\Delta r/\lambda) \quad , \quad (13)$$

where K_0 is the modified Bessel function of order zero and imaginary argument and Δr is the distance between \vec{r} and \vec{r}_0 :

$$\Delta r = |\vec{r} - \vec{r}_0| \quad (14)$$

With the fundamental solution the value of ϕ can be expressed in terms of its Cauchy data (i.e. the value of ϕ and its normal derivative at the boundaries).

In order to find this relation multiply eq (2) by $F(\vec{r}/\vec{r}_0)$, eq (12a) by $\phi(\vec{r})$, and integrate the difference over all \vec{r} to obtain

$$\int (F \nabla^2 \phi - \phi \nabla^2 F) d^2 r = \phi(\vec{r}_0) \quad (15)$$

The surface integral is transformed into a line integral with the help of Greens theorem since the integrand is the divergence of the vectorfield $F \nabla \phi - \phi \nabla F$. The line integral should be taken along a boundary enclosing a surface region without steps. In the present case this contour consists of

three parts. First, starting at the origin, it follows the spiral infinitely close to its negative side during a large number (say N) of turns, second it crosses the step free region perpendicularly to the (N-1)th turn, and third it follows the spiral infinitely close to its positive side back to the origin. In such a way the step free region up till N-1 turns is enclosed. Finally if N approaches infinity the exponential fall off of the Bessel function eq (13) at large Δr assures that the integral converges to a value where the contribution of the second (cross-over) part of the contour vanishes. Greens theorem then states that the left hand side of eq (15) equals the line integral of $\vec{n}_0 (F\nabla\phi - \phi\nabla F)$ over the first and third part of the contour. In both cases the contour approaches the curve \vec{R} but the outer normal \vec{n}_0 is equal and opposite to the normal \vec{n} of the spiral for the first and the third part respectively. Therefore eq (15) becomes

$$-\oint_0^\infty \left\{ \left[F \frac{\partial \phi}{\partial n} \right] (p) - \left[\phi \frac{\partial F}{\partial n} \right] (p) \right\} dS(p) = \phi(\vec{r}_0) \quad (16)$$

In this equation we can substitute eq (13) for F, the boundary conditions eqs (3-5) and $[F] = [\partial F / \partial n] = 0$ to get

$$\omega_0 \int_0^\infty \frac{K_0(\Delta r / \lambda)}{\lambda^2} R(p) R^1(p) dp = 1 - g(\rho) - 2\pi \omega_0 \lambda^* R(p_0) R^1(p_0) / (S^1(p_0) \lambda^2), \quad (17)$$

where the point \vec{r}_0 has been chosen on the spiral at $\vec{R}(p_0)$, and it has been used that $ds = S^1 dp$ by definition of the arc length. For further use we give the distance Δr in polar coordinates

$$\Delta r(p, p_0) = \left[R(p)^2 + R(p_0)^2 - 2R(p)R(p_0) \cos(\theta(p) - \theta(p_0)) \right]^{\frac{1}{2}} \quad (18)$$

by the cosine rule.

Summarizing this section we have transformed the original differential equation eq (2) with the boundary conditions eq (3-5) into a single integral equation eq (17) which has to be solved for functions $R(p)$ and $\theta(p)$, with the restriction that eqs(10,11) have to hold. Again this equation seems intractable by standard methods, hence an approximate method is treated in the next sections.

In previous theories a differential equation for the spiral shape has

been given. This equation is known to hold for the case of direct integration and hence it is supposed to be relevant in the case $\lambda \gg 0$. It is therefore natural to investigate whether eq (17) reduces to this differential equation in the limit that λ tends to zero. Consider then

$$\lim_{\lambda \rightarrow 0} F(\vec{r}/\vec{r}_0) = \frac{1}{2} \delta \left(\frac{\Delta r}{\lambda} \right) \quad (19)$$

Upon substituting eq (19) into eq (16) the following relation results:

$$2\pi \left(\frac{1}{2} + \lambda^* / \lambda \right) \frac{\omega_0 R R^1}{\lambda S^1} = 1 - g(\rho) \quad (20)$$

where it has been used that $dS = d(\Delta r)$ in this limit (since differences in the distance measured along the curve (dS) or directly (Δr) are of second order and give negligible contributions to the integral).

It is precisely this equation which has been studied earlier for the case $\lambda^* = 0$ and $r_1 \rightarrow 0$ [2, 4, 5] (with the parametrization $R(\rho) = \rho$, $R^1(\rho) = 1$).

In view of the present derivation it is seen that eq (20) is valid if (i) r_c the smallest radius of curvature of the resulting spiral, is much larger than λ , and (ii) $R(\rho) \gg \lambda$. The first condition is well known and is generally believed to be the condition for which spirals with and without surface diffusion mechanism become equivalent [4, 5, 6]. So far it seems that eq (20) could be used indeed in the limiting case $\lambda \rightarrow 0$.

The second condition, however, shows that series expansions (which form the basis of those analyses) around $R(\rho) = 0$ are invalid, even for arbitrarily small λ . Indeed, upon observing that when $R \rightarrow 0$ only one "wing" of the function $K_n(\Delta r/\lambda)$ contributes to integrals of the following type, one obtains

$$\lim_{\lambda \rightarrow 0} \lim_{R_0 \rightarrow 0} \int_0^{\infty} K_n \left(\frac{|R-R_0|}{\lambda} \right) f(R) dR = \frac{1}{2} \lim_{R_0 \rightarrow 0} \lim_{\lambda \rightarrow 0} \int_0^{\infty} K_n \left(\frac{|R-R_0|}{\lambda} \right) f(R) dR$$

for any order n of the Bessel function and for any function f for which the integral exists. Clearly, the left hand side represents the physically interesting case. Since derivatives of K_0 are expressible in terms of K_n functions, it follows that, in order to obtain series expansions for small $R(\rho)$ one should not use eq (20) but instead the slightly different expression

$$2\pi \left(\frac{1}{2} + \frac{\lambda^*}{\lambda} \right) \frac{\omega_0 R R^1}{\lambda S^1} = 1 - g(\rho) \quad (20a)$$

In the spirit of the previous theories it is possible now to study the spiral shape in case $\lambda \rightarrow 0$ by the combination of a Taylor expansion of eq (20a) and an asymptotic expansion of eq (20).

The difference of eqs (20) and (20a) is the mathematical consequence of the physical difference between steps with and without end points. The latter ones have a larger effective area from which they can absorb growth units.

3 THE SPIRAL CLOSE TO THE CENTRE

In this region of small $|\vec{R}|$ values it is convenient to parametrize the curve \vec{R} by its distance to the origin, using λ as the unit of length:

$$R(p) = p\lambda, \quad R^1(p) = \lambda, \quad S^1(p) = \lambda\sqrt{1+(\theta^1(p)p)^2} \quad (21)$$

Eq (17) is a non-linear integral equation for $\theta(p)$, which can be studied by the Taylor expansion in the variable p_0 of the following equation:

$$\omega_0 \int_0^\infty K_0 \left(\frac{\Delta r}{\lambda}\right) p dp = 1 - g(\varrho(p_0)) - 2\pi\omega_0 \frac{\lambda^*}{\lambda} p_0 / S^1(p_0) \quad (22)$$

The first term of the expansion is found by substitution of $p_0 = 0$. This gives $\Delta r = p\lambda$ by eq (18) and $\varrho(0) = \lambda(2\theta^1(0))^{-1}$ by eq (8), and hence

$$\omega_0 \int_0^\infty K_0(p) p dp = 1 - g(\varrho(0)) \quad (23)$$

The integral is standard [7] and equals unity. Hence eq (23) gives a relation between the fractional growth rate ω_0 and the central radius of curvature $p(0)$.

$$\omega_0 = 1 - g(\varrho(0)) \quad (24)$$

Note that in this relation λ^* does not occur, that hence the step integration kinetics do not influence the central radius of curvature directly (only through their influence on ω_0).

The second term of the Taylor expansion is found by differentiation of eq (22) with respect to p_0 and putting $p_0 = 0$ afterwards. Upon using $\partial \Delta r / \partial p_0 = -\lambda \cos \theta(p_0)$, $\partial \varrho(0) / \partial p_0 = -3\theta^{11}(0) \varrho(0)^2 / \lambda$ and $K_0^1 = -K_1$ one obtains

$$\omega_0 \int_0^\infty K_1(p) p \cos \theta(p) dp = 3\theta^{11}(0) \varrho(0)^2 g^1(\varrho(0) / \lambda) - 2\pi\omega_0 \lambda^* / \lambda \quad (25)$$

In order to get an idea of the value of the left hand side of this equation let us assume that in the region which contributes to the integral the spiral can be approximated by an archimedean one with an effective central radius of curvature $\rho_{\text{eff}}(o) \equiv \lambda / (2\theta^1(p))$. Then the integral is [7].

$$\int_0^{\infty} K_1(p) p \cos \frac{p\lambda}{2\rho_{\text{eff}}(o)} dp = \frac{\pi}{2} (1 + \frac{1}{4}(\lambda/\rho_{\text{eff}}(o))^2)^{-3/2} \quad (26)$$

Let us now consider the classical limit $\lambda \rightarrow 0$. Since g is a monotonically increasing function with $g(r_c) = 0$, it follows from eq (24) that $\rho(o) > r_c$. Below it will be shown that $\rho(p)$ is increasing as well, such that $\rho_{\text{eff}}(o) \geq \rho(o)$. These inequalities guarantee that $\lambda/\rho_{\text{eff}}(o) \rightarrow 0$ if $\lambda \rightarrow 0$ such that in this limit eq (25) reads

$$\pi\omega (\frac{1}{2} + 2\lambda^*/\lambda) = 3\theta^{11}(o)\rho(o)^2 g^1(\rho(o))/\lambda \quad (27)$$

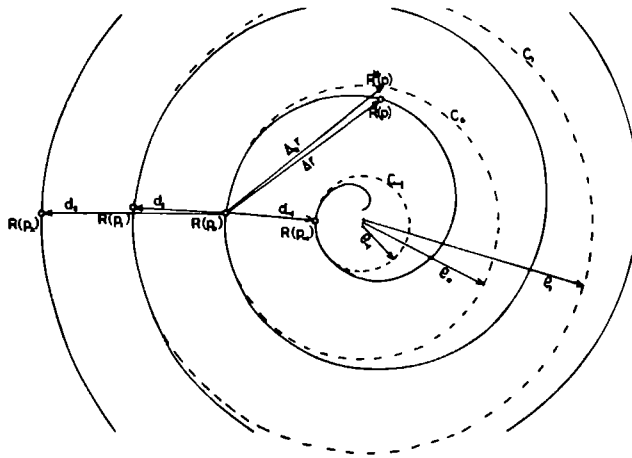
When we would have constructed Taylor expansions in p of eqs (20) and (20a) eq (27), multiplied by p , would be the linear term in eq (20a), not in eq (20). This again illustrates that, close to the centre, eq (20a) is the correct differential equation as soon as the surface diffusion mechanism operates.

4 THE SPIRAL FAR FROM THE ORIGIN

Far from the origin the spiral steps become straight and their velocity depends on the mutual distance to the preceding and succeeding step. A set of parallel equidistant steps moves stationary. This means that at large distances the spiral tends to an archimedean shape. We denote the interstep distance by d (not by δr as in ref [1] in order to keep the formulae transparent). In view of this we are led to consider an asymptotic representation of the spiral shape of the following form (a gives the deviation from the archimedean shape):

$$R^1(p)/\theta^1(p) = \frac{d}{2\pi} (1 + \frac{a}{R(p)} + \dots) \quad (28)$$

Before turning to the asymptotic representation of eq (17) we perform some differential geometry manipulations in order to obtain asymptotic expansions of some relevant functions. See fig. 1 for the following explanation.



1. The geometrical representation of the quantities defined in the text. Counted from $\vec{R}_0 = \vec{R}(p_0)$ the -1-th, 0-th, 1-st and 2nd spiral turn are shown as well as the osculating circles with radii ρ_{-1} , ρ_0 , ρ_1 and ρ_2 , and distance d_{-1} , d_0 , d_1 and d_2 from \vec{R}_0 , and $\Delta_n r - \Delta r$ determines the error in the integrand of eq (17).

The first to consider is the arc length S , or rather its derivative $S^1(p)$, given in eq (17). Using eq (28) we find

$$S^1/\theta^1 = R(1 + \frac{1}{2} (\frac{d}{2\pi R})^2 + \frac{a}{R} (\frac{d}{2\pi R})^2 + \dots) \quad (29)$$

This result can be used too in eq (8) for the radius of curvature

$$\rho = R(1 - \frac{1}{2} (\frac{d}{2\pi R})^2 + \dots) \quad (30)$$

The distance $|d_n|$ from the fixed point $\vec{R}_0 = \vec{R}(p_0)$ to the n -th spiral turn after \vec{R}_0 is going to play an important role in the discussion below. This n -th turn is defined as that part of the spiral for which $\theta(p) - \theta(p_0)$ is between $(2n+1)\pi$.

Let $\vec{R}_n = \vec{R}(p_n)$ be the projection of \vec{R}_0 on this turn, and T_n and N_n the tangent and normal vectors at R_n . The following relations then hold:

$$(\vec{R}_n - \vec{R}_0) \cdot T_n = 0 \quad , \quad (31)$$

$$(\vec{R}_n - \vec{R}_0) \cdot N_n = d_n \quad . \quad (32)$$

Upon using eq (1) to express T_n and N_n in terms of $R_n = R(\rho_n)$ and $\theta_n = \theta(\rho_n)$, eq (28) together with eq (31) show that

$$\theta_n - \theta_0 = 2\pi n \left(1 - \left(\frac{d}{2\pi R_0} \right)^2 + \dots \right) \quad , \quad (33)$$

$$R_n - R_0 = dn \left(1 + \frac{a}{R_0} + \dots \right) \quad , \quad (34)$$

and substituting this in eq (32) gives

$$d_n = dn \left(1 + \frac{a}{R_0} + \dots \right) \quad (35)$$

In the following it is useful to parametrize the spiral with the arc length S , whose derivative with respect to the general parameter p is given by eq (7). If $S_n = S(\rho_n)$ is the arc length at the point \vec{R}_n , the n -th spiral turn is, to order $(S-S_n)^4$, given by [8]:

$$\begin{aligned} \vec{R}(S) = & \vec{R}_n + (S-S_n) \vec{T}_n + \frac{(S-S_n)^2}{2\rho_n} \vec{N}_n + \frac{(S-S_n)^3}{6\rho_n^2} (\dot{\rho}_n \vec{N}_n - \vec{T}_n) + \\ & \frac{(S-S_n)^4}{24\rho_n^3} (\rho_n \ddot{\rho}_n + 1 - 2\dot{\rho}_n^2) \vec{N}_n + 3\dot{\rho}_n \vec{T}_n \quad , \quad (36) \end{aligned}$$

where $\rho_n = \rho(S_n)$ and dots above symbols denote derivatives with respect to S , e.g.

$$\dot{\rho}_n = \frac{d\rho}{dS}(S_n) = \frac{d\rho/dp}{dS/dp} = \frac{d}{2\pi R_n} \left(1 + \frac{a}{R_n} + \dots \right) \quad . \quad (37)$$

The last equality follows from eqs (28) - (30). In order to obtain an asymptotic expression for eq (17) we approximate the n -th spiral turn by the osculation circle at \vec{R}_n , (see fig. 1). If that circle is parametrized with the arc length too, its points $\vec{C}_n(S)$ are given, to order $(S-S_n)^4$, by [8]

$$\vec{C}_n(S) = \vec{R}_n + (S-S_n) \vec{T}_n + \frac{(S-S_n)^2}{2\rho_n} \vec{N}_n - \frac{(S-S_n)^3}{6\rho_n^2} \vec{T}_n + \frac{(S-S_n)^4}{24\rho_n^3} \vec{N}_n \quad . \quad (38)$$

Note that, arbitrarily, the arc length at the osculation point \vec{R}_n is taken as S_n .

The approximation which we shall use in eq (20) is to replace the actual distance $\Delta r = |\vec{R}_0 - \vec{R}(S)|$, between \vec{R}_0 and the running point $\vec{R}(S)$ on the spiral, by the distance

$$\Delta_n r = |\vec{R}_0 - \vec{C}_n(S)| \quad (39)$$

between \vec{R}_0 and a point on the osculation circle with the same arc length to \vec{R}_n . Upon using eqs (36) and (38) in eqs (18) and (39) it can be derived that the lowest order

$$\begin{aligned} \Delta r - \Delta_n r &= u^3 \dot{\rho}_n / 6 \rho_n^2 \quad \text{for } n \neq 0 \quad , \\ &= 5u^4 \dot{\rho}_0 / 24 \rho_0^3 \quad \text{for } n = 0 \quad , \end{aligned} \quad (40)$$

where $u = S - S_n$.

The error in replacing $K_0(\frac{\Delta r}{\lambda})$ by $K_0(\frac{\Delta_n r}{\lambda})$ in the region around \vec{R}_n is, to lowest order, given by

$$\begin{aligned} K_0\left(\frac{\Delta r}{\lambda}\right) - K_0\left(\frac{\Delta_n r}{\lambda}\right) &= -\frac{u^3 \dot{\rho}_n}{6 \rho_n^2} K_1\left(\frac{\Delta_n r}{\lambda}\right) \quad (\text{if } n \neq 0) \quad , \\ &= -\frac{5u^4 \dot{\rho}_0}{24 \rho_0^3} K_1\left(\frac{\Delta_0 r}{\lambda}\right) \quad (\text{if } n = 0) \quad . \end{aligned} \quad (41)$$

To evaluate the integral in eq (17) we integrate each turn separately and approximate its contribution by an integration over the corresponding osculation circle. In stead of the general parameter p we use the arc length S and approximate the integrand to second order in u for each C_n :

$$\begin{aligned} \int_0^{\infty} K_0\left(\frac{\Delta r}{\lambda}\right) R(p) R^1(p) dp &\approx \sum_n \int_{C_n} K_0\left(\frac{\Delta_n r}{\lambda}\right) \{R_n \dot{R}_n + u(\dot{R}_n^2 + R_n \ddot{R}_n) + u^2(2\dot{R}_n \ddot{R}_n + R_n \ddot{R}_n)\} dS \quad (42) \\ &= \sum_n \left[R_n \dot{R}_n \rho_n G_0\left(\frac{\rho_n^*}{\lambda}, \frac{\rho_n}{\lambda}\right) + (2R_n \ddot{R}_n + R_n \ddot{R}_n) \rho_n^3 G_2\left(\frac{\rho_n^*}{\lambda}, \frac{\rho_n}{\lambda}\right) \right] \quad , \end{aligned} \quad (43)$$

where G_k are geometrical factors, depending on the radius ρ_n of C_n and the distance ρ_n^* of \vec{R}_0 to the centre of C_n which is, to order $1/R^2$ given by

$$\rho_n^* = \rho_n - d_n \approx R_0 \quad . \quad (44)$$

The general expression for G_k is

$$G_k(x, y) = \int_{-\pi}^{\pi} K_0(\sqrt{x^2+y^2-2xy \cos \theta}) \theta^k d\theta \quad (45)$$

It is seen immediately that $G_k = 0$ for odd values of k , such that the second term in eq (42) vanished identically in eq (43). The factor G_k can be found using Neumann's addition theorem

$$K_0(\sqrt{x^2+y^2-2xy \cos \theta}) = \sum_{m=-\infty}^{\infty} I_m(Z_-) K_m(Z_+) \cos m \theta, \quad (46)$$

where Z_- and Z_+ are the smaller and the larger of x and y respectively.

For $k = 0$ only the $m = 0$ term of eq (46) contributes to eq (45) such that

$$G_0(x, y) = 2\pi I_0(Z_-) K_0(Z_+) \quad (47)$$

For $k \neq 0$ all terms for which $m + k$ is even contribute, and upon interchanging summation and integration it is found that e.g.

$$G_2(x, y) = \frac{2\pi^3}{3} I_0(Z_-) K_0(Z_+) + 2 \sum_{m=1}^{\infty} \frac{\pi}{m^2} I_{2m}(Z_-) K_{2m}(Z_+) \quad (48)$$

These expressions for G_k will be used now to obtain an asymptotic expressions for the basic integral, eq (42).

First, note that the two terms in eq (42) are the first terms in an asymptotic series.

Indeed, if eqs (28) and (29) are used it follows that to lowest order

$$\dot{R}_n = d/2\pi R_n, \quad \ddot{R}_n = -d^2/4\pi^2 R^3, \quad \dddot{R}_n = 3d^3/8\pi^3 R^5 \quad (49)$$

Consequently, the factor in front of G_0 in eq (43) is of order R , the factor in front of G_2 of order $1/R$. From the asymptotic expansions of I_m and K_m it is readily seen that the asymptotic expansion of the G_k is of the form

$$G_k(x, y) = \frac{1}{\sqrt{xy}} \exp(-|x-y|) \left(a_k - b_k \frac{|x-y|}{(x+y)^2} + \dots \right) \quad (50)$$

$$a_0 = \pi, \quad a_2 = \pi^3/2, \quad b_0 = \pi/8 \dots \quad (51)$$

Finally, combination of eqs (30), (35), (43), (44), (49) and (50) gives

$$\lambda^{-2} \int_0^{\infty} K_0 \left(\frac{\Delta r}{\lambda} \right) R(p) R^1(p) dp = \sum_n \frac{d}{2\pi\lambda} \left(1 + \frac{a}{R_0} + \dots \right) \sqrt{1 + \frac{nd}{R_0} + \dots} \exp(-|n|d \left(1 + \frac{a}{R_0} + \dots \right)) \times$$

$$\times \left(a_0 - b_0 \frac{d|n|\lambda}{4R_0^2} \left(1 + \frac{a}{R_0} + \dots \right) + \dots \right) \quad (52)$$

The summation variable n runs from a certain negative number (namely the smallest integer above $-\theta_0/2\pi$) to $+\infty$, but because of the cut-off factor $\exp(-|n|d)$ it makes no difference for the asymptotic expansion when n is running from $-\infty$ to $+\infty$.

Upon expanding the square root and using the following sums

$$\sum_{n=-\infty}^{\infty} \exp(-|n|x) = \coth(x/2) \quad , \quad (53)$$

$$\sum_{n=-\infty}^{\infty} n \exp(-|n|x) = 0 \quad , \quad (54)$$

it is found that

$$\lambda^{-2} \int_0^{\infty} K_0 \left(\frac{\Delta r}{\lambda} \right) R(p) R^1(p) dp = \frac{d}{2\lambda} \coth \frac{d}{2\lambda} + \frac{a}{R_0} \left(\frac{d}{2\lambda} \coth \frac{d}{2\lambda} - \frac{d^2/4\lambda^2}{\sinh^2(d/2\lambda)} \right) + \dots \quad , \quad (55)$$

when terms of order $1/R_0^2$ are neglected.

In the same way as we obtained the first terms of the Taylor expansion of eq (17) in the preceding section (the eqs (24) and (25)) we are now in a position to give the first terms of the asymptotic expansion, using eq (55) and the asymptotic expansion of the right hand side of eq (17). Indeed, using the explicit form eq (15) of g and the expansion, eq (30), of φ , it is found that

$$\omega_0 \frac{d}{2\lambda} \coth \frac{d}{2\lambda} = 1 - \omega_0 \lambda^* \frac{d}{\lambda^2} \quad , \quad (56)$$

$$\omega_0 a \left(\frac{d}{2\lambda} \coth \frac{d}{2\lambda} - \frac{d^2/4\lambda^2}{\sinh^2(d/2\lambda)} \right) = \frac{r_1}{1 - \exp\left(\frac{r_1}{r_c}\right)} - \omega_0 \lambda^* a \frac{d}{\lambda^2} \quad (57)$$

The first expression, eq (58), has been given by Chernov [9] and Bennema and Gilmer [6] too, assuming that at large distances from the origin the spiral is constituted from parallel equidistant steps, for which the diffusion problem has been solved by a straight forward approach.

They gave eq (56) in the form

$$\omega_0 = \frac{2\lambda}{d} \zeta \tanh \frac{d}{2\lambda} \quad , \quad (58)$$

where ω_0 determines to the growth rate of the crystal face under consideration, and ζ is a factor

$$\zeta = \left[1 + \frac{2\lambda^*}{\lambda} \tanh \frac{d}{2\lambda} \right]^{-1} \quad , \quad (59)$$

which measures the influence of finite integration times ($\lambda^* \neq 0$)

From the second expression, eq (57) it is seen that ω must always be negative (since $\text{cotanh } x$ is larger than $x/\sinh^2 x$ for all positive x). In view of eq (28) this means that the step distance far from the centre is larger than close to it. This qualitative result should have been expected, since a stationary spiral means that the step flux (the product of step density and step velocity) is constant for the whole spiral. The spiral is the more curved, and hence moving the slower, the closer the centre is approached and this has to be compensated with a higher step density, i.e. smaller step distance.

5 THE TAPERING FACTOR AND THE BASIC EQUATION

In the preceding sections we have seen that the spiral can be approximated by an archimedean spiral both close to the centre and far away from it. However, these approximations do not necessarily have the same characteristic length. More precisely $r^1(p)/\theta^1(p)$ tends to different constants for $p \rightarrow 0$ and $p \rightarrow \infty$. The most obvious object to investigate at present is therefore

$$T = \lim_{p \rightarrow \infty} \frac{R^1(p)}{\theta^1(p)} / \lim_{p \rightarrow 0} \frac{R^1(p)}{\theta^1(p)} \quad (60)$$

This quantity will be termed tapering factor since it measures the difference of tapering of the spiral hillock at the top and at the base. If the spiral is archimedean $T = 1$ and the hillock has a constant tapering. If $T > 1$ the spiral is more curved in the centre and the corresponding hillock is stronger tapered at the top. It is of interest to note that the growth rate and the slope of the spiral hillock are the physically most important quantities and they can easily be obtained as soon as T is known.

In order to obtain an estimate of T the spiral shape $R^1(p)/\theta^1(p)$ is approximated by a trial function which we choose to be of the following form:

$$\frac{R^1(p)}{\theta^1(p)} = A\lambda \frac{1+TBp}{1+Bp} \quad , \quad (61)$$

where A and B are adjustable positive numbers.

From the definition eq (8) of the radius of curvature it follows that

$$\rho(o) = \frac{1}{2}A\lambda \quad . \quad (62)$$

Upon using eq (21) again for the dependence of R on p it follows

$$\theta^{11}(o) = \frac{B}{A} (1-T) \quad . \quad (63)$$

On the other hand, the asymptotic expansions of eqs (28) and (61) should coincide and this gives

$$T = \frac{d}{2\pi A\lambda} = \frac{d}{4\pi\rho(o)} \quad , \quad (64)$$

$$\frac{ad}{2\pi} = \frac{A\lambda^2}{B} (1-T) \quad . \quad (65)$$

At this point we have eight relations eqs (24), (25), (56), (59) and (62) - (65) between eight unknowns A, B, T, $\rho(o)$, a, d, $\theta^{11}(o)$ and ω_o . We now proceed to reduce this set to a single equation for the distance d between spiral turns. Indeed, eq (58) expresses ω_o in terms of $d/2\lambda$ and, using eq (24) we find for $\rho(o)$

$$\frac{r_1}{\rho(o)} = \ln \left[1 - (1-\omega_o) (r_1 \exp(r_1/r_c)) \right] \quad (66)$$

Upon multiplying eq (56) by a and subtracting the result from eq (57)

$$\frac{r_1}{a} = (1-\omega_o) \left(\frac{d/2\lambda}{\sinh(d/2\lambda)} \right)^2 (r_1 \exp(r_1/r_c)) \quad , \quad (67)$$

substitution of eq (64) in eq (65) gives

$$\frac{B}{A} = \frac{2\pi\lambda^2}{ad} \left(1 - \frac{d}{4\pi\rho(o)}\right), \quad (68)$$

and hence

$$\theta^{11}(o) = \frac{2\pi\lambda^2}{ad} \left(1 - \frac{d}{4\pi\rho(o)}\right)^2 \quad (69)$$

In this way the seven quantities A, B, T, $\rho(o)$, a, $\theta^{11}(o)$ and ω_o are given in terms of $d/2\lambda$. It is also straight forward to integrate eq (61) in order to obtain θ as a function of $p = R/\lambda$

$$\begin{aligned} \theta(p) &= \frac{p}{AT} - \frac{1-T}{ABT^2} \ln(1+BTp) \\ &= \frac{2\pi\lambda p}{d} - \frac{2\pi a}{d} \ln\left(1 + \frac{\lambda}{a}(1-T)p\right) \end{aligned} \quad (70)$$

Substituting these results in eq (25) we may conceive that equation as a non-linear equation for $d/2\lambda$:

$$\omega_o \left(\int_0^\infty K_1(p) p \cos \theta(p) dp + 2\pi \frac{\lambda^*}{\lambda} \right) + 3\theta^{11}(o) \frac{r_1}{\lambda} \frac{e^{r_1/\rho(o)}}{e^{r_1/r_c-1}} = 0 \quad (71)$$

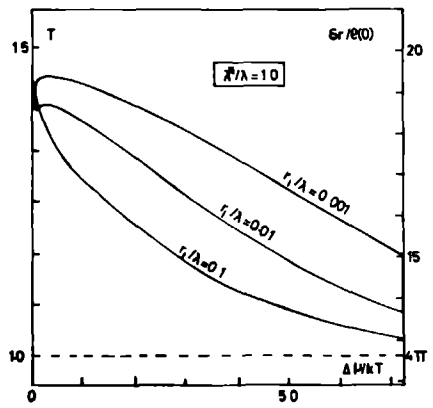
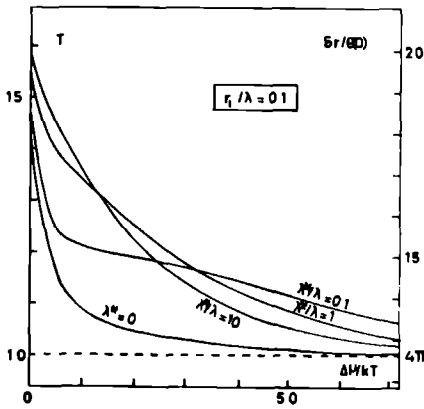
This equation can be solved numerically for different values of λ^*/λ , r_1/λ and r_1/r_c and from the so obtained $d/2\lambda$ all other spiral characteristics are easily traced back.

Indeed, the fractional growth rate ω_o is given by eq (58), the slope of the growth hillock is proportional to $d/2\lambda$, and the tapering factor satisfies

$$(T-1)^2 = \frac{d\omega_o \left(\int_0^\infty K_1(p) p \cos \theta(p) dp + 2\pi\lambda^*/\lambda \right) \exp(r_1/r_c)}{6\pi\lambda \left(1 - \omega_o \left(\frac{d/2\lambda}{\sinh(d/2\lambda)}\right)^2\right) (1 - \omega_o (1 - \exp(r_1/r_c)))} \quad (72)$$

This equation is obtained by substitution of eq (69) in (71) using the eqs (64), (66) and (67) for T, $\rho(o)$ and a.

The behaviour of ω_o and T in dependence on the supersaturation r_1/r_c is, for some values of λ^*/λ and r_1/λ given in fig (2). When r_1/r_c increases from zero to infinity then ω_o increases from 0 to 1 and T decreases from a finite value to 1, sometimes after a maximum has been passed.



- 2a. The supersaturation (r_1/r_c) dependence of the tapering factor T , for $r_1/\lambda = 0.1$ and different values of λ^*/λ . This figure is the same as fig. 1a of ref. [1].
- 2b. The supersaturation dependence of the tapering factor T , for $\lambda^*/\lambda = 1.0$ and different values of r_1/λ . This figure is the same as fig. 1b of ref. [1].

6 QUALITATIVE BEHAVIOUR AND THE BACK FORCE EFFECT

In this reasoning we assume a priori that the tapering factor T remains finite, an assumption which is justified a posteriori. Upon equating the two expressions for ω_0 , eq (24) and eq (58), using eq (64), it follows that

$$1 - \frac{1 - \exp(4\pi\eta/Td)}{1 - \exp(\eta/r_c)} = \frac{2\lambda}{d} \frac{1}{2 \frac{\lambda^*}{\lambda} + \coth \frac{d}{2\lambda}} = \omega_0 \quad (73)$$

The left hand side is zero for $d = d_c \equiv 4\pi r_c T$, i.e. for $\rho(0) = r_c$, and increases thereafter monotonically to 1, with increasing d .

The right hand side decreases from 1 for $d = 0$ to zero for $d \rightarrow \infty$. This means that the equation has a unique solution $d > d_c$, which solution decreases with increasing supersaturation $1/r_c$.

In order to study eq (73) we first linearize it around d_c , i.e. we expand to first order in the parameter $\delta = (d - d_c)/d_c$. After some straight forward operations, using $\sinh 2x = 2 \sinh x \cosh x$, it readily follows that the solution of the linearized eq (73) reads

$$\delta \equiv \frac{d-d_c}{d_c} = \omega_c \cdot \frac{r_1/r_c}{1-e^{-r_1/r_c}} + \omega_c \left(1 - \frac{\mathfrak{J}_c d_c/\lambda}{\sinh(d_c/\lambda)}\right)^{-1}, \quad (74a)$$

where ω_c and \mathfrak{J}_c are the values of ω_0 and \mathfrak{J} when $\rho(0)$ would equal r_c . This solution, however, approximates the real solution of eq (73) only if $\delta \ll 1$. An upper bound for δ is found by observing that the second term in the square brackets in eq (74) is positive:

$$\delta < \omega_c \frac{1-\exp(-r_1/r_c)}{r_1/r_c} < \omega_c \frac{r_c}{r_1} \left[\frac{\lambda}{2\pi T r_1} \frac{r_c}{\lambda} + \coth \frac{d_c}{2\lambda} \right]^{-1} \quad (75)$$

It thus follows that $d = d_c (1 + \delta)$ is an approximate solution of eq (73) unless r_1/r_c , r_1/λ , λ^*/λ and $r_c/2\lambda$ are all small. To this case we shall refer as the back force regime since now the central turn of the spiral is forced to a curvature considerably different from r_c by the outer spiral turns. The fact that r_1/r_c and d/λ are small allows to expand both sides of eq (73) in r_1/r_c and $d/2\lambda$:

$$1 - \frac{d}{d_c} + \dots = 1 - \frac{\lambda^* d}{\lambda^2} + \left(\left(\frac{\lambda^*}{\lambda} \right)^2 - \frac{1}{12} \right) \left(\frac{d}{\lambda} \right)^2 + \dots \quad (76)$$

When the terms with λ^*/λ are neglected the solution is

$$d \approx (12 d_c \lambda^2)^{1/3} = 5.32 (T r_c)^{1/3} \lambda^{2/3} \quad (74b)$$

This solution remains valid as long as λ^*/λ is small compared to $(d_c/\lambda)^{1/3}$; when, on the other hand $\lambda^*/\lambda \gg (d_c/\lambda)^{1/3}$ (but still $\lambda^*/\lambda \ll 1$) then

$$d \approx \lambda (d_c/\lambda^*)^{1/2} = 3.54 (T r_c)^{1/2} \lambda \lambda^{*-1/2} \quad (74c)$$

Note that in both cases d/λ is small as soon as $d_c/\lambda \ll 1$ such that eq (73) is a good approximation to eq (73).

Finally, using eqs (74) approximate expressions for ω_0 and T can be given in the different limiting cases. First, outside the back force regime $\omega_0 \approx \omega_c$, and the tapering factor is found from eq (72) substituting ω_c for ω_0 , and d_c for d . Let us consider the r_1/r_c dependence of T .

For $r_1/r_c \rightarrow 0$ the integral approaches $\pi/2$, $\omega_0 \rightarrow 0$ and $d_c \omega_c / 2\lambda \rightarrow (1 + 2\lambda^*/\lambda)^{-1}$ such that

$$\lim_{r_1/r_c \rightarrow 0} T = 1 + (1/3) \frac{\frac{1}{2} + 2\lambda^*/\lambda}{1 + 2\lambda^*/\lambda} \frac{1}{2} \quad (77)$$

For $r_1/r_c \rightarrow \infty$, on the other hand, the integral tends to zero, $d_c \omega_c / 2\lambda \rightarrow 1$, the numerator in eq (72) approaches zero as a polynomial in $d_c / 2\lambda$, and the factor $\exp(-r_1/r_c)$ in the denominator vanishes exponentially fast, hence

$$\lim_{r_1/r_c \rightarrow \infty} T = 1 \quad (78)$$

showing that the spiral becomes archimedean at large enough supersaturations.

For intermediate values of r_1/r_c the tapering factor would be large if at the same time $d_c \omega_c / 2\lambda \approx 1$, $r_1/r_c \ll 1$ (otherwise the exponential decay sets on), and $\omega_c \approx 1$ (such that the numerator is small). Inspection of the formulae shows that these conditions are equivalent to the conditions of the back force regime.

Turning then to the back force regime, let us first consider the case that $\lambda^*/\lambda \approx 0$, such that eq (74b) holds. Then $\omega_o \approx 1 - \frac{1}{12} (d/\lambda)^2$ (right hand side of eq (76)), the integral in eq (72) is about $\frac{\pi}{2} (d/2\pi\lambda)^3$ (assuming that the main contribution is from the outer part of the spiral), and upon substituting these results in eq (72) it follows that

$$(1-T)^2 \approx \left(\frac{d}{\lambda}\right)^2 \left(\frac{1}{2\lambda}\right)^3 \quad (79a)$$

Similarly, when eq (74c) holds, it is found that

$$(T-1)^2 \approx \frac{1}{12} \frac{\lambda}{\lambda^*} \left(\frac{d}{2\pi\lambda}\right)^3 \quad (79b)$$

Since one of the conditions of the back force regime is $d/2\lambda \ll 1$, the right hand sides of eqs (79) remain bounded, in contrast to eq (72) which would lead to large values of $(T-1)^2$ in these parameters ranges. It is thus seen that the back force effect reduces the tapering. This explains why the tapering curves in fig. (2) do not predict very large tapering factors, even in the region where the substitution of d_c and ω_c in eq (72) would do so. The existence, however, of a maximum in some of the curves is reminiscent of the competing effects of the free spiral and the back force effect.

7 CONCLUSIONS

The free boundary diffusion problem in two dimensions for a boundary with a stationary spiral shape has been studied. Exact relations between the rotational frequency, the central radius of curvature and the distance between spiral turns far from the centre have been derived, using the potential theory technique.

An approximate expression for the tapering factor, which characterizes the deviation from the archimedean shape, has been obtained from the numerical solution of a characteristic equation which connects the local behaviour of the spiral in the centre with that in the outer regions. Some limiting cases and the influence of the back force effect have been studied too.

REFERENCES

1. J.P. van der Eerden, the manuscript going herewith.
2. H.Müller Krumbhaar, T.W. Burkhardt and D.M. Kroll, J. Crystal Growth 38 (1977) 13-22.
3. I. Stakgold, "Boundary Value Problems of Mathematical Physics" II (Mac Millan, New York, 1968).
4. N.K. Burton, N. Cabrera and F.C. Frank, Phil. Mag. 243 (1951) 299.
5. N. Cabrera and M.M. Levine, Phil. Mag. 1 (1956) 450.
6. P. Bennema and G.H. Gilmer in "Crystal Growth, an Introduction", ed. P. Hartman (North Holland, Amsterdam, 1973) 263.
7. For this and other properties of Bessel functions see e.g. G.N. Watson, "a treatise on the theory of Bessel functions" (Cambridge, 1962).
8. See e.g. K. Rektorys "Survey of Applicable Mathematics" (M.I.T. Press, Cambridge, 1969) Ch 9.
9. A.A. Chernov, Sov. Phys. Usp. 4 (1961) 116.

TRANSITION FROM ISLAND TO LAYER GROWTH OF THIN FILMS: A MONTE CARLO SIMULATION

D. KASHCHIEV *, J.P. VAN DER EERDEN and C. VAN LEEUWEN

Laboratory of Physical Chemistry, Delft University of Technology, Delft, The Netherlands

Received 20 August 1976, revised manuscript received 25 March 1977

The results of a Monte Carlo simulation of the process of thin film deposition on to a face of Kossel crystal as a substrate are presented. The island and the layer modes of film growth are illustrated by morphological observations at different supersaturations β . It is shown that the cluster growth shape differs noticeably from the theoretical equilibrium one and changes with β and time. The time dependence of the degree of coverage of the successive layers and the mean film height are measured for different β . For deposition on to the own substrate it is found that the interface width at the moment t_{99} of 99% substrate coverage increases with β from about 2 to 10 monolayers, values being limiting for low and high β , respectively. The observed strong β dependence of the mean film height N_{99} at t_{99} is used for determination of the critical supersaturation β_c for changing the mode of film growth. A very good quantitative agreement is established between the simulation data for N_{99} and β_c and the predictions of a recently proposed generalized theory of layer growth.

1. Introduction

In a previous paper [1] a generalization was made of the theory of layer growth of an interface free of screw dislocations and it was shown that it can be used for description of the growth of a thin film on a foreign substrate. It was established that depending on the correlation between the intensities of the kinetics of filling up the successive layers the film may grow either by simultaneous spreading of only a few layers (layer growth) or via formation and growth of island-like crystallites of multiautomic height (island growth). With the aid of a concrete example it was shown how one can find the critical supersaturation at which a change of the mode of film growth occurs.

The different modes of thin film growth as well as the existence of a critical supersaturation of transition between them are known experimental facts [2–9] and a number of theoretical works [2,9–12] is concerned with them. So far, however, there is not yet a firmly established correspondence between theory and experiment.

In this work our aim is to simulate by Monte Carlo

technique the process of thin film deposition on to a foreign substrate. Special attention will be paid to the phenomenon of changing the mode of film growth, as it may prove very important for understanding the epitaxial growth of thin films. The exact knowledge of the physical parameters and the state of the system is an unique feature of the simulation method, which we shall use to confront the simulation results with the newly-proposed analytical theory [1]. It will be seen that this theory provides a fairly good description of the simulation findings concerning the supersaturation dependence of the mean height of the film and the value of the critical supersaturation for changing the mode of the film growth.

2. Simulation model

We are compelled to simulate the process of thin film deposition by means of a system which (i) permits obtaining results within reasonably short computing times, and (ii) is accessible to an analytical description, as exact as possible. This is why the physical model and the numerical values of the parameters used for simulation do not correspond necessarily to the experiments which offer a con-

* Permanent address: Institute of Physical Chemistry, Bulgarian Academy of Sciences, Sofia 1113, Bulgaria.

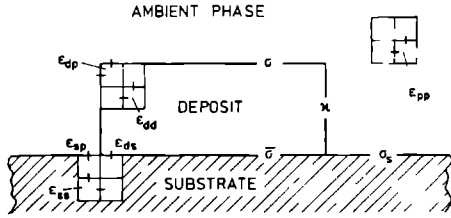


Fig 1 The deposition model

siderably variety of particular cases. Mainly because of the second requirement, our model is the simplest possible and is characterized as follows (fig 1)

(1) The substrate is of ideal simple cubic structure with a lattice constant a (cm) and is held at a constant absolute temperature T (K). The strong interaction of energy ϵ_{ss} (erg/atom) between the nearest neighbours in the bulk of the substrate ensures perfect atomic smoothness of its surface at the given temperature

(2) The deposited material has the lattice constant and the temperature of the substrate and a nearest neighbour binding energy ϵ_{dd} . The interaction between the deposit and the substrate is also within the range of nearest neighbours only and the bond energy is ϵ_{ds} . For the deposition conditions used the solid on solid restriction is a reasonable approximation [13] and because of that we do not allow formation of overhangs during the process

(3) The ambient phase has the same temperature and its homogeneity permits describing it by the same lattice structure. The bond energies ϵ_{pp} , ϵ_{dp} and ϵ_{sp} refer to the interaction between neighbouring cells within the ambient phase and on its boundary with the deposit and the substrate, respectively

(4) The adatom surface diffusion is fully prohibited during the deposition process. The simulation of surface diffusion is not difficult [14–16], but its presence hinders considerably the reliable interpretation of the computer results by analytical formulae

The elementary events of direct adding and losing single atoms are specified by the frequencies (in atoms per sec per site) of attachment to whatever site on the surface of both the substrate and the deposit (k^+) and of detachment from a site on to the deposit (k_i^-) or the substrate ($k_{s,i}^-$) having $i = 0, 1, 2, 3, 4$ lateral nearest neighbours

As seen, the model chosen can be conceived as a generalization of the lattice gas model [17,18]. Application of the principle of microscopic reversibility to this model [15,19] gives us the following expressions for the dependence of the elementary frequencies on ι , the bond energies and the super saturation $\Delta\mu$ (erg/atom)

$$k^+ = k_e^+ e^\beta, \quad (2.1)$$

$$k_i^- = k_e^- e^{2\omega(2-i)}, \quad (2.2)$$

$$k_{s,i}^- = k_e^+ e^{2\omega(2-i) + 2\Delta\omega} \quad (2.3)$$

In these relations k_e^+ stands for the frequency of single atom addition at equilibrium between the deposit and the ambient phase and the parameters β , ω and $\Delta\omega$ are introduced for brevity by the definition equalities (k_B is the Boltzmann constant)

$$\beta = \Delta\mu/k_B T, \quad (2.4)$$

$$\omega = (\epsilon_{dd} + \epsilon_{pp} - 2\epsilon_{dp})/2k_B T, \quad (2.5)$$

$$\Delta\omega = (\epsilon_{dd} - \epsilon_{ds} + \epsilon_{sp} - \epsilon_{dp})/2k_B T \quad (2.6)$$

The three kinds of elementary frequencies from (2.1)–(2.3) are sufficient for simulation of the process and at any given ambient phase and temperature varying β , ω and $\Delta\omega$ physically means using different supersaturations, deposits and substrates, respectively. For this reason it is worth noting how ω and $\Delta\omega$ are connected with the specific surface free energies (in erg/cm²) of the interfaces deposit/ambient phase (σ), substrate/ambient phase (σ_s) and deposit/substrate ($\bar{\sigma}$). For low enough temperatures these quantities can be approximated by the formulae

$$\sigma = \omega k_B T/a^2, \quad (2.7)$$

$$\sigma_s = (\epsilon_{ss} + \epsilon_{pp} - 2\epsilon_{sp})/2a^2,$$

$$\bar{\sigma} = (\epsilon_{ss} + \epsilon_{dd} - 2\epsilon_{ds})/2a^2,$$

and if we introduce the quantity

$$\Delta\sigma = \sigma + \bar{\sigma} - \sigma_s, \quad (2.8)$$

we shall obtain

$$\Delta\sigma = 2\Delta\omega k_B T/a^2 \quad (2.9)$$

Besides, statistical calculations on the basis of the same model [20] show that the specific edge free energy κ (erg/cm) of the clusters of the deposited

material is related to the parameter

$$\gamma = \omega + \ln[(1 - e^{-\omega})/(1 + e^{-\omega})], \quad (2\ 10)$$

by the equality

$$\kappa = \gamma k_B T/a \quad (2\ 11)$$

The logarithmic term in (2 10) is a correction allowing for the roughening of the cluster periphery at higher temperatures. The familiar low temperature approximation $\gamma = \omega$ (i.e. $\kappa = a\sigma$) follows from (2 10) at $\omega \gg 1$.

The physical meaning of the correlations between ω and σ and between $\Delta\omega$ and $\Delta\sigma$ is most easily seen if the ambient phase is a gas, as then practically $\epsilon_{pp} = \epsilon_{dp} = \epsilon_{sp} = 0$. One characteristic case is the deposition on to the own substrate. Then $\epsilon_{ds} = \epsilon_{dd}$ and $\epsilon_{sp} = \epsilon_{dp}$ and consequently the condition $\Delta\omega = 0$ (or $\Delta\sigma = 0$) will refer to the growth of a given interface.

Moreover eq (2 3) shows that at $\Delta\omega < 0$ the adsorption is promoted as compared with that on the own substrate (then $k_s^- < k_t^-$). On the contrary $\Delta\omega > 0$ implies more weakly adsorbing substrate. In particular when the interaction between the substrate and the deposit is identical to that between the latter and the ambient phase, $\epsilon_{ds} = \epsilon_{dp}$ and $\epsilon_{sp} = \epsilon_{pp}$ hold. Then $\Delta\omega = \omega$ and the deposition is not influenced energetically by the presence of the substrate.

3 Theory

For interpretation of the simulation results we need to know what is the influence of the supersaturation on the mean film height h_{99} (cm) at the moment t_{99} of reaching 99% substrate coverage. In the simulation model only the atoms of the first layer feel the presence of the substrate and the filling of the second, the third, etc. layers occurs exactly as on to the own one. This allows a straightforward use of the analytical formulae in section 6 of ref [1] (all notations to follow are defined in ref [1] and the equations referring to it are supplied with the Roman numeral I). If N_{99} is the mean height h_{99} measured in number of monolayers, according to (I 6 7) (I 3 16), (I 6 4) and $N_{99} = h_{99}/a$ we can write

$$N_{99} = \nu_k + \psi\theta_1/\theta_2 \quad (3\ 1)$$

It is seen that the supersaturation dependence of N_{99} is determined first and foremost by the ratio of

the time constants θ_1 (sec) and θ_2 (sec) for overall filling up the first and the second layers as they are strong functions of β . The numerical factor ψ is almost β independent and is defined by

$$\psi(m_1, m_2) = [(4.61)^{1/m_1} - \Gamma(1 + 1/m_1)]/\Gamma(1 + 1/m_2) \quad (3\ 2)$$

Here Γ is the complete gamma function and $m_1, m_2 > 0$ are kinetic coefficients varying usually from 1 to 3, so that for example $\psi(3,1) = 0.77$ and $\psi(1,1) = 3.61$. The height ν_k (atoms) of the flat nucleus is given by the expression

$$\nu_k = \begin{cases} 4\Delta\omega/\beta, & 0 \leq \beta \leq 4\Delta\omega, \\ 1, & 4\Delta\omega \leq \beta, \end{cases} \quad (3\ 3)$$

resulting upon combining (I 5 5), (2 4) and (2 9) and using table 1 of ref [1]. Eq (3 3) shows that the nucleus is of monoatomic height only at high enough β (fig 2).

Clearly, to make further use of the general equation (3 1) we must know m_1, m_2, θ_1 and θ_2 , quantities which can be found only by means of a concrete model for the kinetics of overall filling of the first two layers.

Let us first consider the filling of the second layer in order to determine m_2 and θ_2 . Under our simulation conditions this layer may be filled in the way which is characteristic for the continuous (called also normal or liquid-like) growth of a given interface. In accordance with section 4c of ref [1] and eq (I 4 9) such kinetics of filling are specified by

$$m_2 = 1, \quad (3\ 4)$$

$$\theta_2 = (a^2 J_2)^{-1} = (k^+ - k_2^-)^{-1}, \quad (3\ 5)$$

since the area occupied by an atom is a^2 and the net rate J_2 ($\text{cm}^{-2}\text{sec}^{-1}$) of depositing single atoms within the second layer is given by the difference between the rate k^+/a^2 of attachment to and the rate k_2^-/a^2 of

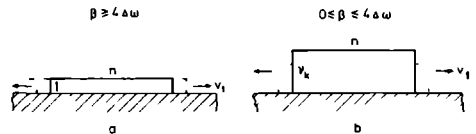


Fig 2 The first layer and the flat clusters within it have monoatomic (a) and ν_k atomic (b) height at high and low supersaturations, respectively

their detachment from sites with two lateral neighbours. Of course, the atom detachment rate is different for each $i = 0, 1, 2, 3, 4$, but one must choose k_2^-/a^2 as a characteristic one, for $i = 2$ refers to an atom in a kink position. Thus, in view of (2.1) and (2.2), from (3.5) we find

$$\theta_2 = 1/k_2^+(e^\beta - 1) \quad (3.6)$$

The determination of m_1 and θ_1 is somewhat more complicated. Depending on β , under the simulation conditions the building of the first layer occurs in two ways: at higher β as discussed above (continuous growth mechanism), and at lower β via formation and growth of flat clusters of height ν_k (nucleation growth mechanism). This demands a separate consideration of each one of these cases.

(a) Nucleation growth mechanism of filling the first layer

Let us assume that steady state nucleation and time independent lateral growth of flat clusters with square bases are operative within the first layer. Since the nucleation rate J_1 ($\text{cm}^{-2}\text{sec}^{-1}$) and the velocity v_1 (cm/sec) of spreading do not depend on time, recalling section 4a of ref. [1], in this case we may write

$$m_1 = 3, \quad (3.7)$$

$$\theta_1 = (3/4 v_1^2 J_1)^{1/3} \quad (3.8)$$

Expressions for J_1 and v_1 are given in the Appendix. If we put (A.7), (A.8) and (A.10) into (3.8) we shall get θ_1 for the two supersaturation regions. Insertion of the obtained result into (3.1) and accounting for (3.2)–(3.4), (3.6) and (3.7) will give us the sought dependence of N_{99} on β when the deposition occurs through nucleation and growth of flat clusters within the first layer and continuous growth within the second one

$$N_{99} = \begin{cases} 4\Delta\omega/\beta + 0.77(9\pi\Delta\omega/8)^{1/6}\beta^{-1/3} \\ \times e^{4\omega/3+2\Delta\omega/3} \\ \times e^{-\beta}(e^\beta - 1)(e^{\beta/2} - 1)^{-2/3} e^{32\gamma^2\Delta\omega/3\beta^2} \\ 0 \leq \beta \leq 4\Delta\omega, \\ 1 + 0.77[9\pi/64(\beta - 2\Delta\omega)]^{1/6} \\ \times e^{4\omega/3+2\Delta\omega/3} e^{-2\beta/3} \\ \times (e^\beta - 1)(e^\beta - e^{2\Delta\omega}) e^{4\gamma^2/3(\beta-2\Delta\omega)}, \end{cases} \quad (3.9)$$

(b) Continuous growth mechanism of filling of the first layer

As this is the mechanism of filling of the second layer which has already been considered, by analogy with (3.4) and (3.5) we can write

$$m_1 = 1, \quad (3.10)$$

$$\theta_1 = (k^+ - k_s^-)^{-1} \quad (3.11)$$

Here k_s^- allows for the fact that now the atoms desorb from the foreign atoms of the substrate. In view of (2.1) and (2.3) eq. (3.11) is equivalent to

$$\theta_1 = 1/k_c^+(e^\beta - e^{2\Delta\omega}), \quad \beta \geq 4\Delta\omega \quad (3.12)$$

This expression is valid only provided the first layer is of monoatomic height. If we want to extrapolate formally the continuous growth mechanism at $\beta < 4\Delta\omega$, too, we must use again (3.11), but with k_{col}^+ and k_{col}^- approximated by (A.5) and (A.9). This will give

$$\theta_1 = 1/k_c^+(e^\beta - e^{\beta/2}), \quad 0 \leq \beta \leq 4\Delta\omega \quad (3.13)$$

Thus, when the deposition within both the first and the second layers occurs by the continuous growth mechanism, with the help of (3.2)–(3.4), (3.6), (3.10), (3.12) and (3.13) from (3.1) we find that the dependence of N_{99} on β is

$$N_{99} = \begin{cases} 4\Delta\omega/\beta + 3.61(e^\beta - 1)/(e^\beta - e^{\beta/2}), \\ 0 \leq \beta \leq 4\Delta\omega, \\ 1 + 3.61(e^\beta - 1)/(e^\beta - e^{2\Delta\omega}), \\ 4\Delta\omega \leq \beta \end{cases} \quad (3.14)$$

We shall need a formula for one more quantity – the number N_{99}^{ow} of monoatomic layers giving the mean film height at the moment t_{99} in case of deposition on to the own substrate (i.e. at $\Delta\omega = 0$). Now $\nu_k = 1$ and all layers are filled by one and the same mechanism, so that $m_1 = m_2$, $\theta_1 = \theta_2$. Then, according to (3.1) and (3.2)

$$N_{99}^{\text{ow}} = (4.61)^{1/m_1} / \Gamma(1 + 1/m_1), \quad (3.15)$$

and in particular

$$N_{99}^{\text{ow}} = 4.61, 2.43, 1.86 \quad \text{for } m_1 = 1, 2, 3, \quad (3.16)$$

respectively. It is clear that if N_{99}^{ow} is an experimentally known function of β , using (3.15) we can judge about the influence of the supersaturation on the

kinetic index m_1 which may be expected to vary from $m_1 = 3$ (low β , nucleation growth mechanism) to $m_1 = 1$ (high β continuous growth mechanism)

4 Simulation results

The present Monte Carlo simulation is similar to those of Abraham et al [14,16] on heterogeneous deposition. The simulation results were obtained by means of the computer programs described elsewhere and used for studying the structure [21] and the growth [15] of a face of a Kossel crystal. Minor changes were made in order (i) to eliminate the adatom surface diffusion, (ii) to forbid detachment of atoms belonging to the substrate, and (iii) to allow for the difference in the probabilities of detaching an atom staying on top of foreign or own atom. In this way the deposition started on a bare substrate of size 50×50 atoms which remained perfectly smooth throughout the whole process. It was covered as a result of many elementary acts of single atom attachment and detachment occurring with the frequencies k^+ , k_t and $k_{s,l}^-$ from (2.1)–(2.3). The necessary information about the time dependences of the cluster sizes, the total amount of the deposited material and the degree of coverage of the different layers was provided by a subroutine for lateral scanning within each one of the populated layers. The above quantities are integral ones and the substrate size was large enough to ensure measuring them with good reproducibility. Indeed, repeated computer experiments showed that, except for the lowest substrate coverages, the deviations between the data taken from different outputs were less than 5%. The simulation results reported below were obtained by single runs performed with various β and $\Delta\omega$, but always with one and the same $\omega = 1.3$.

4.1 Growth shape of the crystallites

With respect to morphology the growth history of the thin film is the same as that observed during physical experiments [9]. At lower supersaturations first separate island-like clusters form on the substrate, then they grow laterally and vertically, coalesce without, of course, producing grain boundaries, and finally fill up entirely the substrate. At higher β ,

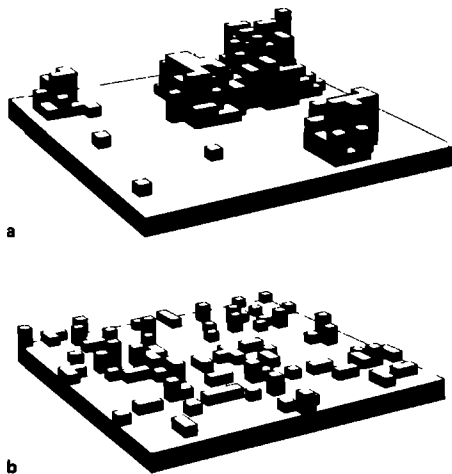


Fig 3 Thin film morphology at about 20% substrate coverage (a) island growth ($\beta = 2.8$, $\Delta\omega = 1.3$), and (b) layer growth ($\beta = 5.2$, $\Delta\omega$ – the same)

instead of by large and high islands, the substrate is covered by a multitude of smaller clusters which start coalescing, when containing several atoms only. The morphology of the film during the initial stage of the process is shown in fig 3 at $\Delta\omega = 1.3$ and at the moment of about 20% substrate coverage. The two modes of film growth, the island one at $\beta = 2.8$ (fig 3a) and the layer one at $\beta = 5.2$ (fig 3b), are clearly revealed.

The simulation results permit testing the reliability of the frequently used assumption that the island-like clusters grow by keeping their equilibrium shape. In our model the equilibrium shape is a square prism with an edge of n atoms and a height of ν atoms whose ratio is given by the ratio ν_k/n_k characteristic for the nucleus, i.e.

$$\nu/n = \nu_k/n_k = \Delta\omega/\gamma, \quad 0 \leq \beta \leq 4\Delta\omega, \quad (4.1)$$

in accordance with (3.3) and (A.2). It may be noted that the right hand side of (4.1) passes into the familiar approximation $\nu_k/n_k = \Delta\omega/\omega$ [2,22–24], if in (2.10) $\omega \gg 1$. With the chosen $\omega = 1.3$, eq (2.10) yields $\gamma = 0.75$ – a value which will be used in all further numerical calculations of analytical formulae.

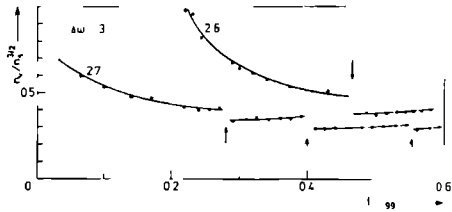


Fig 4 Time variation of the shape ratio during growth for the largest cluster at $\beta = 2.6$ and 2.7 when $\Delta\omega = 1.3$. The arrows indicate the moments of growth coalescence

It is more convenient to represent (4.1) in the equivalent form

$$n_v/n_s^{3/2} = \Delta\omega/\gamma, \quad 0 \leq \beta \leq 4\Delta\omega \quad (4.2)$$

Indeed, the total volume number n_v and surface number n_s of atoms constituting the cluster and forming its base, respectively are defined for all cluster shapes and therefore accessible to direct determination from the simulation data. As seen, when the clusters grow preserving their equilibrium shape, the quantity $n_v/n_s^{3/2}$ should not depend on time t , neither on β . Fig 4 shows the measured ratio $n_v/n_s^{3/2}$ referring to the largest cluster on the substrate. The substrate is of $\Delta\omega = 1.3$ and the time evolution of $n_v/n_s^{3/2}$ is presented as a function of the variable t/t_{99} at $\beta = 2.6$ and 2.7 (the figures at the corresponding curves). It is clearly visible that for small t/t_{99} the shape ratio is closer to the equilibrium value 1.7 calculated from (4.2) with $\Delta\omega = 1.3$ and $\gamma = 0.75$. This may be expected, as at the beginning of its growth the cluster is closer to the nucleus, i.e. to the equilibrium conditions. For longer times, however, the growth shape differs noticeably from the equilibrium one: it depends on both supersaturation and time. The physical reason for this is that the correlation between the velocity of lateral growth of the first layer and the rate of filling of the upper layers is different at different β and besides it changes with time. The arrows in fig 4 mark the first moments of growth coalescence between the largest cluster and its smaller neighbours. It is worth noting that the coalescence acts affect sharply the shape ratio which afterwards, however, increases as if to reach some undisturbed value.

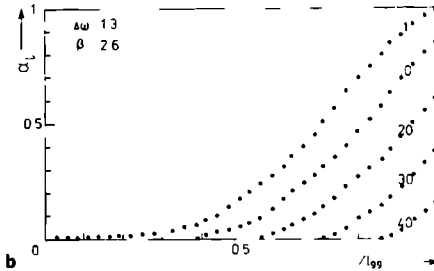
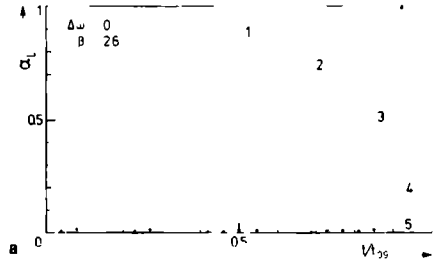


Fig 5 Time dependence of the degree of coverage of the successive monolayers at $\beta = 2.6$ (each figure gives the number i of the corresponding monolayer). In (b) the intermediate curves are not shown as they are too close to each other.

4.2 Coverage-time curves for the successive layers

Through lateral scanning within each layer the simulation method offers the unique opportunity the time dependence of the coverage α_i ($i = 1, 2, \dots$) of the i th layer to be traced. In this way the effect of the substrate is immediately seen: at a given β it slows down (if $\Delta\omega > 0$) the filling of the first layer (then $\theta_1 > \theta_2$) and a great many of the next layers has time to deposit on to it. This effect is clearly visible in figs 5 and 6 which depict the curves of filling up the first layers, i.e. α_i as functions of t/t_{99} at $\beta = 2.6$ and $\beta = 5.2$, respectively (the figure at each curve gives the number i of the corresponding layer). Fig 5a refers to the own substrate ($\Delta\omega = 0$) and shows that till the moment of building up the first layer the first few atoms within the fifth layer only just appeared. When, however, the substrate is weakly attaching the deposit ($\Delta\omega = 1.3$), fig 5b reveals an altogether different picture: until the filling of the first layer is

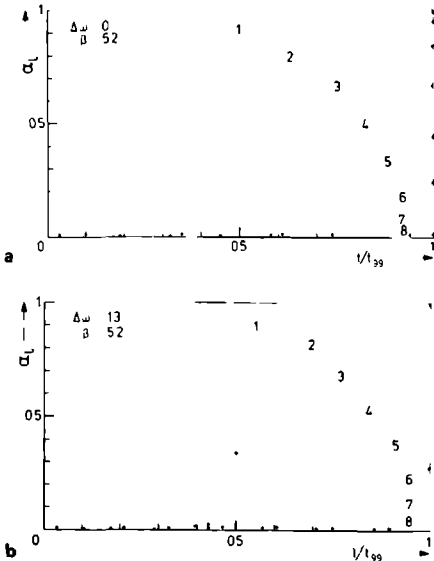


Fig. 6 Time dependence of the degree of coverage of the successive monolayers at $\beta = 5.2$. Now only 9 monolayers are seen in (b) in sharp contrast with fig. 5b

finished, 3 more almost completely and 48 partially built up layers have time to amass on top of it – so much is θ_1 greater than θ_2 . Increasing β , i.e. the flux of atoms arriving at the substrate, we can suppress its energetic inhospitality, make θ_1 equal to θ_2 and obtain the same number of layers at $t = t_{99}$ as on the own substrate. This effect manifest itself in fig. 6 which is for the same two substrates ($\Delta\omega = 0$, fig. 6a and $\Delta\omega = 1.3$, fig. 6b) as in fig. 5, but now $\beta = 5.2$. It is seen that at this β the two filling kinetics are practically identical.

One has to notice also that at $\Delta\omega = 1.3$ and $\beta = 2.6$ (fig. 5b) the α_1 curve is of the sigmoidal shape characteristic for nucleation growth mechanism (with $m_1 > 1$) of layer filling. The increased supersaturation ($\beta = 5.2$) leads to continuous growth mechanism ($m_1 = 1$) of filling and α_1 takes the simple exponential form $\alpha_1 = 1 - \exp(-t/\theta_1)$ (fig. 6b). In the case of the own substrate, however, the shape of α_1 in figs. 5a and 6a shows that both β values are high enough to ensure filling of the first layer with $m_1 = 1$. It is seen from figs. 5 and 6 as well that regardless of the sub-

strate and of the filling mechanism all $\alpha_i(t)$ curves with $i = 2, 3, \dots$ have a sigmoidal shape because the deposition of the 2nd, 3rd, etc. layers occurs on to the variable area of the 1st, 2nd, etc. layers, respectively. For this reason the mechanism of filling up the second and the next layers during deposition on to a foreign substrate may be revealed in pure form only through the curve $\alpha_1(t)$ obtained by deposition on the own substrate at the same β .

4.3 Mean height of the film at the moment of 99% substrate coverage

The facilitated or impeded deposition of the atoms on to the substrate when changing $\Delta\omega$ and/or β leads to a different mean film thickness or height h (cm) at any given moment t , i.e. to a different number N of deposited monolayers, as $N = h/a$. The computer experiment gives directly the dependence of N on t , thus making possible the theoretical equations (1.3.19) and (1.3.25) to be tested. In this section we shall use the simulation data for N versus t in order to determine N_{99} from the condition $N_{99} = N(t_{99})$ and to confront the found dependence on β with the theoretical formulae (3.9), (3.14) and (3.16). To that purpose let us present separately the results for deposition on to the own and foreign substrates.

(a) Own substrate

Fig. 7 shows the dependence of N on t/t_{99} for deposition on to the own substrate ($\Delta\omega = 0$) at different values of β (the figures at the corresponding curves) from 0.87 to 5.2. All curves are in good qualitative agreement with eq. (1.3.25) and fig. 5 of ref. [1] and especially the predicted initial bends of the curves at lower β are to be noticed. At time t_{99} the curves indicate that the film is of different thickness. The dependence of N_{99}^{ow} on β is given in fig. 8 by the circles. The dashed curve 1 is drawn arbitrarily in order to connect the points and the horizontal straight lines are traced according to (3.16). As seen, $m_1 = 1$ predicts well the asymptote $N_{99}^{ow} = 4.61$ at higher supersaturations when the continuous growth mechanism is operative. As it is to be expected, at lower β the nucleation growth mechanism starts manifesting itself and m_1 increases smoothly, thus leading to a decrease of N_{99}^{ow} in conformity with (3.15). The value $m_1 = 3$ gives satisfactorily the mean

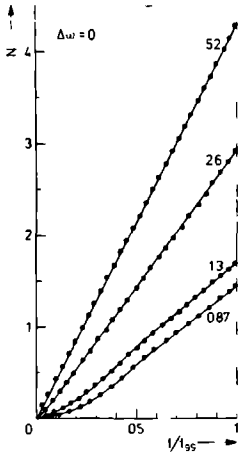


Fig. 7 Time dependence of the mean film height (in number of monolayers) for deposition on to the own substrate at different β (the figures at the curves). The bends in the curves at the lower β values are a direct indication for nucleation growth of the interface

height $N_{99}^{ow} = 1.86$ in the region of the lowest supersaturations when the nucleation growth mechanism is most pronounced. Using (3.16), we may conclude that $m_1 = 2$ at $\beta \approx 2.2$, as then $N_{99}^{ow} = 2.43$.

Fig. 8 presents also the simulation data (the triangles) for the β dependence of the width Δ_b of the interface at t_{99} which is defined as the difference between the numbers of the first empty (<1%) and the last full (>99%) layer at this moment. The dashed

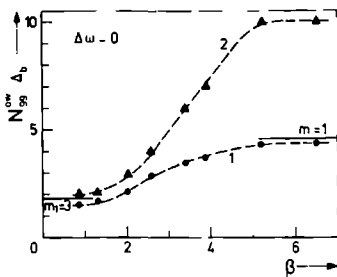


Fig. 8 Mean film height N_{99}^{ow} (the circles) and interface width Δ_b (the triangles) at time t_{99} in dependence of supersaturation for deposition on to the own substrate

line 2 is drawn arbitrarily to point out the existence of a minimal and a maximal interface width of 2 and 10 layers at $\beta \leq 1.5$ and $\beta \geq 5$, respectively. These values are in agreement with the theoretical estimate $\Delta_{b,min} = 2.7$ and $\Delta_{b,max} = 8.2$ obtained on the basis of eq. (16.6) at low (with $m_1 = 3$) and high (with $m_1 = 1$) supersaturations, respectively. Fig. 8 is physically interesting in that it demonstrates the intuitively expected widening of the interface with increasing β . The rise of Δ_b ceases, however, after reaching the region where the continuous growth mechanism is effective, as this is the most intensive mechanism of growth at all. Of course, the upper limit of Δ_b appears because the simulation experiment satisfies the condition for one and the same supersaturation within all successive layers. Breaking this condition may result in an infinite increase of Δ_b with increasing β , i.e. in a loss of the interface morphological stability.

(b) Foreign substrate with $\Delta\omega > 0$

The change of N with time during deposition on

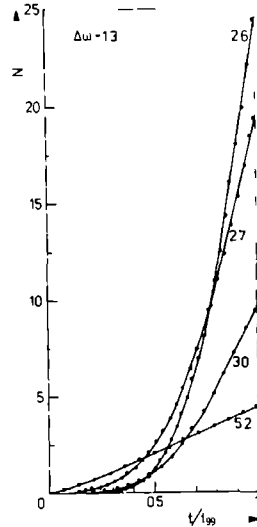


Fig. 9 Time dependence of the mean film height (in number of monolayers) for deposition on to a foreign substrate with $\Delta\omega = 1.3$ at different supersaturations (the figures at the curves)

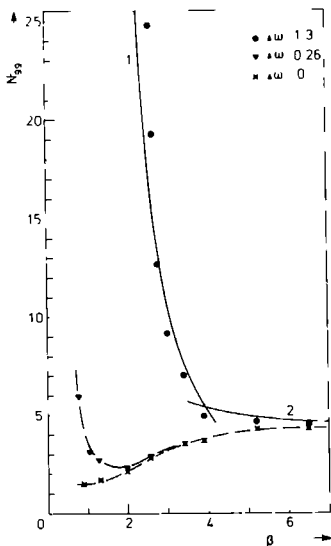


Fig. 10 Mean film height at time t_{99} in dependence of super saturation for the own and two foreign substrates. The dashed curves are drawn to fit the data, whereas curves 1 and 2 are calculated theoretically from (3.9) and (3.14), respectively

to a foreign substrate with $\Delta\omega = 1.3$ is shown in fig. 9 at different β (the figures at the corresponding curves). The time dependence of N is similar, too, for the substrate with $\Delta\omega = 0.26$ used for simulation. The curves in fig. 9 are in good qualitative accordance with eq. (1.3.19) and they reveal clearly the strong increase of N_{99} with decreasing β . Establishing and analyzing this effect is just our main aim and because of this N_{99} is presented separately in fig. 10 as a function of β . The circles and the triangles denote the simulation results for the substrates with $\Delta\omega = 1.3$ and $\Delta\omega = 0.26$, respectively, and the crosses are the data from fig. 8 for the own substrate ($\Delta\omega = 0$) shown once again for comparison. Unfortunately, at low supersaturations N_{99} and N_{99}^{sw} cannot be determined theoretically from (3.1) and (3.15) with a sufficient accuracy, since then the concrete dependences of m_1 , m_2 , θ_1 and θ_2 on β are not well known. For that reason the triangles and the crosses in fig. 10 are connected by arbitrary curves.

The data for the substrate with $\Delta\omega = 1.3$, however, are accessible to theoretical description. Indeed, fig. 10 indicates that they fall into the region of the high enough supersaturation at which the filling of the second layer (characterized by the dashed curve for the own substrate) occurs according to the continuous growth mechanism for which $m_2 = 1$ and θ_2 is given by (3.6). In addition, the morphology of the film as well as the $\alpha_1(t)$ curve attest to analogous kinetics within the first layer, too, but only at higher β (figs. 3b and 6b). At lower β the filling of the first layer is due to formation and lateral growth of flat clusters within it (fig. 3a). This combination of kinetics of overall filling within the first and the second layers was already examined in section 3 and eqs. (3.9) and (3.14) describe theoretically the dependence of N_{99} on β . In fig. 10 these two formulae are confronted with the simulation results for $\Delta\omega = 1.3$. The bold curves 1 and 2 are drawn according to (3.9) and (3.14), respectively, with $\omega = 1.3$, $\gamma = 0.75$ and $\Delta\omega = 1.3$ in them. As seen, the theoretically predicted values of N_{99} are in a fairly good quantitative agreement with the simulation data. The extrapolations of curves 1 and 2 show the supersaturation regions in which (3.9) and (3.14) do not apply any more because the kinetics of filling up the first layer change their character at about $\beta = 4$. This means that the correct determination of the β dependences of θ_1 and θ_2 in the general formula (3.1) is of primary importance when using it in concrete cases.

At this point it is of particular interest to note that for the substrate with $\Delta\omega = 1.3$ the classical expression (A.1) for J_1 provides sufficiently exact determination of θ_1 and therefore of N_{99} at $2.6 < \beta < 4$, although in this supersaturation region the nucleus is constituted of $\nu_k n_k^2 \approx 3$ to 1 atoms. The sole requirement for a good fit between curve 1 and the simulation points is the edge energy parameter γ to be calculated from eq. (2.10) which accounts for the roughening of the cluster periphery. If, for example, the familiar approximation $\gamma = \omega$ is used to evaluate γ , depending on β curve 1 shifts up by a factor of 3 to 10 and finds itself in a strong quantitative discrepancy with the simulation data. The conclusion is, therefore, that connecting γ and ω (i.e. κ and σ) by means of eq. (2.10) may be very useful when analyzing nucleation and growth phenomena.

4.4 Critical supersaturation for changing the mode of growth

The simulation findings in fig 10 demonstrate clearly the phenomenon of changing the mode of thin film growth at deposition on to a foreign substrate. Indeed, if $\beta < 3.9$, at the moment t_{99} the substrate with $\Delta\omega = 1.3$ is covered by a thick deposit of multi-atomic height which means that formerly high island like clusters have been growing on it. At the critical supersaturation $\beta_c = 3.9$ the island growth passes sharply into a layer growth which operates within the region $\beta > 3.9$ (with the used values for ω and $\Delta\omega$ this is practically the region of the continuous growth of the film). Theoretically β_c is defined by the equation

$$N_{99}(\beta_c) - N_{99}^{0W}(\beta_c) = 1 \quad (4.3)$$

resulting from (1.6.15) and $\beta_c = 3.9$ is also the solution of (4.3) with $N_{99}^{0W} = 4.61$ and N_{99} from (3.16) and (3.9) respectively, in it. As seen from fig 10, this value of β_c corresponds very well to the sharp bend in the dependence of N_{99} on β obtained through the simulations.

Fig 10 gives evidence that a transition between island and layer growth occurs also when the deposition takes place on to the foreign substrate with $\Delta\omega = 0.26$. As now the deposit is attached stronger to the substrate, the critical supersaturation is lower $\beta_c \approx 1.5$. This value is determined only experimentally by finding that β at which the two dashed curves in fig 10 satisfy eq (4.3), since in this case theoretical formulae for N_{99} and N_{99}^{0W} are not available.

It must be finally noted that the simulation findings are not in favour of the existing criteria for transition between the two modes of growth. According to Bauer [2], at both $\Delta\omega = 0.26$ and $\Delta\omega = 1.3$ the film has always to exhibit island growth because these $\Delta\omega$ correspond to $\Delta\sigma > 0$. In other words, a transition should not exist at all and this is in complete discrepancy with the results in fig 10. Markov and Kaischew [12] admit the existence of critical supersaturation for transition and determine β_c by $\beta_c = 4\Delta\omega$ provided at this supersaturation the nucleus is large enough. With $\Delta\omega = 0.26$ this formula gives $\beta_c = 1.04$ against the value 1.5 obtained from the simulation data in fig 10 referring to the substrate with the same $\Delta\omega$.

5 Conclusion

In conformity with the observations in physical experiments [2,3,6–9] our simulation results convincingly manifest the existence of a transition between island and layer growth at deposition of thin films on to a foreign substrate. The simplicity of the simulation model and the exact knowledge of the physical parameters pertinent to it make the obtained data most suitable for theoretical description. The established fairly good quantitative agreement between the simulation findings and eqs (3.9), (3.14), (3.15) and (4.3) is at the same time a corroboration of the validity of the general theory of layer growth developed in ref [1]. This enables the new approach to be also used for analyzing the layer growth kinetics operating under real experimental conditions. Based on it, in a forthcoming paper a theory will be proposed for the change of the mode of thin film growth concerning the particular case of deposition from the vapour phase when the adatom surface diffusion is of primary importance for the process.

Our simulation gives also information about the deviation of the actual shape of the island like clusters from their equilibrium shape. It turns out that at a given substrate (i.e. fixed $\Delta\omega$) their growth shape changes with time and is different at different supersaturations. This is a result which does not support the widely used approximation for equilibrium shape of the clusters during their growth. The simulation data for the β dependence of N_{99} confirm the possibility of using the classical nucleation theory by formal extrapolation to those high supersaturations at which the nucleus contains a few atoms only. The theoretical curve 1 in fig 10, however, fits well the simulation points only upon using the formula (2.10) of Van Leeuwen and Bennema [20] for the connection between γ and ω (i.e. between κ and σ) and this way be regarded as a proof for its validity. The conclusion is, therefore, that allowing for the decrease of κ , due to the roughening of the cluster periphery, is sufficient for a proper quantitative description of the layer growth. To take into account the roughening of the cluster top surface is not necessary, since the theory allows automatically for it by the different filling of the successive layers.

Acknowledgements

The authors would like to thank Dr P Bennema for his interest and criticism during this work One of them (D K) is grateful to the Research Fellowship Committee of the Delft University of Technology for granting him a fellowship which made it possible this investigation to be carried out

Appendix

When determining θ_1 from (3.8) we need to know J_1 and v_1 Let us first find J_1 Supposing that the classical nucleation theory holds good, we can use the known formula [4]

$$J_1 = (\Delta G_k / 4\pi k_B T \nu_k^2 n_k^4)^{1/2} \lambda_k C_1 \exp(-\Delta G_k / k_B T) \quad (A 1)$$

for the frequency of steady state formation of flat nuclei of ν_k atomic height Here n_k is the number of the atoms in the edge of the nucleus square base, ΔG_k is the nucleation work, λ_k (sec^{-1}) is the frequency of an atom joining the nucleus, and C_1 (cm^{-2}) is the adsorption equilibrium concentration of single atoms on the substrate Using the already obtained equations (1.5.4), (1.5.7), (1.5.14) and (1.5.15) in combination with (2.4), (2.9) and (2.11) yields

$$n_k = \begin{cases} 4\gamma/\beta, & 0 \leq \beta \leq 4\Delta\omega, \\ 2\gamma/(\beta - 2\Delta\omega), & 4\Delta\omega \leq \beta, \end{cases} \quad (A 2)$$

$$\Delta G_k / k_B T = \begin{cases} 32\gamma^2 \Delta\omega / \beta^2 & 0 \leq \beta \leq 4\Delta\omega, \\ 4\gamma^2 / (\beta - 2\Delta\omega), & 4\Delta\omega \leq \beta \end{cases} \quad (A 3)$$

In so far as the adatom surface diffusion is fully expelled from the simulation model, the nucleus incorporates atoms solely by direct additions with the frequency k^+ to any one of the $4n_k$ sites on its periphery, i e

$$\lambda_k = 4n_k k_e^+ e^\beta \quad (A 4)$$

We shall use this equality not only for the monoatomically high nuclei (when $\beta \geq 4\Delta\omega$), but also for the nuclei of polyatomic height (i e at $\beta \leq 4\Delta\omega$) Indeed, then the frequency k_{col}^+ of attachment of a column of monoatomic base and ν_k -atomic height

(fig 2b) is approximately given by the mean frequency

$$[(k^+)^{\nu_k}]^{1/\nu_k}$$

of attachment of one atom belonging to the column Hence

$$k_{\text{col}}^+ \approx k^+, \quad (A 5)$$

and $\lambda_k = 4n_k k_{\text{col}}^+$ leads again to (A 4) And finally, since C_1 is the product of the atom incidence rate k^+ / a^2 and the life time $(k_s^- a)^{-1}$ of the adatoms on the substrate, bearing in mind (2.1) and (2.3) we may write

$$C_1 = a^{-2} e^{-4\omega - 2\Delta\omega} e^\beta \quad (A 6)$$

Thus, upon inserting (3.3) and (A 2)–(A 6) in (A 1) we find the following different β dependences of J_1 in the two supersaturation regions

$$J_1 = \begin{cases} a^{-2} (2\pi\Delta\omega)^{-1/2} k_e^+ \beta e^{-4\omega - 2\Delta\omega} e^{2\beta} \\ \quad \times e^{-32\gamma^2 \Delta\omega / \beta^2}, & 0 \leq \beta \leq 4\Delta\omega, \\ a^{-2} [4(\beta - 2\Delta\omega) / \pi]^{1/2} k_e^+ e^{-4\omega - 2\Delta\omega} e^{2\beta} \\ \quad \times e^{-4\gamma^2 / (\beta - 2\Delta\omega)}, & 4\Delta\omega \leq \beta \end{cases} \quad (A 7)$$

Next we have to determine v_1 At $\beta \geq 4\Delta\omega$ the flat clusters are of monoatomic height (fig 2a) and in the absence of surface diffusion they grow laterally only by direct incorporation of atoms from the ambient phase The growth velocity is the product of the atomic volume a^3 and the net rate $(k^+ - k_{s,2}^-) / a^2$ of depositing atoms on to kink sites and therefore, in view of (2.1) and (2.3),

$$v_1 = a k_e^+ (e^\beta - e^{2\Delta\omega}), \quad \beta \geq 4\Delta\omega \quad (A 8)$$

At lower supersaturations ($0 \leq \beta \leq 4\Delta\omega$) the flat clusters are of ν_k -atomic height and v_1 is to be determined analogously by means of the difference between the frequencies k_{col}^+ and k_{col}^- of attachment and detachment, respectively, of a column of monoatomic base and ν_k -atomic height (fig 2b) Besides, the column should be regarded as an entity being in a "kink" position which implies that each atom of it has two lateral neighbours Finding v_1 in this case is a rather complicated problem, but for the further considerations it is sufficient to express approximately k_{col}^+ by (A 5) and k_{col}^- by the mean frequency

$$[(k_2^-)^{\nu_k - 1} k_{s,2}^-]^{1/\nu_k} = k_2^- (k_{s,2}^- / k_2^-)^{1/\nu_k}$$

of an atom detachment from the column Using (2 2), (2 3) and (3 3) leads to

$$k_{\text{col}}^- \approx k_e^+ e^{\beta/2}, \quad (\text{A } 9)$$

and hence

$$v_1 = ak_e^+ (e^{\beta} - e^{\beta/2}), \quad 0 \leq \beta \leq 4\Delta\omega \quad (\text{A } 10)$$

References

- [1] D Kashchiev, *J Crystal Growth* 40 (1977) 29
- [2] E Bauer, *Z Krist* 110 (1958) 372, 395
- [3] W A Jesser and J W Matthews *Phil Mag* 15 (1967) 1097, 17 (1968) 461, 17 (1968) 595
- [4] R A Sigsbee in *Nucleation*, Ed A C Zettlemoyer (Dekker, New York, 1969) p 109
- [5] F Bauer and H Poppa, *Thin Solid Films* 12 (1972) 167
- [6] D G Lord and M Prutton, *Thin Solid Films* 21 (1974) 341
- [7] C T Horng and R W Vook, *J Vacuum Sci Technol* 11 (1974) 140
- [8] R W Vook, C T Horng and J E Macur, *J Crystal Growth* 31 (1975) 353
- [9] J A Venables and G L Price, in *Epitaxial Growth* Ed J W Matthews, (Academic Press, New York, 1975) p 215
- [10] L N Aleksandrov and I A Entin *Soviet Phys -Cryst* 20 (1975) 1140
- [11] T Halicioğlu, *J Crystal Growth* 29 (1975) 40
- [12] I Markov and R Kaischew *Thin Solid Films* 32 (1976) 163
- [13] J P van der Eerden *Phys Rev B* 13 (1976) 4942
- [14] F F Abraham and G M White, *J Appl Phys* 41 (1970) 1841
- [15] G H Gilmer and P Bennema, *J Appl Phys* 43 (1972) 1347
- [16] A I Michaels, G M Pound and G F Abraham, *J Appl Phys* 45 (1974) 9
- [17] T L Hill, *Statistical Mechanics* (McGraw Hill, New York 1956)
- [18] H J Leamy G H Gilmer and K A Jackson, in *Surface Physics of Materials*, Ed J H Blakely (Academic Press, New York, 1975) p 121
- [19] J P van der Eerden, C van Leeuwen, P Bennema W L van der Kruk and B P Th Veltman, *J Appl Phys* 48 (1977)
- [20] C van Leeuwen and P Bennema, *Surface Sci* 51 (1975) 109
- [21] C van Leeuwen and J P van der Eerden, *Surface Sci* 64 (1977) 237
- [22] R Kaischew, *Commun Bulg Acad Sci (Phys)* 1 (1950) 100
- [23] R Lacmann, *Z Krist* 116 (1961) 13
- [24] S Toshev, M Paunov and R Kaischew, *Commun Dept Chem Bulg Acad Sci* 1 (1968) 119

SURFACE MIGRATION OF SMALL CRYSTALLITES - A MONTE CARLO SIMULATION WITH CONTINUOUS TIME

J. P. VAN DER FERDEN, D. KASHCHIEV* and P. BENNFMA

RIM Laboratory of Solid State Chemistry, Catholic University of Nijmegen, Toernooiveld Nijmegen, The Netherlands

The migration of crystallites on an amorphous substrate by the mechanism of morphological changes was studied with a Monte Carlo simulation technique which used, in contrast to the usual methods, time as a continuous parameter. In this case an enormous increase in computational efficiency was achieved. As an example the activation energies for Au or Ag on alkali halide substrates were used. It was shown that the theory of this migration mechanism has to be improved.

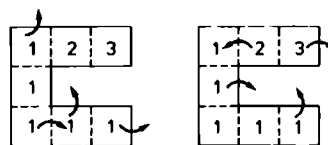
1 Introduction and model description

Classical nucleation and growth theories are often based on the assumption that only single atoms (adatoms) are able to move over the surface. The experiments of Masson, Metois and Kern [1, 2] however, clearly showed that even gold grains of over 50 atoms are executing random walks over an amorphous carbon substrate. Venables [3] and Stowell [4] showed that the movement of dimers and trimers would decrease both the saturation concentration of stable (growing) clusters and the nucleation rate. The analytical results of a theory for the coalescence of large clusters [5] show that also here the diffusion of clusters may play an important role. In some cases direct information about the motion of adatoms and dimers [6, 7] can be obtained from ion field observations. Such results can then be used to determine interactions between deposited atoms mutually and with the substrate. Using Monte Carlo simulations we start the other way around: given certain interactions we determine the diffusion constants D_n of n atomic clusters and reconsider the relevant features for a quantitative theory.

We use a very simple model. The substrate is a square lattice and atoms of a cluster can be present only at its lattice points or at positions above them on top of other cluster atoms. These restrictions imply that the deposited material is building up a

tetragonal structure and that we use the solid on solid restriction [8]. Nearest neighbour potential energies ϵ_0 (between cluster atoms) and ϵ_0^* (between deposit and substrate) are assumed. The cluster as a whole moves as a consequence of jumps of single atoms to a neighbouring position. This mechanism is known as diffusion by morphological changes [1]. Jumps which would split the cluster in the sense of first nearest neighbour approximation are forbidden (fig. 1). For simplicity we assume that the jump frequencies are merely determined by binding energies in the original position, although in general the future bonds also play a role. As an atom is not completely separated from the cluster during a jump, the activation energies ϵ_d and ϵ_d^* which enter in the jump frequencies are smaller than ϵ_0 and ϵ_0^* . Stowell [4] and Bonzel [9] estimate $\epsilon_d = 0.5$ eV, $\epsilon_d^* = 0.2$ eV for Au or Ag on NaCl, KCl or KBr substrates. Inspired by these estimations we varied the simulation parameters

$$\omega = \epsilon_d / 2kT, \quad \Delta\omega = (\epsilon_d - \epsilon_d^*) / kT, \quad (1)$$



FORBIDDEN ALLOWED
 Fig. 1. Examples of allowed and forbidden jumps.

* Institute of Physical Chemistry, Bulgarian Academy of Sciences, Sofia 1113, Bulgaria.

in such a way that $\Delta\omega/\omega = 0.6$. Moreover we varied ω between 7.0 and 1.0, corresponding to 400 and 3000 K for these systems. Of course, the high temperature results are not directly applicable to the physical case, but enough general conclusions can be drawn to justify these efforts. Indeed, these results will be applicable for even smaller activation energies.

2 The simulation technique

Using the principle of detailed balance in the usual way [8,10] we get the following expressions for the frequencies with which an atom jumps to any neighbouring position if it has z lateral bonds with the cluster

$$k_i^* = k_0^* \exp(-2i\omega), \quad (2)$$

$$k_i = k_0^* \exp[-2(i\omega + \Delta\omega)] \quad (3)$$

Here k_i^* or k_i have to be used if the vertical bond is with the substrate or with the cluster respectively. Consequently the average time between two such jumps is given by

$$\tau_i^* = \tau_0^* \exp(+2i\omega), \quad (4)$$

$$\tau_i = \tau_0^* \exp[2(i\omega + \Delta\omega)] \quad (5)$$

As successive jumps may be considered as independent, the actual time t between jumps will be Poisson distributed around the corresponding average value τ

$$P(t) = (1/\tau) \exp(-t/\tau) \quad (6)$$

From random number $R \in (0, 1)$ we obtain corresponding waiting periods by

$$t_i^* = -\tau_i^* \ln R, \quad (7)$$

$$t_i = -\tau_i \ln R \quad (8)$$

These expressions can be verified by computation of the interval in which R should fall in order that t_i^* or t_i is between t and $t + dt$.

Therefore, it is at any moment possible to determine for all atoms in the cluster the time at which they will jump. The following algorithm can then be used: Step 1 determine for all atoms in the cluster the time at which they will jump. Step 2 execute the jump which is first in time. Step 3 determine new

times for those atoms whose state is influenced by this jump. Step 4 go back to step 2, unless the desired amount of jumps is carried out. It should be mentioned that step 3 is justified for Poisson processes: the waiting period after the change of state is independent of the history of the atom, in particular whether the atom has "waited" already some time in its previous state.

In order to compare the computational efficiency of the present continuous time algorithm with the usual [8] discrete time simulation we compare the time necessary to simulate the same arbitrary number of processes

$$T_{\text{cont}}/T_{\text{disc}} = N_p T_{23}/N_i T_0 \quad (9)$$

Here the T_{cont} in the continuous algorithm is approximately the number of processes N_p times the average time T_{23} for steps 2 and 3, which will in turn be almost proportional to n . The necessary time T_{disc} in the discrete algorithm is the number of trials N_i times the execution time T_0 of one trial (successful or not). But N_p/N_i is the ratio of the frequencies for the most often occurring process and for a trial. In many cases the jump from a kink site (k_2^*) is the most common one and the jump of an adatom has the highest frequency k_0^* . Therefore

$$T_{\text{cont}}/T_{\text{disc}} \propto (k_2^*/k_0^*) n = n e^{-4\omega} \quad (10)$$

Generally speaking, the continuous algorithm will be faster for small systems and for low temperatures (ω large). E.g. we found for the 12 atomic cluster at $\omega = 7$ a decrease in computation time with a factor 10^{10} .

3 Results

We studied the movement of clusters containing 2, 3, 4, 8, 12, 16 or 20 particles. It turned out that the square displacement r_n^2 (of the center of mass from its original position) increased linearly with time. Therefore it is justified to consider the cluster movement as a random walk, characterized by a diffusion constant D_n .

$$r_n^2 = 4D_n t + b \quad (11)$$

The constant b describes an initial effect: the cluster with which we start needs not to have the average

shape Therefore a certain initial displacement of the center of mass corresponds to the rearrangement of the atoms As the time unit is arbitrary in the simulations we can choose it in such a way that the jump frequency of an adatom equals 1 For the adatom we have

$$r_1^2 = 4D_1 t = k_0^* t \equiv t_{SIM} \quad (12)$$

Upon combining eqs (11) and (12) we see that

$$r_n^2 = (D_n/D_1) t_{SIM} + b \quad (13)$$

Concluding we see that a straight line fit of r_n^2 versus t_{SIM} gives us the ratio of diffusion coefficients D_n/D_1 The displacement should be at least some lattice distances to damp out the initial transient effect, especially for the larger (12, 16, 20-atomic) clusters

In fig 2 we see that the dependence of $\ln(D_n/D_1)$ on ω is linear both for high ($\omega < 2.0$) and for low ($\omega > 4.0$) temperatures which means that D_n is characterized by a diffusion free energy ΔG_n

$$D_n \propto \exp(-\Delta G_n/kT) \quad (14)$$

Using the fact that $\epsilon_d^* = 0.4 \epsilon_d$ is the diffusion free energy for an adatom, it is seen that the slope of the $\ln(D_n/D_1)$ versus ω curves is $0.8 - 2\Delta G_n/\epsilon_d$ The so found ΔG_n values are given in table 1 To understand these results we introduce the concept of an "essential jump" With this we mean a jump which attacks the "core" of the cluster Eg the 12 atomic cluster has, at low temperature, often the shape shown in table 1 A $2 \times 2 \times 2$ cube as a core, surrounded by

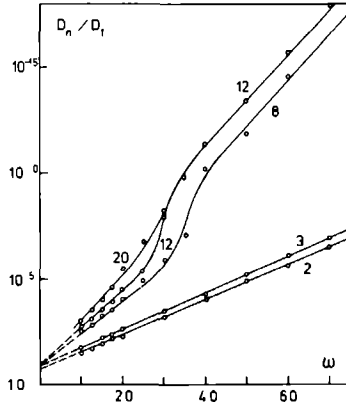


Fig 2 Temperature dependence ($\omega \propto T^{-1}$) of the diffusion coefficient for several cluster sizes (n -values indicated)

4 "satellites" which move around it without changing its position Therefore jumps of one of the core atoms are essential in the sense that they initiate a real displacement and their activation energies ΔE_{ess} will give the main contribution to the diffusion free energy of the cluster as a whole

The validity of this assumption is investigated in table 1 Ordinary shapes of the clusters were guessed, keeping in mind that the mutual interaction between cluster atoms is stronger than with the substrate ($\epsilon_d > \epsilon_d^*$) Therefore at low temperatures the clusters will be relatively high and tend to form facets [10],

Table 1

Ordinary shapes, activation energies for essential jumps, ΔE_{ess} , and observed diffusion free energies, candidate atoms for essential jumps are underlined

Size	Low temperature ($\omega > 4.0$)			High temperature ($\omega < 2.0$)		
	Shape	ΔE_{ess}	ΔG_n	Shape	ΔE_{ess}	ΔG_n
2	$\frac{1}{1}$	$\epsilon_d + \epsilon_d^* = 1.4 \epsilon_d$	$1.34 \epsilon_d$	$\frac{1}{1}$	$\epsilon_d + \epsilon_d^* = 1.4 \epsilon_d$	$1.34 \epsilon_d$
3	$\frac{1}{1}$	$\epsilon_d + \epsilon_d^* = 1.4 \epsilon_d$	$1.39 \epsilon_d$	$\frac{1}{1}$	$\epsilon_d + \epsilon_d^* = 1.4 \epsilon_d$	$1.39 \epsilon_d$
8	$\frac{1}{2}$ $\frac{2}{2}$	$3\epsilon_d$	$2.86 \epsilon_d$	$\frac{1}{1}$ $\frac{1}{2}$ $\frac{1}{1}$	$2\epsilon_d + \epsilon_d^* = 2.4 \epsilon_d$	$2.16 \epsilon_d$
12	$\frac{1}{2}$ $\frac{2}{2}$ $\frac{2}{2}$ $\frac{2}{2}$ $\frac{1}{1}$	$3\epsilon_d$	$2.86 \epsilon_d$	$\frac{1}{1}$ $\frac{1}{2}$ $\frac{1}{1}$ $\frac{2}{2}$ $\frac{1}{1}$ $\frac{1}{2}$	$2\epsilon_d + \epsilon_d^* = 2.4 \epsilon_d$	$2.40 \epsilon_d$

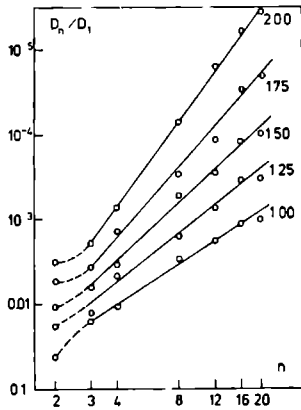


Fig. 3 Size dependence of the diffusion coefficient for several high temperatures (ω values indicated)

whereas at higher temperatures a gain in entropy makes them more flat. The atoms whose jumps would be essential are easily recognized and the close correspondence between their activation energies ΔE_{ess} and the observed ΔG_n confirms the essence of our model that the activation energy of an essential jump is a good approximation for the diffusion free energy of the clusters

The size dependence of D_n is shown [1] to be $D_n \propto 1/n$ for an isotropic hemisphere. It is seen in fig. 2 that such a dependence will not hold for low temperatures but may hold for high temperatures. Indeed the linearity of the $\ln(D_n/D_1)$ versus $\ln n$ curves in fig. 3 shows that at constant temperature

$$D_1/D_n = \text{const } /n^\alpha, \quad n = 3, 4, \dots, 20 \quad (15)$$

The exponent α , however, is temperature dependent and varies between 1.5 and 3.4 in the high temperature range. Indeed it turns out that

$$\alpha \approx 1.9 \omega - 0.3 \quad (16)$$

4 Conclusion

We used time as a continuous, instead of discrete, parameter in our Monte Carlo simulations which led to an enormous increase in computational efficiency

In general this method is advisable if only a few particles join actually in the processes and if the characteristic time for the most often occurring process is much larger than the smallest possible one. E.g. for the description of smooth (low temperature) surfaces the method may prove useful.

Physically, our results show that the motion of small crystallites by morphological changes is governed by essential jumps, jumps which attack the rigid core of the crystallite. Therefore the cluster diffusion free energy will vary between the value ϵ_n^* for an adatom and the activation energy $3\epsilon_n$ for a jump from a kink site (for large clusters and at low temperatures). At all temperatures a strong size dependence was found, D_n fell off faster than with $1/n$.

As both these results differ from the theoretical results in ref. [1], it is necessary to reconsider their arguments to reject the mechanism of diffusion by morphological changes for the random walk of gold grains on (100) KCl substrates: (i) if $D_n \propto 1/n^\alpha$ for constant temperature then $\alpha \approx 3.0$, (ii) a size dependent diffusion free energy was found, and (iii) the absolute value of D_n compared to an estimation of D_1 is much higher than predicted. Our results show that the first two arguments can not be used, the last one, however, is even stronger since we predict an even faster decrease in D_n with n .

References

- [1] A. Masson, J.J. Metois and R. Kern, in *Advances in Epitaxy and Endotaxy*, Eds H.G. Schneiders and V. Ruth (VEB, Leipzig 1971) p. 103.
- [2] A. Masson, J.J. Metois and R. Kern, *J. Crystal Growth* 3/4 (1968) 196.
- [3] J.A. Venables and G.L. Price in *Epitaxial Growth*, Ed J.W. Matthews (Academic Press, New York 1975).
- [4] M.J. Stowell, *Thin Solid Films* 21 (1974) 91.
- [5] D. Kashchiev, *Surface Sci.* 55 (1976) 477.
- [6] G. Ehrlich and G. Hudda, *J. Chem. Phys.* 44 (1966) 1039.
- [7] K. Stolt, W.R. Graham and G. Ehrlich, *J. Chem. Phys.* 65 (1976) 3206.
- [8] J.P. van der Eerden, P. Bennema and T.A. Chrepanova, in *Progress in Crystal Growth and Assessment*, Ed B.R. Pamplin (Pergamon, Oxford, 1977).
- [9] H.R. Bonzel, in *Surface Physics of Materials*, Ed J.H. Blakely (Academic Press, New York, 1975).
- [10] D. Kashchiev, J.P. van der Eerden and C. van Leeuwen, *J. Crystal Growth* 40 (1977) 47.

MEAN FIELD THEORY AND MONTE CARLO SIMULATION OF MULTISITE ADSORPTION

J.P. VAN DER EERDEN

RIM Laboratory of Solid State Chemistry, Toernooiveld, Nijmegen, The Netherlands

G. STAIKOV and D. KASHCHIEV

Central Laboratory of Electrochemical Power Sources and Institute of Physical Chemistry, Bulgarian Academy of Sciences, 1000 Sofia, Bulgaria

W.J. LORENZ

Institute of Physical Chemistry and Electrochemistry, University of Karlsruhe, Karlsruhe, Germany Fed. Rep.

and

E. BUDEVSKI

Central Laboratory of Electrochemical Power Sources and Institute of Physical Chemistry, Bulgarian Academy of Sciences, 1000 Sofia, Bulgaria

Received 27 July 1978; manuscript received in final form 20 November 1978

Multisite or $1/n$ adsorption on single crystal surfaces takes place when the adatom diameter is greater than the distance between two neighbouring adsorption sites. The adsorption isotherm has been deduced using a mean field approximation. The same problem was studied by Monte Carlo simulation. The results show asymmetric adsorption isotherms with respect to a degree of coverage of 0.5. The critical temperature of a first order phase transition is increased as compared with the case of $1/1$ adsorption. The theoretical and the simulated isotherms are in a good agreement for low adatom–adatom attraction. The theoretical and simulated isotherms obtained were used for interpretation of experimental results on electrolytic underpotential adsorption of Tl and Pb on Ag(100) faces.

1. Introduction

When atoms or molecules adsorb on different faces of single crystals the surface of the adsorbent can be considered as a two-dimensional lattice of adsorption sites with a given geometry. If the thermal fluctuations of the adatoms about their equi-

librium positions of lowest energy (i.e. the adsorption sites) are negligibly small, localized monolayer adsorption takes place and its theoretical description reduces to two-dimensional lattice gas models equivalent to the Ising one [1,2]. The lattice gas model corresponds to the simple Ising model when each adatom of the compact monolayer covers only one adsorption site, a case which will be further referred to as one-to-one (1/1) adsorption for brevity. This case can be easily described in the limit of no interaction between the adatoms, and the classical adsorption isotherm of Langmuir represents the exact solution of the problem [1,3-6]. Isotherms accounting for the adatom interaction are derived by Frumkin [5], Fowler and Guggenheim [4,6] and Honig [4] by different approximate methods. Using Monte Carlo simulation technique, Abraham and White [7] have found a good quantitative agreement between their isotherms and the theoretical isotherms of Honig at temperatures above the critical temperature for the first-order phase transition. Onsager [8] has shown that the critical temperature can be calculated exactly and its value for lattice with different geometry may be found in ref. [2], p. 191.

In many physically important cases of adsorption each adatom of the compact monolayer covers effectively $n > 1$ adsorption sites [4,9,10]. Obviously, the theoretical model for such multisite or one-to- n ($1/n$) adsorption will be different from the simple Ising model of 1/1 adsorption. In principle one can distinguish between two kinds of localized $1/n$ adsorption:

(i) Adsorption of molecules which are so large that each of them occupies n adsorption sites. This is the situation, for example, when large organic molecules or radicals adsorb on single crystal faces. This kind of adsorption has been considered theoretically by Honig [4] and very recently by Mutaftschiev and Bonissent [9] as well as by Gurevich and Kharkats [10].

(ii) Adsorption of atoms with diameter greater than the distance between two neighbouring adsorption sites on the substrate surface. In this case each adatom occupies only one adsorption site, but at the same time, due to its size, it blocks neighbouring adsorption sites and prevents them from being occupied by other adatoms. Typical examples for $1/n$ adsorption of this kind are the adsorption of noble gases on (0001) graphite substrate [11] and the electrolytic underpotential adsorption of metals on single crystal electrodes [12-16].

The type (ii) models have been studied in the past from the point of view of a hard core lattice gas. Until recently most effort was devoted to mean field approximations, low temperature series expansions and the transfer matrix method [17-19]. The general feeling is that such theories provide for a good description of the model properties far enough from critical conditions.

Monte Carlo simulations, on the other hand, turn out to be a reliable tool both close to and far away from critical conditions, e.g. for the 1/1 adsorption on a triangular lattice this was shown by Metcalf [20]. Similarly, a correspondence was found for 1/3 adsorption on a triangular lattice between Monte Carlo simulation [21] and exact renormalization group results [22].

In view of these considerations we feel that it is useful to carry out Monte Carlo

simulations in order to get information about the critical region of type (ii) models. On the other hand a mean field treatment is useful to get a closed form for the adsorption isotherm which is reliable far from critical conditions. In this paper we discuss both methods.

2. Physical model

The theoretical analysis is restricted to one-component monolayer adsorption. The model is based on the following assumptions:

- (a) The surface of the adsorbent is a two-dimensional lattice with a given geometry and a given number N_s of adsorption sites which have equal adsorption energy ϵ_a .
- (b) Each adatom remains attached to one adsorption site during its residence on the substrate, i.e. adsorption is localized.
- (c) The adatom diameter exceeds the distance between two neighbouring adsorption sites to such an extent that although one adatom occupies only one site, it blocks neighbouring adsorption sites and does not allow their occupation by other adatoms (fig. 1).

Thus, if the compact adsorbed monolayer, i.e. the saturation coverage, consists

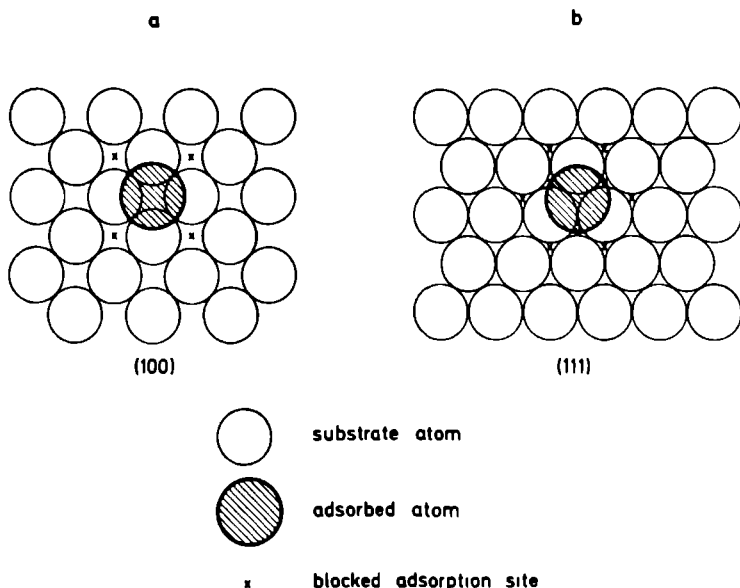


Fig. 1. Blocking effect of adatoms on different faces of fcc single crystals: (a) (100) face (square lattice) yielding a 1/2 adsorption; (b) (111) face (hexagonal lattice) yielding a 1/4 adsorption.

of $N_{a,max}$ adatoms, each covers effectively

$$n = N_s / N_{a,max} \quad (1)$$

adsorption sites from the two-dimensional lattice of the substrate. One of these sites is occupied by the adatom itself, and the other $(n - 1)$ sites are blocked by it. If $N_{b,max}$ is the maximum number of blocked sites in the compact adsorbed monolayer, combining (1) and the conservation of sites condition,

$$N_{a,max} + N_{b,max} = N_s ,$$

results in

$$N_{b,max} = (n - 1)N_{a,max} . \quad (2)$$

3. Mean field treatment of the problem

The problem is to find the adsorption isotherm corresponding to the above model. In doing that, according to the standard statistical method one has first to determine the free energy F of the adsorbed phase. If F , given by

$$F = U - TS , \quad (3)$$

is known, the adsorbate chemical potential μ_a can be easily found. Equating μ_a with the chemical potential of the ambient phase yields then directly the adsorption isotherm. Thus, the solution of the problem reduces to the determination of the entropy S and the internal energy U of the adsorbed phase at constant temperature T .

3.1. Determination of S

In the two-dimensional lattice of the substrate each adsorption site can be either free, or blocked, or occupied. This is exemplified in fig. 2 for a square lattice of adsorption sites denoted by circles which are open, labeled b , or solid.

Let us consider the general case of a lattice with arbitrary geometry. If the probabilities that a given site is occupied or blocked are θ/n and $\theta_b(1 - 1/n)$ respectively, the number N_a of the occupied and the number N_b of the blocked adsorption sites will be given by the equalities.

$$N_a = N_{a,max}\theta , \quad (4)$$

$$N_b = N_{b,max}\theta_b . \quad (5)$$

Normally, θ is denoted as the degree of coverage in adsorption processes.

Since the number N_0 of the free adsorption sites is determined by

$$N_0 = N_s - N_a - N_b ,$$

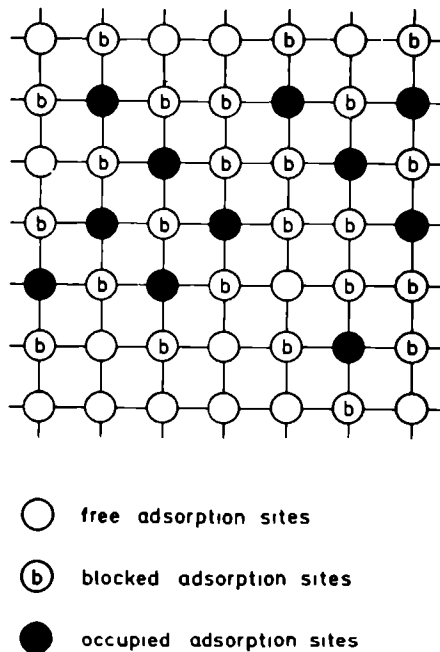


Fig. 2. Free, blocked and occupied adsorption sites in case of 1/2 adsorption on a square lattice.

combining eqs. (1), (2), (4), and (5) yields

$$N_0 = N_{a,\max} [n - \theta - (n - 1)\theta_b] . \quad (6)$$

The sum of the free and the occupied adsorption sites is then

$$N_0 + N_a = N_{a,\max} [n - (n - 1)\theta_b] . \quad (7)$$

To find exactly the number W of all possible ways in which N_a adatoms can occupy N_s adsorption sites with accounting for the effect of blocking is a difficult and possibly insoluble problem. It simplifies, however, upon assuming that a fixed number N_s of blocked sites corresponds to the number N_a of the adatoms on the substrate whatever the actual configuration may be. One can then express W by the number of the permutations of N_a adatoms on $N_0 + N_a$ adsorption sites when no blocking takes place. Thus,

$$W = (N_0 + N_a)! / N_a! N_0! . \quad (8)$$

Since $N_0 + N_a = N_s - N_b$, in physical terms eq. (8) means that, due to the effect of blocking, the N_a adatoms are distributed on a lattice with an effectively reduced number $N_s - N_b$ of adsorption sites.

The configurational part S_c of the entropy is determined according to the known

Boltzmann formula

$$S_c = k \ln W, \quad (9)$$

where k is the Boltzmann constant. The thermal component S_T of the entropy arising from the presence of N_a adatoms localized on the substrate surface is given by

$$S_T = N_{a,\max} \theta s_T, \quad (10)$$

where s_T is the thermal entropy per adatom. As $S = S_c + S_T$, using eqs. (4), (6), (7)–(10) and the Stirling approximation $\ln(x!) \approx x \ln x - x$ results in

$$S = kN_{a,\max} \{ [n - (n-1)\theta_b] \ln [n - (n-1)\theta_b] - [n - \theta - (n-1)\theta_b] \ln [n - \theta - (n-1)\theta_b] - \theta \ln \theta \} + N_{a,\max} \theta s_T. \quad (11)$$

3.2. Determination of U

To find the exact dependence of U on θ is also a difficult problem if adatom–adatom interaction has to be taken into account. In the following, the so-called mean field or Bragg–Williams [23] approximation for U will be used. In this approximation U is given by the expression [1,6]

$$U = N_{a,\max} [-\theta \epsilon_a - \frac{1}{2} c \theta^2 \epsilon + \theta u_T]. \quad (12)$$

Here ϵ_a is the adatom adsorption energy, ϵ is the adatom–adatom interaction energy between nearest neighbours in the adsorbate (positive for attraction, negative for repulsion), u_T is the thermal component (per adatom) of U , and c is the number of nearest neighbours of an adatom in the compact adsorbed monolayer.

3.3. Determination of θ_b

In eq. (11), θ_b is a function of θ . The explicit dependence of S on the degree of coverage θ can be found only after specifying the way in which θ_b depends on θ .

To obtain an approximate expression for θ_b as a function of θ let us first consider the case of $1/2$ adsorption on a square lattice of adsorption sites (fig. 2) by choosing a lattice element of the type shown in fig. 3a. Let us suppose that adatoms are present only on the sublattice of the $N_{a,\max}$ adsorption sites which are occupied by the compact adsorbed monolayer (fig. 3b). As illustrated in fig. 3c, this excludes the possibility of two nearest adsorption sites being simultaneously blocked. In this approximation the probability, $1 - \theta_b$, that the central adsorption site of the element in fig. 3 is not blocked, equals the probability that the peripheral four adsorption sites are free at the same time:

$$1 - \theta_b = (1 - \theta)^4.$$

Similarly, in the general case of $1/n$ adsorption on a lattice with arbitrary geometry

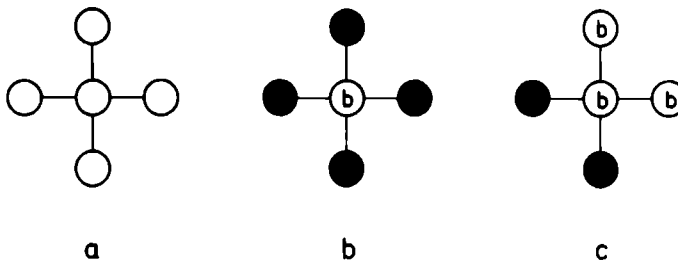


Fig. 3. Different occupied unit elements in case of $1/2$ adsorption on a square lattice in order to determine θ_b . In the present approximation the peripheral four sites may be occupied, the central one may be blocked.

θ_b may be written in the form

$$\theta_b = 1 - (1 - \theta)^b. \tag{13}$$

Here b stands for the number of adatoms in the compact adsorbed monolayer blocking one and the same adsorption site.

It is of importance to note that in eq. (13) only one configuration that leads to blocking of a given site is taken into account.

It can be expected that eq. (13) is valid under the following assumptions:

- (i) the adatoms are localized on the same sublattice corresponding to the final regular structure of the compact adsorbed monolayer;
- (ii) the distribution of the adatoms on their sublattice is uncorrelated, i.e. assuming a mean field approximation for the entropy may be used.

The condition (i) is valid for a high coverage ($\theta \approx 1$) or strong lateral attraction ϵ , whereas the condition (ii) holds only for low lateral fields. Therefore, eq. (13) will be a nearly correct description of $\theta_b(\theta)$ in the case of high coverage and low adatom–adatom attraction.

3.4. Adsorption isotherm

The chemical potential μ_a of the adsorbed phase is given by the definition

$$\mu_a = \left(\frac{\partial F}{\partial N_a} \right)_T = \frac{1}{N_{a,\max}} \left(\frac{\partial F}{\partial \theta} \right)_T. \tag{14}$$

In the case of adsorption from the vapour the thermodynamic equilibrium is characterized by the condition

$$\mu_v = \mu_a, \tag{15}$$

where μ_v is the chemical potential of the vapour phase.

In the electrochemical case of adsorption of charged particles the equilibrium condition (15) changes to

$$\bar{\mu}_e = \bar{\mu}_a, \tag{16}$$

where $\bar{\mu}_e$ and $\bar{\mu}_a$ are the electrochemical potentials of the particles in the electrolyte and in the adsorbed phase, respectively. These are defined by the equations [24]

$$\begin{aligned} \bar{\mu}_e &= \mu_e + ze_0\varphi_e, \\ \bar{\mu}_a &= \mu_a + ze_0\varphi_s, \end{aligned} \tag{17}$$

in which μ_e is the chemical potential of the electrolyte, z is the valency, e_0 is the electron charge, and φ_e and φ_s are the Galvani potentials of the electrolyte and the substrate, respectively.

Thus, combining (11)–(14) and using (15) or (16) leads to the following isotherm for $1/n$ localized monolayer adsorption in the mean field approximation:

$$\begin{aligned} \beta &= \ln\left(\frac{\theta}{1-\theta}\right) - \ln[1 + (n-1)(1-\theta)^{b-1}] \\ &+ b(n-1)(1-\theta)^{b-1} \ln\left(\frac{1 + (n-1)(1-\theta)^b}{1-\theta + (n-1)(1-\theta)^b}\right) - c\omega(\theta - 1/2). \end{aligned} \tag{18}$$

Here $\omega = \epsilon/kT$ and $\beta = \Delta\mu_i/kT$, where $\Delta\mu_i$, with $i = v$ or e , is given by

$$\Delta\mu_v = \mu_v - \mu_v^x, \quad \Delta\mu_e = -ze_0(E - E^x),$$

for adsorption from the vapour and in the electrochemical case, μ_i and $E = \varphi_e - \varphi_s$

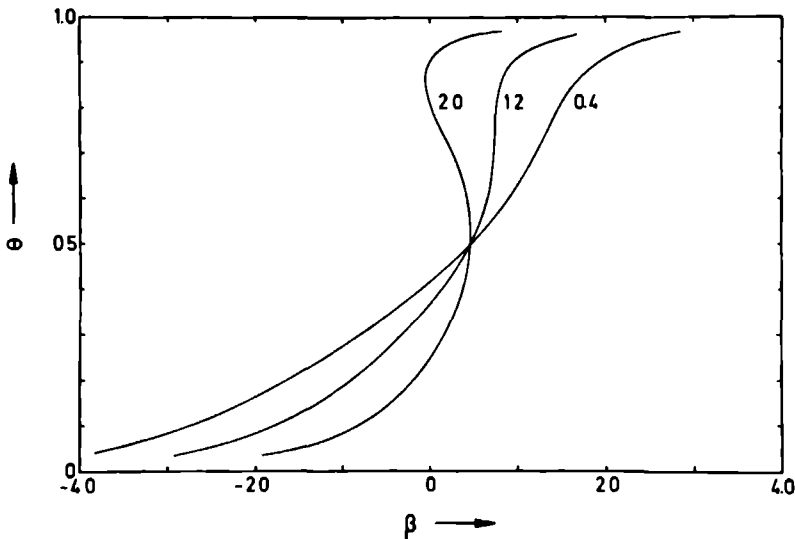


Fig. 4. Mean field $1/4$ adsorption isotherms for a hexagonal lattice calculated from eq. (18) with $n = 4$, $b = 3$, $c = 3$ (ω values indicated).

Table 1

Values of ω_c for 1/1 and 1/n adsorption on different lattices determined according to several methods

Lattice	n	b	c	ω_c	Method
Triangular	1	–	6	0.67	Mean field (eq. (18))
	3	3	6	0.66	
Square	1	–	4	1.0	Mean field (eq. (18))
	2	4	4	0.92	
Hexagonal (honeycomb)	1	–	3	1.33	Mean field (eq. (18))
	4	3	3	1.22	
Triangular	1	–	6	1.1	Onsager (ref. [2], p. 191)
Square	1	–	4	1.76	Onsager (ref. [2], p. 191)
	2	–	4	1.3	Monte Carlo (this paper)
Hexagonal (honeycomb)	1	–	3	2.51	Onsager (ref. [2], p. 191)
	4	–	3	1.9	Monte Carlo (this paper)

being the actual chemical and electrode potentials. The reference chemical and electrode potentials, μ_v^x and E^x are given by

$$\mu_v^x = -ze_0E^x = -\epsilon_a + u_T - Ts_T - \frac{1}{2}c\epsilon.$$

As seen, when $n = 1$ eq. (18) reduces to the known mean field or Frumkin isotherm for 1/1 adsorption.

Fig. 4 shows isotherms for the case of 1/4 adsorption on a hexagonal (honeycomb) lattice (see fig. 1b) calculated from eq. (18) with $n = 4$, $b = 3$, $c = 3$ at different values of the parameter of lateral interaction ω . Two points are worth noting. In contrast with the case $n = 1$, for $n > 1$ the isotherms are asymmetric with respect to $\theta = 1/2$ i.e.

$$\theta(\beta) \neq 1 - \theta(-\beta).$$

This asymmetry is seen more clearly at large values of ω where the curves become s-shaped. There is also a change in the critical value ω_c above which the two-dimensional first-order phase transition takes place. The ω_c value calculated from the 1/n isotherm (18) for $n > 1$ is smaller than the mean field value for 1/1 adsorption corresponding to the same structure of the adsorbed monolayer. The results are given in table 1. The values of ω_c for 1/n adsorption are computed from eq. (18) with an accuracy to ± 0.002 .

4. Monte Carlo simulation

In recent years, the Monte Carlo simulation has been used successfully for studying the processes of adsorption and deposition [7,20,21,25–29]. The first simula-

tion of 1/2 adsorption on a rectangular lattice with repulsion of the adatoms in [111] direction was carried out by Ertl and Plancher [28] to explain LEED data on deposition of oxygen on (211) faces of W. In particular, the rearrangement of the adatoms before reaching the equilibrium substrate coverage θ was investigated.

The present Monte Carlo simulation deals with 1/2 and 1/4 adsorption on square (fig. 1a) and hexagonal (fig. 1b) lattices of adsorption sites, respectively. Adsorption isotherms $\theta(\beta)$ are obtained for a number of ω values by means of kinetic measurements.

4.1. Simulation model

The simulation model includes both, the case of localized adsorption as well as the adsorption in the presence of adatom surface diffusion characterized by a mean diffusion distance λ_s . The value of this parameter is used for distinguishing between the above two cases. In the first one $\lambda_s = 0$ and the simulation model corresponds exactly to the physical model for localized 1/n adsorption described in section 3.1. In the second case $\lambda_s > 0$ and the adatoms can migrate along the substrate surface by jumping at random to neighbouring adsorption sites.

The kinetics and the equilibrium of the adsorption process are governed by the elementary frequencies of single atom adsorption (k^+), desorption (k_i^-) and jumping (k_i^j) to a neighbouring adsorption site. In the simulation model these frequencies are defined in the usual way [25] by the expressions:

$$k^+ = \begin{cases} \nu \exp \beta, & \text{if the site is free,} \\ 0, & \text{else,} \end{cases} \quad (19)$$

$$k_i^- = \nu \exp[-\omega(i - c/2)], \quad (20)$$

$$k_i^j = \lambda_s^2 k_i^-, \quad (21)$$

where i is the number of the nearest neighbours of the adatom, and ν is a frequency factor. In adsorption from the vapour and in the electrochemical case, ν may be estimated from the relationships

$$\nu = p^x \Omega (2\pi m k T)^{-1/2} \exp(-\Delta\epsilon/kT),$$

and

$$\nu = i_0(E^x)\Omega/ze_0,$$

respectively. Here p^x is the pressure corresponding to μ^x , Ω is the area corresponding to an adsorption site, m is the mass of an atom, $\Delta\epsilon$ is the activation energy for the transfer of an atom from the vapour to the adsorption site and i_0 is the exchange current density at the reference electrode potential E^x .

The simulation experiment was carried out in the way described elsewhere [26] A substrate with 40 X 40 adsorption sites was used and periodic boundary conditions were imposed to eliminate edge effects. For each point of an isotherm at least 1000 elementary events per adsorption site (i.e. 1.6×10^6 in total) were used. This

number was larger when the equilibrium coverage of the substrate was not yet reached.

4.2. Simulation results

One way to obtain the equilibrium coverage θ at a given driving force β is to start with a bare substrate and to inspect the resulting coverage versus time curve. Such curves are shown in fig. 5 for 1/2 adsorption. At small ω values (i.e. high temperatures and/or small interaction energies ϵ) they are steadily increasing until θ starts to fluctuate around a saturation value which is then to be used in the isotherm. As can be expected, adatom surface diffusion does not affect this value. At larger ω and sufficiently small β a time delay is observed indicating a metastable state at small coverages. A metastable state may also appear at higher coverages. This is seen in fig. 5 for the $\omega = 2$ curve at $\theta \approx 0.88$. The reason for this kind of metastability is understood from figs. 6 and 7. Domains with a completely ordered structure are separated by mismatch boundaries, each of the domains containing adatoms on either "normal" or "twin" adsorption sites. In case of a square lattice (fig. 6) these "normal" and "twin" sublattices may be illustrated by the nets of white and black fields on a chess board. During the filling of the monolayer "normal" and "twin" clusters are formed at different parts of the substrate and each of them spreads out building up a domain of its own kind. If the equilibrium is to be reached by trans-

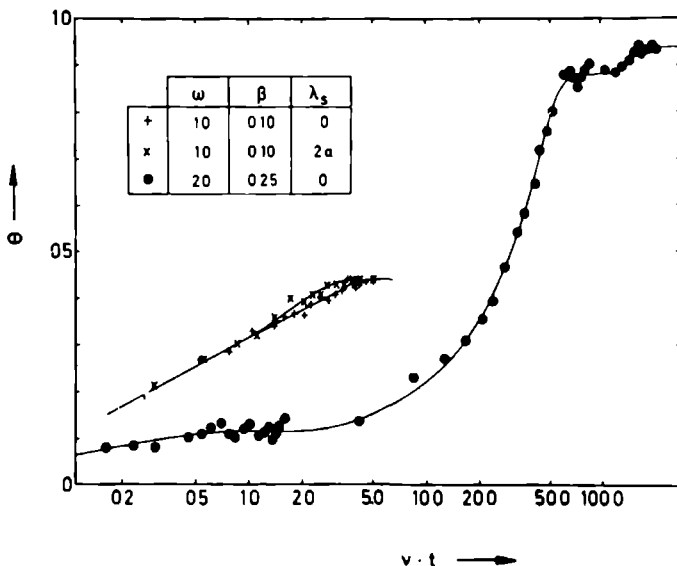


Fig. 5. Simulated time dependence of θ for 1/2 adsorption on a square lattice. At $\omega = 1.0$ no metastable state is observed. At $\omega = 2.0$ metastable states at low and high coverages exist.

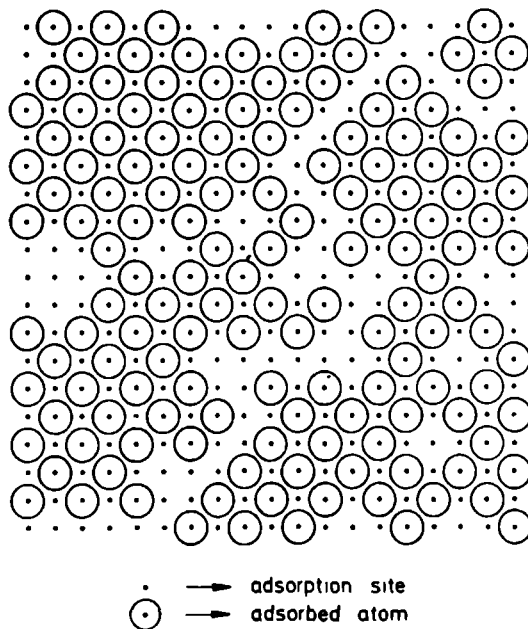


Fig. 6. Structure of the adsorbed monolayer at $\theta \approx 0.80$ as given by the computer in the case of $1/2$ adsorption on a square lattice at $\omega = 1.0$, $\beta = 0.7$. There are two ordered regions separated by a mismatch boundary.

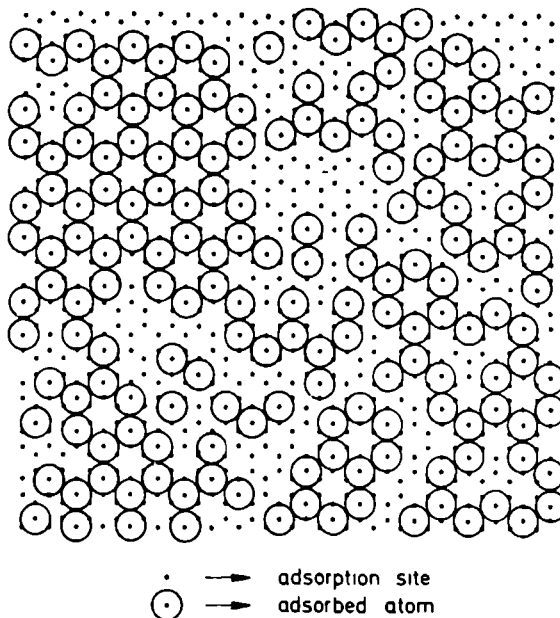


Fig. 7. Structure of the adsorbed monolayer at $\theta \approx 0.77$ as given by the computer in the case of $1/4$ adsorption on a hexagonal lattice at $\omega = 1.0$, $\beta = 1.5$. Several ordered regions, isolated small clusters and mismatch boundaries are seen.

formation of some of the clusters from “twin” to “normal” ones, for example, this could be time-consuming and the state may appear as metastable. This mismatch metastability is most pronounced at large ω values, but it is noticeable at small ω too, if β is sufficiently high.

A slightly different way to obtain a complete isotherm turned out to be faster and was used for most of the data presented. Namely, one first starts from an initially bare substrate to get one point of the isotherm at low θ as described above. After that the next points result from slight successive increases of β and the determination of the corresponding saturation values of the coverage–time curves which now start at $\theta \neq 0$.

The simulation $1/n$ isotherms are shown in figs. 8 and 9 for square and hexagonal lattices, respectively. As seen, they are asymmetric with respect to $\theta = 1/2$ in the way predicted theoretically by eq. (18) (see fig. 4). The Monte Carlo simulation method enables one to find also the critical ω_c value for two-dimensional first-order phase transition. The values of ω_c obtained with an accuracy to ± 0.1 in the two studied cases of $1/n$ adsorption are presented in table 1. As seen, they are smaller than the exact values for $1/1$ adsorption corresponding to the same structure of the adsorbed monolayer. This important result is also in agreement with the decrease in ω_c predicted by the theoretical isotherm (18) for $n > 1$.

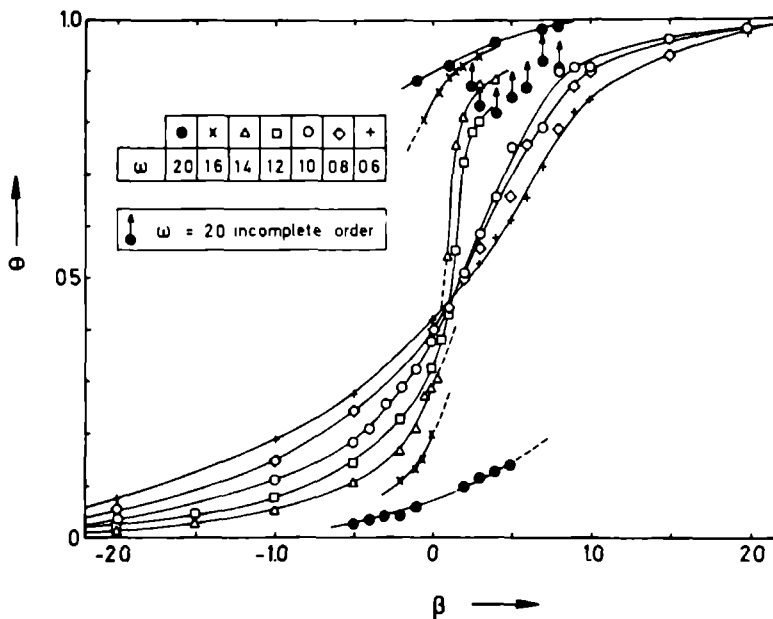


Fig. 8. Simulation adsorption isotherms for $1/2$ adsorption on a square lattice.

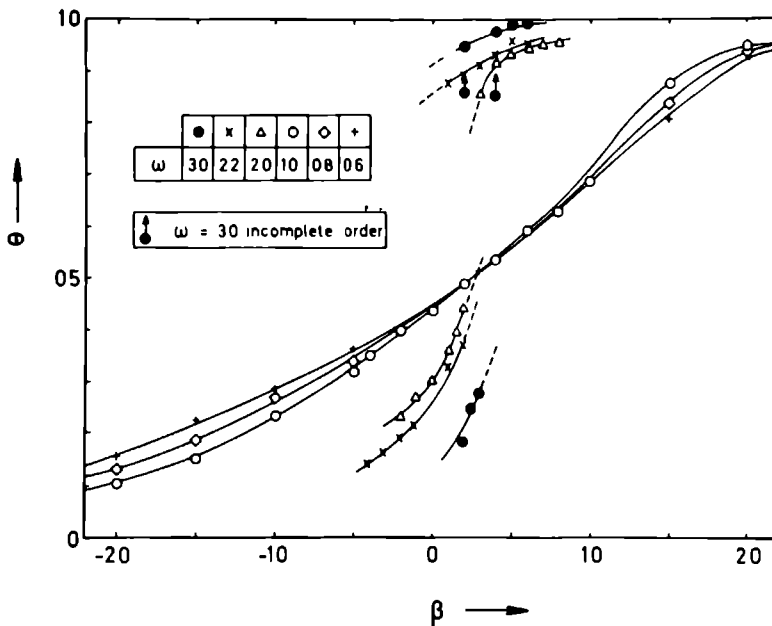


Fig 9 Simulation adsorption isotherms for 1/4 adsorption on a hexagonal lattice

5. Conclusion

The $1/n$ isotherm (18) is derived theoretically on the basis of approximate expressions for both the configurational entropy S_c and the internal energy U of the adsorbed phase. One can estimate the quality of the approximation for S_c by comparing the theoretical isotherm (18) with Monte Carlo simulation isotherms for various n and b in the absence of adatom–adatom interaction i.e. at $\omega = 0$. Figs 10 and 11 represent the theoretical (dashed curves) and the simulation (points) isotherms at $\omega = 0$ in the cases of 1/2 adsorption on a square lattice (fig 1a) and 1/4 adsorption on hexagonal lattice (fig 1b). As seen, the theoretical curve fits well the simulation data for the case 1/2 adsorption on square lattice, a higher deviation is observed in the case of 1/4 adsorption on a hexagonal lattice. In both cases a better approximation can be obtained by adjusting the b values. The lines drawn in figs 10 and 11 are obtained using $b = 2.5$ and 1.8 in eq (18). These differences between the theoretical and the empirical values of b may be regarded as due to the approximations involved in the calculations of $S_{c, i.e.}$ in the determination of W and θ_b . In view of the complexity of this problem it is interesting to note that the assignment of an effective value of b results in a virtual coincidence of the approximate $1/n$ isotherm (18) at $\omega = 0$ with the exact $\theta(\beta)$ dependence obtained by the simulation method.

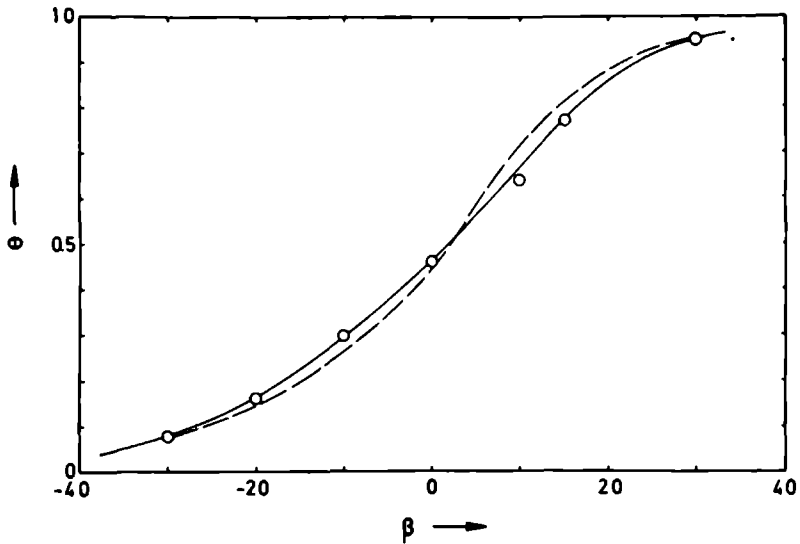


Fig 10 Adsorption isotherms for 1/2 adsorption on a square lattice at $\omega = 0$ (o) simulation data, (—) eq (18) with $b = 2.5$, (- - - -) eq (18) with $b = 4$

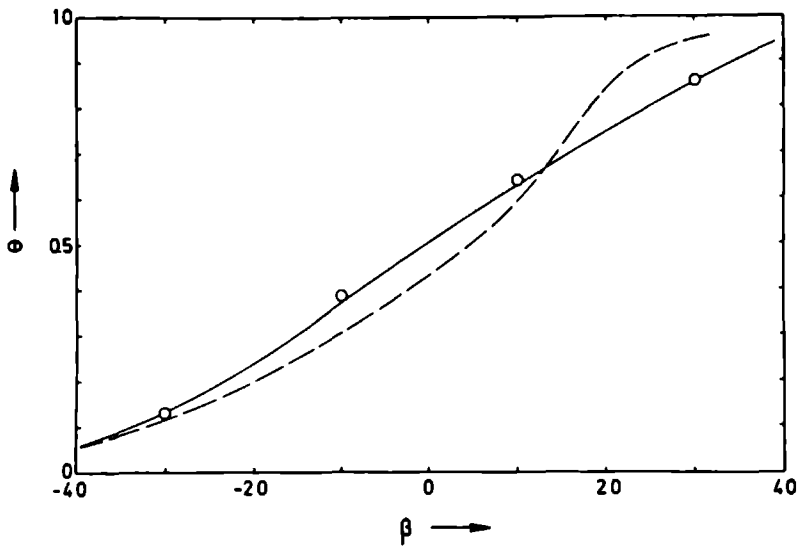


Fig 11 Adsorption isotherms for 1/4 adsorption on a hexagonal lattice at $\omega = 0$ (o) simulation data, (—) eq (18) with $b = 1.8$, (- - - -) eq (18) with $b = 3$

In the presence of adatom–adatom attraction, the adatoms on the substrate are arranged in comparatively large domains with the regular structure characteristic of the compact adsorption monolayer as can be seen from the Monte Carlo simulation results in figs. 6 and 7. In these cases the validity conditions of eq. (13), namely $0 < \omega \ll \omega_c$ and $\theta \rightarrow 1$, seem to be roughly fulfilled. Therefore, it can be expected that b tends to its theoretical value, i.e. 4 for 1/2 and 3 for 1/4 adsorption on square and hexagonal lattices, respectively. On the other hand, from eq. (18) follows that the precise $\theta_b(\theta)$ function is not important at small θ values. Consequently, eq. (13) is then likely to become a better approximation to the exact dependence of θ_b on θ in the whole coverage range as long as $\omega \ll \omega_c$.

This seems to be supported by comparing the simulation isotherm for 1/2 adsorption on square lattice at $\omega = 0.6$ with the theoretical one calculated from eq. (18) with $b = 4$ (fig. 12). The residual discrepancy could rather be attributed to the mean field approximation eq. (12) used for calculation of U than to an inexact determination of θ_b from eq. (13) affecting S . Indeed, a discrepancy of the same order of magnitude is seen in fig. 13 where the simulation isotherm for 1/1 adsorption on square lattice at $\omega = 0.7$ is compared with the known mean field isotherm for this case given by eq. (18) with $n = 1$ and $c = 4$. The deviation is now only due to the mean field approximation in the calculation of U .

It should be noted that the Monte Carlo isotherm of fig. 10 (1/2 adsorption on a square lattice with $\omega = 0$) fits remarkably well the numerical isotherm of Runnels (fig. 1 of ref. [19]) obtained by the transfer matrix method. For higher ω values, a

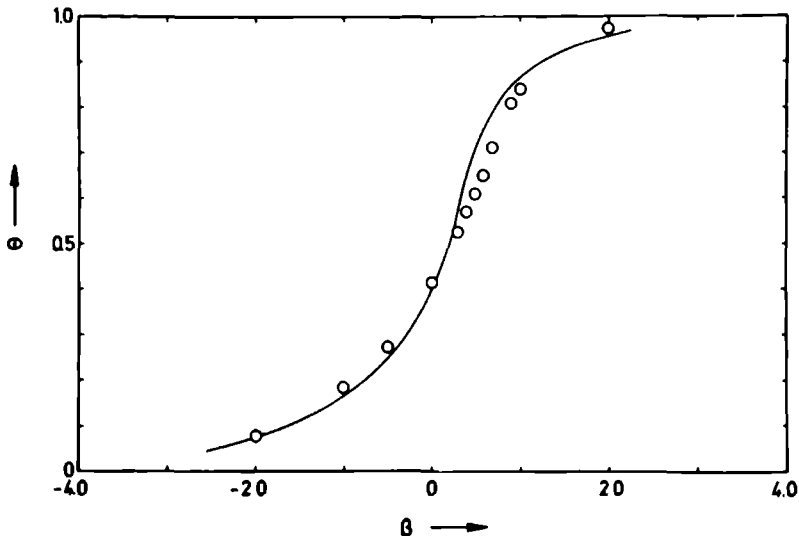


Fig. 12. Isotherm of 1/2 adsorption on a square lattice at $\omega = 0.6$: (o) simulation data; (—) eq. (18) with $b = 4, c = 4$.

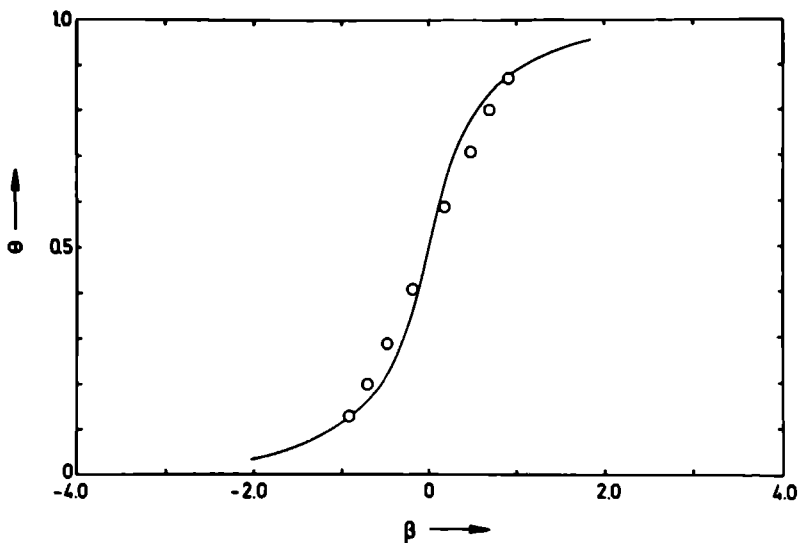


Fig. 13. Isotherm of 1/1 adsorption on a square lattice at $\omega = 0.7$: (o) simulation data; (—) eq. (18) with $c = 4$.

deviation is found between these isotherms which increase with ω tending to ω_c .

The existing treatments [17–19] of the hard core lattice gas model indicate a second order (“continuous”) transition at $\omega = 0$. The points of the present Monte Carlo simulation (figs. 10 and 11) are unfortunately rather limited in number to allow any conclusion about the existence of a second or higher order transitions. Runnel’s analysis [17,19] for 1/2 adsorption on a square lattice suggests that the second order transition could change to a first order phase transition with increasing attractive forces which agrees qualitatively with the present results.

The theoretical and the simulation isotherms obtained in the present work on the basis of the considered model for 1/ n adsorption can be used for interpretation of a number of experimental results on electrolytic underpotential adsorption of metals and adsorption of noble gases on single crystal faces. For example, the underpotential adsorption of Tl and Pb on (100) faces of Ag single crystals [14–16] corresponds to 1/2 adsorption on a square lattice. The experimental data for the formation of the first adsorption monolayer of Tl and Pb on Ag(100) in the underpotential region and the present simulation findings are compared in fig. 14. It is seen that the experimental isotherms agree well with the simulation isotherm for 1/2 adsorption on a square lattice at $\omega \approx 0.6$. Since the experimental isotherms are obtained at $T = 298$ K, this is equivalent to $\epsilon \approx 2.5 \times 10^{-14}$ erg, which is a reasonable value. In comparison to that a value of $\epsilon_e = 2.1 \times 10^{-6}$ erg cm $^{-1}$ for the specific edge energy in the case of monoatomic steps of silver has been found [30,

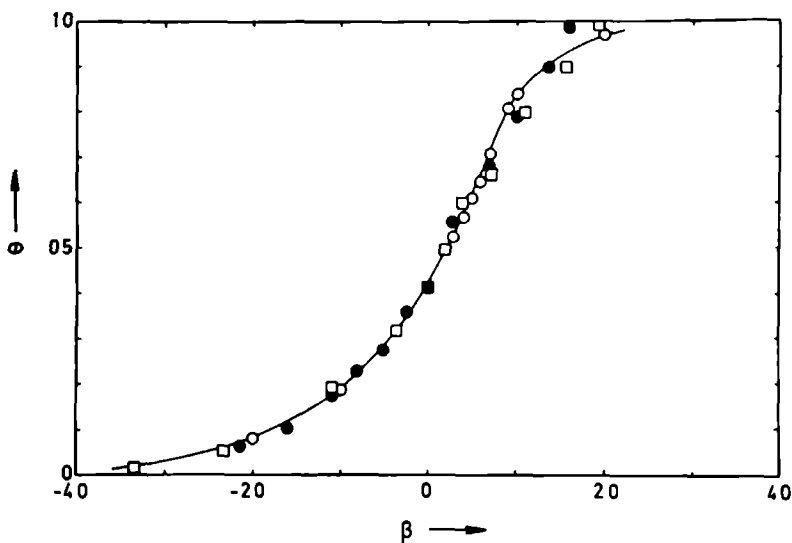


Fig. 14. Experimental and simulation isotherms: (○) simulation data for 1/2 adsorption on a square lattice at $\omega = 0.6$; (●) and (□) experimental results for underpotential adsorption of Tl and Pb on Ag(100) [14–16], respectively.

31]. From this value an attraction energy of $\epsilon = 6.05 \times 10^{-14}$ erg for the silver–silver interaction can be estimated taking into account only first next neighbours.

References

- [1] T.L. Hill, *Statistical Thermodynamics* (Addison-Wesley, Reading, MA, 1960).
- [2] J.G. Dash, *Films on Solid Surfaces* (Academic Press, New York, 1975).
- [3] I. Langmuir, *J. Am. Chem. Soc.* 40 (1918) 1361.
- [4] J.M. Honig, in: *The Solid Gas Interface*, Ed. E.A. Flood (Dekker, New York, 1967) p. 371.
- [5] A.N. Frumkin, *Z. Physik. Chem.* 116 (1925) 466.
- [6] R.H. Fowler and E.A. Guggenheim, *Statistical Thermodynamics* (Cambridge Univ. Press, Cambridge, 1965) p. 421.
- [7] F.F. Abraham and G.M. White, *J. Appl. Phys.* 41 (1970) 1841.
- [8] L. Onsager, *Phys. Rev.* 65 (1944) 117.
- [9] B. Mutaftschiev and A. Bonissent, *J. Phys. (Paris), Colloq. C4 (Suppl. No. 10)* 38 (1977) 82.
- [10] Yu.Ya. Gurevich and Yu.I. Kharkats, *J. Electroanal. Chem.* 86 (1978) 245.
- [11] J. Suzanne and H. Bienfait, *J. Phys. (Paris) Colloq. C4 (Suppl. No. 10)* 38 (1977) 31.
- [12] W.J. Lorenz, H.D. Herrmann, N. Wüthrich and F. Hilbert, *J. Electrochem. Soc.* 121 (1974) 1167.
- [13] G. Staikov, K. Jüttner, W.J. Lorenz and E. Budevski, *Electrochim. Acta* 23 (1978) 319.
- [14] H. Bort, K. Jüttner, W.J. Lorenz and E. Schmidt, *J. Electroanal. Chem.* 90 (1978) 413.

- [15] W J Lorenz, E Schmidt, G Stakov and H Bort, *Trans Faraday Soc* , in press
- [16] H Siegenthaler, K Juttner, E Schmidt and W J Lorenz, *Electrochim Acta*, in press
- [17] L K Runnels, in *Phase Transitions and Critical Phenomena*, Vol 2, Eds C Domb and M S Green (Academic Press, London, 1977) p 305
- [18] D M Burley, see ref [17], Vol 2, p 329
- [19] L K Runnels, J P Salvant and H R Streiffer, *J Chem Phys* 52 (1970) 2352
- [20] B D Metcalf, *Phys Letters* 45A (1973) 1
- [21] B Mihura and D P Landau, *Phys Rev Letters* 38 (1977) 977
- [22] M Schick, J S Walker and M Wortis, *Phys Rev* B16 (1977) 2205
- [23] W L Bragg and E J Wilhams, *Proc Roy Soc London* 145A (1934) 699
- [24] K J Vetter, *Electrochemical Kinetics* (Academic Press, New York, 1967)
- [25] G H Gilmer and P Bennema, *J Appl Phys* 43 (1972) 1347
- [26] J P van der Eerden, P Bennema and T A Cherepanova, in *Progress in Crystal Growth and Characterization*, Vol 1 (Pergamon, Oxford, 1978) pp 219–254
- [27] G Frtl and J Koppers, *Surface Sci* 21 (1970) 61
- [28] G Frtl and M Plancher, *Surface Sci* 48 (1975) 364
- [29] K Binder and D P Landau, *Surface Sci* 61 (1976) 577
- [30] E Budevski, V Bostanov, T Vitinov, Z Stoynov, A Kotzewa und R Kaischew, *Electrochim Acta* 11 (1966) 1697
- [31] F Budevski, *Some Fundamental Aspects of Electrocrystallization*, in *Progress in Surface and Membrane Science*, Vol 11 (Academic Press, New York, 1976) p 71

J.P. van der Eerden werd geboren 6 - 9 - 1950 te Amsterdam. Na te zijn opgegroeid en zijn gymnasium β diploma te hebben behaald in Doetinchem begon hij in 1968 zijn natuurkunde studie aan de Katholieke Universiteit van Nijmegen. In 1971 behaalde hij het kandidaatsexamen N2 en in 1974 het doctoraal examen in de theoretische natuurkunde van de Vaste Stof, op het onderwerp 'soft modes in structurele vaste stof faseovergangen'. Zijn belangstelling voor didaktiek (en het overdragen van kennis in het algemeen) leidde o.a. tot student assistentschappen (wiskunde en algemene mechanica) en tot een tijdelijk leraarschap (MAVO, wiskunde). Hij begon zijn promotie onderzoek in 1974 aan de technische hogeschool te Delft en sinds 1976 zet hij dit voort aan de Katholieke Universiteit. Van het begin af aan verheugde hij zich in de ruime mogelijkheden tot interdisciplinaire, inter-universitaire en internationale kontakten en samenwerking die binnen die onderzoeksgroepen bestonden en uitgebouwd konden worden. Na zijn promotie zal hij dit onderzoek aan de Katholieke Universiteit voortzetten.

- 1) Men moet er naar streven het samenstellen van een proefschrift zo in te richten dat dit de wetenschappelijke vorming en de sociale kontakten van de promovendus niet onderbreekt, maar juist verdiept.
- 2) Het vertrouwen in diskrete kristalgroeimodellen is momenteel intuïtief. Een toekomstig onderzoek naar het geldigheidsbereik van deze diskrete benadering zal de relatieve ligging van de oppervlakteverruwings- en de smeltemperatuur moeten verklaren.
- 3) Bij de numerieke bepaling van partiële gas druk velden bij kristalgroei door middel van gas fase depositie (CVD) is het onlogisch (gezien de huidige kennis van oppervlakteprocessen) en onnodig (gezien het gebruik van een komputer) te veronderstellen dat aan het oppervlak een eerste orde reactie plaatsvindt (C.H.J. v.d. Brekel, proefschrift Nijmegen 1978).
- 4) De huidige stand van de kristalgroei theorie leidt tot de konklusie dat het kweken van een éénkristal gewoonlijk niet ver van zijn (dynamische of evenwichts) verruwingsovergang plaatsvindt.
- 5) De berekening van de golffuncties van het waterstof atoom is vanuit didaktisch oogpunt ongewenst in een inleiding in de kwantummechanika. Het eerder introduceren van observabelen en toestandsvektoren vermijdt ingewikkelde wiskunde en leidt tot meer begrip van ingewikkelder systemen.
- 6) In het wiskunde onderwijs op middelbare scholen wordt te veel nadruk gelegd op het feit dat een plaatje niets bewijst. Het is zinniger de leerling voor te houden dat inzichten bijna altijd groeien uit en verruimd worden door beelden.
- 7) Naarmate er over een bepaalde behandeling of kwaal meer verschillende opvattingen bestaan in de medische wereld, moet een behandelend arts het eigen oordeel van de patient zwaarder laten wegen.
- 8) Het is onrechtvaardig boeren te beboeten voor de aanwezigheid van schadelijke stoffen in hun produkten als een overheidskommissie, na zorgvuldig onderzoek, konkludeert dat die besmetting niet opzettelijk wordt

veroorzaakt, dat de bron niet aangewezen kan worden, en dat er geen aanbeveling ter voorkoming van verdere besmetting kan worden gegeven.

- 9) Ingenieurs zijn in staat problemen op te lossen voor ze die volledig begrijpen, doctorandi kunnen problemen begrijpen zonder dat ze een oplossing geven.

